Titre: Title:	Fabrication of Mullite-Bonded Porous SiC Ceramics from Multilayer-Coated SiC Particles Through Sol-Gel and In-Situ Polymerization Techniques
Auteur: Author:	Omid Ebrahimpour
Date:	2013
Type:	Mémoire ou thèse / Dissertation or Thesis
Référence: Citation:	Ebrahimpour, O. (2013). Fabrication of Mullite-Bonded Porous SiC Ceramics from Multilayer-Coated SiC Particles Through Sol-Gel and In-Situ Polymerization Techniques [Thèse de doctorat, École Polytechnique de Montréal]. PolyPublie. https://publications.polymtl.ca/1321/

UNIVERSITÉ DE MONTRÉAL

FABRICATION OF MULLITE-BONDED POROUS SIC CERAMICS FROM MULTILAYER-COATED SIC PARTICLES THROUGH SOL-GEL AND IN-SITU POLYMERIZATION TECHNIQUES

OMID EBRAHIMPOUR

DÉPARTEMENT DE GÉNIE CHIMIQUE

ÉCOLE POLYTECHNIQUE DE MONTRÉAL

THÉSE PRÉSENTÉE EN VUE DE L'OBTENTION

DU DIPLÔME DE PHILOSOPHIAE DOCTOR

(GÉNIE CHIMIQUE)

DÉCEMBRE 2013

UNIVERSITÉ DE MONTRÉAL

ÉCOLE POLYTECHNIQUE DE MONTRÉAL

Cette thèse intitulée:

FABRICATION OF MULLITE-BONDED POROUS SIC CERAMICS FROM MULTILAYER-COATED SIC PARTICLES THROUGH SOL-GEL AND IN-SITU POLYMERIZATION TECHNIQUES

présentée par: EBRAHIMPOUR Omid

en vue de l'obtention du diplôme de : Philosophiae Doctor

a été dûment acceptée par le jury d'examen constitué de :

M. BERTRAND François, Ph.D., président

M. CHAOUKI Jamal, Ph.D., membre et directeur de recherche

M. DUBOIS Charles, Ph.D., membre et codirecteur de recherche

M. PATIENCE Gregory S., Ph.D., membre

M. GITZHOFER François, Ph.D., membre

DÉDICACE

*To my lovely parents :(**Eshagh** and **Jila**), and my brothers **Ehsan** and **Ali**.*

*To my love: **Pardis***

ACKNOWLEDGEMNTS

I would like to express my sincere gratitude to my research supervisor, Prof. Jamal Chaouki, and my co-advisor, Prof. Charles Dubois, for their extensive support and guidance and the great opportunity to study under their supervision. Their innovative attitude, encouragement, patience led me to undertake this project.

I would like to extend my thanks to all my professors during my undergraduate and graduate studies at Sharif University, particularly Dr. Baghalha and Prof. Meghdari, for encouraging me to continue my graduate studies.

My sincere appreciation goes to all the technical and administrative staffs of École Polytechnique de Montreal, Chemical Engineering department, especially Ms. Valérie Baudart and Ms. Évelyne Rousseau for providing me with administrative assistance, Mr. Gino Robin and Ms. Martine Lamarche for providing the materials, and Mr. Guillaume Lessard, Ms. Claire Cerclé, Mr. Robert Deris and Ms. Carole Massicote for their technical assistance. My special thanks go to Ms. Sylvie St-Amour from FPInnovations for her collaboration in working with mercury porosimetry and Dr. Josianne Lefebvre for measuring the surface analysis via XPS. I would like to thank Ms. Nicole MacDonald, M. Jean-Philippe Masse and M. Philippe Plamondon from CM^2 group for their great help in morphological and characterization studies for this thesis.

I would like to acknowledge the helpful discussions with and assistance from my colleagues in my research group as well as Dr. Babak Esmaeili, Mr. Ahmad Zohrevand, Dr. Hamed Heidari, Mr. Amyeric Guy, Mr. Milad AghabararNejad, Mr Farzam Fotovat and Ms. Lucie Griffon and Ms. Sophie Bussiere. I would appreciate the assistance of Odile and Soumaya to translate the Abstract of this work into French. I would like to thank Dr. Amirhossein Maani and Dr. Hessam Tabatabaei for their valuable assistance since my arrival in Canada.

I would like to thank all of my friends, especially Ehsan, Forough, Ahmad, Maryam, Ashkan, Naghmeh, Andrew, Olivier, Evan, François-Xavier, Hamed, Maryam Fereidooni, Babak, Mahsa, Amir, and Atefeh for supporting me, during my studies and their assistance during the difficult situation.

Finally, all my special and deepest gratitude go to my family, especially my parents, wife, and brothers for their love, understanding, and support during my PhD.

RÉSUMÉ

Les céramiques poreuses en carbure de silicium (SiC) ont un avenir prometteur au sein d'une large variété d'applications, que ce soit en tant que produits finaux, ou encore au sein de nombreux procédés à haute température où elles peuvent servir de support de combustion gazeuse, de membranes ou de supports catalytiques, de filtres à haute température et autres. Cette large gamme d'applications potentielles est due à leur excellente et unique combinaison de propriétés mécaniques et physiques, telles qu'une haute conductivité thermique, un faible coefficient d'expansion thermique (CET) et une forte stabilité mécanique. En fonction de l'application à laquelle se destine la céramique de SiC, différents procédés de fabrication ont été développés et proposés. Parmi ceux-ci on retrouve la technique de liaison par réaction. Cette technique nécessite le mélange des particules de SiC avec un additif de frittage, tel que des poudres de Al_2O_3 ou de Y_2O_3, ainsi qu'avec un agent formateur de pores, tel que des particules de graphite ou des billes de polymère. Ce mélange est ensuite pressé et chauffé en présence d'air, contrairement à d'autres techniques qui utilisent une atmosphère inerte. Cette technique a prouvé être efficace pour la production de céramiques poreuses de SiC avec des propriétés satisfaisantes et ce à faible température de frittage (1500 °C). Néanmoins, les propriétés des céramiques poreuses de SiC, quelles soient mécaniques ou physiques, ainsi que le contrôle précis de la porosité et de la distribution de taille des pores peuvent encore être améliorés, nécessitant dès lors la révision de ce procédé ainsi que le développement d'une nouvelle voie de fabrication des céramiques poreuses de SiC. Afin d'atteindre une amélioration significative des performances de fabrication, une bonne dispersion de l'additif de frittage et de l'agent formateur de pores dans le matériel initial est requis.

Dans ce travail, des céramiques poreuses de SiC liées par de la mullite sont préparées via la technique de liaison par réaction, assistée d'une part par la technique dite sol-gel, et d'autre part par la technique de polymérisation in-situ. La procédure typique de formation de ces céramiques consiste premièrement à enduire les particules de SiC par de l'alumine. Ceci est fait via la technique sol-gel avec comme réactifs des poudres calcinées et un sol d'alumine. Cette première étape est suivie par le séchage et le tamisage des poudres produites. Ensuite, ces dernières sont enduites de la quantité désirée de polyéthylène par la technique de polymérisation in-situ au sein d'un réacteur en suspension avec un catalyseur de type Ziegler-Natta. Après la polymérisation in-

situ, les poudres enrobées sont à nouveau séchées et tamisées avant d'être pressées au sein d'un moule rectangulaire afin de former un corps vert, qui est ensuite chauffé. Durant le procédé de chauffage, à une température d'environ 500 °C, le polyéthylène est dégradé, et les pores sont formés au sein du matériel. L'augmentation de la température au dessus de 800°C mène à l'oxydation partielle de particules de SiC en silice. A plus haute température encore, supérieure à 1400°C, la silice nouvellement formée réagit avec l'alumine pour former de la mullite, qui joue alors le rôle de liant entre les particules restantes de SiC. Les spécimens de SiC poreux ainsi formés sont alors caractérisés à l'aide des essais de flexion en trois points, d'un porosimètre au mercure, de la technique de diffraction aux rayons X et d'un microscope électronique à balayage.

Étant donné que l'oxydation des particules de SiC est une étape critique du procédé de fabrication des céramiques poreuses de SiC, la première partie de ce projet est consacrée à son étude à l'aide d'un appareil d'analyse thermogravimétrique (TGA). Les paramètres étudiés sont l'effet de la taille des particules (micro- et nanoparticules), de la température d'oxydation (910 °C – 1010 °C), ainsi que la masse initiale de particules de SiC sur l'oxydation des poudres de SiC. Les analyses TGA ont révélé que pour les échantillons avec une plus grande surface spécifique (et donc une plus petite taille de particules), l'oxydation débute à plus basse température. Dans le système étudié, la vitesse d'oxydation est contrôlée par la cinétique de réaction à la surface ainsi que la diffusion intra-particulaire. En plus de ces facteurs, il semblerait qu'une diffusion inter particules ait également lieu, qui doit alors être prise en compte au sein de la description de la vitesse globale de réaction. Afin d'évaluer la vitesse globale d'oxydation de SiC au sein d'un lit fixe de particules, un modèle réactionnel inédit a été développé. Il prend en compte toutes les étapes de diffusion (jusqu'à la surface du lit de particules, entre les particules au sein du lit, et au sein des particules elles-mêmes) ainsi que la cinétique d'oxydation. Finalement, l'état d'oxydation des particules de SiC a été analysé par diffraction aux rayons X. Il a été trouvé qu'aux températures supérieures à 1200°C, la structure amorphe de la silice se modifie pour former de la cristobalite.

L'effet des différentes sources d'alumine (Al_2O_3 calcinés, le sol d'alumine ou une combinaison des deux) sur la structure mécanique, physique et cristalline de céramique SiC poreuse liée par mullite est étudié dans la deuxième partie du projet. Un sol d'alumine est synthétisé par hydrolyse de isoproxide d'aluminium selon la méthode Yoldas. L’observation par microscopie électronique en transmission (MET) montre que le sol d'alumine était homogène et avait une forme d'aiguille avec une épaisseur de 2-3 nm. Les changements cristallins au cours du processus de chauffage de

sol d'alumine sont étudiés par diffractométrie de rayons X (DRX). En outre, spectroscopie infrarouge à transformée de Fourier (IRTF) est réalisée afin d'identifier les groupes fonctionnels sur la surface d'alumine sol en fonction de la température. Dans cette phase, il a été constaté que l'augmentation de l'alumine calcinée nano poudre de 0 % en masse à 40% en masse permet d'améliorer la résistance mécanique et de diminuer la porosité des échantillons. Cependant, l'addition de l'alumine sous forme de sol conduit à augmenter la porosité et diminuer la résistance. L'analyse DRX et et la microscopie électronique à balayage (MEB) montrent que, à une faible quantité d'alumine (10 % en masse) sous forme de sol, toute l'alumine réagit avec la silice pour former la mullite ; tandis que, lorsque l'alumine est ajoutée sous forme calcinée, une fraction d'alumine reste dans le système. Les analyses de caractérisation montrent que lorsqu'une partir d'alumine calcinée (20% en masse) est remplacée par de l'alumine sol, les forces mécaniques et physiques sont améliorées (30%) par rapport à quand 100 % d'alumine calcinée est utilisée comme source d'alumine.

Dans la troisième partie du projet, la faisabilité de la technique de polymérisation in situ est étudiée pour fabriquer des céramiques SiC poreuses. Dans cette partie, le mélange de SiC et de poudres d'alumine calcinés ont été recouverts par du polyéthylène par polymérisation in situ appelée la polymérisation processus cumulatif dans une phase de suspension. La polymérisation a été effectuée dans des conditions d'opération très modérées (T = 65 ° C, P = 48 kPa) en utilisant le système de catalyseur Ziegler-Natta (TiCl4 comme catalyseur et trois éthyl-aluminium en tant que co-catalyseur). La calorimétrie différentielle à balayage (DSC) et l'analyse thermogravimétrique (TGA) et des études morphologiques (SEM et MET) révèlent la présence d'une forte densité de polyéthylène sur la surface de SiC et de poudres d'alumine. La quantité de polymère est commandée par la durée de la réaction de polymérisation. Les analyses MET et spectroscopie de photoélectrons X (XPS) ont démontré que la plupart des parties de particules sont recouvertes d'une fine couche de polyéthylène et de polymère. Les céramiques SiC poreuses fabriqués par ces particules traitées–possèdent des propriétés mécaniques et physiques supérieures par rapport aux échantillons réalisés sans aucun traitement. La caractérisation DRX du produit montre que l'intensité relative de mullite est plus élevée par rapport aux échantillons préparés par le procédé traditionnel. Les effets sur les propriétés physiques et mécaniques du produit final de la température de frittage (1500 °C et 1550 °C), la pression de formage (25 MPa, 50 MPa, 100 MPa) et la teneur en polymère (0% -19 % en masse) sont également étudiés.

Dans la dernière phase de ce travail de recherche, l'objectif est de combiner le traitement sol-gel et le procédé de polymérisation in situ pour développer un nouveau procédé de fabrication de céramique SiC poreuses liés par mullite aux propriétés mécaniques et physiques améliorées. Par conséquent, les premières particules de SiC et les poudres d'alumine nano sont mélangées dans un sol d'alumine pour ajuster le poids d'alumine à 35 % en masse. Ensuite, la quantité désirée de catalyseur, qui dépend de la superficie totale de la surface des particules, est greffé sur la surface des poudres sous atmosphère inerte. En conséquence, la polymérisation commence à partir de la surface du substrat. Les poudres traitées ont été caractérisés par MEB, XPS et TGA. En outre, la quantité de photogène est déterminée par l'analyse TGA. L'analyse DRX confirme que, dans les échantillons produits par le nouveau procédé, les quantités de mullite et de cristobalite sont beaucoup plus élevées par rapport à celui préparé par la méthode conventionnelle. Selon les analyses DRX, céramiques SiC poreuses fabriqués par le procédé novateur, sont constitués de mullite, SiC, cristobalite et une petite quantité de l'alumine et de TiO_2. L'analyse de la distribution des tailles des pores illustre que les céramiques fabriqués en utilisant le nouveau procédé conduit à une distribution de taille des pores étroite avec une taille de pores moyenne supérieure et une porosité élevée par rapport à la méthode traditionnelle. En outre, une résistance mécanique améliorée de plus de 35 % . L'analyse SEM confirme que la plupart des particules de SiC sont bien reliées entre elles et la croissance du cou entre les particules est bien développé. De plus, l'effet de la température de frittage (1500 °C, 1550 °C et 1600 °C) sur la structure cristalline des échantillons poreux est étudiée. Il est constaté que, dans les échantillons préparés à 1600 ° C pendant 3 heures dans l'air, les principales phases ont été la mullite et le carbure de silicium. En outre, il est suggéré que la conversion de $TiCl_4$ à TiO_2, introduit auparavant comme étant le catalyseur pour la formation du polymère, agit comme additif de frittage pour former de la mullite à une température de frittage inférieure. On conclut que l'application de la technique sol-gel et la polymérisation in situ est un moyen efficace pour améliorer la dispersion des poudres d'additifs de frittage et des pores anciens avec les matières premières, ce qui entraîne la formation de céramiques poreuses avec des propriétés améliorées à basse température de frittage .

ABSTRACT

Porous silicon carbide (SiC) ceramics have been regarded as promising candidates in a wide variety of applications as end products and in several high temperature processes, such as gas burner media, catalyst membrane reactors, catalyst supports, hot-gas particulate filter and molten metal filter due to the unique excellent combination of mechanical and physical properties, such as high thermal conductivity, a low coefficient of thermal expansion (CTE) and high mechanical stability. Depending on the application of porous SiC ceramics various fabrication processes have been developed and proposed. One of them is the reaction bonding technique, which involves the addition of a sintering additive, such as Al_2O_3 and Y_2O_3 powders, and a pore former, such as graphite particles or polymer beads, to the SiC particles and heating the pressed powders under air instead of an inert atmosphere. This has been shown as an effective way to produce porous SiC ceramics at a lower sintering temperature (1500 °C) with enhanced properties. However, there still is a need to improve the process and develop a new manufacturing route to fabricate porous SiC ceramics, precisely control the porosity and pore size distribution and improve both mechanical and physical properties of the final product. To achieve significant performance enhancements, good dispersion of the sintering additive as well as pore former into the starting materials is required.

In this work, mullite-bonded porous SiC ceramics were prepared via a reaction bonding technique with the assistance of a sol-gel technique or in-situ polymerization as well as a combination of these techniques. In a typical procedure, SiC particles were first coated by alumina using calcined powder and alumina sol via a sol-gel technique followed by drying and passing through a screen. Subsequently, they were coated with the desired amount of polyethylene via an in-situ polymerization technique in a slurry phase reactor using a Ziegler-Natta catalyst. Afterward, the coated powders were dried again and passed through a screen before being pressed into a rectangular mold to make a green body. During the heating process, the polyethylene was burnt out to form pores at a temperature of about 500 °C. Increasing the temperature above 800 °C led to the partial oxidation of SiC particles to silica. At higher temperatures (above 1400 °C) derived silica reacted with alumina to form mullite, which bonds SiC particles together. The porous SiC specimens were characterized with various techniques, such as a three point bending test, mercury porosimetry, XRD and SEM.

As the oxidation process is an important step during the fabrication of porous SiC ceramics, the first part of the project was devoted to investigating the oxidation of SiC particles using a Thermogravimetric analysis (TGA) apparatus. The effects of particle size (micro and nano) and oxidation temperature (910 °C-1010 °C) as well as the initial mass of SiC particles in TGA on the oxidation behaviour of SiC powders were evaluated. TGA analysis revealed that in the samples that have a higher surface area (lower particle size) the oxidation started at a lower temperature. In the studied system, it was found that both surface kinetic and intra particle diffusion control the oxidation rate. Beside these factors, it was revealed that inter particle diffusion must also be taken into account to describe the overall kinetic rate. To illustrate the oxidation rate of SiC in the packed bed state, a new kinetic model, which takes into account all of the diffusion steps (bulk, inter and intra particle diffusion) and surface oxidation rate, was proposed. Furthermore, the oxidation of SiC particles was analyzed by the X-ray Diffraction (XRD) technique. It was found that at temperatures above 1200 °C, the amorphous structure of silica was transferred to cristobalite.

The effect of different alumina sources (calcined Al_2O_3, alumina sol or a combination of the two) on the mechanical, physical, and crystalline structure of mullite-bonded porous SiC ceramics was studied in the second part of the project. Alumina sol was synthesized by the hydrolysis of Aluminum isopropoxide using the Yoldas method. Transmission electron microscopy (TEM) observation showed that alumina sol was homogenous and had a needle-like shape with a thickness of 2-3 nm. Crystalline changes during the heating process of alumina sol were studied using XRD. In addition, Fourier transform infrared (FTIR) spectroscopy was performed to identify the functional groups on the alumina sol surface as a function of temperature. In this phase, it was found that increasing the calcined alumina nano powder (0 wt% to 40 wt %) improved the mechanical strength and decreased the porosity of the specimens. However, the addition of alumina in the sol form resulted in increasing porosity and decreasing strength. XRD analysis and scanning electron microscope (SEM) characterization revealed that at a low amount of alumina (10 wt%) in the sol form, all of the alumina reacted with silica to form mullite while when alumina was added in the calcined form, some of the alumina remained in the system. Characterization analysis showed that when some sources of calcined alumina (20 wt %) were replaced by alumina sol, both mechanical and physical strengths were enhanced (30%) compared to when 100% calcined alumina was used as the source of alumina.

In the third part of the project, the feasibility of the in-situ polymerization technique was investigated to fabricate porous SiC ceramics. In this part, the mixture of SiC and calcined alumina powders were coated by polyethylene via in-situ polymerizing referred to as the polymerization compounding process in a slurry phase. The polymerization was conducted under very moderate operational conditions (T= 65 °C, P= 48 kPa) using the Ziegler-Natta catalyst system ($TiCl_4$ as catalyst and three ethyl aluminum as co-catalyst). Differential scanning calorimetry (DSC) and TGA analysis and morphological studies (SEM and TEM) revealed the presence of a high density of polyethylene on the surface of SiC and alumina powders. The amount of polymer was controlled by the polymerization reaction time. TEM and X-ray photoelectron spectroscopy (XPS) analysis demonstrated that most parts of particles were coated by a thin layer of polyethylene and polymer. The porous SiC ceramics, which were fabricated by these treated particles showed higher mechanical and physical properties compared to the samples made without any treatment. The XRD characterization of the product showed that the relative intensity of mullite was higher compared to the samples prepared by the traditional process. The effects of the sintering temperature (1500 °C and 1550 °C), forming pressure (25 MPa, 50 MPa, 100 MPa) and polymer content (0%-19 wt%) were also studied on the physical and mechanical properties of the final product.

In the last phase of this research work, the focus of the investigation was to take advantage of both the sol-gel processing and in-situ polymerization method to develop a new process to manufacture mullite-bonded porous SiC ceramic with enhanced mechanical and physical properties. Therefore, first the SiC particles and alumina nano powders were mixed in alumina sol to adjust the alumina weight to 35 wt%. Then, the desired amount of catalyst, which depends on the total surface area of the particles, was grafted onto the surface of the powders under an inert atmosphere. Consequently, the polymerization started from the surface of the substrate. The treated powders were characterized by SEM, XPS and TGA. In addition, the amount of pore-former was determined by TGA analysis. The XRD analysis demonstrated that in the samples produced via the novel process the amount the mullite and cristobalite were much higher compared to the one prepared by the conventional method. According to the XRD analysis, porous SiC ceramics, which were fabricated by the novel process, consist of mullite, SiC, cristobalite and a small amount of alumina and TiO_2 as a result of reaction of $TiCl_4$ with air. Pore size distribution analysis illustrated that ceramics manufactured using the novel process resulted

in a narrow pore size distribution with a larger average pore size and higher porosity compared to the traditional method. In addition, mechanical strength improved more than 35 %. The SEM investigation confirmed that most of the SiC particles were well connected together and the neck growth between particles was well developed. Furthermore, the effect of the sintering temperatures (1500 °C, 1550 °C and 1600 °C) on the crystalline structure of the porous samples was investigated. It was found that for the samples prepared at 1600 °C for 3h in air the main phases were mullite and silicon carbide. Furthermore, it was proposed that converting $TiCl_4$ to TiO_2, which was initially introduced as the catalyst during the polymer formation, acted as the sintering additive to form mullite at a lower sintering temperature. It was concluded that implementation of the sol-gel technique and in-situ polymerization was an effective way to enhance dispersion of sintering additive powders and pore-former with the starting materials, which results in the formation of porous ceramics with enhanced properties at a low sintering temperature.

TABLE OF CONTENTS

LIST OF TABLES

LISTE OF FIGURES

LIST OF SYMBOLS

A	Gas reactant
A_b	Bed surface area
b	Stoichiometric coefficient
C_A	Concentration of gas reactant
C_{As}	Concentration of gas reactant at the surface of the bed
ρ_{SiC}	Molar density of SiC
C_t	Total molar density of gas
D_0	Pre-exponential factor in Arrhenius equation in Eq. 4.24
D_{air-co_2}	Diffusion coefficient of the reactant in gas in the bulk system
D_e^s	Effective diffusivity of the reactant gaseous in solid
k_0	Pre-exponential factor in Arrhenius equation in Eq. 4.25
H.D.P.E	High density polyethylene
L	Bed height
L_0	Crucible height
m_0	Initial sample weight
$N_A^{'}$	Molar flux of gaseous reactant inside the powder
N_A	Molar balance of the gaseous reactant in the crucible
R_0	Radius of the crucible
r_c	Radius of un-reacted shell of powder
r_0	Initial powder radius
S_v	Total surface area of the powder per unit volume
t	Time

T	Temperature
τ_S	Time for a complete reaction of the particles as defined in Eq. 4.4
τ_r	Time to complete oxidation of the particles as defined in Eq. 4.4
τ_b	Time to complete oxidation of the particles as defined in Eq. 4.10
τ_c	Time to complete oxidation of the particles as defined in Eq. 4.27
X	Fractional conversion as defined in Eq. 4.5
x_0	Thickness of the oxide layer
x_A	Mole fraction of gas A in crucible
x_{Ab}	Mole fraction of gas A at bulk
$x_{As}(t)$	Mole fraction of gas A at the surface of the bed
$X_{A,Loc}^{'}$	Local fractional conversion defined by Eq. 4.22
Z	Dimensionless of bed height in the crucible (z/L)
Z^*	Dimensionless of moving boundary in the bed
Ω	Function defined by Eq. 4.19
η	Function defined by Eq. 4.18
θ	Function defined by Eq. 4.27
Φ	Function defined by Eq. 4.B1
ε	Porosity
σ	Stress
τ	Tortuosity

INTRODUCTION

Porous silicon carbide (SiC) ceramics have been attracting a great deal of research attention as they are found in a wide variety of high-temperature processes in the metallurgical and chemical fields. Due to their unique combination of physical and mechanical properties, such as excellent mechanical strength, good chemical resistance, high thermal conductivity and low thermal expansion number, these materials are known as the best material candidates in filters, catalytic supports, separation membranes, high-temperature structural materials, kiln furniture, thermoelectric energy conversion, and the reinforcement of composites [1]. Depending on the special application of the porous ceramic, several processing routes have been proposed and developed for the manufacture of porous SiC ceramics, which can be grouped into 5 categories [1]: (i) partial sintering, (ii) replica, (iii) sacrificial template, (iv) direct foaming, and (v) reaction bonding techniques. To self-bond porous SiC ceramics a very high sintering temperature (above 2000 °C) is required due to the high covalent nature of the Si-C bond [2] and low self diffusion coefficient of SiC. In addition, during the operation of self-bonded porous SiC ceramics at high temperature in a humid environment and an oxidizing atmosphere, these materials are partially oxidized and elongated and eventually fail.

To fabricate porous SiC ceramics at lower sintering temperatures with a higher oxidation resistance, a reaction bonding technique was developed, which involves a mixture of a sub-micron sintering additive, such as alumina, and a pore former, such as graphite, with the SiC particles followed by pressing the powders to make a green body and heating the compact powders under air [3]. However, the main drawback of this process is the agglomeration of the sintering additive and poor dispersion of pore former in the starting materials, which degrades the mechanical and physical properties of the porous ceramics. Therefore, developing a new process at a low sintering temperature to improve control in pore size distribution and increase the mechanical properties and porosity simultaneously would be an interesting subject.

The main objective of this study is to develop mullite-bonded porous SiC ceramics with a combination of sol-gel and in-situ polymerization techniques with a reaction bonding process. Sol-gel processing is a well-known method to fabricate ceramic composite due to the low cost and high homogenous mixing. In addition, in-situ polymerization is a promising technique to synthesize organic-inorganic composites with enhanced mechanical properties. It is believed that

the addition of a sintering additive via the sol-gel route and a pore former by in situ polymerization is an appropriate choice to overcome the inhomogeneity of the starting particles and enhance and control the properties of the final ceramics. This method can fabricate a porous ceramic, which is strongly resistant to oxidation and with the desired filtration properties. It will make it possible to create a multifunctional, responsive and adaptive filter for various operating conditions, such as for advanced coal and biomass-based gas turbine power generation applications. In this method, SiC particles are coated by alumina via alumina sol and calcined alumina powders. Subsequently, polyethylene is layered on particles using in situ polymerization. By heating the green body, polyethylene is removed as a result of the reaction of the polymer with oxygen and consequently pores are created. Mullite is formed by the reaction between alumina and silica derived from SiC during the sintering process to bond SiC particles together.

To help follow the results presented in this dissertation, a literature review concerning the important properties of the starting materials (SiC, alumina and mullite), sol-gel processing, in-situ polymerization technique, oxidation of SiC and previous works carried out on the porous SiC ceramics fabrication is given in Chapter 1. The materials used and our methodology to achieve the objectives are presented in Chapter 2. Chapter 3 briefly describes the organization of the papers. In Chapter 4, the passive oxidation of SiC powders is discussed from experimental results with high-temperature thermogravimetry analysis. The effects of oxidation temperature and particle size on the oxidation rate of SiC powders are investigated. In addition, the effect of the diffusion resistance on the oxidation rate of SiC powders is discussed in depth. Chapter 5 presents the results on the fabrication of porous SiC ceramics via reaction bonding with different amounts of alumina contents and sources (alumina in sol or calcined powders or a combination of them). The results showed that the alumina content and form played a crucial role on the mechanical and physical properties and morphology of the pore structure of the porous samples. In chapter 6, porous SiC ceramics were fabricated with the cooperation of the in-situ polymerization method and reaction bonding technique. It will be demonstrated that controlling the processing parameters, such as polymer content, and forming pressure make it possible to adjust the porosity and mechanical properties of the porous SiC ceramics. In Chapter 7, the application of sol-gel and in situ polymerization methods is investigated in detail to fabricate mullite bonded porous SiC ceramics via in-situ reaction bonding. The effect of the sintering temperature on the crystalline structure and morphology of the manufactured porous ceramics are

discussed. In Chapter 8 (general discussion), a full review regarding the most important factors affecting the mullite-bonded porous SiC ceramics and the effects of the implementation of sol-gel and in-situ polymerization are presented. Finally, Chapter 9 summarizes the most important conclusion of this thesis and lists some recommendations for future work in this area.

CHAPTER 1 LITERATURE REVIEW

1.1 Hot gas filtration

Since the 1990s ceramic filters, with fine pore size distribution, have been reported being used in a number of dust removal and gas treatments, especially when hot gases are present [4]. Typical industrial applications of hot gas filters include the following: biomass pyrolysis, biomass gasification [5], metal refining, incineration [6], metal recycling, coal gasification [7] radioactive waste, integrated gasification combined cycle (IGCC) [8] and pressurized fluidized bed combustion (PFBC) [5, 9]. The goals of hot gas filtration are to protect the downstream equipment, such as the gas turbine, to save energy and meet environmental regulations. The efficiency of ceramic filter test results versus particle size is compared to other particulate filters in Figure1-1 [16]. It has been reported that implementing the ceramic filters instead of the wet scrubber method results in increasing the efficiency of a coal gasification process by about 3%. Moreover, in a wide variety of processes, such as biomass gasification, in order to avoid undesirable condensation or desublimation reactions, the effluent gas must be cleaned at high temperature via ceramic filters.

Hot gas filters should operate reliably for more than 10,000 hours, with a high particulate removal efficiency, a high flow capacity and a low pressure drop. In addition, they should have high durability and reliability against mechanical and thermal stresses [4]. In ceramic filters, phase and matrix composition have been critical to the impact of the long-term thermal and chemical stability of the component during operation in porous ceramic candle filters.

Ceramic filters can be divided into high and low densities in terms of media. High density porous ceramics consist of sintered grains, preferably of silicon carbide, alumina or cordierite, with a porosity in the range of about 40% and have a stable mechanical strength (O-ring pressure strength of above 20 MPa). While in low density ceramics, the main component is typically alumosilicate fibers and the porosity can reach up to 90%. The low density ceramic filters have high porosity, they suffer from a low mechanical structure due to the loose structure of fibers and, consequently, break easily. Also, during the cleaning process of the low density ceramic filter, the intensity of the back pulse should be controlled to protect the fiber structure [10].

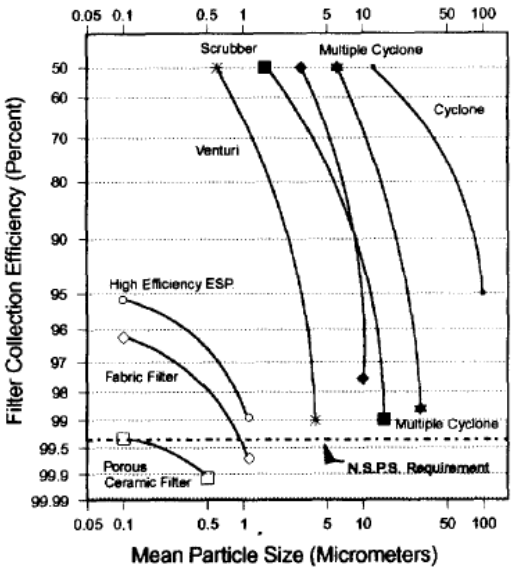

Figure 1-1Efficiency of various separation processes

Figure 1-2 presents a typical structure of low and high densities of porous ceramics. In the high density porous ceramics a thin membrane layer with smaller pores covers the support material. The efficiency of this kind of filter is very high (in the order of 99.99%).

Figure 1-2 The structure of a low density (left) and high density (right) of porous ceramics[10]

1.2 Ceramic materials and their properties

With respect to filter materials, strength, thermal shock resistance, thermal expansion, thermal conductivity, fracture toughness, hardness and chemical reactivity are important parameters in the selection of a reliable, durable, filter material. Generally, porous ceramic filter material can be divided into non-oxide and oxide materials. Among these materials, SiC, alumina and mullite are the most common [11].

1.2.1 Silicon carbide

Silicon carbide (SiC) known as carborundum offers without a doubt one of the most important structural ceramics in various industrial products, such as abrasive materials, refractories and heating elements [12]. It is produced worldwide in tonnage quantities using the Acheson process by reaction in a batch consisting principally of high-purity sand and low-sulfur coke at 2200-2500 °C in an electric arc furnace according to the following reaction:

$$SiO_2 + 3C \rightarrow SiC + 2CO \qquad 1\text{-}1$$

After crushing the crystalline product, it is washed in acid and alkali. Then the iron is removed by magnetic techniques and, finally, the product is dried. SiC can resist the attack of any acids, alkalis or molten salts up to 800 °C. Also, SiC has excellent mechanical and physical properties, such as high thermal conductivity coupled with low thermal expansion and high strength. Therefore, silicon carbide is an outstanding ceramic for severe environments. The properties of silicon carbide are shown in Table 1.1 [12].

1.2.2 Alumina

Aluminum oxide (Al_2O_3) is mostly produced on a commercial scale using the Bayer process. The Bayer process includes the physical beneficiation of bauxite, digestion, clarification, precipitation and calcination, followed by crushing, milling and sizing. The temperature of calcination of washed aluminum hydroxide is between 1100-1200 °C. The most common crystalline form of alumina is known as corundum [13, 14]. It has Al^{3+} in octahedral coordination, which occupies two-thirds of the available sites [15]. Table1.2 presents the property of alumina.

Table 1.1 Mechanical and physical properties of SiC

Property	Metric
Density (gm/cc)	3.1
Flexural strength (MPa)	550
Poisson modulus	0.14
Thermal conductivity (W/m.K)	120
Coefficient of thermal expansion (/ C)	4×10^{-6}
Specific heat (J/Kg.K)	750

Table 1.2 Mechanical and physical properties of alumina

Property	Metric
Density (gm/cc)	3.97
Flexural strength (MPa)	379
Poisson modulus	0.22
Thermal conductivity (W/m.K)	35
Coefficient of thermal expansion (/ C)	8×10^{-6}
Specific heat (J/Kg.K)	880

1.2.3 Mullite

In contrast to the Al-Si-oxides, like sillimanite ($Al_2O_3.SiO_2$, 62.92 wt% Al_2O_3), andalusite, and cyanite, mullite ($2SiO_2.3Al_2O_3$) has been recognized as the only stable crystalline compound under normal atmospheric pressure in the binary system of SiO_2-Al_2O_3 [16]. The structure of mullite crystal consists of edge-sharing AlO_6 octahedra chains parallel to the *c*-axis bounded by

aluminum and/or silicon tetrahedral. In the X-ray diffraction of mullite at 26° (2Θ-CuKα), a double peak can be observed due to the orthorhombic structure or a single pick can be detected at 26° related to the tetragonal structure, which is a metastable phase [17]. The mullite material has two stoichiometric crystalline ($2SiO_2.3Al_2O_3$ or $SiO_2.2Al_2O_3$).

The properties of mullite, such as the high temperature melting point (>1800°C), low thermal expansion ($4.5–5.6\times10^{-6}$ K^{-1} in a range of 20 °C and 1000 °C), good thermal shock resistance, low density (3.16-3.22 $g.cm^{-3}$), high creep resistance and good chemical stability, are similar to the properties of SiC. As a result, it has found widespread applications in high temperature structural materials where the environment temperature changes rapidly [18].

During the past few decades, various preparation methods, such as the reaction sintering of mechanically mixed powder [19], hydrothermal treatment of mixtures of sols [20, 21], and chemical vapor deposition [22], were applied to synthesize mullite. In general, mullite formation can be classified into three different routes as follows: sinter-mullite, fused-mullite and chemical mullite. Sinter-mullite is a conventional process, i.e., the mixing of alumina and silica powders [23]. In this method, mullitization occurs by the interdiffusion of the solid-solid or transient liquid phase reactions of aluminium, silicon and the oxygen atom [24]. Thus, the particle size of the starting powders is an important factor, which affects the mullitization temperature [19]. The drawback of this method is that the size of the particles is not enough to accomplish the complete mullitization at a relatively low sintering temperature. Nurishi et al. [25] investigated the effect of the crystallization of cristobalite by X-ray diffraction studies on the reaction sintering of Al_2O_3 and amorphous SiO_2 compacts at temperatures of 1300-1500 °C. In the system consisting of amorphous silica and α-Al_2O_3, mullitization involves two steps. Prior to mullitization in the temperature range of 1300-1500 ^oC liquid formation was observed. In this system first the transformation of quartz to cristobalite occurred. Moreover, mullitization during the reaction sintering of quartz and α-Al_2O_3 powders was studied by means of TEM. It was suggested that the reaction sequence begins with the formation of a transient glass phase on the surface of quartz grains. This viscous silica melt penetrates into α-Al_2O_3 particles and concurrently incorporates Al by the dissolution of α-Al_2O_3 [26]. Nucleation of mullite was observed mainly at the α-Al_2O_3/silica melt contact [27, 28]. Saruhan et al. [24] observed two different mullite mechanisms depending on the use of quartz or cristobalite. They prepared two different green samples consisting of SiO_2 glass plus α-Al_2O_3 and cristobalite-α-Al_2O_3. They proposed that mullite

formation is a multiple-step process: mullite nucleation, high mullitization, a temperature range of low mullitization and the area of high mullite formation rates. In the quartz-alumina system they suggested that before the beginning of mullite formation, densification occurs in the SiO_2-Al_2O_3 sample through the viscous flow sintering and in the other sample it was characterized by solid-state sintering. They reported that at high temperatures the content of mullite in the crisoblite-α-Al_2O_3 system is higher than in SiO_2-α-Al_2O_3 (Figure 1-3) [24].

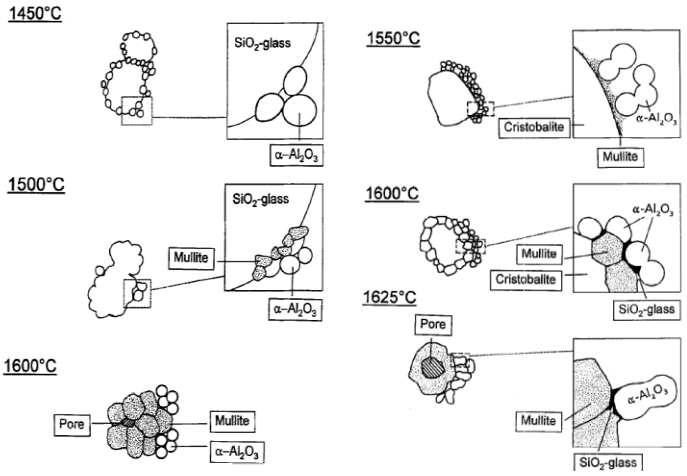

Figure 1-3 Mechanism of mullite formation using silica/ cristobalite with alumina [24]

Also, Amar P.S. Rana and his coworkers[29] investigated the mullite formation from cristobalite and quartz in mixtures with α-Al_2O_3 at 1415 °C. Similarly, they reported in quartz, a liquid first forms on the surfaces of quartz that result in the occurrence of an intermediate liquid phase on the transformation of quartz to cristobalite. The liquid acts as the precursor to the formation of mullite by reacting with α-Al_2O_3. They observed that mullite was detected earlier in the cristobalite containing mixtures under a similar sintering process to quartz [29].

In 1924, Bowen and Greig [30] reported the first phase equilibrium diagram at standard conditions and showed that mullite crystallized from a stoichiometric $2SiO_2.3$α-Al_2O_3 contained 71.8% Al_2O_3. It was reported that this is the only composition that melted incongruently at 1828 °C with no solid solution range determined (Figure 1-4) [30].

In 1962, Aramaki and Roy [31] observed mullite with a solid solution of alumina in the range of 71.8-74.3 wt% Al_2O_3. They reported that mullite melts congruently at 1850 °C. In another study, it was shown that at temperatures above 1828 °C, mullite does not form, and α-Al_2O_3 is dissolved in the SiO_2 liquid to form aluminosilicate liquids. In summary, the source of species, their chemical purity and particle size distribution are the most important factors in the rates and temperature of mullite formation [24].

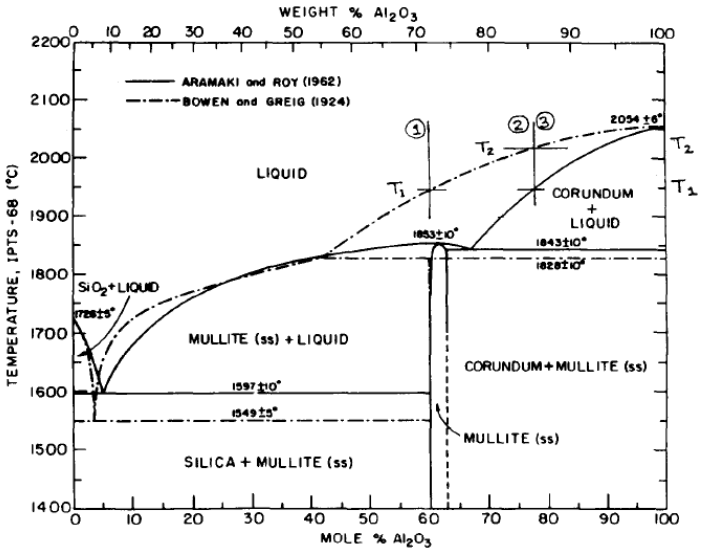

Figure 1-4 Phase diagram of alumina and silica[30]

The physical and mechanical properties of mullite are shown in Table 1.3. Regarding more recent developments in processing technologies, sol-gel, precipitation, hydrolysis, spray pyrolysis and chemical vapour deposition are other possible techniques for the synthesis of mullite [32].

1.2.3.1 Synthesis of mullite using the sol-gel method

In this method mullite is produced by adding sols or mixing sols and salts as starting materials. The main difference of this method from the conventional method is the particle size. In the sol-gel method, usually the particle size of sols is very small (nano sized), about ten to several tens nano-meters. Alumina sol and silica sol are major starting materials.

Silica sol can be obtained from fumed silica, colloidal silica as well as the hydrolysis of silicon alkoxides. Alumina sol can be obtained by various sources, such as isopropylate, aluminium chloride, aluminium sulphate, aluminium acetate, the dispersion of ultra-fine particles of γ-Al_2O_3 and the dispersion of pseudo-boehmite γ-Al(OH). Boehmite is the most common starting precursor of alumina sol [33]. Sacks et al. [34] fabricated mullite by coating silica on α-Al_2O_3 particles. First, α-alumina with an average particle size of 0.2 μm was suspended in ethanol. The suspension was mixed with the TEOS/ethanol solution to form a composite powder. The hydrolysis of TEOS was carried out by adding ammonia solution. The pH was kept in the 9-10 range to make a surface charge for electrostatic stabilization. After precipitation, the composite particles were filtrated and washed followed by the preparation of green compacts by slip casting and drying at 80 °C. Finally, the green compacts were fired in air. It was observed that powder compacts converted to mullite at temperatures ≥1400 °C.

Table 1.3 Physical and mechanical properties of mullite [35]

Density	3.2 (g/cm^3)
Young' Modlus	130 (GPa)
Fracture of Rupture	2-4(MPa.$m^{-1/2}$)
Modulus of Rupture	160(MPa)
Thermal Expansion Co- Efficient	4.5-5.6 (× 10^{-6}/°C)
Thermal conductivity	4-6 (100 -1400 °C) (W/m.K)
Maximum operating temperature	1725°C in air
Flexural strength	180(MPa)

Similarly, Bartsch et al. [36] successfully produced mullite at sintering temperatures below 1300 °C via ɣ-Al_2O_3 nano particles with silica by the sol-gel method. They proposed that the viscosity of amorphous silica-coated ɣ-Al_2O_3 is lower than amorphous silica-coated α-Al_2O_3, which

enhanced the densification process. We can conclude from the literature review that in the reaction sintering of SiO_2 and alumina compound, the sintering behaviour and properties of mullite strongly depend on the sources of SiO_2 and alumina.

1.3 Sol-gel processing and coating of particles

As stated in the previous section, sol-gel is one technique, which can be applied to the synthesis of ceramic and also to coat the ceramic substrate. Thus, a brief discussion of the fundamentals of the sol-gel process is required. The definition of the sol-gel (solution-gelation) process is "a preparation process of precursors using liquid colloidal solutions of metal salts to obtain a gel by a subsequent heat treatment." In other words, this method is a wet chemical route to synthesize materials starting from either a colloidal suspension of solid particles or clusters in a liquid (sol) and later to produce an integrated solid skeleton filled with a solvent (wet gel). A sol consists of a dispersion of solid particles (colloids), which are very small (1nm~1μm), such that gravitational force is negligible in a liquid. The dominant interactions in sol are Vander Walls, columbic and steric forces. In order to stabilize a sol, an electric double layer or steric repulsion, or their combination must be established [37]. When solvent from the gel is removed, depending on the type of drying either through ambient pressure or under supercritical conditions a xerogel or aerogel will be formed. Changing the temperature, evaporation and some chemical reactions affect the sol gel process.

In the aqueous-based process, there are two distinct reactions: hydrolysis and condensation or polymerization. Hydrolysis of the metal cations is often given by the following general mechanism:

$$M^{n+} + nH_2O \rightarrow M(OH)_n + nH^+ \qquad 1\text{-}2$$

Ceramic powder can be synthesized mostly from cation metal ions (M^{Z+}) sol. The hydrolysis of this sol is given by the following:

$$M(H_2O)_b^{Z+} \Leftrightarrow \left[M(H_2O)_{b-1}OH\right]^{(z-1)+} + H^+ \qquad 1\text{-}3$$

Moreover, adding dilute acid breaks up aggregates of hydrous metal oxide or hydroxides. Size distribution of the sol is controlled by temperature and reactant concentrations. In alkoxide

various factors, such as pH, solid content, temperature, organic and inorganic additive addition and starting materials, influence the hydrolysis and condensation rate of the sol-gel process [37]. For instance, in acidic solutions, the hydrolysis reaction is faster than condensation, which increases the development of larger and linear molecules and under basic conditions; the rate of condensation reaction is more than hydrolysis [38]. Colloidal and polymeric methods are two techniques used to obtain a homogeneous sol. In the colloidal method, a large quantity of water is added to hydrolyze the alkoxide followed by the addition of acid in order to peptize the agglomerates. Acid breaks the agglomerates by electric charge repulsion. Yoldas developed clear bohemite sol (aluminium hydroxide) with the colloidal method. He applied aluminum isopropoxide (AIP) and the molar ratio of distillated water to AIP was 100:1. Peptization was observed with nitric acid or HCL at 90 °C with 0.07 moles of acid per mole of precursor [39].

The crystal structure of boehmite is composed of double AlO_6 octahedral chains as shown in Figure 1-5 giving rise to a dimer, which is interconnected by hydrogen bonds between the hydroxyl groups. The specific density of boehmite is 3.01 g/cm^3 [15].The morphology cell of boehmite is cubic orthorhombic [40].

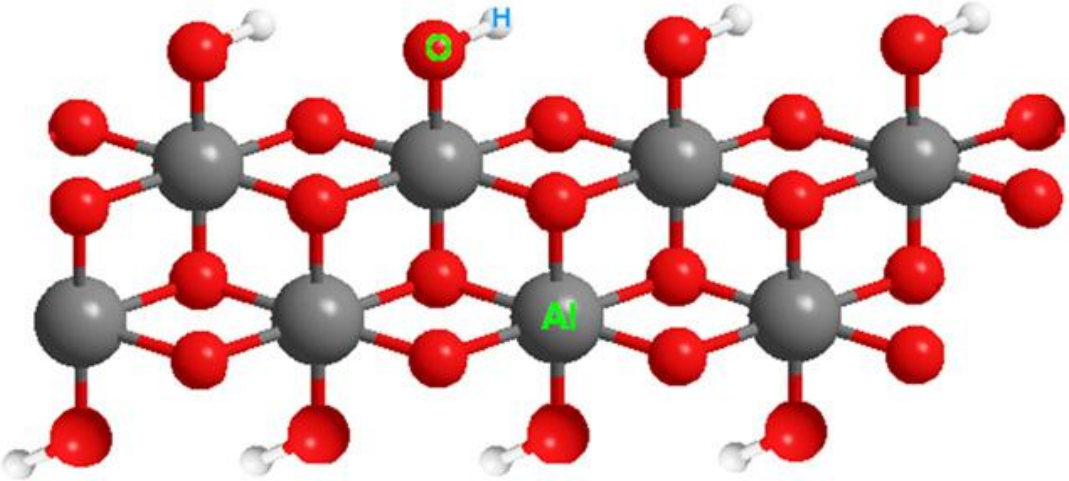

Figure 1-5 The crystal structure of boehimite[41]

Among metal alkoxides, aluminum, titanium, and zirconium alkoxides are the most common starting materials for the sol-gel process because of their relatively high reactivity, especially to water.

In addition to the synthesis of ceramic, the coating of the substrate with sol-gel processing is especially suitable for corrosive protection and a thermal barrier for various materials. Besides the sol-gel method, various technologies have been applied for coating ceramic on a substrate. These include chemical vapour deposition (CVD), physical vapor deposition (PVD), sputtering and plasma spray. The sol-gel coating has several advantages over the mentioned methods. It is simple, relatively low cost, has high homogeneity and potential for use in the coating of complex geometries.

Prior to gelation, a sol can be applied for the formation of thin, uniform films by either dip coating, spinning or spraying a film onto an appropriate substrate. Dip coating is more common than the spinning method and was first commercially used for preparing thin films in 1939 using sol–gel technology [42]. A simple approach for depositing a thin film of solution onto various shaped objects, dip coating involves five stages: immersion of a substrate into a reservoir of solution, start up, deposition, drainage and evaporation. This method does not require any special apparatus. The liquid film formation is attained by gravity draining the liquid solution and solvent evaporation. A thick film can be applied through multiple coating. During drying, by removing the water or alcohol between the colloidal units, the sol is transformed to a gel. The final step is firing at temperatures above 150 °C, which leads to the gel becoming consolidated. In the drying step, the formation of cracks may occur due to the significant stress [38]. It is well known that the thickness of the deposited liquid film (position c in Figure 1-6) strongly depends on the selected withdrawal speed and is directly proportional to the withdrawal speed as well as the soaking time.

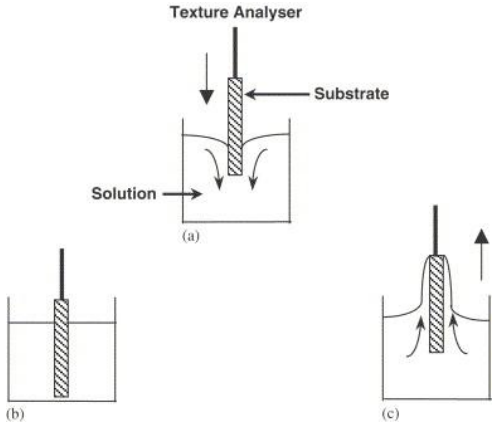

Figure 1-6 Step processing in dip coating technique: a) immersion, (b) wetting, and (c) withdrawal [38, 42]

Furthermore, the sol concentration has to be carefully selected. A high concentration sol may lead to crack formation during the drying and firing process. Landau et al. [43] estimated the thickness of the liquid film with the help of following equation:

$$h = 0.944 \frac{(\eta_L U)^{\frac{2}{3}}}{\gamma_{LV}^{\frac{1}{6}} (\rho_L g)^{\frac{1}{2}}} \qquad 1\text{-}4$$

where h is the deposited film thickness, η_L , ρ_L are the viscosity and density of the liquid, U is the substrate speed of the liquid, g, the gravitational acceleration constant and γ_{LV} is the liquid-vapor surface tension. M. Guglielmi et al. investigated the effect of withdrawal speed on the thickness of the SiO_2 and TiO_2 coating. They reported that the relation between thickness and speed is $U^{1/2}$ instead of $U^{2/3}$ [44]. Shih et al. [45] applied the sol-gel method to distribute the additives onto the surface of silicon nitride. They observed that with the sol-gel technique boehimite was distributed uniformly on the surface of silicon nitride.

Therefore, the sol-gel method can be applied as a way to create the secondary phase and improve the homogeneity of the microstructure. The creation of the secondary phase helps to meet two goals: sintering aid to lower the sintering temperature, or application of grain growth inhibitor to improve the thermal stability of the core particles. Chia-Yi Yang et al. [46] extended the work of Shih et al [45]. They investigated the coating of aluminium oxide on SiC particles. They used

coated α-SiC powder with the mean size of 0.6 μm and 3 wt% boehmite. They studied the effect of pH on coating SiC particles from 0.5 to 11 at 90 °C. Results showed that adding acid to deagglomerate alumina sol in the SiC suspension is critical for achieving a homogeneous boehmite coating on SiC at pH 4. Adding HCl causes the gel network of aluminum hydroxide to break up or dissolve. Besides, the addition of acid may result in charging the network, which helps in the dispersion of the suspension. It should be noted that the solubility of aluminum hydroxide increases with decreasing pH [47]. Also, the effect of the ceramic coating thickness on the rheological and consolidation properties of a coated ceramic suspension has been investigated. The coating thickness of the second phase is varied by changing the boehmite concentration in the suspension. TEM results revealed that increasing the concentration of boehmite from 1% to 10 wt% increases the thickness of boehmite. Increasing it by more than 10 wt%, however, results in the formation of individual boehmite particles. It was observed that the concentration of sol reaches a maximum amount and beyond this amount the coating thickness begins to saturate. The reason for this phenomena was studied by measuring the zeta potential of the coated particles [48].

As mentioned earlier, sol-gel can be used in the formation of ceramic composites. Generally, when mixing ceramic particles in a wet source, various competitive interaction forces, such as electrostatic repulsion forces, van der Waals attractive forces, and steric repulsion forces, affect the dispersion of ceramic particles in liquids [49]. Zhang et al. [50] investigated the dispersion of kaolin powders in silica sol via electro-kinetic, viscosity and rheological analysis. It was shown that silica sol is an efficient dispersant for kaolinite particles in comparison with the dispersions of powders in deionized water. Prabhakaran et al. [51] modified the surface of SiC powders with alumina sol to behave like alumina. The pH range of the suspension was reported to be 3-4.5. They suggested that their method can be applied in the preparation of concentrated SiC and SiC–Al_2O_3 composites. Similarly, the surface properties of sub micro and nano sized SiC powders were coated by a thin layer of ALOOH, which may act as a homogeneously distributed source of sintering additive in the fabrication the SiC-based composites for fusion application [52]. Yang et al. [53] applied the sol-gel method for making SiC-Al_2O_3 composites. They used alumina sol and alumina grains as a source of alumina. They compared two SiC-Al_2O_3 composites with and without alumina sol. The research results indicated that adding alumina sol decreased the sintering temperature. It was found that the sol–gel phase acts as a sintering additive through the

formation of a continuous inter-granular film around both alumina and silicon carbide particles. This active inter-granular phase acts as a fast diffusion path during the sintering of the composite. They found that the dispersion of alumina and SiC particles was substantially improved in alumina sol compared to water at the same pH. This result can be interpreted as the alumina sol formed a thin layer of SiC particles and these sols had a positive charge [53]. The inherent SiO_2 on the surface of SiC in a wet environment is hydrolyzed to form a negatively charged species, $Si(OH)^-$. Putting these particles in contact with alumina sol leads to the absorption of the positively charged sol clusters ($AlO_4Al_{12}(OH)_{24}(H_2O)_{12}^{7+}$ as in the following reaction (Figure 1-7):

$$Si(OH)^- + AlO_4Al_{12}(OH)_{24}(H_2O)_{12}^{7+} \rightarrow Si-O-Al-AlO_4Al_{11}(OH)_{23}(H_2O)_{12}^{6+} + H_2O \qquad 1\text{-}5$$

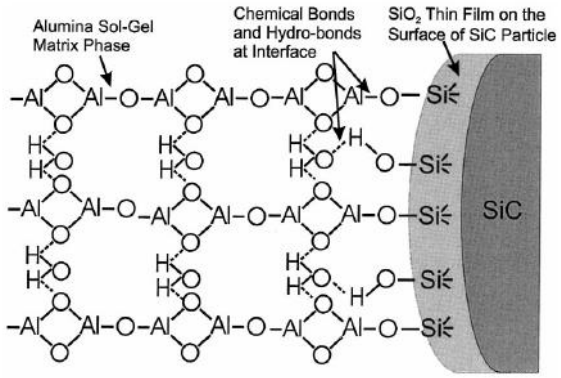

Figure 1-7 Interaction of inherent hydrated silica film on SiC surface with the alumina gel[53].

1.4 Sintering

Sintering is the heat treatment process in which a powder compact known as the green body bonds together resulting in a dense final body. It is considered as a key step in controlling the ceramics microstructure. Among various types of sintering processes, solid state and liquid phase mechanisms are the most important. In these processes particle size, particle packing of the green body, temperature, sintering atmosphere, additives, pressure during sintering, time and ramp rate used during heating are the most effective parameters. The solid state process can be divided into three stages according to the sequence in physical changes. During the initial stage of sintering, at

the contact point between each particle, the neck growth occurs and particles are bonded resulting in atomic movement at high temperature. During this stage the neck size can grow to about 20% of the particle size. The initial step occurs at a reasonably low temperature and no shrinkage happens during this stage as well as no changes in the grain size. During the intermediate stage, the mechanism of transport shifts from surface to bulk and grain boundary transport. It involves neck growth, grain growth, and considerable shrinkage and the pore phase continues. Most of the shrinkage results in this stage. At the end of this stage, pores start to close. In the final stage, which is the slow elimination of the porosity by vacancy, diffusion to the grain boundaries is observed. Individual isolated pores will be closed through the bulk diffusion mechanism. Generally, the driving force for solid-state sintering is in the reduction of total free energy, which consists of energy in volume, boundaries and surfaces of the particles. It is obtained by the diffusional transport of material from the centers of grains to the particle–particle necks [54-56].

Due to the very low sinterability of the covalent nature of SiC itself, particularly to the low surface energy and self-diffusion coefficient, it is very difficult to achieve full densification of SiC without using additives. Since sintering SiC in solid state requires very high temperatures, abnormal grain growth occurs, causing problems to control the microstructure and the related mechanical properties. The use of boron [57] and carbon [58, 59] for the solid sintering of SiC are reported. In the system of B and C additions, sintering is controlled by the grain boundary diffusion phenomenon. The role of these additives is the reduction of the grain boundary energy through the segregation of additives to the grain boundaries and the increase of surface energy.

While solid state sintering is successful, the sintering temperature of such systems is generally very high, above or around 2100 °C. Due to the extremely high temperature needed in the solid state sintering of SiC, expensive sintering equipment is required and also easily results in abnormal grain growth. Therefore, significant work is focused on developing an alternative method to the sintering of silicon carbide [55].

In contrast to the solid state sintering process, liquid phase sintering can be carried out at lower temperatures. In this method, the liquid phase is formed by the selection of the proper powder composition and temperature. The liquid phase reduces inter-particle friction and increases the diffusion rate. During sintering, the liquid phase is formed as a result of a eutectic reaction among the different sintering aids. Similar to solid-solid sintering, liquid phase sintering also involves

three steps: the primary densification mechanism changes due to rearrangement, to solution reprecipitation, to the final pore removal stage (Figure 1-8). During the rearrangement step, the open pore space between the powders in the green body is filled by the wetting liquid, which increases the packing density. In the second step, finer grains transferred into the solution due to the presence of liquid in the system. The effect of the addition of sintering aids for liquid sintering has been studied on various ceramics.

Generally, the combination of rare-earth oxides with Al_2O_3 and/or boron compounds, the most common additives, is used to generate the conditions for liquid phase sintering in the SiC system [60-64]. These sintering additives react with SiC and the surface oxide silica on the surface of grains to provide the liquid phase in order to densify the ceramics. During densification, the liquid phase provides a medium for mass transport. The dense α-SiC powder was obtained at a temperature of about 1800-2000 °C by the addition of Al_2O_3 and Y_2O_3 [62, 65, 66].

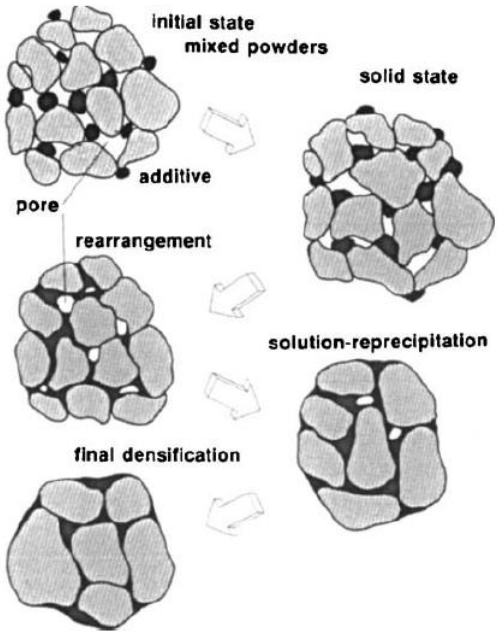

Figure 1-8 A schematic drawing of liquid phase sintering [67]

1.5 Oxidation behavior of silicon carbide

As silicon carbide is applied in an oxidized environment, numerous studies have been conducted on the oxidation of SiC materials. It has been demonstrated that the oxidation of SiC materials can be divided into two regimes: active and passive oxidation [68]. In active oxidation, which causes corrosion in SiC based materials, SiO is produced by the reaction of SiC and O_2.

$$SiC + O_2 \rightarrow SiO + CO \qquad 1\text{-}6$$

Vaporization of the oxides SiO and CO results in sample weight loss. For most applications, the oxidation of SiC should be limited within the passive oxidation regime. The following equations represent the passive oxidation weight gain due to conversion to silica:

$$SiC + 1.5\ O_2 \rightarrow SiO_2 + CO \qquad 1\text{-}7$$

The active to passive transition is determined by the oxidation conditions, such as impurity in the system, oxidation temperature, and partial pressure of oxygen[69]

In the literature there is a general agreement that the reaction product was amorphous at the beginning of the oxidation and at low temperatures, but with the increase in temperature and for longer durations it tended to crystallize.

Most researchers describe the oxidation of SiC by the diffusion-reaction model developed by Deal and Grove[70]. According to this model, the thickness of the oxide layer, x_0, can be predicated by the following equation:

$$x_0{}^2 + A^* x_0 = B^* (t + t_0) \qquad 1\text{-}8$$

Where B^*/A^* and B^* represent the linear and parabolic rate constants, respectively. t_0 is a correction constant used to adjust the time coordinate to the presence of an initial oxide layer. Typically, at temperatures above 800 °C in air, SiC reacts with air to form silica on the surface layer. Results show that the oxidation of SiC above 1200 °C follows a parabolic rate law, which can be attributed to the oxidation rate and is controlled by oxygen diffusion through the oxide product [71].

Chou [72] developed a new kinetics model, which can be applied to calculate the oxidation rate of SiC in powder form. This model assumes that the powders are spherical in shape with a constant density. The main advantage of the Chou model is that it gives a clear physical meaning

to the kinetics parameters it contains, and it can better describe the oxidation process compared to the parabolic models [72]. However, it is worth mentioning that the basic assumption of the Chou model is the same as the shrinking core model, which is very famous for describing the reaction where the solid particles are consumed [73]. The difference between the Chou and shrinking core models is based on the assumption of the flux calculation. The former applied Cartesian coordinates to obtain a concentration profile of oxygen inside the oxide layer (thin film approximation) while the latter used spherical coordinates, which are more accurate as the conversion increases [72-74].

Xinmei Hou et al. [75] proposed a model for the oxidation of micro particles with time as follows:

$$\frac{\Delta m}{m_0} = 50\left(1-\left[1-0.6483t^{0.5}\left(-\frac{11216.0}{T}\right)\right]^3\right) \qquad 1\text{-}9$$

Where T is the absolute temperature, time in seconds and m is the mass of samples. During the passive oxidation, both bulk volume and bulk mass of the original SiC body will increase because silica is less dense than silicon carbide. The equation reaction in the passive process shows that the number of produced SiC moles is the same as moles of SiO_2 produced. The thickness of SiO_2 can be estimated by assuming that the density of SiC and silica are 3.21g.cm^{-3} and 2.2 g.cm^{-3}, respectively, and all the particles are spherical and the same size (Figure 1-9).

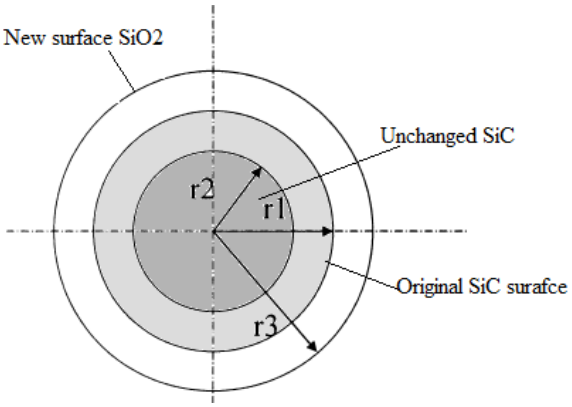

Figure 1-9 A schematic diagram of the SiC particle size change after oxidation

The following equation assumes that the mass of the sample before and after oxidation is M_S and M_S', respectively.

$\frac{M_S' - M_S}{M_S} = C_M$ where C_M is the factor of relative mass change after oxidation, and the oxidation fraction of SiC is as follows: $f = \frac{X}{M_S} = 2C_M$. The mass balance equation between SiC and SiO_2 is solved and the thickness of SiO_2 is calculated using the following equations:

$$r_3 = r_1\sqrt[3]{1+1.186f} \quad 1\text{-}10$$

$$\Delta r = r_3 - r_2 = r_1\left[\sqrt[3]{1+1.186f} - \sqrt[3]{1-f}\right] \quad 1\text{-}11$$

In the literature, it was reported that during the oxidation of SiC, the volume rate of SiO_2 changes greatly only in the initial 5 hours of holding time [76]. Shi et al. [77] probed the oxidation behavior of SiC particles in the passive state using XRD characterization. They showed that with the increase in temperature, the amorphous SiO_2 is transferred to the cristobalite phase. The XRD analysis demonstrates that for the oxidized powder a new peak at 2θ =22.15 is formed, which is attributed to the cristobilite, whereas the SiC diffraction peak (2θ = 35.65°) decreased [77].

In fact, SiC oxidation is influenced by various parameters, such as moisture in the environment, particle size, and metal impurities in the powders. Opila [78] investigated the oxidation of chemical vapor deposited (CVD) SiC in the oxygen via thermogravimetry (TGA) using high purity alumina and fused quartz reaction tubes. She observed the difference in the oxidation rate, which was attributed to the impurities in the alumina tubes. It was shown that in the oxidation environment containing water vapor, oxidation derived silica reacts with water to volatize silica by forming $Si(OH)_4$.[79] Ramberg [80] investigated the oxidation of the high purity CVD SiC thick films and single crystal SiC between 800- 1100 °C. Results revealed that the activation energy oxidation depends on the crystal orientation of the SiC face.

1.6 In situ polymerization

Like the coating of particles with ceramic, polymers can also be used for the preparation of a layer on the surface of particles at low temperatures. Typically, inorganic particles, especially nano particles, can be incorporated into polymers to produce composites to enhance the various properties, such as thermal, mechanical, rheological, and electrical [81-83].

In-situ polymerization is one of the methods, which can lead to the coating of fibers or particles with a desired thickness. In situ polymerization or polymerization compounding is the well-known technique for solving the problems encountered when making a new composite material in polymer science. The usual problems encountered in coating a substrate are poor wetting of the particle and insufficient dispersion into the substrate. As shown in Figure 1-10 in the traditional polymer composite, such as melt polymerization, the nano particles are agglomerated, but in the grafting polymerization, monomer typically penetrates inside the agglomeration and supports the existing active sites on the particles. Therefore, polymerization starts from the surface of particles. As a result of macromolecular chain growth, the nanoparticle aggregation will break and the dispersion of particles inside the polymer will be improved.

The basic principle of graft polymerization referred to as the polymerization compounding approach is strongly dependent on the existing active sites, such as the hydroxyl group on the surface of particles. Ait-Kadi et al. [84] developed this technique for coating particles with polyethylene using Ziegler Natta catalyst.

In this method the catalyst is chemically anchored on the surface of the filler and the monomer is polymerized from the surface of the samples. In fact, OH groups on the surface of the fillers play the role of the reactive sites for the bonding of the catalyst. It should be noted that during the polymerization with the Ziegler-Natta catalyst, the size of the monomer strongly controls the reactivity of polymerization. For example, ethylene is five times more reactive than propylene because of ethylene’s smaller size. In polymerization compounding, polymer chains grow from the active surface sites by a sequential monomer polymerization.

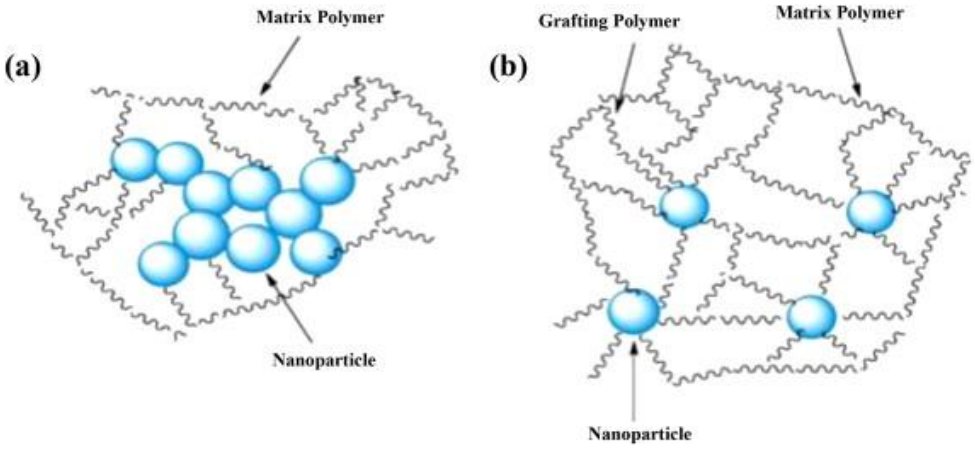

Figure 1-10 Preparation of nano-composite without: (a) without grafting polymer and (b) separation with grafting polymer.[82]

Dubois et al. [85] coated fumed silica particles with polyurethane at concentrations of about 25 wt%. Roy et al [86] performed the in-situ synthesis of high density polyethylene (H.D.P.E) on the surface of aluminium nanoparticles using the Ziegler-Natta catalyst in the solvent extraction with hexane. Similarly, Esmaili et al. [87] successfully coated a nano particle of zirconia with polyethylene. Contents of the polymer can be controlled by temperature, pressure, concentration of monomer and time. A comparison of the results of the coated-zirconia with coated-aluminium particles showed that the surface properties of fillers affect the characterization of product. Rong et al. [88] prepared a nanocomposite of polyethylene/clay via the simplest coordinated catalyst, $TiCl_4/AlR_3$. They first activated the surface of the silicate nanowhiskers by the reaction of a $TiCl_4$ catalyst with magnesium vacancies present in the clay structure. Similarly, Zhongjie Du et al. [89] produced a polyethylene-palygorskite nanocomposite using in-situ coordination polymerization. They used $TiCl_4$-$MgCl_2$-AlR_3 as a catalyst system. Ramazani et al [90] prepared polyethylene/clay nanocomposites by in situ Ziegler-Natta catalyst polymerization. In their work, they first activated the substrate with a co-catalyst. They found that the optimum temperature and pressure for polymerization were 60 °C and 7 bars. Wei L. et al. [91] successfully prepared polyethylene on clay-silica nanocomposites to improve the mechanical properties of nanocomposites. In their work, they fixed a zirconocene catalyst [bis(cyclopentadienyl)zirconium dichloride/methylaluminoxane] on the montmorillonite/silica hybrid before ethylene

polymerization. The catalyst was supported on the particles by mixing methylaluminoxane (MAO) solution under an inert atmosphere followed by adding Cp2ZrCl2 solution to the system. Yang F. [92] prepared polyethylene/montmorillonite (MMT) nanocomposites via graft polymerization using a MMT/$MgCl_2$/$TiCl_4$ catalyst and co-catalyst of $Al(Et)_3$. The molar ratio of (Al/Ti) was fixed to be 20 at a polymerization reaction of 50 °C. Alexandre et al. synthesized polyethylene-layered silicate nanocomposites via in situ polymerization of ethylene by attaching the methylaluminoxane to the filler [93]. Takamura M. et al. [94] grafted poly(L-1actide)(PLLA) from the surface of a silica nanoparticle via ring-opening polymerization. Before the polymerization, they initially treated the surface of the silica with amino groups to fix an amidine base catalyst. They showed that the dispersibility of silica was significantly enhanced after the graft polymerization and the coated particles were stable in polar solvents.

All of the previously mentioned research works have proven that graft polymerization is an effective technique to enhance the dispersion of nano particles in the polymer matrix.

1.7 Fabrication of porous SiC ceramics

As mentioned in the Introduction, various methods for the manufacture of porous SiC ceramics have been proposed and can be grouped into the five following categories [95]: (i) partial sintering, (ii) replica, (iii) sacrificial template, (iv) direct foaming, and (v) bonding techniques, as schematically presented in Figure 1-11.

Among the above mentioned methods, partial sintering is the simplest process, which includes pressing the powder compact and heating the compact powders. During the partial sintering powders were bonded as a result of the surface diffusion, evaporation–condensation, or re-crystallization process [96-98]. In this method, pore size, porosity, and mechanical properties are dependent on the size of the starting powders and the degree of partial sintering [95, 99, 100]. Typically, the final pore sizes are between two to five times smaller than the starting particle sizes [95]. In this method, the sintering temperature is reported between 1500 °C to 2300 °C [97, 100-102].

In the replica method, porous ceramics are fabricated from either the impregnation of polymer foams with a SiC suspension or precursor solution, chemical vapor deposition (CVD) of SiC on polymeric foams, or the infiltration of natural wood-derived or artificial carbon foams with Si

sources [103-105]. The products have a very high porosity (up to 95 %) with a large pore size (more than 10 um to 5 mm), which is useful to form open-cell SiC ceramics[106].

In the sacrificial template technique, porous SiC ceramics are fabricated by mixing of sacrificial template, which acts as a pore former, with SiC powders or SiC precursors. During the heating process the template is removed, creating pores [107]. The porosity and pore size depend on the amount of pore former content and the structure of the pore former. The porosity can reach up to 95% but the final products have the wide pore size distribution [95].

The carbothermal reduction technique involves the carbothermal reduction of silica by carbon. Kim et al. [108] developed microcellular silicon carbide ceramics by carbothermal reduction. They used polysiloxane, phenol resin, polymer beads, alumina and Y_2O_3 as sintering additives. They heated the compact powders under an inert atmosphere at 1650 °C for the carbothermal reduction of SiOC ceramics to produce SiC. Pyrolysis of polysiloxane and phenol resin generates SiOC and carbon, respectively. Eom et al. [109] fabricated porous silicon carbide ceramics by the carbothermal reduction of polysiloxane at sintering temperatures between 1800 °C to 1900 °C. They showed that pore size distribution is a tri-model in the range of 0.003 to 30 µm with porosity in the range of 40 % with high mechanical strength, 100 MPa. Youngseok [98] and his co-workers fabricated porous SiC ceramics at a sintering temperature of 2100 °C via the recrystallization process. They fabricated porous SiC ceramics with a pore size of 6-7 µm, porosity of 47% and strength of 45 MPa.

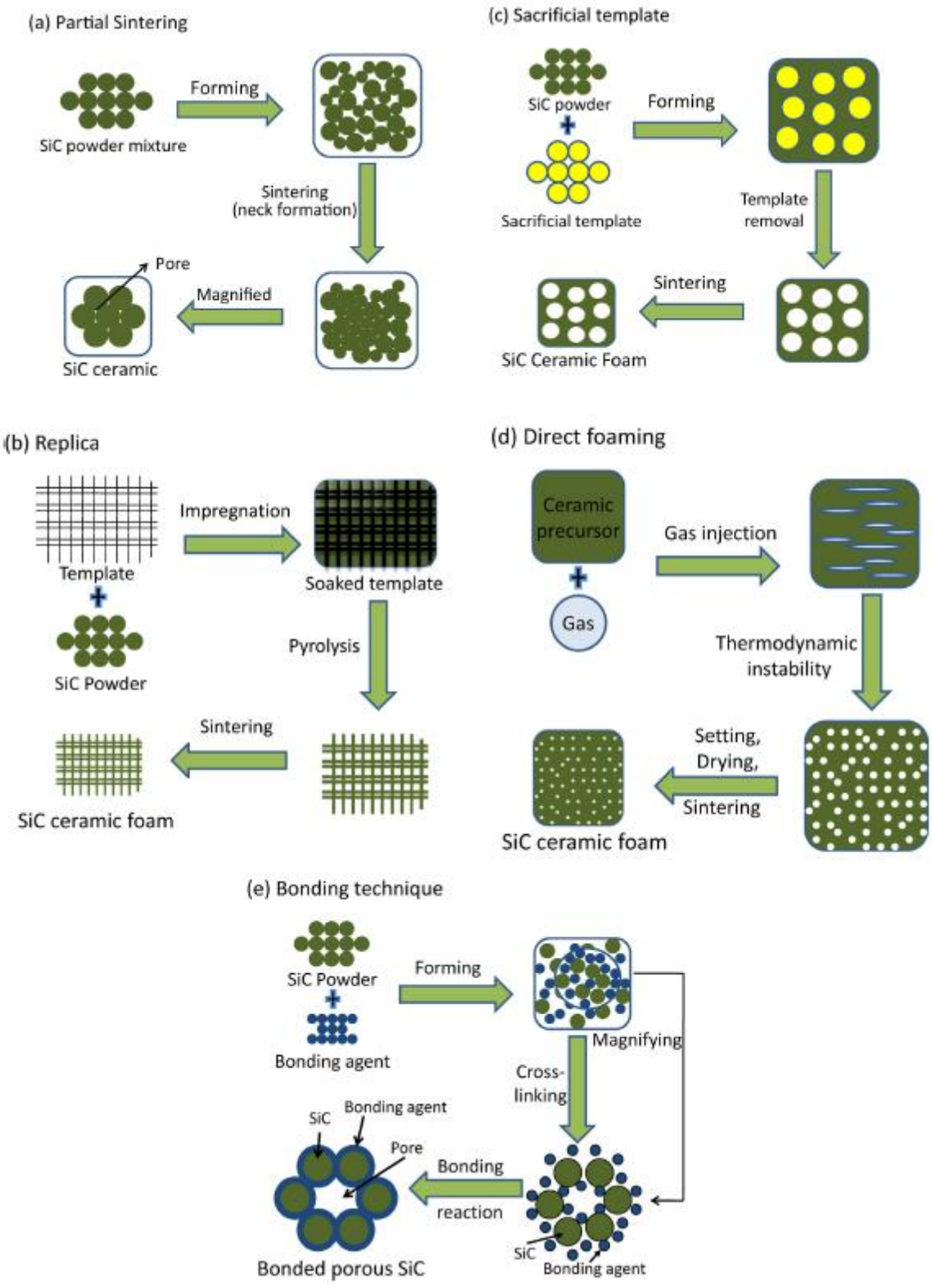

Figure 1-11Schematic of different processing routs of porous SiC ceramics

In the above mentioned methods to fabricate porous ceramic grains, usually a higher sintering temperature is needed to bond SiC particles together due to the strong covalent nature between the Si-C bonds and the sintering process is carried out under inert gas. However, changing the sintering atmosphere may lead to an increase in mechanical stability at lower temperatures. In 2002, She et al. [3] developed a low temperature fabrication technique of porous SiC-based ceramics with good resistance to oxidation. The most important feature of the process was in the sintering process where they applied air instead of an inert atmosphere. In the other work, they used alumina as the sintering additives. As a result of the increase in temperature, a layer of silica was formed on the outer surface of the SiC grains and with an increase in temperature silica reacted with alumina to form mullite, which subsequently bonded silicon carbide together. This method, which is well-known as the reaction bonding technique, has been applied by numerous researchers to fabricate porous ceramics. For controlling the porosity and pore size distribution organic or inorganic materials, such as graphite, can be used. During heat-treatment, these particulates burn out and produce stable voids [3]. Dey [110] and his coworkers fabricated porous SiC ceramics by the infiltration technique. They first infiltrated the SiC powder compact with tetraethylorthosilicate (TEOS) sol. During sintering, SIC particles were bonded by silica. They reported flexural strength of 48 MPa with a porosity of 28%. The sintering temperature was 1300 °C under air. Ding S. [111] and his coworkers studied the effect of Y_2O_3 addition on the phase composition and mechanical and physical properties of the products, which was produced by the reaction-bonded technique. They concluded that the addition of 1.5 wt% Y_2O_3 causes the formation of mullite at lower temperatures and increases the mechanical strength of the product. Liu S. et al. [112] extended their work by investigating the CeO_2 addition to the cordierite–bonded porous SiC ceramics. They reported that the addition of 2 wt % CeO2 promotes cordierite formation and crystallization. Flexural strength of 26 MPa with a porosity of 44 % was reported when 10 μm SiC and graphite as the pore former were used at the temperature of 1350 °C. Kumar et al. fabricated mullite bonded SiC ceramics using aluminum hydroxide ($Al(OH)_3$) powders as the source of alumina. They studied the effect of aluminum hydroxide from 14 to 47 wt% at the sintering temperatures of 1450 °C to 1550 °C for 2 hours. It was demonstrated that flexural strength was enhanced with the increase in aluminum hydroxide content [113]. Jin et al. prepared SiC/mullite porous ceramics by heating the mixture of calcined kaolin, aluminum hydroxide, silicon carbide, and graphite under air [114]. In the another work, the effect of

different alkaline earth metal oxidation additions, such as MGO, CaO and SrO, on the physical and mechanical properties of mullite-bonded porous SiC ceramics was investigated [115].

Dey [116] fabricated SiO_2- bonded porous SiC ceramics with a porosity in the range of 36 to 56 % and a pore size from 3 to 15 µm and they evaluated the air permeation. More recently they investigated the flirtation efficiency of mullite-bonded porous SiC ceramics at room temperature with different ranges of porosity and it was demonstrated that the perforce of the filtration was more than 99%.

1.8 Problem identification

To manufacture self-bonded SiC ceramics a very high sintering temperature (2100 °C) is required due to the covalent nature and low self diffusion coefficient of SiC. In order to decrease the sintering temperature, some sintering additives are added to the starting powder. For example, non-oxide-based clay-bonded SiC is used in various plants throughout the world [117]. Schumacher and Pall manufactured SiC particle candle filters with a different binder and it has been tested worldwide for various particulate removal processes. The filter matrix of Schumacher Dia Schumalith consists of silicon carbide grains that are held together by a clay binder containing alkali and aluminosilicates. Research has demonstrated that the behavior of the candle filters is controlled by the ceramic binder. Based on engineering reports, a major disadvantage of SiC is its oxidation to silica at high temperature, particularly in humid environments. During the process, the micro-structure of these types of filters has been changed. Silicon carbide particles have been oxidized due to the diffusion of the process gas through the binder coating. Initially, the coalescence and crystallization of the binder increased the strength of the clay bonded filter matrix and the thickness of the crystalline silica-enriched layer increased as well, encapsulating the silicon carbide grains. As shown in Figure 1-12, two distinguished parts were formed. The outer surface layer was formed with silica while an underlying crystalline aluminosilicate was observed. With extended service operation, thermal fatigue at the junction of the crystallized silica-enriched encapsulating layer occurred and led to a reduction in the bulk strength of the filter matrix exposing the underlying silicon particles to further oxidation (Figure 1-12) [118]. In the presence of Na_2O, K_2O and Fe_2O_3, the softening temperature of siliceous glassy phases dropped significantly low and, therefore, clay-bonded SiC filters could be irreversibly damaged

during long-term operation at higher temperatures. Moreover, during the pulse cycle (for cleaning a filter) the crystallized binder and oxide-enriched is removed. The edge abrasion of particles has been found to cause a degradation of material strength in service.

In summary, although SiC filters are one of the most attractive candidates in hot gas cleaning, due to harsh conditions they are faced with problems, such as the oxidation of the silicon carbide grains, volume expansion of the component, loss of permeability of flow gas due to the formation of the amorphous glassy phase and cracks because of thermal shock during the long-term pulse cycling of the elements [119, 120].

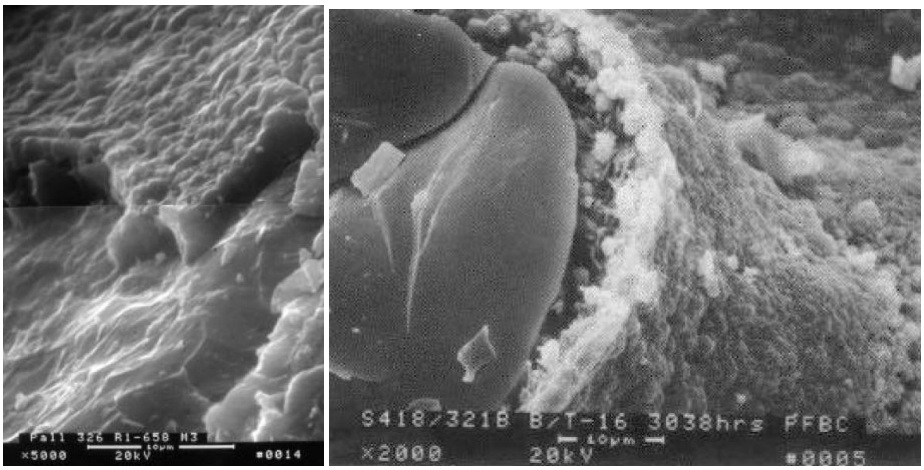

Figure 1-12 Crystallization of the Schumacher Dia Schumalith F40 filter matrix during operation (right) and the silica-enriched layer on the surface of the silicon carbide grains within the Pall filter matrix (left)[118]

As in the reaction bonding technique, SiC particles are already partially oxidized during the manufacturing process. The porous ceramics are resistant to oxidation and thus suitable to be applied in oxidizing atmospheres. In the case of mullite bonded SiC particles, since the thermal expansion number of SiC and mullite is similar they are expected to show more thermal shock resistances as well.

Ding et al. [121] fabricated porous SiC with different fractions and particle sizes of graphite to produce ceramic porous on the basis of the reaction bonding method. They reported that graphite content had a significant effect on the open porosity of porous SiC ceramics and open porosity

increased with the graphite content, however, mercury porosimetry showed that the pore size distribution of SiC ceramic by this method was bi-model, where one of them contributed to the stacking of SiC grains while the other was due to graphite burning out (Figure 1-13). Similarly, Liu S. et al. [112] exhibited a similar bi-model pore size distribution in the fabricated porous ceramics even when they started with a similar size pore former and starting particle.

Theses researchers contributed to this effect because of the wide particle size distribution of graphite particles, which were partly dispersed into the voids among SiC grains. The uniformity of pore structure in porous ceramic depends significantly on how uniformly the pore former is dispersed in the slurry as well as the size and particle size distribution of the pore former. Porosity and pore size distribution strongly depend on the shape, size, and amount of pore former.

Another shortcoming of this method is the weak dispersion of sintering additives in the starting materials and strong agglomeration of nano particles due to the nature of nano materials. For example, SEM analysis showed (Figure 1-13, right) that in some parts of the ceramic porous, Al_2O_3 agglomerates together [121]. This agglomeration significantly decreases the constitutive properties of the product. Due to the in-homogeneity of the starting material during the preparation of the green body, mullite formation cannot bond all of the SiC particles and, consequently, some parts of the final product do not possess enough mechanical strength [81].

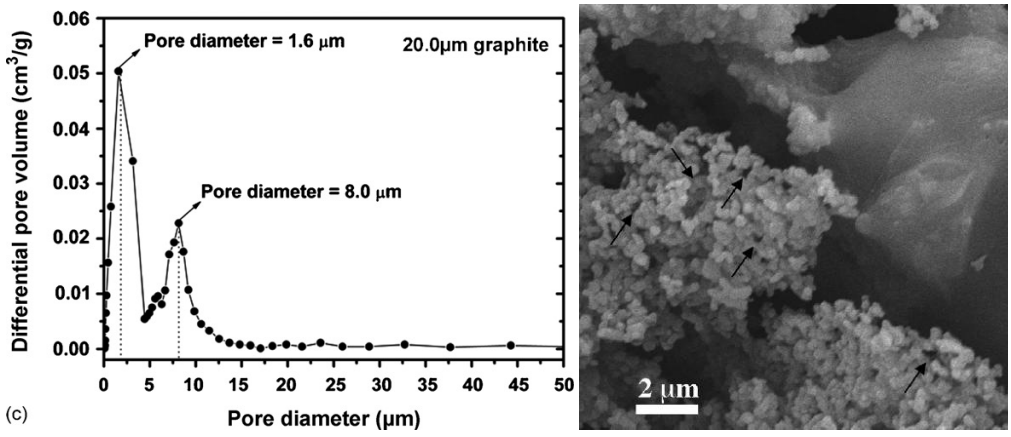

Figure 1-13 Pore size distribution of porous SiC ceramic (addition of the20μm graphite) (left) and agglomeration of α-Al_2O_3 particles in porous SiC ceramics [81].

Therefore, developing a new method to obtain a porous ceramic, which can better control pore size distribution and increase the mechanical properties and porosity simultaneously would be an interesting subject.

1.9 Objectives

The literature review showed quite a few studies to increase the dispersion of sintering additives onto the starting materials. In addition, there is the need to develop porous SiC ceramics with a narrow pore size distribution. Furthermore, based on the literature study the optimum conditions of alumina nano particles as the sintering additive on the starting powders are not systematically studied.

The broad goal of this research is to develop a method to control the microstructure of porous silicon carbide to improve the mechanical and physical properties. Accordingly, the main objective of this research is as follows:

'Fabrication of mullite-bonded porous silicon carbide ceramics using combination sol-gel and polymerization compounding methods'

Inherent to the main goal are more specific objectives, which are as follows:

- To experimentally and theoretically study the oxidation of SiC powders and porous SiC with different particle sizes
- To fabricate porous SiC ceramics using the Sol-gel method
- To fabricate porous SiC ceramics prepared by in situ polymerization and a reaction bonding technique
- To develop mullite bonded porous SiC ceramics using sol-gel and polymerization compounding methods.

CHAPTER 2 METHODOLOGY

2.1 Materials

For the kinetic studies of SiC particles and the effect of particle size on the oxidation rate of SiC, two different particle sizes were selected (1.5 μm and 0.12 μm). For the fabrication porous SiC samples via various processing techniques, the larger particle size of SiC was chosen (11.1 μm). In this work, the ceramic materials (SiC and Al_2O_3) were supplied by LABMAT, Inc, Canada. Some of their physical properties are listed in Table 2.1.

Table 2.1 Powder compositions and characterization of materials used in this study

Material	Particle size μm	Surface area m^2/gr	Crystalline phase	Density g/cm^3
SiC	1.5	15.27	β	3.2
SiC	0.12	34.73	β	3.2
SiC	11.1	0.87	α	3.2
Al_2O_3	0.27	8.5	α	3.95

2.2 Synthesis of alumina sol

Alumina sol was prepared by the hydrolysis of Aluminum isopropoxide (AIP, Aldrich, 98%), which was used as the alkoxide source of alumina according to the method developed by Yoldas [122]. In a typical experiment, 350 grams of distilled water were heated up to 85 °C in a four neck reactor equipped with a heater and magnetic stirrer, followed by adding 40 grams of AIP in the form of powder to the medium. The molar ratio of water to AIP was fixed at 100:1. After vigorously stirring for about 1 hr, the resultant white precipitate was peptized by adding a small amount (9 cc) of 10% HCL (Merck, 37%) in order to set the pH of the solution to 3.5–4. This mixture was kept under the reflux condition and temperature of (85-90 °C) for another 24 hrs to form a clear solution. After cooling it down to ambient temperature, the resultant sol was kept for

the fabrication of porous ceramics and characterization. A schematic of the set up is illustrated in Figure 2-1.

Figure 2-1 Processing set-up for the synthesis of alumina sol

2.3 In-situ polymerization processing

Ethylene polymerization was performed in the solvent by means of a Ziegler–Natta catalyst. Titanium tetrachloride ($TiCl_4$, Fluka) was used as the catalyst and triethylaluminum 1M in hexane ($AlEt_3$, Sigma-Aldrich) was used as the co-catalyst. As the catalyst and co-catalyst are highly sensitive to moisture and oxygen, they were stored and handled in a glove box under argon in an inert atmosphere. Ethylene gas with a purity of 99.5% was obtained from Canadian liquid air and used as a monomer for the polymerization reaction. Hexane was supplied by Sigma

and used as the reaction solvent. In order to adsorb the water, it was dried and stored for at least 24 hours on a molecular sieve.

The polymerization experiments were carried out in slurry phases using a two liter pressurized BUCHI reactor. The heating of the reaction system was provided through an external fluid bath circulator and mixing was performed by a magnetic drive impeller, which was located on top of the reactor. The pressure in the system was monitored by a pressure gauge, which was located on top of the reactor (Figure 2-2).

Figure 2-2 A BUCHI reactor system for polymerization

In a typical reaction, a mixture of powders, which was previously dried in an oven at temperature of 150 °C, was added to 1.5 liter of dried hexane. The powders were dispersed in hexane at a temperature of 65 °C for about 1 hour by mechanical agitation (400 rpm) and the system was purged with N_2, which was further dried by passage through a molecular column sieve to eliminate oxygen in the medium. At this step, the desired amount of catalyst, $TiCl_4$, was added to the system using a syringe through a septum feeding port in the reactor. In order to be sure that the catalyst had sufficient time to adhere onto the powders, the system was mixed for another 15

min. Subsequently, the pre-determined amount of co-catalyst, $AlEt_3$, was also injected through the same position and the mixture was agitated for another five minutes to allow the system to form a catalyst-co-catalyst complex. The reaction started by shifting nitrogen to the ethylene monomer. The relative pressure of the system was kept to 48 kPa. After the desired reaction time, the reaction was terminated by an injection of ethanol in the medium to hydrolyze the catalyst complex.

2.3.1 Calculation of catalyst and co-catalyst

The amount of catalyst was calculated based on the ideal assumption where all the surface of the powders can be covered by the catalyst. Therefore, it depends on the total surface area of powders in the system that can be coated by $TiCl_4$. In all of the experiments, the molar ratio of co-catalyst to catalyst was kept constant at two.

It was thought that the $TiCl_4$ molecule had a spherical shape with a radius equal to the size of the Ti-Cl bond. When the catalyst was adhering onto the surface of the substrate, it was assumed that each molecule of the catalyst occupied the surface of the substrate according to the surface of a disk with the ratios of the Ti-Cl length (1.18 A°) and surface area of 1.493×10^{-19}. For example, in a case where 25g of powders with the specific surface area of 21.3 m^2/g were used for polymerization, 3.56×10^{21} molecules of catalyst are needed to cover all surfaces of the powders ($25\times 21.3/1.493\times10^{-19}$). This amount of molecule is equal to the 5.9×10^{-3} mole or 1.12 gr of catalyst (TiCl4 molar mass =189.9 g and ρ= 1.72 g/cm^3). Consequently, for this system, 650 micro liters of catalyst and 11.85 cc of co-catalyst must be used.

2.4 Fabrication of porous SiC ceramics

In this part, different approaches were used to assess the effect of various parameters, such as the effect of alumina sources and contents, sintering temperature, forming pressure and pore-former content on the properties of porous SiC ceramics.

2.4.1 Mixing of powders in calined form

In the first approach a conventional method was applied to fabricate porous ceramic. Initially, a given mass of silicon carbide and sub-micron alumina powders at certain weight ratios were placed in a plastic vial. Subsequently, 2.5 wt. % of polyvinyl butyral (PVB) binder, which was dissolved in ethanol, was added to the powders followed by mixing the powders in a high-energy ball mill (Spex 8000 M) for 30 minutes. The volume percentage of the amount of polyvinyl butyral was equal to 7 Vol.%. Two plastic balls were used during the mixing. The resulting slurries were transferred into a baker, dried under stirring using a magnetic stirrer and, finally, crushed by a mortar and pestle. Then, they were passed through an 80-mesh size screen.

2.4.2 Mixing of powders in alumina sol

In the samples fabricated by the sol-gel technique, SiC particles were added to different amounts of alumina sol and calcined alumina powders and the slurry was stirred-dried at room temperature. The amount of alumina sol was determined to yield the desired alumina content in the final product with respect to the SiC powders. For example, when 40 g of AIP were dissolved in 350 cc of water, according to the mole balance it results in 10 g of Al_2O_3 in the final product. The resulting powders were then further dried in an oven at 100 °C, before being crushed and passed through an 80-mesh sieve. The weight ratio of SiC to alumina was calculated from the quantity of sol that was finally converted to calcinated α-Al_2O_3.

2.4.3 Preparing coated powders with polyethylene

The calcined alumina powders and SiC particles with a weight ratio of 35 wt% were first dried at 150 °C and then coated by the desired amount of polymer according to the procedure explained in section 2.3. Then, the coated powders were dried at 80 °C to evaporate the hexane under vacuum conditions. The resultant powders were screened through an 80-mesh sieve.

2.4.4 Preparing the samples by a combination of sol-gel and in-situ polymerization

In this step, first the SiC and alumina powders were placed in a baker and mixed in the alumina sol until the solvent evaporated. In other words, a fraction of alumina was formed from alumina sol to yield the total mass ratio of 35 wt% alumina. After being crushed and passed through a screen, they were placed in a vacuum oven to be further dried. The resultant sample was coated by polyethylene similar to the procedure as described above followed by drying and passing through a screen for a second time.

2.4.5 Preparation of green body and sintering processing

At this point, the powders were uniaxially pressed into rectangular bars of 4.5 mm × 10.0 mm × 50.0 mm under a typical 50 MPa pressure in a stainless steel die. At least three samples were prepared, carefully handled, and placed in a box furnace (CM furnace 1700 °C). At the beginning of the heating, the temperature was increased with the slow heating rate of 2 °C/min to 900 °C to avoid failure of the samples, especially during the burning out of the pore-former. In the second step of heating, the samples were heated at a heating rate of 5 °C/min and ramped up to the desired sintering temperature, at which they were sintered for 3 hours in air. It should be noted that before and after the firing step the weight of the sampled was measured.

2.5 Characterization techniques

During the fabrication of porous SiC ceramics, the oxidation of SiC particles, the synthesis of alumina sol and in-situ polymerization of polyethylene on the surface of particles, and different characterization techniques have been used to analyze the synthesis of the materials and measure the physical and mechanical properties of the specimens.

2.5.1 Thermal analysis TGA and DSC

During the oxidation kinetic studies of SiC particles, for thermal analysis of alumina sol and polyethylene and to determine the quantity of polymer or degradable components on the particles, thermogravimetric analysis (TGA) was applied using a TGA Q 5000 apparatus (TA Instruments, USA) or a Mettler Toledo thermogravimetric analyzer. The flow rate of gas was 20 ml/min and the typical heating rate was 10 °C/min. The thermal properties of the synthesized polymer were further investigated using differential scanning calorimetry (DSC Q 2000, TA Instruments, USA) to measure the melting temperature and crystallization behavior of the polymer, which grafted on the particles. The samples were heated up to 200 °C with heating and cooling rates of 10 °C/min. The crystallinity of polyethylene was calculated as follows:

$$\Delta X(\%) = \frac{\Delta H_m}{\Delta H_0(1-\emptyset)} \times 100 \qquad 2\text{-}1$$

Where $\emptyset$ is the weight fraction of ceramic powders, ΔH_m is the enthalpy of melting and ΔH_0 represents the heat of fusion of 100% crystalline high density of polyetheylene.

2.5.2 Surface characterization: FTIR and XPS analysis

BIO-RAD Excalibur series FT-IR 3000 was used for fourier transform infrared (FTIR) spectroscopy measurements to detect the functional groups on the surface of dried and calcined alumina sol. In this technique the intensity of a beam from FTIR is determined before and after the interaction with the specimen according to the light frequency. FTIR tests were carried out using the pellet technique in a wide range of frequencies, 400-4000 cm^{-1}. Sixty-four scans at a resolution of 4 cm^{-1} were taken per spectrum. The specimens for the FT-IR analysis were prepared by mixing the samples with dried KBr at a ratio of 1:100 followed by compressing them to form a transparent disc.

Furthermore, the surface analysis of the coated samples by polymer and alumina sol as well as the original samples was analyzed by X-ray photoelectron spectroscopy (XPS) in a VG Scientific ESCALAB Mk II with Mg Kα radiation (1253.6 eV) operated at 300 W without a monochromator. During the analysis, the pressure of the chamber was about 8×10^{-9} Pa. In this

technique, the substrate is bombarded by monoenergetic soft X rays to leave electrons of elements, which will be recognized by the kinetic energies of these photoelectrons.

2.5.3 Crystalline examination: XRD

X-ray diffraction (XRD) measurements were performed using a Philips X'Pert diffractometer (The Netherlands) with Cu-Kα radiation in which a collimated beam of X rays with a wavelength of 1.542 A° was radiated on the samples followed by diffraction in the crystalline phase. The generator was set up at a voltage of 50kV and a current of 40 mA. The scanning rate was 1.2 °/min at an interval of 0.02°. This technique was performed to investigate the crystalline structure of dried alumina sol at different calcined temperatures, the crystalline changes of SiC during oxidation as well as the crystalline structure of porous SiC ceramics prepared by different approaches.

2.5.4 Morphological characterization: SEM and TEM

The morphology of the porous ceramics, starting materials and coated particles was observed by scanning electron microscopy (SEM, Model JSM-7600 TFE, JEOL, Japan) operated at 2 kV with an LEI imaging mode and a working distance of 8.5 mm. During the analysis with SEM beams interact with the specimen and form various signals, such as secondary electron and ternal currents, which are highly localized to the place directly under the beam to produce an image. It should be mentioned that before the characterization of the porous samples, they were coated with a very thin layer of gold.

Transmission electron micrographs (TEM, JEOL JEM-2100F) were utilized at a 200 kV acceleration voltage to bombard the synthesized alumina sol and coated particles with a polymer under vacuum for morphology studies. During the analysis, the beam was passed through the specimens. Before characterization of the coated particles by polyethylene, they were ultrasonically dispersed in water or ethanol for a few seconds and dried at room temperature.

2.5.5 Physical properties: BET, PSD, and pycnometer

The surface area of ceramic powders before and after modification was measured by gas adsorption using a Quantachrome Autosorb-1 apparatus. Before analysis, samples were degassed at 150 °C for 3 hours to drive off any adsorbed water on the sample. In summary, the total volume of nitrogen gas adsorbed on the surface of particles was measured at different pressures. By plotting of $P/[V(P_0-P)]$ versus P/P_0, the monolayer capacity, V_m, and the constant c were determined where P is the experimental pressure, P0 is the saturation pressure at the temperature of adsorption and V_m is the monolayer capacity. By knowing these parameters the specific surface area of the powders can be calculated as explained by Brunauer, Emmett and Teller, BET [123].

The particle size distribution of ceramic samples was measured by a Horiba LA-950 laser diffraction particle size analyzer. The calculation was based on the volume calculation. The true densities of porous samples were measured by the gas volume displacement method using a gas pycnometer (Accupyc II 1330 helium pycnometer). In this method the predetermined weight of the samples was placed in a vessel filled with helium. Knowing the volume of the empty calibrated vessel, mass of the samples and volume of the fluid filling the void space in the vessel gives the true density of the samples.

Mercury porosimetry (Micromeritics Autopore IV) was utilized to show the pore size distribution of porous samples. Open porosity was ascertained from the total mercury intrusion volume and the skeletal density of the sample. During the operation the pressure and temperature of the ambient were monitored to determine the density of mercury and measure the pore size distribution. This analysis was performed by increasing the imposed pressure in small increments and measuring the volume of mercury entering the sample during each pressure increment. The imposed pressure is generally related to the pore size via the Washburn equation [124].

2.5.6 Mechanical Property

The flexural strength of porous samples was determined by a three-point bending test with a support distance of 30 mm at a constant crosshead velocity of 0.5 mm/min using an Instron Universal Testing machine (Model 1123, Instron, Canton, MA, USA) with a 500 N load cell. The

deflection measurement was taken using LVDT with a resolution of 0.05% and Young's modulus was calculated via standard software (Instron Bluehill-2, UK). Typically beams were machined and polished to 3.0 (±0.1 mm) × 4.0 (±0.1 mm) × 36.0 mm and at least three specimens were tested to obtain the average strength. The strength of the beam in a three point flexure is calculated as follows:

$$S=3PL/(2bd^2) \quad 2\text{-}2$$

Where P is the break force, L is the outer span, b is the width of the bar, and d is the sample thickness.

CHAPTER 3 ORGANIZATION OF THE ARTICLES

The following four chapters contain the articles representing the results of this study.

The first paper of this work is presented in Chapter 4, "*Diffusional effects for the oxidation of SiC powders in thermo-gravimetric analysis experiment*". This work investigates the oxidation behavior of two different particle sizes of SiC powders in the temperature range of 910 °C to 1010 °C by means of thermogravimetric analysis (TGA). TGA results revealed that the oxidation of SiC particles began at lower temperatures for the samples, which had a smaller particle size. The effect of the height of the samples into the crucible on the oxidation of particles was also investigated. It was found that for the same particles, the oxidation rate depends on the initial mass of sample placed in the crucible. Furthermore, in the studied system, the analysis of the results showed that both inter-particle and intra-particle diffusion as well as surface kinetics control the overall oxidation rate. As the previous models cannot describe the oxidation rate of SiC particles, especially in the pack state, it was necessary to develop a new one. A new kinetic model was proposed which can be applied for describing non-catalytic gas-solid reactions, which include all diffusion steps (bulk, inter- and intra-diffusion) and the chemical reaction. The developed model was found to describe the oxidation behaviors of SiC powders well, especially for the compact case. This article has been published in the *Journal of Materials Science, 2013, Vol. 48 (12), pp 4396-4407*.

The second article presented in Chapter 5 is entitled *"Fabrication of Mullite-bonded Porous SiC Ceramics via a Sol-gel Assisted In-situ Reaction Bonding"*. In this work the influence of different sources of alumina (alumina in powder and sol form) and the contents of the physical and mechanical properties of porous SiC ceramics produced via in-situ reaction bonding have been investigated. The resulting porous ceramics are characterized using XRD, SEM, and mercury porosimetry and three point bending. It was found that the implementation of the sol–gel technique improved the porosity and flexural strength of the samples compared to the traditional method. This article has been published in the *Journal of the European Ceramic Society* (2014, *Vol. 34(2), pp 237-247).*

The third article presented in chapter 7 is entitled *"A Novel Fabrication Route for Porous SiC Ceramics by Combining In-situ Polymerization and Reaction Bonding Techniques"*. In this article SiC and alumina particles were coated by polyethylene via in situ polymerization using a

Ziegler-Natta catalyst. The aim of this section is to investigate the application of in-situ polymerization, known as the graft polymerization technique, as a means of improving the dispersion of the polymer (pore former) and sintering additive to fabricate porous SiC ceramics. The effects of the polymer content on the mechanical and physical properties of fabricated porous SiC have been studied and discussed. The pore size distribution, porosity and flexural strength of the products, which were fabricated with the assistance of in situ polymerization techniques, have been compared to the traditional methods. This article has been submitted to the *Journal of Applied Polymer Science* in 2013 and received minor correction.

The fourth article presented in chapter 8 is entitled *"Manufacturing Process for In situ Reaction-bonded Porous SiC Ceramics using a Combination of graft Polymerization and Sol-Gel Technique".* In this article for the first time a new method, which includes the combination of in-situ polymerization and sol-gel techniques, has been proposed to fabricate in situ reaction bonded porous SiC ceramics. The resulting products have been characterized by means of flexural strength, mercury porosimetry and morphological studies. In addition, the effect of sintering temperatures from 1500 °C to 1600 °C was investigated on the properties of the resulting porous ceramics and the crystalline structure of the specimens. This article will be submitted to the *Journal of Industrial & Engineering Chemistry Research.*

CHAPTER 4 ARTTICLE 1: DIFFUSIONAL EFFECTS FOR THE OXIDATION OF SIC POWDERS IN THERMOGRAVIMETRIC ANALYSIS EXPERIMENTS

Omid Ebrahimpour, Charles Dubois and Jamal Chaouki[1]

Journal of Materials Science, 2013, Vol. 48 (12), pp 4396-4407.

Department of Chemical Engineering, École Polytechnique de Montréal, P.O. Box 6079, Station Centre-Ville, Montréal, Canada

Parts of this work have been presented 33rd International Conference & Exposition on Advanced Ceramics & Composites**,** USA

Abstract

The oxidation behavior of SiC powders was studied using a thermogravimetric analysis (TGA). The effects of temperature (910-1010°C), particle size (120 nm, 1.5 µm) and the initial reactant mass on the oxidation behavior of SiC were investigated. Kinetics analysis showed that intra-particle diffusion and chemical reaction controls the oxidation rate. Moreover, a new kinetics model was proposed to describe the oxidation rate of where all diffusion steps (bulk, inter- and intra-diffusion) and the chemical reaction may affect the overall reaction rate. The model was validated through a comparison with the experimental results obtained from the oxidation of SiC powders in TGA experiments. It was found that during the experiments, inter diffusion must also be taken account to describe adequately the oxidation rate. Numerical analysis indicated that inter-particle diffusion has significant effect on the oxidation rate especially for larger system.

Keywords: SiC powder, Passive oxidation, Particle size, Diffusional effects, Kinetics model

[1] Jamal.chaouki@polymtl.ca Tel.: +1-(514) 340-4711 x. 4034; fax: +1-(514)340-4159

4.1 Introduction

Silicon carbide has been recognized as a promising member of the high temperature structural materials due to its excellent combination of physical and mechanical properties. Because of wide use of silicon-based material in a high temperature, it is important to study its oxidation [1].

It is well-known that the oxidation behavior of SiC is categorized into passive and active regimes. During passive oxidation [2], a layer of SiO_2 is formed on the SiC surface causing a net weight gain according to Eq. (1):

$$SiC + 2O_2 \rightarrow SiO_2(s) + CO_2(g) \quad 4\text{-}1$$

On the other hand, the active state [2] results in gaseous species of SiO and CO, which leads to a net mass loss, where:

$$SiC + O_2 \rightarrow SiO(g) + CO(g) \quad 4\text{-}2$$

At a well defined temperature (typically more than 800°C), when the level of partial pressure of oxygen in the bulk gas is higher than the critical pressure of oxygen, passive oxidation takes place [2]. Jacobson N.S. [3] listed the previous works which have been studied on the determination of active-to-passive or passive-to-active transition in the oxidation of SiC.

Several factors affects on the oxidation rate of SiC based materials. Opola [4] investigated the effect of impurity on the oxidation rate of chemically vapor deposited SiC. He performed the experiments in alumina (99.8%) and fused quartz (99.995%) reaction tube. It was observed that the impurities in alumina tubes increased the oxidation rate. Zheng et al. [5] investigated the effect of sodium contamination on the oxidation rate of CVD SiC at the temperature range of 1100-1300 °C. Ramberg et al. [6] showed that oxidation rate of SiC is depended on the crystal orientation of SiC faces. Quanli et al. [7] studied the effect of particle size on the oxidation rate of SiC powders over the temperature range 1100 to 1200°C. Tortorelli P.F. [8] showed that the presence of water vapor enhanced both oxidation and crystallization rate.

Most investigators describe the growth of the oxide layer using the diffusion-reaction model developed by Deal and Grove [9]. According to this model, the thickness of the oxide layer, x_0, can be predicated by the following equation:

$$x_0{}^2 + A^* x_0 = B^* (t + t_0) \quad 4\text{-}3$$

Where B^*/A^* and B^* show the linear and parabolic rate constants, respectively. t_0 is a correction factor used to adjust the time coordinate to the presence of an initial oxide layer. For a long reaction time, the equation reduces to the popular parabolic oxidation model. Lately, Chou [10] proposed a new kinetics model to calculate the oxidation rate of Si-Al-O-N materials in powder form when the intra-diffusion is the rate control of the reaction. It was shown that it describes better the oxidation process as compared to the parabolic model [11]. Typically, at higher oxidation temperature, intra-particle diffusion is the rate step controlling of the reaction. Some of the previous works for the oxidation of silicon carbide including the experimental conditions and the rate-controlling steps are summarized in Table 4.1.

Table 4.1 Summary of previous studies on the oxidation of SiC

Temperature range (°C)	Time (min)	Sample type	Rate-controlling Steps	Experiment condition	Gas	Activation energy (kJ mol^{-1})	Ref.
1100-1200	0-120	α-SiC powders	Diffusion	TGA alumina crucible	Dry air	82-110	[7]
800-1100	10-9000	CVD-SiC plate	Reaction-diffusion	Furnace Mullite tube	Dry O2	94-285	[6]
950-1150	15-360	4H-SiC pilayers	Reaction-diffusion	Lindberg furnace	Dry O2	192-301	[25]
1200-1500	0-480	Hexagonal 4 H poly type plate	Diffusion	Mullite tube furnace TGA	Dry O2	120-260	[26]
600-850	30-480	α-SiC powder	Diffusion	Alumina crucible Quartz tube furnace	Dry/wet air	100-138	[27]
1100-1400	0-60	Rhombohedral -SiC Powder	Reaction- diffusion	Alumina crucible TGA	Dry O2/N2	179	[24]

Recently, there has been increasing interest in the investigation of oxidation behavior of SiC in the powders state due to its wide application for the fabrication of porous and composite SiC ceramics in oxidation environment [12]. Typically, thermogravimetric analysis (TGA) is used as one of the most widely characterization techniques for kinetics determination of gas-solid reactions. Although it is a simple and accurate technique, but in order to determine the reliable kinetics parameters in laboratory studies, the diffusion effects (bulk or internal diffusion) should

be considered. For example, Ollero P. et al. [13] and Gomez B. et al. [14] reported that internal diffusion resistance significantly affects the observed gasification reaction rate where the reaction intrinsically controlled by chemical reaction. Likewise, N. Zouaoui[15] studied the combustion of the carbon black in a TGA which is mainly kinetic control. They found that reaction rate is depended on initial sample mass in the crucible which is attributed to the mass diffusion limitation in the TGA. He et al. [12] investigated the influence of the flow rate on the oxidation rate of SiC powder which were laid in the crucible. It was observed that, under the same time and reaction temperature, the oxidation rate in flowing air is higher than the one in static air. This can be attributed to the difference of partial pressure of the oxygen due to the existence of bulk diffusion in the system.

To the best of the author's knowledge, none of the previous researchers considered the effects of bulk or internal diffusion of oxygen during the kinetics parameters determination of the SiC powders. Therefore, it seems to be necessary to do further studies on the oxidation of SiC powders in order to determine the significant affecting the physical diffusion limitations on their oxidation kinetic in TGA.

In this work, the oxidation behavior of SiC micro-sized and nano-sized powders was studied at different temperatures (910°C-1010°C). For the oxidation kinetic of SiC powders, it was assumed that both intra-particle diffusion and chemical reaction controls the growth rate. The objective of the present work was to investigate the importance of the diffusion limitations for the SiC oxidation in TGA. Furthermore, a new model was developed that considers all mass transfer steps (external, inter- and intra-particle) and interface reaction for any non-catalytic gas-solid reaction. The model was validated and applied to describe the oxidation behavior of SiC powders in TGA experiments.

4.2 Model Development

In many gas solid systems, the gas reactant must first diffuse from the bulk to the surface of the fixed bed, followed by diffusion through the pore space between particles in the bed. Afterward, gaseous reactant diffuses into the reactant to reach the surface of the solid where finally reacts.

Reversely, gaseous products must diffuse backward, first through the reacted layer then the bed and finally in the gas film into the bulk atmosphere over of the system. In some cases, such as the oxidation of SiC powders, the control step of the reaction is thought to be the surface interface-reaction and intra-diffusion of the gaseous reactant through the product layer but other phenomena may also limit the overall reaction rate.

Depending on the experimental conditions taking place during TGA tests, four types of regimes can occur as shown in Figure 4-1. The effective diffusion coefficient in the oxide layer can be measured by filling a monolayer of the powders on top of the crucible (type I). In type II, as there is a stagnant gas on top of the powders, external mass transfer and intra-particle diffusion must then be considered. When the crucible is fully filled by the powders, both inter- and intra-particle diffusion effects are found (Type III). Finally, when the crucible is partly filled, all three steps of diffusion effects must be considered (Type IV). As it will be shown in more details later, if only intra-particle and interface reaction diffusion is considered to describe the oxidation of SiC for all four types of regimes, it may cause a significant error to estimate the kinetic parameters especially during the scale up the system.

4.2.1 Model description and main assumptions

The following assumptions are considered in developing the model for the oxidation of SiC powders in TGA cylindrical crucibles:

1- The geometry and physical properties of the sample do not change during the reaction. In other words, the height of the samples in the crucible (Z=L), and the density of the SiC powders remain constant.
2- All SiC particles in the crucible are assumed to be one porous particle and each SiC particle is called a grain (grain-particle model).
3- During the reaction, each SiC is composed of an unreacted core of SiC, which shrinks as the reaction progresses, and a shell of silica. Consequently, a shrinking core system is applied to describe this phenomenon.
4- From a macroscopic view, it is assumed that oxygen diffuses only in the vertical direction (one dimensional) from the mouth of the crucible to the bed surface and through the pores

in the crucible. While from the microscopic standpoint, oxygen diffuses in the radial direction (r) within of the surrounding each SiC particle.

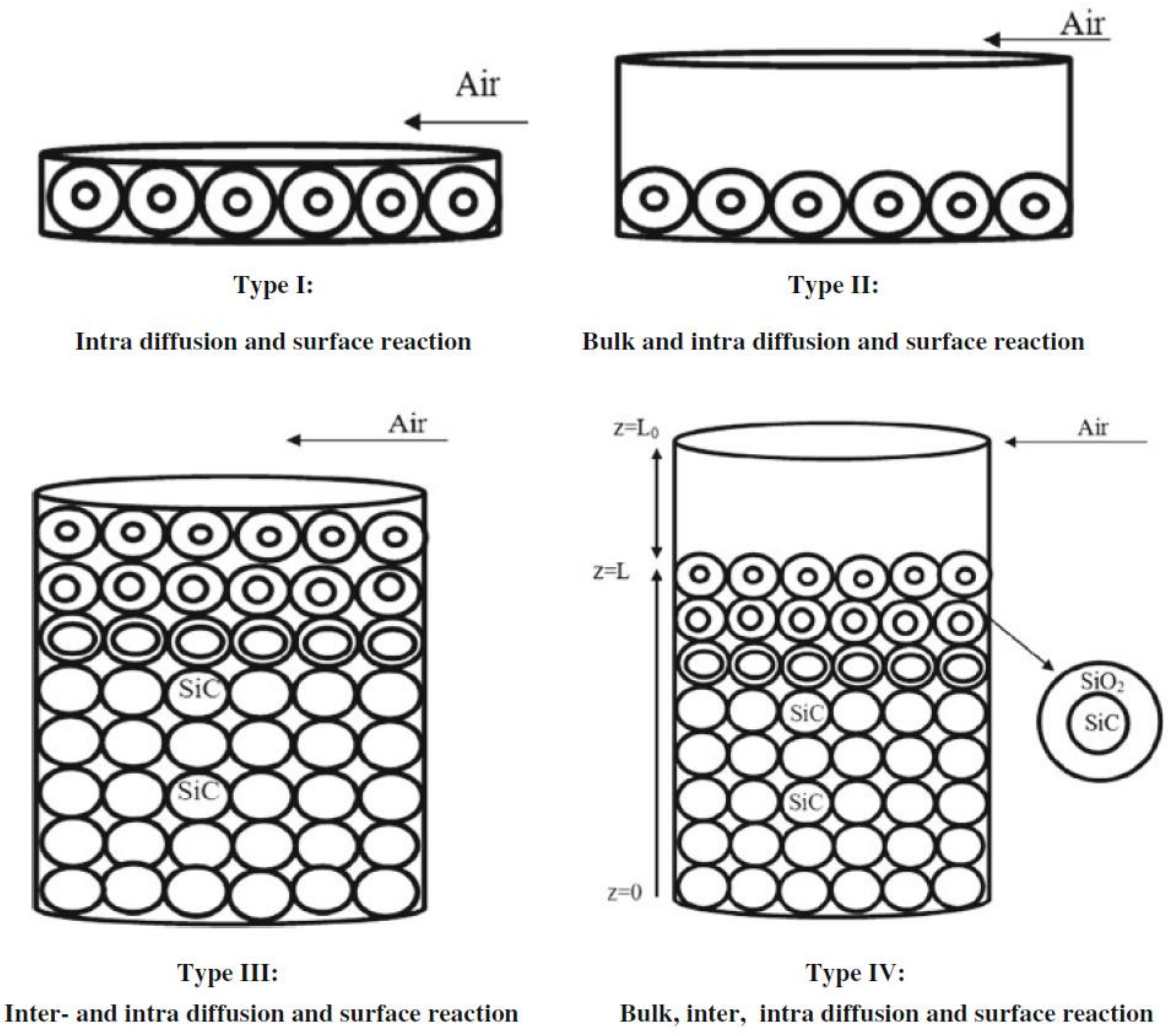

Figure 4-1 Schematic representation of oxidation of SiC in the TGA

5- Although, we are faced with the flux of multiple gases (O_2, N_2, CO_2), but since the gaseous reactant is diluted in an inert nitrogen stream and diffusion occurred through the powders in the bed, to simplify the model, we neglect the effect of the convection term of the flux above the bed.
6- A pseudo-steady sate is assumed.

7- Ideal gas behavior is considered and the total gas pressure and temperature are constant. As the Biot number for SiC powder is less than 0.1, the temperature gradient inside the powders can therefore be neglected.
8- Surface chemical reaction of SiC and oxygen is expressed by the first order law [9].

4.2.2 Model Formulation

4.2.2.1 Types I

In case (I), it is assumed that the oxidation rate is controlled by oxygen diffusion through the silica layer and the surface chemical reaction which act in series. Shrinking core model is very famous to describe the reaction where the solid particles are consumed. This model assumes that the powders are spherical in shape with a constant density. The difference between the Deal and Grove [9] model and shrinking-core model [16] is based on the assumption of flux calculation. The former applied Cartesian coordinates to obtain a concentration profile of oxygen inside the oxide layer (thin film approximation) while the later used spherical coordinates, which are more accurate as the conversion increases in the powder form.

For this system, the fractional conversion (X) in terms of reaction time is as follows:

$$t = \tau_S \times \left[1-3(1-X)^{2/3} + 2(1-X)\right] + \tau_r \times \left[1-(1-X)^{1/3}\right] \qquad 4\text{-}4$$

$$\tau_S = \frac{\rho_{SiC}\, r_0^2}{6bD_e^S C_{Ab}}, \qquad \tau_r = \frac{\rho_{SiC}\, r_0}{bk'' C_{Ab}}$$

τ_S is the time for a complete reaction of the solid when only diffusion resistance through the product layer controls reaction of the particle. τ_r is the required time for a complete consumption of all the reactant when chemical reaction controls throughout reaction of the particle alone. ρ_{SiC}, is the molar density of SiC, r_0 is the radius of the powder and C_{Ab} is the concentration of gas reactant at the bulk system. D_e^S denotes the effective diffusivity of the gaseous reactant, A, within the oxide layer [16]. k'' is the first-order rate constant for the surface reaction. b is the stoichiometric coefficient which for passive oxidation of SiC according to Eq. (1), is 0.5. Details for the deriving the Eq. (1) is explained in the Appendix (A).

The relation between the fractional conversion (X) and the experimental data is given by:

$$X(t) = \frac{\Delta m(t)/m_0}{\Delta m_{max}/m_0} \quad 4\text{-}5$$

Where m_0 is the initial sample weight, Δm_{max} is defined as all of the SiC being completely reacted to silica and (Δm) is the increase in the sample weight with time as measured by TGA [10].

4.2.2.2 Type II

As depicted in Figure 4-1, for type II, the system is divided into two parts: In part (a) air is diffuses through a stagnant gas. In part (b), the interface reaction and inter-particle diffusion phenomena are dominant similar to the type (I).

As there is no reaction in part (a), mole balance of the gaseous reactant is written as follows:

$$\frac{\partial N_A}{\partial z} = 0 \quad 4\text{-}6$$

Where, boundary conditions are:

$$z=L_0 \quad x_A = x_{Ab} \qquad t>0 \quad 4\text{-}7$$

$$z=0 \quad x_A = x_{As}(t) \qquad t>0$$

L_0 is the height of the crucible. x_{Ab} and x_{As} are the mole fraction of reactant gaseous at the bulk and the surface of the particles, respectively. Substituting $N_A = -C_t D_{air-CO_2} \frac{\partial x_A}{\partial z}$ (as the gaseous reactant is diluted in the inert gas for the simplicity of the model, the convection term of the flux is not considered) yields:

$$N_A = -C_t D_{air-CO_2} \frac{x_{Ab} - x_{As}}{L_0} \quad 4\text{-}8$$

Where, $D_{air-CO_2}$is the diffusion coefficient of the reactant in the bulk. C_t is the total mole concentration of the gaseous reactant.

Under pseudo-steady state conditions, the rate of mass diffusion of the gaseous reactant to the bed is related to the overall gaseous consumption in the bed, based on the stoichiometric equation (Eq. (1)) as follows:

$$N_A|_{z=0} \times A_b = N_A^{'}|_{r=r_0} \times S_t \quad 4\text{-}9$$

Where, A_b is the cross section of the crucible and S_t is the total surface area of the particles. $N_A^{'}|_{r=r_0}$ is the molar flux of gaseous reactant at the surface of the SiC particles within the crucible.

For this system similar to the type (I), it can be shown that the fractional conversion (X) in terms of reaction time is determined as:

$$t = \tau_b \times X + \tau_S \times \left[1-3(1-X)^{2/3} + 2(1-X)\right] + \tau_r \times \left[1-(1-X)^{1/3}\right] \quad 4\text{-}10$$

$$\tau_b = \frac{\rho_{SiC} S_t r_0 L_0}{3bC_{Ab} D_{air-CO_2} A_b}$$

τ_b is the time to complete oxidation of the particle when only external diffusion is taken into account. In this case, all three steps (bulk diffusion, intra particle diffusion and the reaction surface) occur in series. In fact, depending on the reaction mechanism and the physical condition of the experiment, one or mixing of these phenomena can control the overall reaction rate.

4.2.2.3 Type III

Molar balance on the gaseous reactant (A), in the bed is given by:

$$\frac{\partial N_A}{\partial z} - S_v \times N_A^{'}|_{r=r_0} = 0 \quad 4\text{-}11$$

Where, S_v is the total surface area of the powder per unit volume of the crucible. The molar flux of component (A) in the bed can be expressed as:

$$N_A = -C_t \frac{\varepsilon}{\tau} D_{air-CO_2} \frac{\partial x_A}{\partial z} \quad 4\text{-}12$$

Where τ and ε are the tortuosity and the porosity, respectively. In the literature, the value of the tortuosity can be found in a range of 1.25 to 4 for the packed bed depending on various parameters such as the packing arrangement or the uniformity of the particles [17]. In practice, the value of $\frac{\varepsilon}{\tau}$ is changed as reaction proceed [18].

Substituting the Eq. (12) into Eq. (11) gives:

$$\frac{\partial^2 x_A}{\partial z^2} = -\frac{S_v}{C_t \frac{\varepsilon}{\tau} D_{air-CO_2}} \times N_A^{'}|_{r=r_0} \quad 4\text{-}13$$

Boundary conditions are written as follows:

z=L_0 $x_A = x_{Ab}$ t> 0 4-14

and

z=0 $\frac{\partial x_A}{\partial z} = 0$ t> 0

The local rate of the reaction in the SiC particle is determined as the following:

reaction rate of SiC particle $(\frac{mol}{t}) = -4\pi r_c^2 \rho_{SiC} \frac{\partial r_c}{\partial t}$ 4-15

where, r_c is the radius of the unreacted SiC particle.

Based on Eq. (1) (stoichiometry) $N_{O_2} = 2N_{SiC}$, therefore at r=r_c, it gives

$\frac{\partial r_c}{\partial t} = N_A^{'} |_{r=r_c} \times \frac{1}{2\rho_{SiC}}$ 4-16

According to the molar balance of gaseous (A), at r = r_0 and r = r_c we have the following relation:

$4\pi {r_0}^2 \times N_A^{'} |_{r=r_0} = 4\pi {r_c}^2 \times N_A^{'} |_{r=r_c}$ 4-17

Substitution of Eqs (16) and (17) into Eq. (13) results

$\frac{\partial}{\partial z}\left(\frac{\partial x_A}{\partial z}\right) = -\eta \times r_c^2 \times \frac{\partial r_c}{\partial t}$ $\eta = \frac{S_v \times 2 \times C_{SiC}}{r_0^2 \times C_t \times \frac{\varepsilon}{\tau} D_{air-CO_2}}$ 4-18

The relation between the local rate of the reaction in the SiC $(\frac{\partial r_c}{\partial t})$, in term of the mole fraction of gaseous reactant in the bed, x_A, can be expressed as follows (Appendix A):

$\frac{\partial r_c}{\partial t} = -\Omega \frac{x_{A(Z,t)}}{\left(1-\frac{r_c}{r_0}\right) r_c + \frac{D_e^S}{k''}}$ $\Omega = C_t \times D_e^S \times \frac{1}{2\rho_{SiC}}$ 4-19

With the initial condition

t=0, $0 \le z \le L$ $r_c = r_0$ 4-20

The relationship between the total fractional conversion in the bed, $X(t)$, and local fractional conversion, $X_{Loc}^{'}$ is determined by:

$X(t) = \frac{1}{L_0} \int_{z=0}^{z=L_0} X_{A,Loc}^{'}(t, Z, r_c) \times dz$ 4-21

Where $X_{Loc}^{'}$ is the local fractional conversion, which is expressed as follows [16]:

$$X_{Loc}^{'}(t,z,r_c) = 1 - \left(\frac{r_c}{r_0}\right)^3 \quad 4\text{-}22$$

4.2.2.4 Type IV

The formulation for this type, is similar to the type III, excepting for the mole fraction at the top of the bed, x_{As}, which changes with the reaction time. x_{As} is determined from the mole balance between the empty space in the crucible and the overall gaseous consumption in the bed according to the stoichiometric relationship (Eq. (1)) as follows:

$$N_A \times A_b = -2 \times \frac{dmol_{sio_2}}{dt} \quad 4\text{-}23$$

4.2.3 Method of Solution

To calculate the mole fraction in the mentioned systems, all the physical parameters must be known. Since the values of the effective diffusivity inside the powders, the kinetic rate constant and $\frac{\varepsilon}{\tau}$ are unknown, these parameters were determined using the Levenberg-Marquardt method for nonlinear regression.

For the type III, in order to determine the mole fraction profile of gaseous reactant inside the bed, Eqs. (18) and (19) must be solved simultaneously with boundary conditions, which were described in Eq. (14) and one initial condition Eq. (20). The procedure to solve these equations is similar to the works that have been done by Batarseh [19] and Crank [20]. In summary, introducing the Leibnz rule results in reducing the partial differential equations system to the nonlinear ordinary differential equation with the moving boundary layer. Then, the shooting algorithm was applied to convert the boundary-value problem to an initial value equation. Finally, to calculate the total fractional conversion in the bed, Simpson's rule was employed. The computer code has been written in MATLAB.

4.3 Experimental procedure

Two different size of SiC powders used for this work were provided by LABMAT, Inc. Canada. The oxidation of specimens was carried out in a Mettler Toledo thermogravimetric analyser, where the weight gain of a sample is measured during the oxidation at atmospheric pressure under controlled gas flow and temperature. Following procedures were employed during the TGA experiments: samples were placed at 25 °C for 5 munities in the crucible. Then, they were heated in an inert atmosphere of N_2 at a constant rate of 10 °C/min to the preset temperatures followed by maintaining them for 20 min at that temperature to ensure that the temperature in the system was reached to the predetermined condition. Subsequently, the gas was shifted to the dry air with a purity of 99.99 air at a constant temperature for another 150 min. All the TGA experiments were corrected by blank tests under the same oxidation conditions and repeated at least two times. The entire TGA tests were carried out in the high purity alumina crucible. The oxidation process were performed at 910-1010 C to minimize the effect of crystalline and sintering of particles during the oxidation.

To investigate the diffisional effects on the oxidation rate, three sets of the experiments were performed in TGA. In the first set of experiment, to find the kinetic parameters a very thin layer of SiC powders were uniformly laid in a crucible which has the inside diameter of 5 mm (type I). In the second set of the experiment to investigate the effect of bulk diffusion, the same amount of sample was laid in the crucible which has 4.5 mm height and 5 mm diameter (type II). In the last set of experiment (type III), to verify the inter particle diffusion, all the crucible was approximately filled by the sample.

The BET technique was performed to determine the surface area of as-received particles using Autosorb-1 (Quantachrome instrument). Before the measurements, samples were degassed at 300°C for at least 3h. The particle size distribution of the samples was measured by a particle size analyser (Coolter rfz LS 200). Morphological analysis of original powders was conducted by SEM (Model JSM-840A, JEOL Co. Ltd., Japan). Phase composition of the starting samples were conducted by X-ray diffraction using a computer-controlled diffractometer (Model X'pert, PHILIPS) with Cu Kα radiation (wavelength of 1.5418 Å) at 50 kV, 40 mA, and a step size of 0.02° between 10° and 80°. Impurity of the specimens was determined by XRF analysis (Philips, PW2440, XRF Spectrometer).

4.4 Results and discussion

4.4.1 Characterization of the starting materials and TGA results

Table 4.2 gives the measured properties of the specimens. XRD results shows that the main crystalline phase of both particles is β. Results from scanning electron microscopy (SEM) as presented in Figure 4-2, show that micro particles are irregular shapes and some fine powders exist on the surface of the large particles, which cause an increase in the surface area of powders.

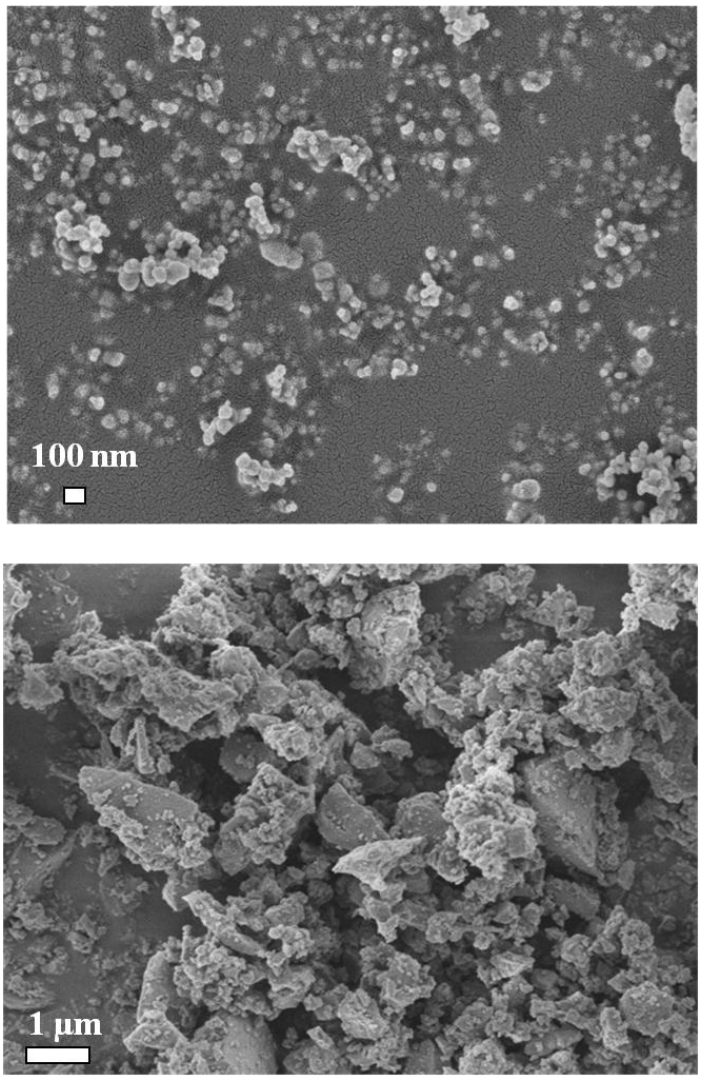

Figure 4-2 SEM images of raw SiC powders: β-SiC-120nm (up) and β-SiC-1.5µm (down)

Figure 4-3 compares the TGA curves of β-SiC powders 1.5 μm and β-SiC 120 nm, plotted as the relative weight gain against temperature. The oxidation of smaller powders starts at a much lower temperature (500 °C) compared to the larger powders (870 °C). Therefore, the smaller powders are more reactive.

Table 4.2 Characteristic of starting materials

Particle type	Specific surface (m^2/g)	Mean size (μm) (Volume method via P.S.A.)	Density (g/cm^3)	Phase	SiC (wt %) Impurity
SiC (1)	15.27	1.5	3.2	β	99%> Mo, Zr, Pb, Fe
SiC (2)	34.73	0.12	3.2	β	99%> Mo, Zr, Pb, Fe

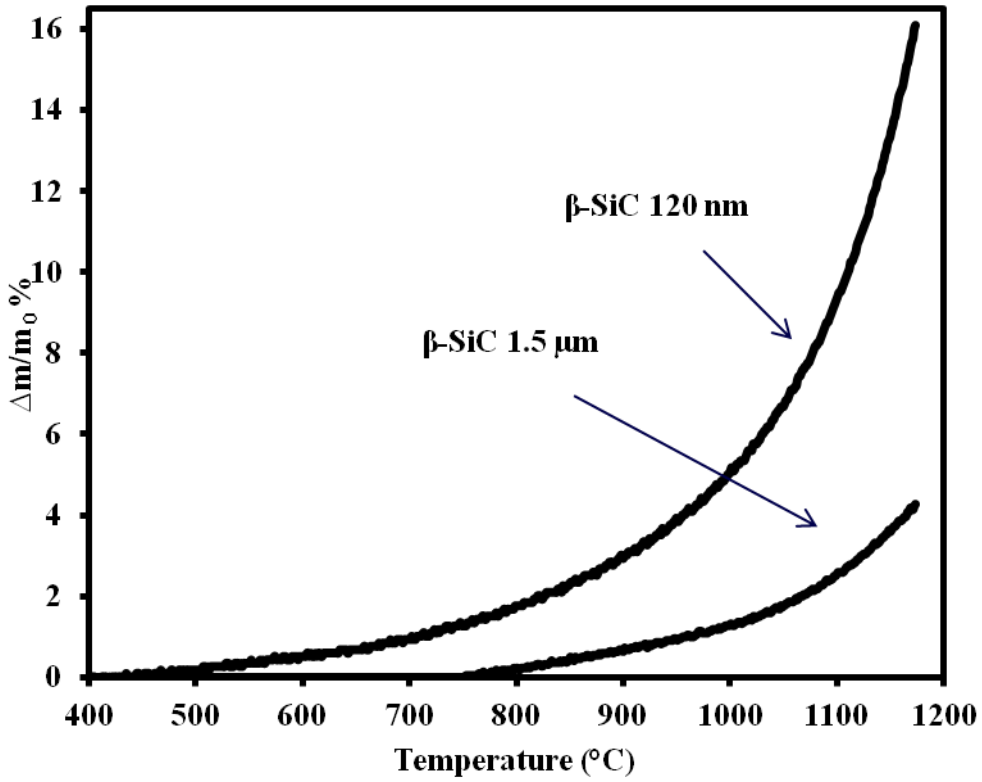

Figure 4-3 TGA curves of β-SiC powders 1.5 μm and 120nm

4.4.2 Oxidation kinetics – Type I

The oxidation data is described in terms of the relative mass changes versus time in Figure 4-4 for different samples during 150 minutes of oxidation. The mass changes are directly linked to the oxidation temperature while it has a reverse relation with the particle size. The explanation is that in finer particles, the total surface area is higher than larger particles which would provide more surfaces for diffusion of O_2 and thus accelerate the oxidation reaction.

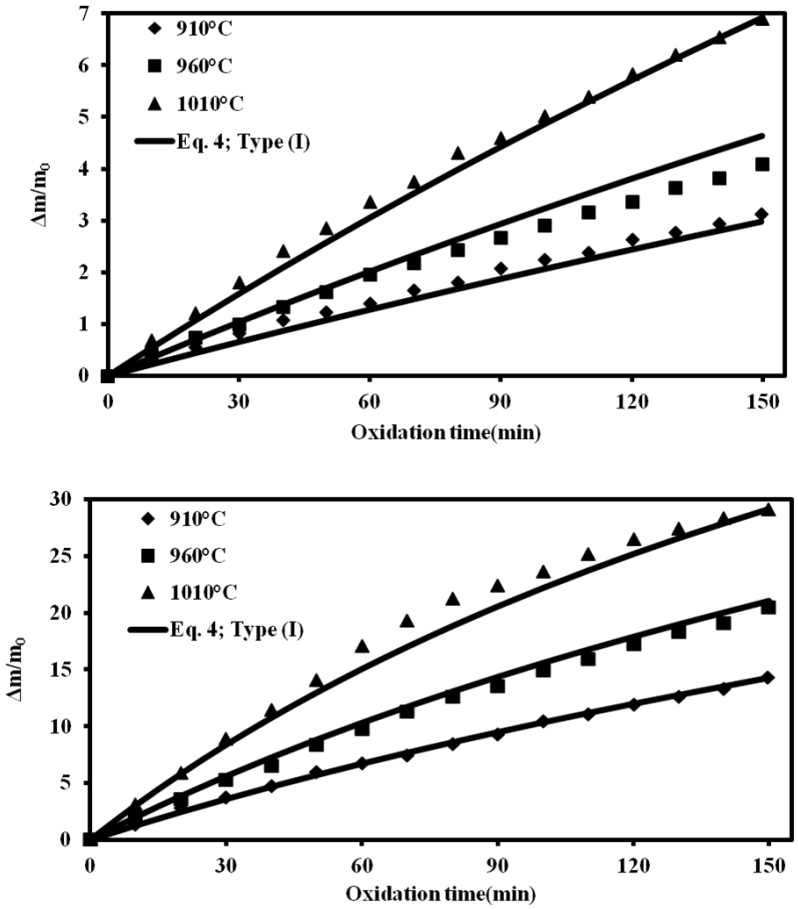

Figure 4-4 A comparison of the oxidation behaviour between experimental and calculated for β-SiC 1.5μm (up) and β-SiC 120 nm (down) at various temperature; type (I)

The relation between the effective molecular diffusivity inside the oxide layer and the reaction rate constant with the temperature are:

$D_e^s = D_0 \exp(-E_a/RT)$ $(\frac{cm^2}{s})$ 4-24

$k'' = k_0 \exp(-E_r/RT)$ $(\frac{cm}{s})$ 4-25

Where E is the activation energy (kJ/mol), R is the universal gas constant (8.314 J/K.mol). D_0 and k_0 are the pre-exponential factors.

Analysis of the data shows that the oxidation rate followed by the reaction-diffusion control for both particles. The kinetics parameters for different temperatures are presented in Table 4.3 using Eq. (4). Activation energies and the pre-exponential factors were determined using onetime multivariate regression method. The calculation error based on the average relative error [21] is less than 8% which shows a quite satisfactory agreement between experiments and model.

Table 4.3 Kinetics parameters values for the system I and III using the Eq. 4 for the temperature range of 910-1010 °C

Type of crucible	K_0	E_r kJ/mol	D_0	E_a kJ/mol
I- SiC- 1.5μm	4.1	123.1	0.09	202.7
I- SiC-0.12 μm	1.9	123.1	0.008	202.7

As shown in Table 4.1, due to the wide variety of experimental conditions and SiC types used in their kinetics determination, the apparent activation energies of oxidation have been reported to be in a wide range from 85 to 500 kJ/mol [1, 22, 23]. Comparing the oxidation kinetics with previous works for the single SiC phase, the obtained values for the activation energy are between the fast oxidation-face (99 kJ/mol) and slow oxidation-face (292 kJ/mole) [24, 25]. It should be noted that as the phase and the impurities of both particles are the same, the value of the activation energy must not depend to the particle size. The difference in the obtained pre-factors for the studied particles (nano-sized and micro-sized) is attributed to the tortusitivity and the porosity inside the powders and also being non-spherical of the particles.

4.4.3 Bulk and inter-particle diffusions in the oxidation (types II and III)

Oxidation rate results for the second series of the experiments are very similar with the first type of the experiment for both powders (results were not reported). Therefore, the external diffusion effects were almost negligible for the studied system. The result is consistent with theory as follows: the calculated values for the T_r and T_s from the Eq. (4) is much larger than the one for the T_b according to the Eq. 10. Therefore, the bulk diffusion effects can be disregarded for this type of system and the concentration of gaseous reactant on the top of the bed is equal to the one at the mouth of the crucible.

The results for the oxidation behavior of the particles when the crucible is completely filled by particles (type III) are shown in Figure 4-5.

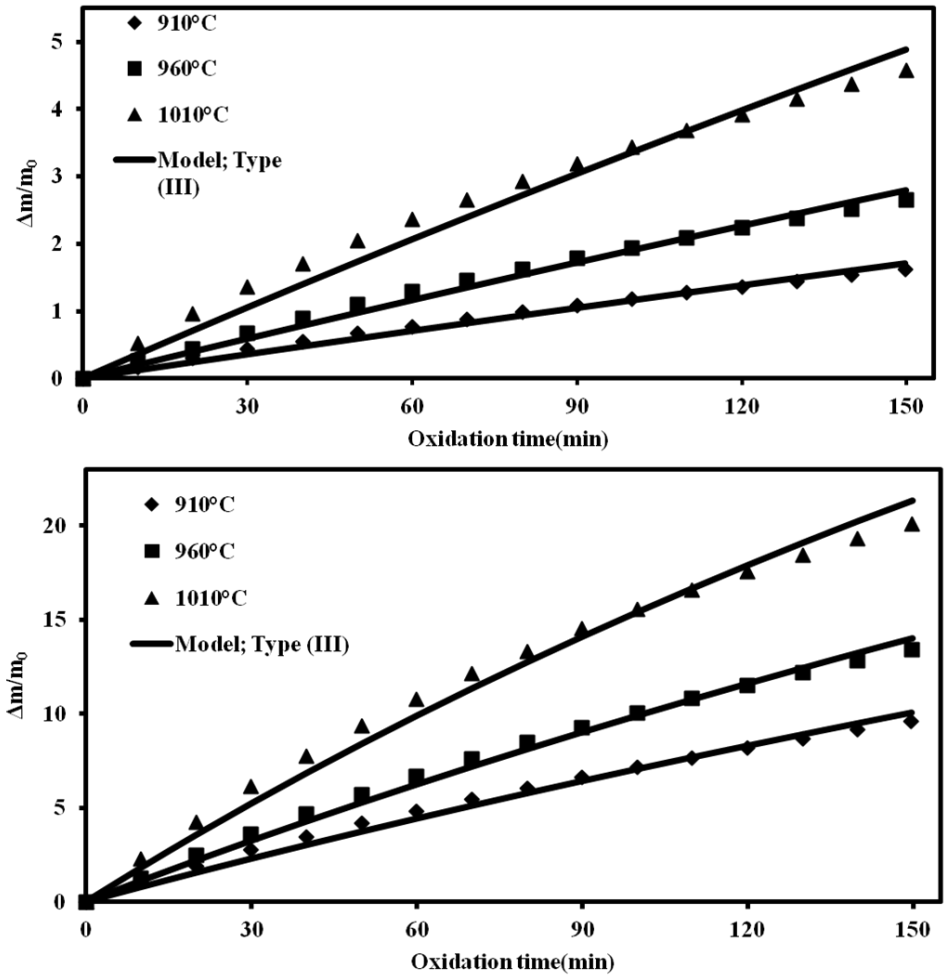

Figure 4-5 A comparison of the oxidation behaviour between experimental and calculated for β-SiC 1.5μm (upper) and β-SiC 120 nm (lower) at various temperature; type (III)

Details of the physical properties of the experiment are given in Table 4.4. Comparing the results from the type I and type III, indicates that for the same experimental conditions, the oxidation rate depends on the initial mass of sample in the crucible. As an example, for the micro-sized particles in type I, at 1100 °C and 150 minutes of the oxidation, the relative mass changes is 31% higher than for the same experimental condition in type III. If the Eq. 4 was applied for type III, the obtained kinetic parameters is different from the same experiments in type I which leads to misleading especially in the scale up of the system, for example in evaluating the predicted time for a complete reaction. Consequently, the diffusion effects of the gaseous reactant between the powders in the crucible must be taken into account to interpret TGA experiments. Although the developed method is more complicated, but the results in type III can not be explained by simpler models.

Table 4.4 Physical properties used in the model

Parameter	β-SiC 1.5 μm TGA	β-SiC 0.12 μm TGA
C_{SiC} (mol/m^3)	8.23×10^{-8}	8.23×10^{-8}
L_0 (m)	5×10^{-3}	5×10^{-3}
R_0 (m)	2.2×10^{-3}	2.2×10^{-3}
ε_0 (%)	67	90
P (pa)	101325	101325
R (J K^{-1} mol^{-1})	8.314	8.314

As shown in Figure 4-5 the curves obtained by numerical solution of Eqs (18) and (19) align very well with the oxidation data in the third experiment series for both particles. In this model, the obtained kinetic values from the first series of the experiment were applied.

Results of the local fractional conversion versus the dimensionless height of the bed (Z/L) at different reaction temperature are plotted in Figure 4-6 for the studied powders. As shown, at higher temperature the difference of the local conversion along the bed increases. In the other words, the effect of the inter-particle diffusion becomes dominant by increasing the temperature.

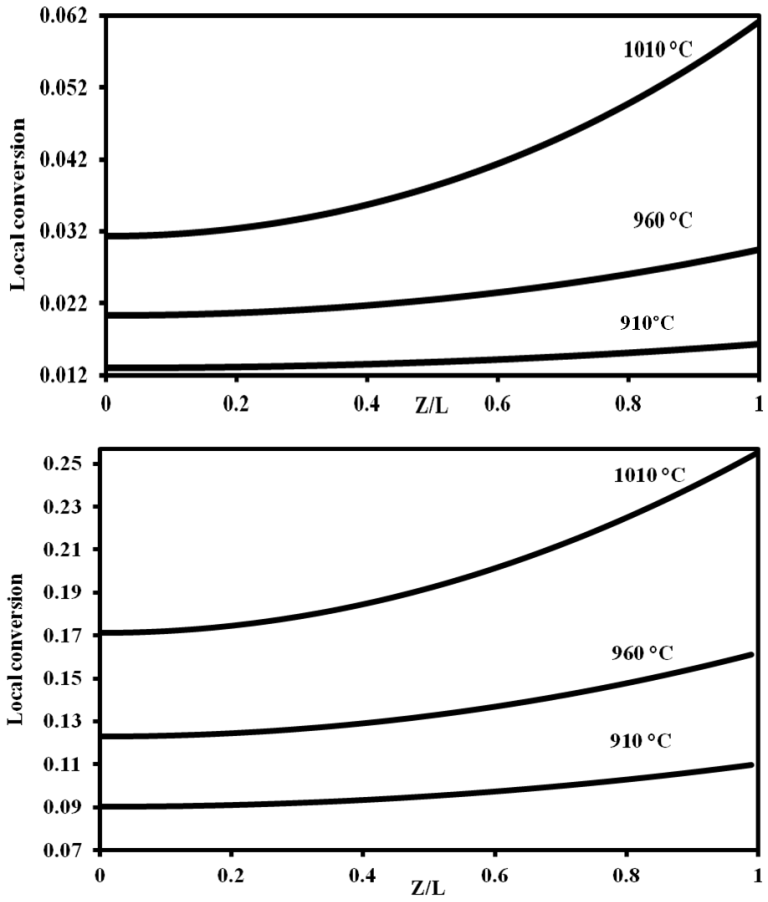

Figure 4-6 Local conversion vs. axial position in the bed for β-SiC 1.5μm (up) and β-SiC 120 nm (down) at different temperature reaction, reaction time 60 min; type (III)

These results can be explained by the sensitivity of the inter-particle (Eq. 26) via reaction rate constant and intra-particle diffusion (Eqs. 24 and 25) to the temperature.

The relation between the bulk diffusion with the temperature is given as

$$D_{air-CO_2} = 0.136 \times \left(\frac{T}{273.2}\right)^{1.75} \quad (\frac{cm^2}{s}) \qquad 4\text{-}26$$

Due to the exponential term, the effective coefficient diffusion in the oxide layer and reaction rate constant is much more temperature-sensitive than bulk diffusion ($T^{1.75}$). For example, increasing the temperature from 910°C to 1010°C increases 4.7 times the value of the effective diffusion

inside the particle, while it only raises the inter-particle diffusion 1.15 times. Therefore, the resistance of the inter-particle diffusion prevails at high temperature.

To show the importance of inter-particle diffusion on the overall rate especially in the larger scale, oxidation rate of the powders is investigated when length of the crucible increases five times. Figure 4-7 shows the local conversion in the bed at the temperature of 1010 °C for a different reaction time.

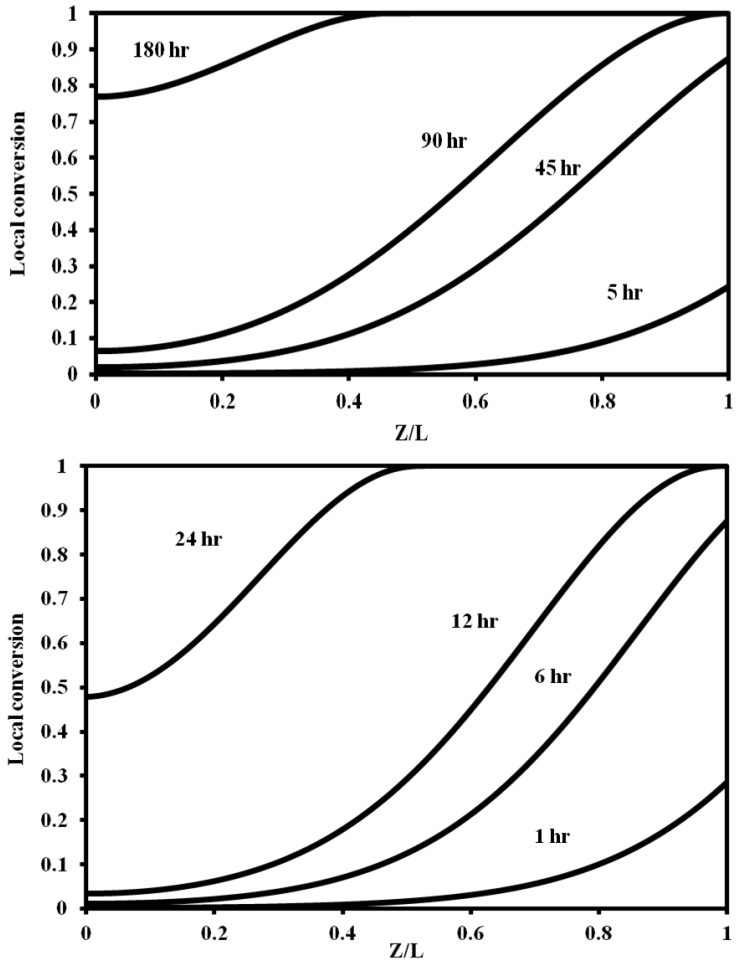

Figure 4-7 Local conversion vs. axial position in the bed for β-SiC 1.5μm (up) and β-SiC 120 nm (down) at 1010 °C for different reaction time; type (III).

Because of the inter particle resistance, in a few times after starting the reaction (1 hr for nano-sized and 5hr. for micro-sized), the powders which are laid on the bottom of the bed did not react with oxygen. At the times of 12 hr and 90 hr for the smaller and larger particles, respectively, all

the powders which are located on the surface of the bed are completely reacted. These times are obtained from the shrinking core model ($t = \tau_r + \tau_s$). After this time, the powders in the crucible are distinguished from the completely reacted particles which are located at the top of the bed and the particles which are reacting.

The total time needed to complete the reaction is calculated from Eq. (27):

$$\tau_c = \tau_s(\theta + 1 + \frac{6D_e^S}{r_0 k''}) \qquad \theta = \frac{S_v \times L^2 \times D_e^S}{r_0 \times \frac{\varepsilon}{\tau} \times D_{air-CO_2}} \qquad \text{4-27}$$

Details for deriving of the equation are explained in Appendix (B). In this case, 313 hr and 55 hr are needed for the complete reaction of all particles in the bed for micro particles and nano-sized powders, respectively. This results show that inter-particle diffusion has significant effect on the oxidation rate, and the model is quite useful especially for the larger system.

According to Eq. 27, if the value of θ is much smaller than other terms, then the inter-particle diffusion does not affect to the reaction and the reaction is controlled by reaction-intra particle diffusion. Physical parameters such as porosity of the bed, the length of the bed and the total surface area of the powder per unit volume affect on the value of θ. For a case when the rate of the reaction is very fast, then both inter and intra particle diffusion controls the growth rate of the oxide layer.

4.5 Conclusion

In this work the passive oxidation behavior of two different particle size of SiC powders has been investigated using thermogravimetry analysis. TGA results showed that particle size has a marked influence on the oxidation rate. Non-isothermal results indicated that for nano sized particles, oxidation reaction started at temperatures much lower than micro sized particles. Furthermore, a new kinetic model was developed for a non-catalytic gas-solid reaction where all diffusion steps and the interface reaction were considered as the overall reaction control rate. The model took into account the influence of particle size, initial mass of particle, porosity and physical characterization of the bed. The model was applied successfully to describe the oxidation of SiC powders taking place in TGA. Based on the analysis of the TGA results, it was found that the oxidation rate was controlled by surface reaction and intra-particle diffusion at the

studied range of oxidation temperature. Although, the bulk diffusion does not influence on the oxidation rate on the studied system, but inter-particle diffusion affects significantly on the oxidation rate. Numerical simulation confirms the importance of the inter-particle diffusion especially for the larger system. Therefore, to determine the kinetics parameters, this phenomenon must be considered.

4.6 Appendix

4.6.1 Appendix A: Calculation of oxidation time in type I

Mole balance of gas reactant inside the oxide layer of powder is described as follows:

$$\frac{\partial}{\partial r}\left(r^2 \frac{\partial C_A}{\partial r}\right) = 0 \qquad \text{(A1)}$$

The boundary conditions are:

r=r_0 $\quad C_A = C_{Ab} \quad$ t> 0 (A2)

and

r=r_c $\quad C_A = C_{As} \quad$ t> 0

Two times integrating with the above boundary conditions yields the concentration profile inside the powder as follows:

$$\frac{C_A - C_{A0}}{C_{As} - C_{A0}} = \frac{\frac{1}{r_0} - \frac{1}{r}}{\frac{1}{r_0} - \frac{1}{r_c}} \qquad \text{(A3)}$$

Where $r_c \leq r \leq r_0$

The concentration of gas reactant at the fresh SiC /oxide layer interface of particle, C_{As}, is calculated according to the flux balance between inside of powder and the reaction rate ($-r''_{SiC} = k'' C_{As}$) at the interface as follows:

$$C_{As} = \frac{1}{2} \frac{C_{A0}}{1 - \frac{k'' r_c^2}{D_e^S}\left(\frac{1}{r_0} - \frac{1}{r_c}\right)} \qquad \text{(A4)}$$

The mole balance on the SiC particles results:

$$\frac{\partial r_c}{\partial t} = \frac{r''_{SiC}}{\rho_{SiC}} = -\frac{k'' C_{As}}{\rho_{SiC}} \quad \text{(A5)}$$

In other words:

$$\frac{\partial r_c}{\partial t} = -\frac{C_{A0}}{2\rho_{SiC}} \frac{1}{\left(1-\frac{r_c}{r_0}\right)\frac{r_c}{D_e^s}+\frac{1}{k''}} \quad \text{(A6)}$$

Integration the above equation and using the Eq. (22) reach us to the Eq. (4)

4.6.2 Appendix B: Deriving the final equations for the type III

To solve the differential equations system (Eqs. 18 and 19), Leibnitz's rule is applied as follows:

Function of $\Phi(z,t)$ is defined as:

$$\Phi(z,t) = \int_0^t x_A(z,t)dt \quad \text{(B1)}$$

According to Leibnitz's rule:

$$\frac{\partial \Phi(z,t)}{\partial z} = \int_0^t \frac{\partial x_A(Z,t)}{\partial z} \partial t \quad \text{(B2)}$$

Therefore, introducing this rule on Eq. 18 results:

$$\int_0^t \frac{\partial}{\partial Z}\left(\frac{\partial x_A(z,t)}{\partial z}\right) \partial t = -\eta \int_{r_0}^{r_c} r_c^2 \, \partial r_c \quad \text{(B3)}$$

$$\frac{\partial}{\partial z}\left(\frac{\partial \Phi(z,t)}{\partial z}\right) = -\frac{\eta}{3}\left[r_c^3 - r_0^3\right] \quad \text{(B4)}$$

and on Eq.19 it gives:

$$6\frac{D_e^s}{k''}(r_c - r_0) + 3r_c^2 - \frac{2r_c^3}{r_0} - r_0^2 = -\Omega\Phi(Z,t) \times 6 \qquad \Omega = \left(\frac{C_t D_e^s}{2C_{SiC}}\right) \quad \text{(B5)}$$

The boundary conditions (Eq. 14) are changed to:

$$z = 0 \quad t > 0 \quad \frac{\partial \Phi(z,t)}{\partial z} = 0 \quad \text{(B6)}$$

$$z = L \quad t > 0 \; \Phi(z,t) = x_{Ab} \times t$$ By

substituting of $\Phi(z,t)$ obtained from Eq. B5 and using the following non-dimension parameters, the previous PDE system is changed to the one non linear second order differential equation with the following boundary conditions:

$$\frac{\partial}{\partial Z}\left(\frac{\partial Y}{\partial Z}\left[Y^2 - Y - \frac{D_e^S}{r_0 k''}\right]\right) = -\frac{\theta}{3} \times [Y^3 - 1], \quad \theta = \Omega \times \eta \times r_0 \times L^2 \tag{B7}$$

$$Z = \frac{z}{L} \qquad Y = \frac{r_c}{r_0}$$

$$\mathrm{Z} = 1 \qquad \mathrm{t} > 0 \qquad 1 + 2\mathrm{Y}^3 - 3\mathrm{Y}^2 + \frac{6D_e^S}{r_0 k''}(1 - \mathrm{Y}) = \beta \times \mathrm{t} \tag{B8}$$

$$\mathrm{Z} = 0 \text{ or } \mathrm{Y} = 1 \quad \mathrm{t} > 0 \qquad \frac{\partial \mathrm{Y}}{\partial \mathrm{Z}} = 0 \qquad \beta = \frac{x_{Ab} \times 6 \times \Omega}{\mathrm{r}_0^2}$$

At the $t = \tau_r + \tau_s = \frac{1}{\beta}(1 + \frac{6D_e^S}{r_0 k''})$ all the powders at the top surface of the bed are completely reacted. When the time is more than τ, the system is divided into two parts: a part that all of the particles are completely reacted (Z^*<Z<1) and a part where the gas solid reaction is occurred.

For the part that all of the SiC particles are completely reacted (Y=0 r_c=0) then Eq. B7 is simplified to:

$$\frac{\partial^2 \Phi(Z,t)}{\partial Z^2} = L^2 r_0^3 \frac{\phi}{3} = 2 \times x_{Ab} \times \theta \times \tau_s \tag{B9}$$

$$Z = 1 \quad \Phi = x_{Ab} \times t \qquad t > \tau_r + \tau_s \tag{B10}$$

$$Z = Z^* \quad \Phi = x_{Ab} \times (\tau_r + \tau_s) \qquad t > \tau_r + \tau_s \tag{B11}$$

This equation can be analytically solved easily.

For the second part of the bed where Z^* < Z< 1 Eq. B7 is valid with the boundary condition of (B9) and (B11).

According to the mass balance of reactant gas at Z= Z^* we have:

$$\left[\frac{\partial \Phi(Z,t)}{\partial Z}\right]_{I,Z=Z^*} = \left[\frac{\partial \Phi(Z,t)}{\partial Z}\right]_{II,Z=Z^*} \tag{B12}$$

This equation results:

$$\mathrm{Z}^{*2} - 2\mathrm{Z}^* + 1 = \frac{\beta}{\theta}(\mathrm{t} - \tau) \qquad t > \mathcal{T} \tag{B13}$$

At Z^*=0, all of the solid in the bed are completely reacted and it results Eq. 27.

4.7 Nomenclature

A	Gas reactant
A_b	Bed surface area
b	Stoichiometric coefficient
C_A	Concentration of gas reactant
C_{As}	Concentration of gas reactant at the surface of the bed
ρ_{SiC}	Molar density of SiC
C_t	Total molar density of gas
D_0	Pre-exponential factor in Arrhenius equation in Eq. 24
D_{air-co_2}	Diffusion coefficient of the reactant in gas in the bulk system
D_e^s	Effective diffusivity of the reactant gaseous in solid
k_0	Pre-exponential factor in Arrhenius equation in Eq. 25
L	Bed height
L_0	Crucible height
m_0	Initial sample weight
$N_A^{'}$	Molar flux of gaseous reactant inside the powder
N_A	Molar balance of the gaseous reactant in the crucible
R_0	Radius of the crucible
r_c	Radius of un-reacted shell of powder
r_0	Initial powder radius
S_v	Total surface area of the powder per unit volume
t	Time
T	Temperature

τ_S	Time for a complete reaction of the particles as defined in Eq. 4
τ_r	Time to complete oxidation of the particles as defined in Eq. 4
τ_b	Time to complete oxidation of the particles as defined in Eq. 10
τ_c	Time to complete oxidation of the particles as defined in Eq. 27
X	Fractional conversion as defined in Eq. 5
x_0	Thickness of the oxide layer
x_A	Mole fraction of gas A in crucible
x_{Ab}	Mole fraction of gas A at bulk
$x_{As}(t)$	Mole fraction of gas A at the surface of the bed
$X_{A,Loc}^{'}$	Local fractional conversion defined by Eq. 22
Z	Dimensionless of bed height in the crucible (z/L)
Z^*	Dimensionless of moving boundary in the bed
Ω	Function defined by Eq. 19
η	Function defined by Eq. 18
θ	Function defined by Eq. 27
Φ	Function defined by Eq. B1
ε	Porosity
τ	Tortuosity

4.8 References

1. Jacobson NS (1993) Corrosion of Silicon-Based Ceramics in Combustion Environments. J Am Ceram Soc 76 (1):3-28

2. Vaughn WL, Maahs HG (1990) Active-to-Passive Transition in the Oxidation of Silicon-Carbide and Silicon-Nitride in Air. Journal of the American Ceramic Society 73 (6):1540-1543

3. Jacobson NS, Myers DL (2011) Active Oxidation of SiC. Oxid Met 75 (1-2):1-25. doi:DOI 10.1007/s11085-010-9216-4

4. Opila E (1995) Influence of Alumina Reaction Tube Impurities on the Oxidation of Chemically-Vapor-Deposited Silicon-Carbide. J Am Ceram Soc 78 (4):1107-1110

5. Zheng Z, Tressler RE, Spear KE (1992) The Effect of Sodium Contamination on the Oxidation of Single-Crystal Silicon-Carbide. Corrosion Science 33 (4):545-556

6. Ramberg CE, Cruciani G, Spear KE, Tressler RE, Ramberg CF (1996) Passive-oxidation kinetics of high-purity silicon carbide from 800 degrees to 1100 degrees C. J Am Ceram Soc 79 (11):2897-2911

7. Jia QL, Zhang HJ, Li SP, Jia XL (2007) Effect of particle size on oxidation of silicon carbide powders. Ceramics International 33 (2):309-313. doi:DOI 10.1016/j.ceramint.2005.09.014

8. Tortorelli PF, More KL (2003) Effects of high water-vapor pressure on oxidation of silicon carbide at 1200 degrees C. J Am Ceram Soc 86 (8):1249-1255

9. Deal BE, Grove AS (1965) General Relationship for Thermal Oxidation of Silicon. Journal of Applied Physics 36 (12):3770-&

10. Chou KC (2006) A kinetic model for oxidation of Si-Al-O-N materials. Journal of the American Ceramic Society 89 (5):1568-1576. doi:DOI 10.1111/j.1551-2916.2006.00959.x

11. Hou XM, Chou KC (2008) Comparison of the Diffusion Control Models for Isothermal Oxidation of SiAlON Powders. J Am Ceram Soc 91 (10):3315-3319. doi:DOI 10.1111/j.1551-2916.2008.02631.x

12. He JY, Ponton CB (2008) Oxidation of SiC powders for the preparation of SiC/mullite/alumina nanocomposites. Journal of Materials Science 43 (12):4031-4041. doi:DOI 10.1007/s10853-007-2332-0

13. Ollero P, Serrera A, Arjona R, Alcantarilla S (2002) Diffusional effects in TGA gasification experiments for kinetic determination. Fuel 81 (15):1989-2000

14. Gomez-Barea A, Ollero P, Arjona R (2005) Reaction-diffusion model of TGA gasification experiments for estimating diffusional effects. Fuel 84 (12-13):1695-1704. doi:DOI 10.1016/j.fuel.2005.02.003

15. Zouaoui N, Brilhac JF, Mechati F, Jeguirim M, Djellouli B, Gilot P (2010) Study of experimental and theoretical procedures when using thermogravimetric analysis to determine kinetic parameters of carbon black oxidation. J Therm Anal Calorim 102 (3):837-849. doi:DOI 10.1007/s10973-010-0831-8

16. Levenspiel O (1999) Chemical reaction engineering. 3rd edn. Wiley, New York

17. Lanfrey PY, Kuzeljevic ZV, Dudukovic MP (2010) Tortuosity model for fixed beds randomly packed with identical particles. Chem Eng Sci 65 (5):1891-1896. doi:DOI 10.1016/j.ces.2009.11.011

18. Niksiar A, Rahimi A (2009) A study on deviation of noncatalytic gas-solid reaction models due to heat effects and changing of solid structure. Powder Technol 193 (1):101-109. doi:DOI 10.1016/j.powtec.2009.02.012

19. Batarseh KI, Swaney GP, Stiller AH (1989) A Mathematical-Model for Heterogeneous Reactions with a Moving Boundary. Aiche Journal 35 (4):625-634

20. Crank J (1975) The Mathematics of Diffusion. Oxford Press

21. Hou XM, Chou KC (2008) Model of oxidation of SiC microparticles at high temperature. Corrosion Science 50 (8):2367-2371. doi:DOI 10.1016/j.corsci.2008.06.006

22. Narushima T, Goto T, Hirai T (1989) High-Temperature Passive Oxidation of Chemically Vapor-Deposited Silicon-Carbide. Journal of the American Ceramic Society 72 (8):1386-1390

23. Shimoo T, Toyoda F, Okamura K (2000) Oxidation kinetics of low-oxygen silicon carbide fiber. Journal of Materials Science 35 (13):3301-3306

24. Das D, Farjas J, Roura P (2004) Passive-oxidation kinetics of SiC microparticles. Journal of the American Ceramic Society 87 (7):1301-1305

25. Song Y, Dhar S, Feldman LC, Chung G, Williams JR (2004) Modified Deal Grove model for the thermal oxidation of silicon carbide. J Appl Phys 95 (9):4953-4957. doi:Doi 10.1063/1.1690097

26. Zheng Z, Tressler RE, Spear KE (1990) Oxidation of Single-Crystal Silicon-Carbide .1. Experimental Studies. Journal of the Electrochemical Society 137 (3):854-858

27. Wittberg TN, Sen Wang P, Hsu SM (2003) Surface oxidation kinetics of SiC powders in wet and dry air studied by x-ray photoelectron spectroscopy and bremsstrahlung-excited Auger electron spectroscopy. Surface and Interface Analysis 35 (10):773-778. doi:Doi 10.1002/Sia.1598

CHAPTER 5 ARTICLE 2: FABRICATION OF MULLITE-BONDED POROUS SIC CERAMICS VIA A SOL-GEL ASSISTED IN SITU REACTION BONDING

Omid Ebrahimpour, Charles Dubois and Jamal Chaouki

Department of Chemical Engineering, École Polytechnique de Montréal, P.O. Box 6079, Station Centre-Ville, Montréal, Canada

Parts of this work have been presented in 62nd Canadian Chemical Engineering Conference, 2012, Vancouver

Abstract

In the present work, mullite-bonded porous SiC ceramics were fabricated using reaction bonding techniques. The morphologies, phase composition, open porosity, pore size distribution and mechanical strength of porous ceramics were examined as a function of alumina sources (calcined nano-sized alumina powder and alumina sol prepared from hydrolysis of aluminium isopropoxide) and contents. It was found that the addition of alumina in powder form effectively enhanced the strength and decreased the porosity. In contrast, when alumina was added in sol form, a reverse effect was observed. Moreover, it was revealed that when a portion of calcined alumina was replaced by alumina sol, the mechanical properties improved significantly (more than 30%) as well as porosity compared to the traditional method. Pore size distribution analysis showed that the dispersion of nanosize alumina powder and SiC micro-particles in alumina sol is strongly improved compared to mixing in ethanol.

Keywords: porous SiC ceramics, mullite, alumina sol, reaction bonding technique, sol-gel rout

5.1 Introduction

The excellent combination of physical, chemical and mechanical properties of porous SiC ceramics makes them one of the most attractive candidates in a wide variety of high temperature

structural applications, such as hot-gas or molten-metal filters, a catalyst support, a thermal insulator and refractory materials [1]. However, to self-bond SiC together, a temperature higher than 2000 °C is required due to the strong covalent nature of the Si–C bond [2]. In order to produce porous SiC ceramics at a lower sintering temperature, changing the sintering environment or adding sintering aids has been proposed. She et al. [3] developed an oxidation bonding technique which involves heating the SiC powder compact in air instead of an inert atmosphere. As a result of the oxidation, the SiC particles were bonded by silica or cristobalite, which exhibited good oxidation resistance [4].

The mechanical and physical properties of oxidation-bonded porous SiC ceramics can be enhanced by the addition of Al_2O_3 to the starting materials. In this method, SiC particles and alumina powders, used as a sintering aid, are mixed in a suitable liquid, such as alcohol or water, followed by drying and pressing and, finally, are heated in air. During the heating stage (over 1400 °C), the SiC particles are bonded by both silica and mullite ($3Al_2O_3.2SiO_2$) by an in-situ reaction-bonding technique [5]. Considering the good oxidation resistance, the high temperature stability, and the slight difference in the thermal expansion coefficient between mullite (5.3×10^{-6}/K at 0–1000 °C) and SiC (4.7×10^{-6}/K at 0–1000 °C) compared to cristobalite (17.5×10^{-6}/K at 0–700 °C), mullite-bonded porous SiC ceramics are expected to exhibit better mechanical properties [5-7].

Recently, the fabrication of porous SiC ceramics via the reaction bonding technique has been studied from different viewpoints. The effects of other additives, such as Y_2O_3, MgO, and CeO_2, on the mechanical properties of porous SiC ceramics have been investigated [8-11]. Li et al. [12] examined the effect of molding pressures, bonding phase contents, and SiC particle sizes on the flexural strength of porous SiC-based ceramics. It was observed that by increasing the molding pressure on the green body, the porosity decreased while the flexural strength increased. In addition, it was also reported that decreasing the particle size of the starting materials increased both porosity and mechanical strength. Kumar et al. [6] studied the role of aluminum sources on microstructure and the strength of mullite-bonded porous silicon carbide. They used four different aluminum sources (Al, AlN, Al_2O_3 and $Al(OH)_3$) to produce porous ceramic and reported that materials based on alumina powders show the highest strength and lowest porosity. To increase the porosity of the final product, some pore seeding additives, such as graphite, yeast

or polymer beads, are incorporated with the starting materials [5, 13, 14]. During the heating of the compact powders, these pore-formers burn out and pores are produced.

Although many studies have been done on forming porous SiC bodies via reaction bonding techniques, more investigation is still required to improve the process. In particular, the effect of sintering aid contents on the final structural properties of the product is yet to be fully understood. For example, Chi et al. [13] reported that the optimal content of Al_2O_3 was about 5-10 wt. % and any increase drastically decreases the flexural strength of the product. They used SiC with an average particle size of 21 μm and 15 μm Al_2O_3 as the starting materials. In contrast, She et al. [3] observed that increasing alumina from 5.5 wt. % to 26.5 wt. % significantly improved the flexural strength. They mixed micro-sized SiC particles with submicron alumina powders. Moreover, Li et al. [12] reported that the maximum flexural strength for their system was governed by the addition of 20 wt% bonding phase content. This method suffers, however, from the strong agglomeration of powders and the difficulty in dispersing particles, especially fine particles (sintering aids), homogeneously into the micro-sized particles (SiC), which substantially degrades the mechanical properties of the final ceramics. Ding et al. [5] showed that alumina submicron-particles were agglomerated and did not make contact with the SiC parts of the porous products.

The dispersion of particles can be improved by using the sol-gel technique [15, 16]. This technique has been applied successfully to fabricate ceramic composites [17-19]. The potential advantages of sol–gel processing for ceramic composites include a better fine-scale mixing and a relatively low densification temperature. Therefore, sol-gel processing is also an attractive approach for the production of porous ceramics. More recently, Kayal et al. [20] fabricated mullite-bonded porous SiC ceramics using the infiltration technique. They first heated the compacted mixture of SiC and petroleum coke powders in air to 1100 °C to have sufficient mechanical strength for holding it. Subsequently, samples were infiltrated with a liquid precursor of mullite sol followed by heating at a temperature between 1300-1500 °C. However, the method required twice the heat (over 1000 °C), which consumed a lot of energy.

The purpose of the present work is to study the effect of alumina content from different sources on characteristic properties of porous SiC ceramics. In addition, implementation of the sol-gel technique as a means of increasing the dispersion of sintering aids into the starting material and

enhancing the mechanical and physical properties of the porous sample is also investigated. In this study, SiC particles were bonded by mullite formed by oxidation-derived SiC and different forms of alumina (powder, alumina sol or a combination of them). A comparison of phase composition, microstructure, flexural strength, open porosity and pore size distribution of the resulting porous SiC ceramics has also been made.

5.2 Experimental procedure

5.2.1 Materials and characterization

The starting material was α-SiC powder (99.7% purity, LabMAT, Canada) and the submicron size sintering additive was α-Al_2O_3 calcined powder (99.95% purity, LabMAT, Canada). The volume averaged mean particle size and the specific surface area of the powders were measured by a Malvern Mastersizer S, UK and a Quantasorb Analyzer, USA, respectively. Physical properties of the materials are listed in Table 5.1. The mean particle size of SiC was found to be 11.5 μm (d_{10}=6.6 and d_{90}=16.2) and for alumina was 270 nm (d_{10}=188 nm and d_{90}=354 nm). As illustrated in Figure 5-1, silicon carbide particles are irregular in shape as compared to alumina powders.

Table 5.1 Powder compositions and characterization of materials used in this study

Material	Phase	Purity (wt. %)	Density (g/cm^3)	Average article size (μm), Volume method	Surface area (m^2/g) (BET)
SiC	α	99 >	3.20	11.1	0.87
Al_2O_3	α	99.9	3.95	0.27	8.5

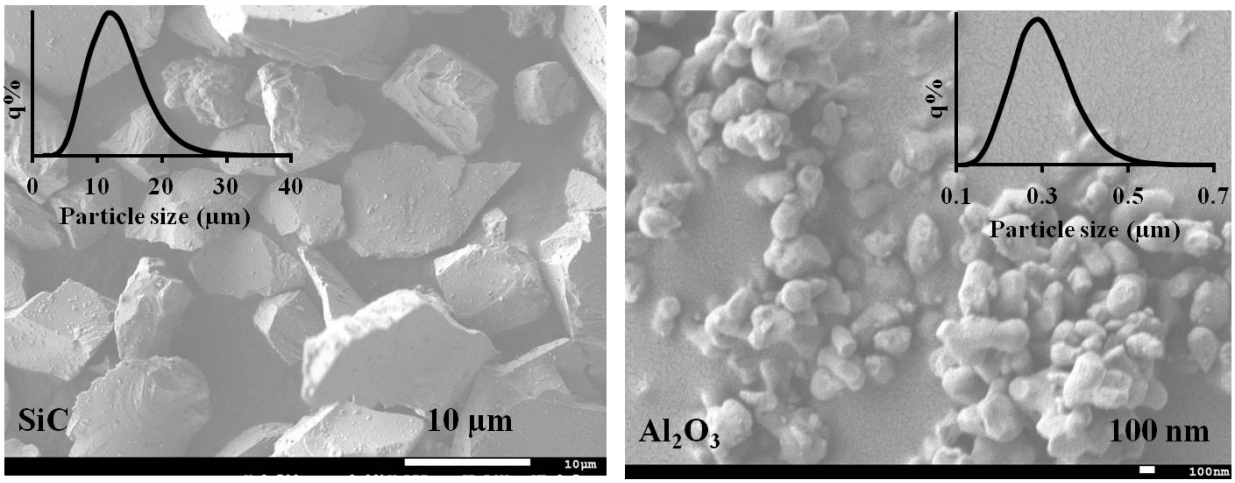

Figure 5-1 SEM micrographs and particle size distribution of starting materials

5.2.2 Synthesis and characterization of alumina sol

Alumina sol was synthesized with the method developed by Yoldas [21]. Aluminum isopropoxide (AIP, Aldrich, 98%) was used as the alkoxide source of alumina. In a typical experiment, distilled water was heated up to 85 °C followed by adding AIP in the form of powder. After stirring for about one hour, the resultant white precipitate was peptized by adding a small amount of 10% HCL (Merck, 37%) in order to set the pH of the solution to 3.5-4. The transparent solution was formed after 24 hours of mixing. The resultant sol was cooled to room temperature. The reaction was performed in the four necks reactor equipped with the heater and magnetic stirrer under reflux. The molar ratio of water to AIP was 100:1.

The morphology of sol was determined by transmission electron microscopy (TEM, Philips CM 30). The crystalline studies were performed via X-ray diffraction XRD analysis. Fourier transform infrared (FTIR) spectroscopy was performed to identify the functional groups on the sample surface. FTIR tests were carried out using the pellet technique in the 400 to 4000 cm^{-1} range, with 64 scans and a resolution of 4 cm^{-1}. The specimens for the IR analysis were obtained by mixing the samples with KBr at a ratio of 1:100 followed by compressing them to form a transparent disc.

5.2.3 Preparation and characterization of SiC porous ceramics

Different approaches were used to assess the effect of alumina sources and contents on the properties of porous SiC ceramics. In the first approach, silicon carbide and sub-micron alumina powders at certain weight ratios were mixed with 2.5 wt. % of polyvinyl butyral (PVB) binder and ethanol in a high-energy ball mill for 30 minutes. The resulting slurries were first dried under stirring and hand-milled in a mortar and pestle. Then, they were sieved through an 80-mesh screen, and, finally, uniaxially pressed into rectangular bars of 4.5 mm × 10.0 mm × 50.0 mm under a 50 MPa pressure in a stainless steel die. The specimens were heated in a box furnace at a heating rate of 2 °C/min to 900 °C followed by a second 5 °C/min ramp to 1500 °C, and then sintered at that temperature for 3 hours in air. It should be noted that in the starting materials, besides a low amount of polyvinyl butyral (7 vol. %), no pore formers, such as graphite, were used and, consequently, most of the porosity results from the stacking of particles.

In the second approach, SiC particles were added to the different amounts of alumina sol and the slurry was stirred-dry at room temperature. The amount of alumina sol was adjusted to yield the desired alumina content in the final product with respect to the SiC powders. The resulting powders were then further dried in an oven at 100 °C, before being crushed and passed through a 80-mesh sieve. The weight ratio of SiC to alumina was calculated from the quantity of sol that was finally converted to calcinated α-Al_2O_3. A similar process has been carried out to fabricate porous SiC ceramics.

In the last process, SiC powders and alumina sub-micron powders were directly mixed in the alumina sol. In other words, a fraction of alumina was formed from alumina sol. From these mixtures, the porous ceramic samples were produced using the procedure already described in the second approach.

Weights of all samples were measured before and after sintering to assess the oxidation degree of SiC particles. Skeletal densities of porous samples were determined by a gas pycnometer (Accupyc II 1330 helium pycnometer). Pore size distribution was obtained using mercury porosimetry (Micromeritics AutoporeIV). The open porosity of the final product was determined from the total mercury intrusion volume and the skeletal density of the sample. Moreover, the porosity of green porous samples was determined by measuring their weights and dimensions. Flexural strength tests were performed using a three-point bending test with a support distance of

30 mm and a cross-head speed of 0.5 mm/min using an Instron Universal Testing machine (Model 1123, Instron, Canton, MA, USA). The procedure was inspired from ASTM C1161-2c. The deflection measurement was based on LVDT with a resolution of 0.05% and Young's modulus was determined using standard software (Instron Bluehill-2, UK). Specimens were machined and polished to 3.0 mm × 4.0 mm × 36.0 mm and at least five specimens were tested to obtain the average strength. The microstructure and morphology of porous SiC ceramics were observed by scanning electron microscopy (SEM, Model JSM-5600LV, JEOL, Japan).

5.3 Results and Discussion

5.3.1 Characterization of alumina sol

The TEM micrographs of boehmite, dried at room temperature and calcined at 550 °C for 2 hours, show the highly homogeneous microstructure in alumina (Figure 5-2-a and b) with a needle-like shape and grain size from 15 to 25 nm that interconnect into nano rods. The thickness of the particles increased from 2.-3 nm to 4.-6 nm as the temperature increased.

Figure 5-3 contains the X-ray diffraction patterns for dried alumina sol after being heat-treated at various temperatures. The XRD pattern of dried alumina is well matched with the reference data of AlOOH (JCPDS 49-0133), which confirms the formation of boehmite [22]. After heating the boehmite powder at 550 °C for 2 hours, two new peaks appeared at 46.2 °C and 67.3 °C, which are the characteristic peaks for γ-Al_2O_3, according to JCPDS 29-0063. Further heating at 1350 °C resulted in a phase transformation to alpha phase as determined by JCPDS 42-1468.

Figure 5-4 presents the FTIR spectra obtained for the dried and heat-treated boehmite samples at different temperatures (150 °C, 350 °C, 550 °C and 1350 °C) for 2 hours. In the dried sol at room temperature, seven major peaks can be identified whereas if the temperature is increased the number of peaks decreases. The broad band in the spectral range of 3300-3500 indicates the presence of the –OH stretching of hydrogen bonded aluminum oxy-hydroxide (AlO(OH)). The next band was observed at 1635 cm^{-1}, which is mainly due to the bending vibration of the residual water molecule [23]. The subsequent absorption peak observed at 1074 cm^{-1} is assigned to the Al-OH bending mode of boehmite [24, 25].

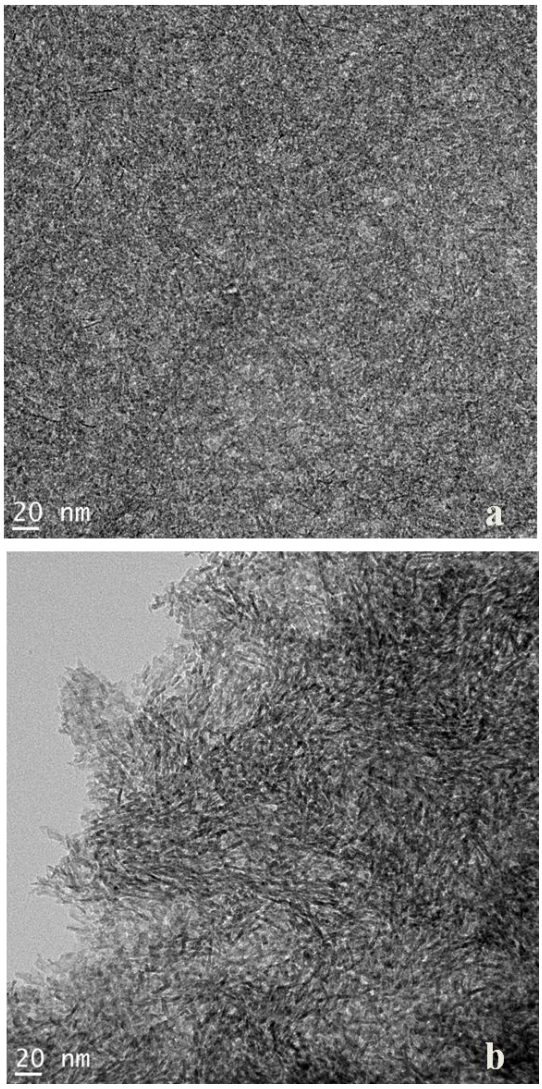

Figure 5-2 TEM images of alumina sol (a) dried and (b) calcined at 550 °C.

It should be noted that when the sample is progressively heated, the intensity of the above peaks decreases. This indicates that the number of -OH sites on the surface of the alumina is reduced during the calcination procedure. The band observed at 738 cm^{-1} corresponds to the bending vibration of the ALO_4 groups and the band at 613 cm^{-1} is assigned to the ALO_6 octahedra [25-27]. The peaks at 889 cm^{-1} and 470 cm^{-1} are both associated with the existence of pseudo boehmite in the sample [26, 28]. As the temperature was increased up to 550 °C, the mentioned peaks disappeared and broad peaks formed in the lower frequency range (500–900 cm^{-1}) due to the coordination of Al atoms and the transition of the alumina phase to γ-Al_2O_3 [24, 29, 30]. Further heating of the boehmite sample at 1350 °C formed three bands at 640, 605 and

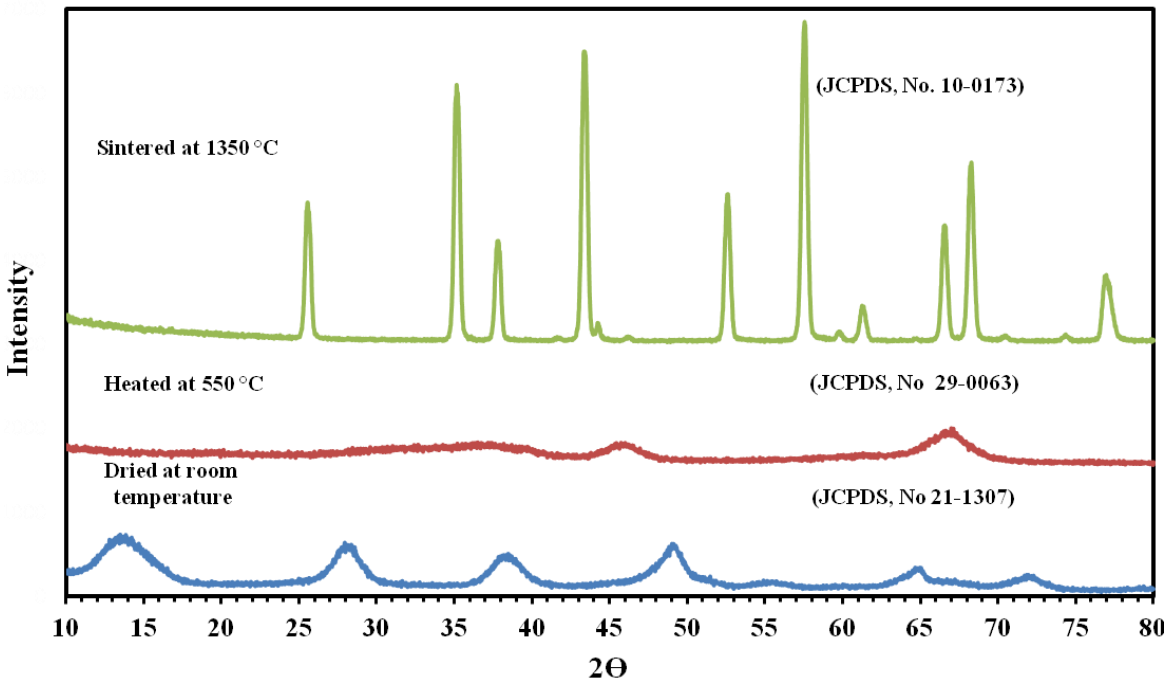

Figure 5-3 X-ray diffraction patterns for dried alumina sol and after heat treated

453 cm^{-1}, which confirms the presence of α-alumina [23, 31]. It should be pointed out that during the heating of the alumina sol at 350 °C, the resulting sample appeared brown in color due to the carbon residue during decomposition. At temperatures higher than 550 °C a white powder was obtained. The FTIR results strongly support the results of the XRD characterization. Consequently, heating the obtained alumina sol resulted in the phase transformation from boehmite to γ as one of the meta-stable phases of alumina and to the stable α-alumina (corundum) phase. Similar results for the transition phases of alumina during heat treatment were reported earlier [32, 33].

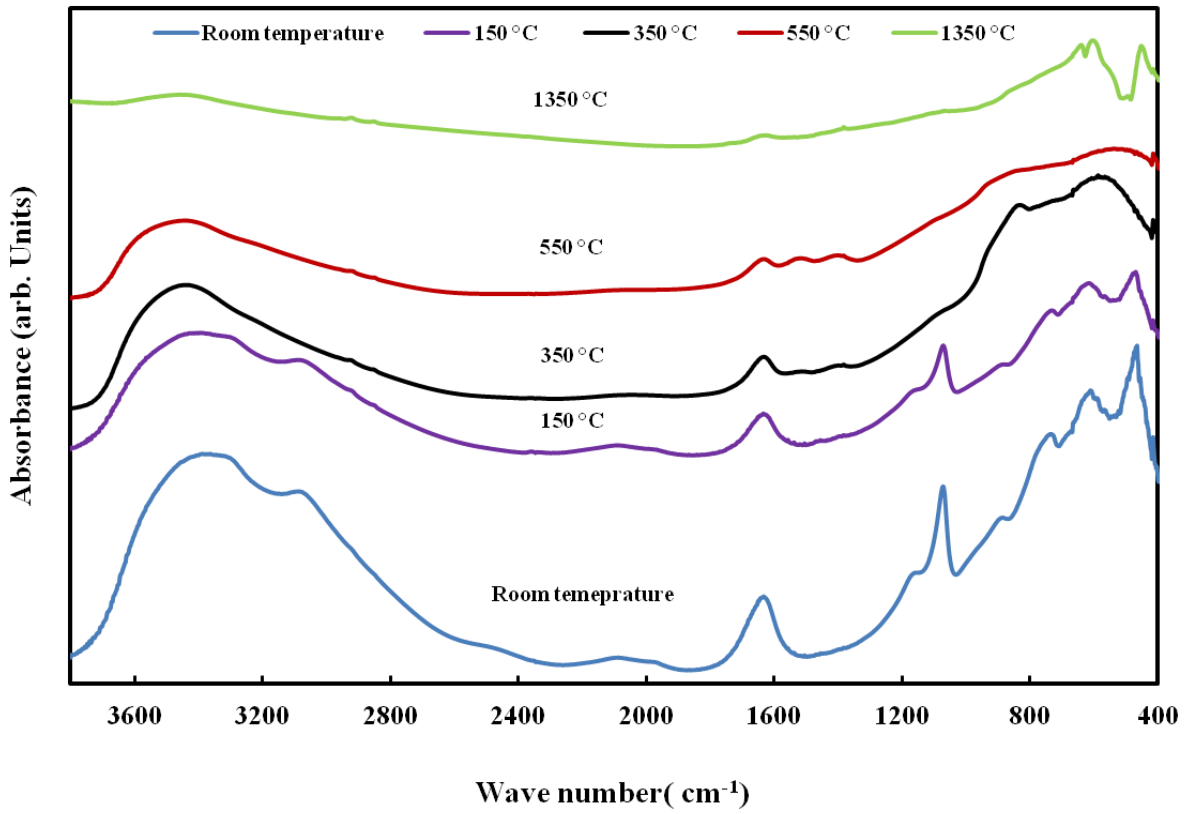

Figure 5-4 FTIR spectra obtained for the dried and heat treated boehmite samples

5.3.2 Fabrication of porous ceramic: the effect of alumina contents and sources

The skeletal density, flexural strength, open porosity and pore size of the porous SiC ceramic with different Al_2O_3 content and sources are summarized in Table 5.2 and Table 5.3. The results indicate (Table 5.2) that the addition of nanopowder to the starting powder resulted in a decrease of porosity and an increase of flexural strength. In contrast, it was observed that introducing alumina in the sol form brought a decrease in flexural strength and increased the porosity. The relation between the strength of porous material and its porosity can be expressed as follows [34]:

$$\sigma = \sigma_0 \exp(-bP) \qquad 5\text{-}1$$

Where σ_0 and σ are the strength of a non-porous structure and the strength of a porous structure at a P porosity, respectively, and b is an empirical constant, which depends on the pore structure and material composition.

Table 5.2 Effect of Al_2O_3 additions in calcined form on the flexural strength, open porosity and pore size

Alumina contents w/w %	Green porosity (≈ %)	Flexural strength (MPa)	Porosity (%)	Average median pore diameter (µm)	skeletal density (g/cm^3)
0	46.5	15.5 ± 1.4	43.1	3.8	2.88
5	44.2	20.3 ± 1.9	41.4	3.26	2.92
10	42.3	22.9 ± 1.3	38.3	2.79	2.95
20	40.5	25.2 ± 2.3	36.5	2.37	3.02
30	36.5	27.8 ± 2.2	34.2	1.7	3.09
35	34.2	30.9 ± 1.3	32.3	1.57	3.11
40	33.1	38.6 ± 0.9	29.5	1.1	3.20

Table 5.3 Effect of Al_2O_3 additions in sol form on the flexural strength, open porosity and pore size

Alumina contents w/w %	Flexural strength (MPa)	Porosity (%)	Average median pore diameter (µm)	skeletal density (g/cm^3)
5	21.9 ± 1.7	41.4	3.11	2.92
10	18.5 ± 0.8	42.6	2.80	2.95
20	13.1 ± 0.7	44.0	2.65	3.03
30	11.5 ± 0.9	46.5	2.7	3.10
40	7.9 ± 0.9	48.3	2.82	3.18

The evolution of the XRD patterns of the specimens with both Al_2O_3 sources and different alumina contents is illustrated in Figure 5-5. When there is no alumina introduced in the specimen, only SiC and cristobalite phases exist (Figure 5-6). At the studied sintering temperature, SiC particles are bonded by silica (Figure 5-6-a) via a passive oxidation reaction:

$$SiC + 2\,O_2 \rightarrow SiO_2(amorphous) + CO_2(g) \qquad 5\text{-}2$$

The exiting of CO_2 from the silica can produce small pores as illustrated in Figure 5-6. It was shown by our research group that the oxidation rate of SiC strongly depends on the reaction temperature and SiC particle size [35]. Increasing the temperature (over 1200 °C) causes the oxidation rate to increase and changes the crystalline structure to the cristobalite phase (Figure 5-6):

$$SiO_2(amorphous) \rightarrow Cristobalite \quad 5\text{-}3$$

The addition of alumina caused a new phase of mullite to be present according to the following reaction during the sintering:

$$3Al_2O_3 + 2\,SiO_2 \rightarrow 3Al_2O_3.2\,SiO_2(mullite) \quad 5\text{-}4$$

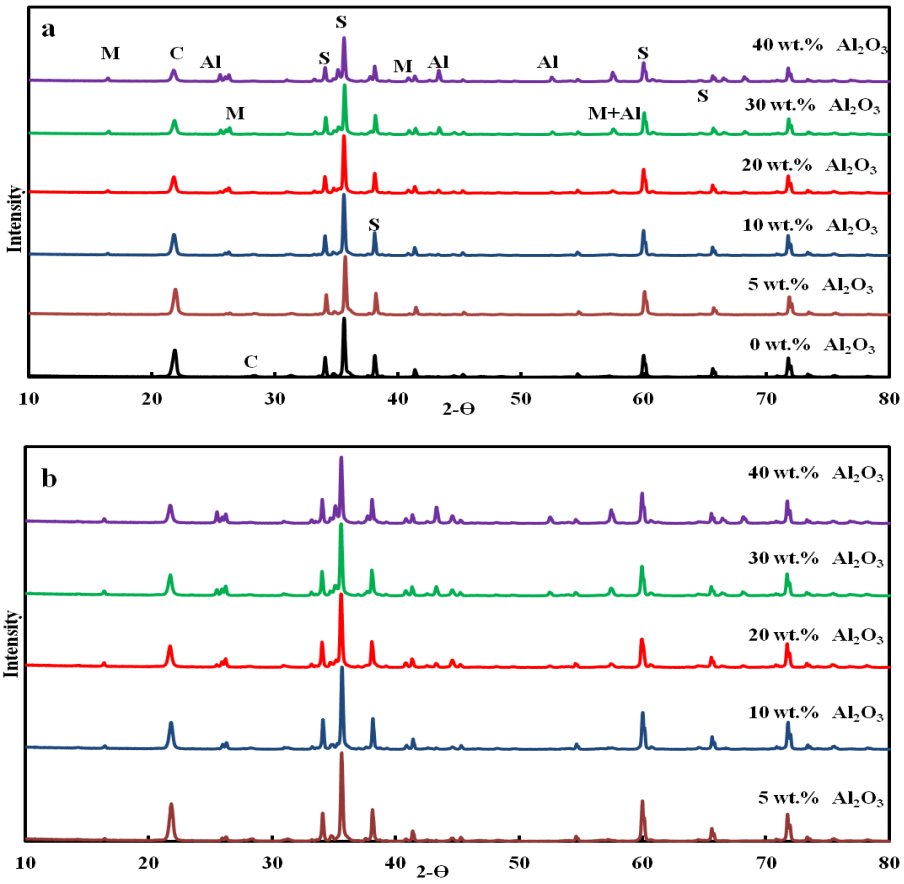

Figure 5-5 XRD patterns of porous SiC ceramics with different content of alumina and sources; a) calcined and b) alumina sol; sintered at the 1500 °C for 3 h (Al: alumina, C: cristobalite, M: mullite and S: silicon carbide).

When more Al_2O_3 was added, the amount of mullite and alumina increased, as demonstrated in Figure 5-5 by the increase in the intensity of their peaks for the two alumina sources. On the other hand, the decrease in the cristobalite peaks in the XRD patterns indicates the consumption of cristobalite by alumina.

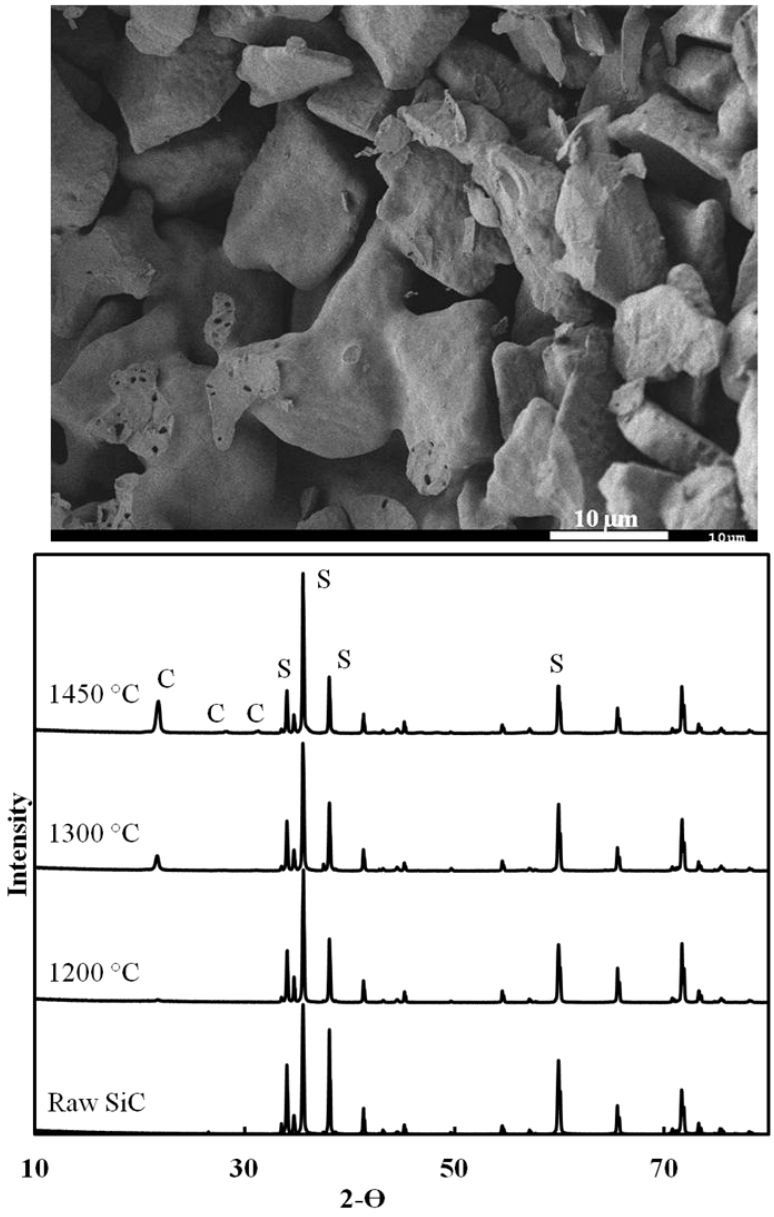

Figure 5-6 SEM micrograph of porous SiC which was prepared by oxidation (0 wt. % alumina) in air at 1500 °C for 3h (up); XRD patterns of raw SiC powder oxidized at indicated temperature in air (down) (C: cristobalite; S: silicon carbide).

When there are no alumina particles added to the starting material, the average pore size is about 4 μm (Table 5.2). This narrow pore size is a result of SiC particles stacking together. When calcined sub-micron alumina particles are mixed with the SiC powders, some of them come in contact with SiC and react with cristobalite to form mullite. The rest filled the pores between SiC particles and caused the average pore size to shift toward lower values as observed from mercury porosimetry results in Figure 5-7.

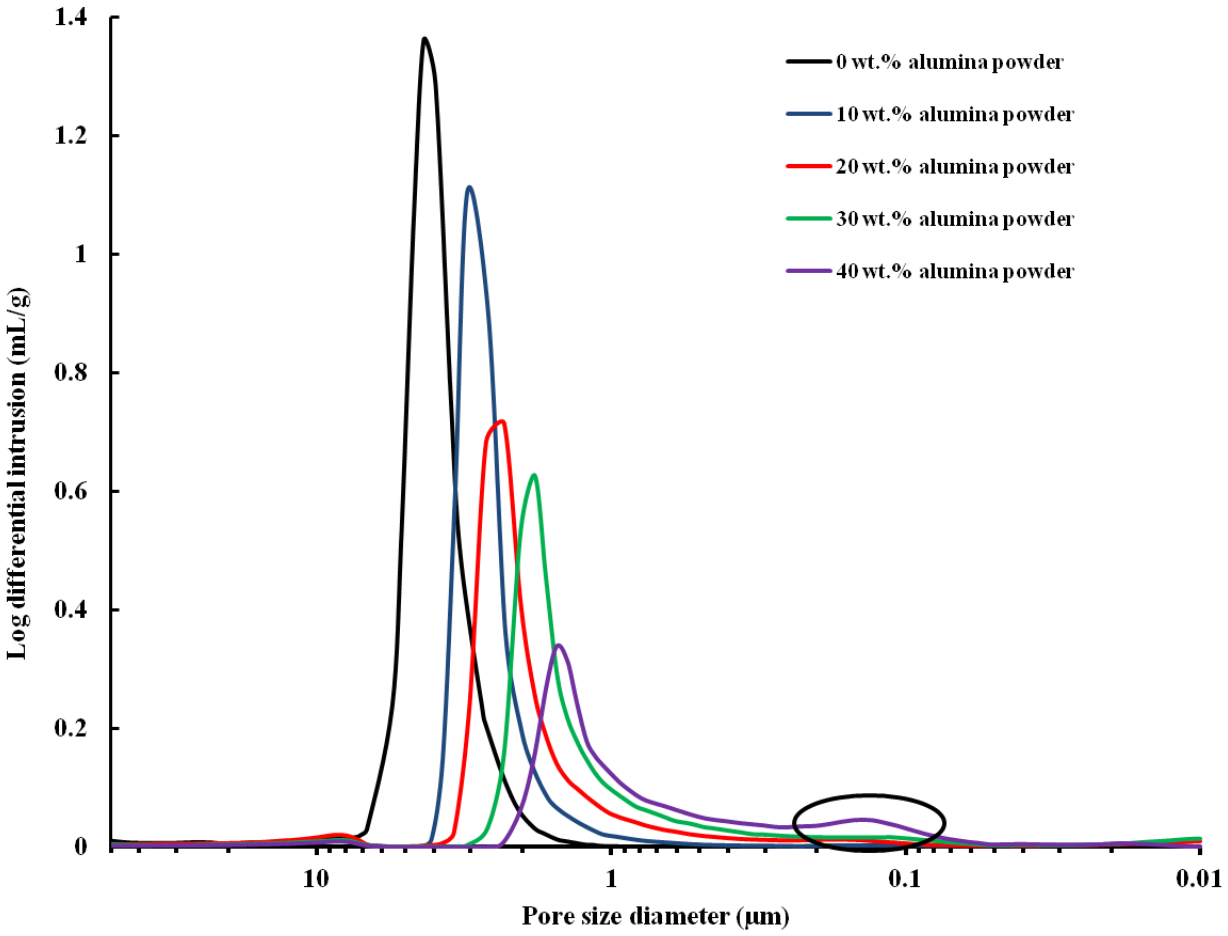

Figure 5-7 Pore size distribution in porous SiC ceramics at different alumina powder contents, sintered at 1500 °C in air for 3 hr

As reported in Table 5.2, the density of the green samples is decreased with an increase in the weight ratio of alumina nano powders to SiC micro particles. For a binary system, the packing density depended strongly on the ratio size of particles and their shape [36, 37]. In the present system, according to a model proposed by Kyrylyuk et al.[36], assuming that both types of particles are spherical, the maximum packing density is 86% when about 33 wt. % of alumina was added to the SiC particles. Adding more fine particles to the system decreases the packing density [36]. For the current system, it was observed that even the addition of the 40 wt. % nanosize alumina powders increased the packing density, which resulted in better mechanical properties and a lower porosity. This higher value (over 33 wt. %) can be attributed to the irregularly-shaped particles, especially SiC. The enhancement of a mechanical property with an increase in alumina nano powder content is in line with the results reported by She et al.[3]. Actually, if the ratio size of SiC to alumina is small, the maximum packing density will be decreased drastically [36]. Therefore, the size ratio of the starting particles is a key factor in determining the optimal contents of sintering aids.

In order to better understand the effect of alumina source and content, the morphology, pore size distribution and crystalline structure (in high magnification) of the porous SiC prepared by alumina sol and calcined alumina powders, where 10 wt. % and 40 wt. % of alumina were added to SiC, are presented in Figure 5-8 and 9, respectively. In the case of 10 wt. % in alumina, pore size distributions for both samples are very similar. As clearly seen from SEM images, when alumina was added in powder form, some of the alumina particles, which were not reacted by cristobalite, can be observed, but when alumina was in the sol form, most of it was probably consumed to produce mullite, which readily bonds SiC together. XRD results (Figure 5-8) reveal that the relative intensity of mullite to alumina peaks increased significantly for the samples prepared with alumina sol in comparison to those where calcined powder was employed. During the mixing of SiC in alumina sol, most SiC surfaces, which are in direct contact with silica, are coated homogenously by a nano layer of alumina. A direct interface between silica and alumina in the sol-state (core-shell structure) decreases the diffusion resistance between them and, consequently, enhances the mullitization rate [38].

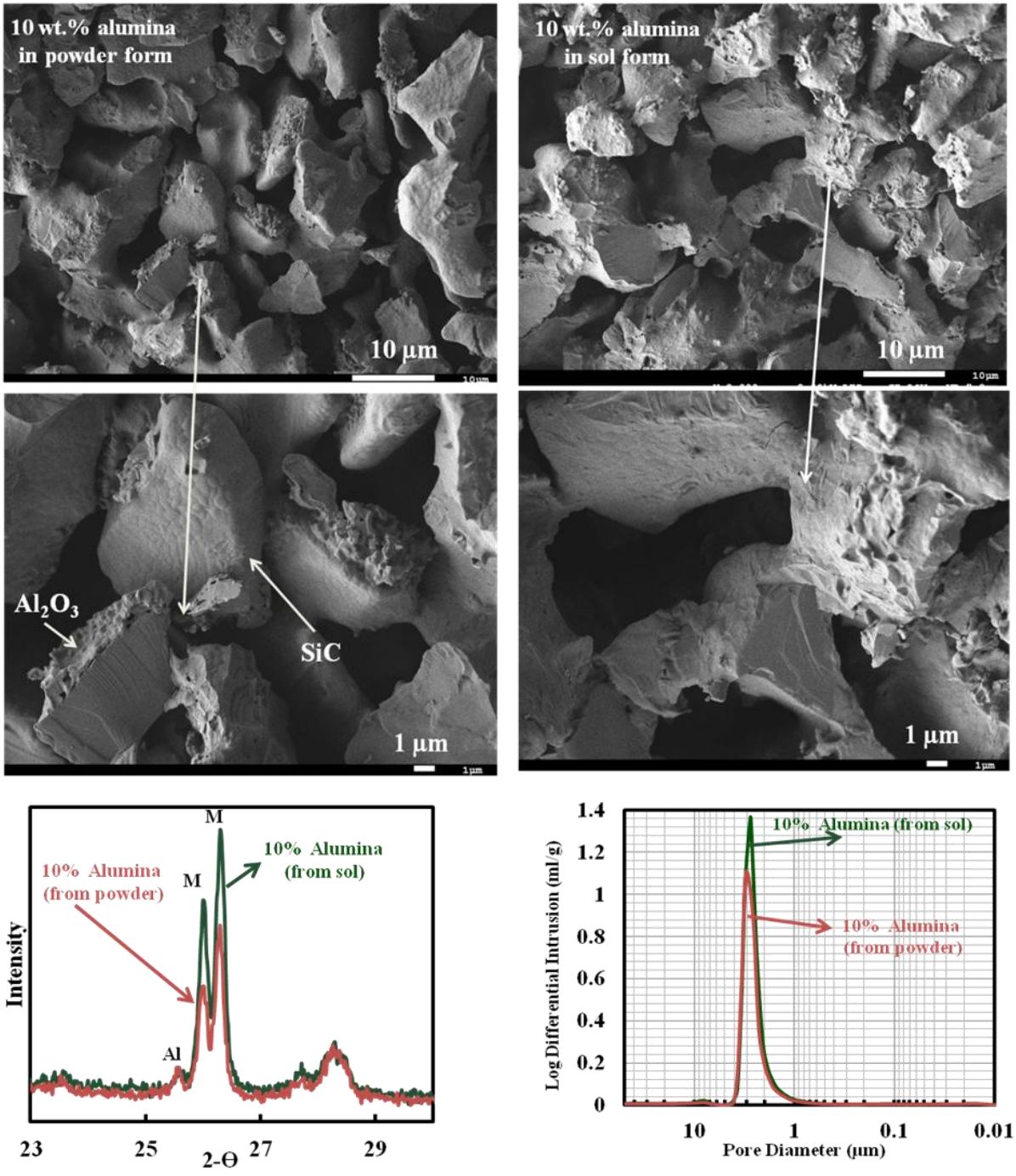

Figure 5-8 SEM micrographs, XRD and pore size distribution of porous SiC ceramics sintered at 1500 °C for 3 hr in air, Where 10%wt. Alumina (in the calcined powder or sol form) was added into SiC particles

For 40 wt. % alumina, SEM micrographs and pore size distribution show (Figure 5-9) that the morphology and structure of the porous samples are notably changed by varying the alumina source. However, XRD results show that the relative intensity of mullite to alumina was not significantly different for both samples. SEM micrographs demonstrate that SiC particles are in less contact when they are prepared by alumina sol compared to adding alumina in powder form. In the samples with calcined powder, most alumina powders are accumulated inside the pores (formed by stacking SiC particles) and between the SiC particles. Strong agglomeration of alumina particles creates small pores as inferred from a bump in the pore size distribution curves (Figure 5-7)

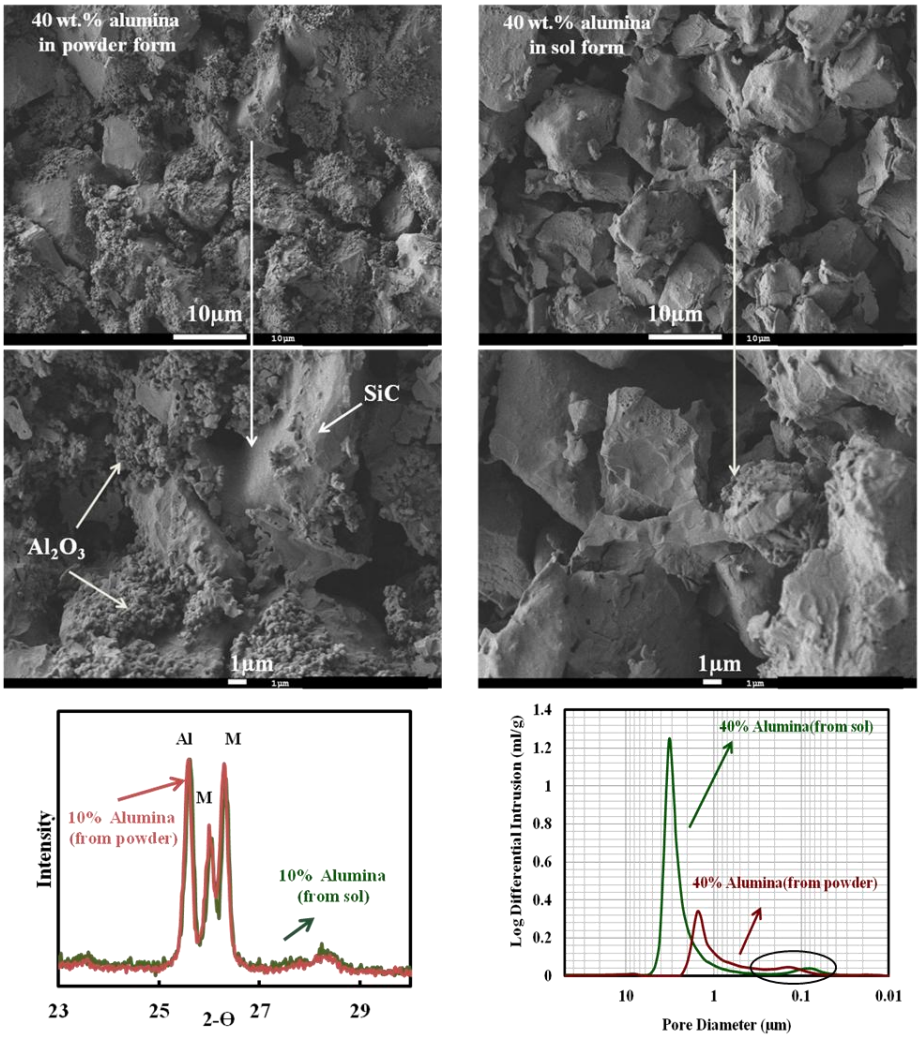

Figure 5-9 SEM micrographs, XRD and pore size distribution of porous SiC ceramics sintered at 1500 °C for 3 hr in air, Where 40%Wt. Alumina (in the calcined powder or sol form) was added into SiC particles

In the case of the addition of 40 wt. % pure sol-gel derived alumina, the green porosity of the samples is lower than the one using alumina powders (about 27%) due to the nature of alumina sol. However, during the heating of the green compact, organic groups in the dried boehmite burn out, which results in the porosity of the sample being increased and causing the SiC particles to have less contact with their neighboring SiC particles. Therefore, the neck bonds which are the result of the mullitization and oxidation between particles are weak. Moreover, when a high amount of alumina in the sol state is employed, the phase changes of alumina and shrinkage as explained previously in the characterization of the alumina sol section may cause stress and in turn lead to the formation of micro cracks in the green body, thus degrading the mechanical properties [39]. Hence, it is reasonable to have modest strength. However, when calcined alumina was used, since the mullite reaction occurs between SiC and alumina particles, which are between the SiC, it consequently bonds SiC together and enhances the mechanical strength.

5.3.3 Fabrication of porous ceramic: the addition of alumina in a combination of the sol and powder form

As shown previously, when the weight ratio of calcined alumina was more than 30 wt. %, the porous samples have sufficient strength for their practical application. However, if alumina in the sol form was added, the flexural strength cannot be reached at that level. In order to take advantage of the sol, it is interesting to investigate the properties of porous SiC ceramic, when prepared with a fraction of the alumina powder being replaced by an alumina sol. Table 5.4 summarizes the mechanical and physical properties of the porous SiC with different mass fractions of alumina sol.

Table 5.4 Effects of Al_2O_3 additions in sol form on the flexural strength, open porosity and pore size where the total alumina was 35 wt. %

Alumina sol contents w/w %	Flexural strength (MPa)	Porosity (%)	Average median pore diameter (µm)	skeletal density (g/cm^3)
0	30.9 ± 1.3	32.3	1.57	3.11
10	36.2 ± 2.5	34.7	1.67	3.09
20	40.6 ± 3.4	35.2	1.85	3.12
30	20.5 ± 1.0	39.0	2.01	3.11
40	18.9 ± 0.9	41.0	2.08	3.12

It was observed that the joint use of alumina sol and alumina powder, where 20 wt. % of alumina powder was replaced by alumina sol, resulted in an increase in porosity and, more notably, the mechanical strength was enhanced significantly (over 30%). It is enlightening to compare the pore size distribution and SEM micrographs when species were prepared with and without alumina sol for the sample with 35 wt. % of total alumina. As shown in Figure5-10, from the pore size distribution curve, the bumps resulting from the agglomeration of nano-particles are much smaller when SiC and alumina nano particles are mixed in alumina sol compared to the one dispersed in ethanol. Typical SEM images depict a good dispersion of alumina nano particles between SiC particles, which decreases the agglomeration of alumina powders for the samples mixed in sol state. In addition, the SEM observations demonstrate that the dispersion of the SiC and alumina nanopowders is considerably superior compared to when they are mixed in ethanol (Figure 5-11). It has been observed that, when they are prepared in the alumina sol, most of the SiC particles are covered by the mixture of alumina sol and sub-micron alumina powders.

It is proposed that the improved dispersion of alumina and SiC particles in alumina sol originates from the electrostatic and steric repulsion effects of the colloidal particle absorption. It is well accepted that the silicon carbide powder surface consists of a nano layer of silica on the surface of SiC particles, which hydrolyzes in alumina sol to form a silanol group, $\equiv Si(OH)^{-}$.

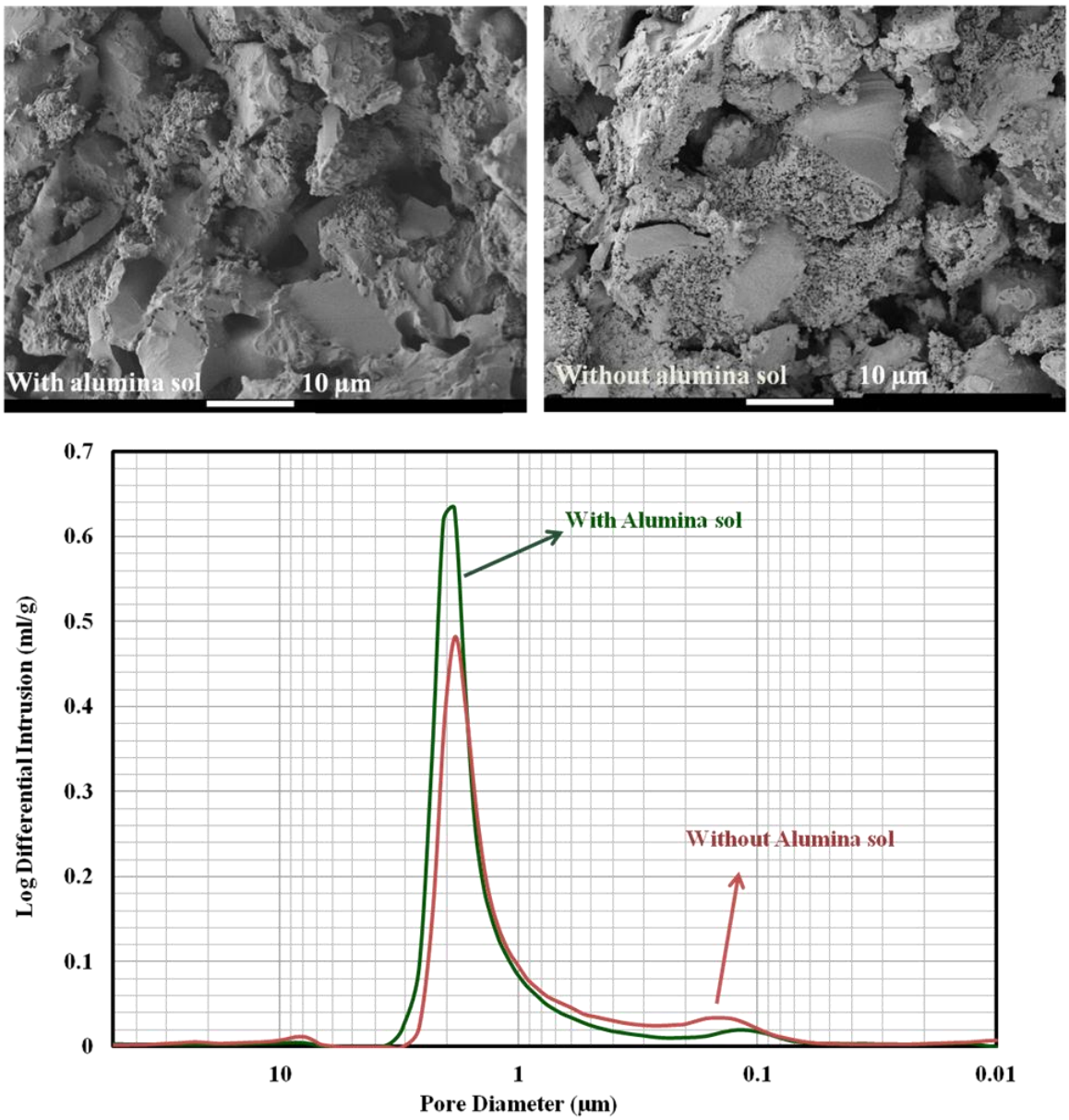

Figure 5-10 SEM micrographs and pore size distribution of porous SiC ceramics sintered at 1500 °C for 3 hr in air, where 35%wt. pure calcined alumina was added into SiC particles and where 20 wt% of calcined alumina was replaced by alumina sol

During the hydrolysis reaction in the pH range of 3.5 to 4, the positive specie, $[AlO_4Al_{12}(OH)_{24}(H_2O)_{12}]^{7+}$, well known as $Al_{13,}$ is produced, which may react with silanol by the following reaction:

(5)

$$\equiv Si(OH)^{-} + [AlO_4Al_{12}(OH)_{24}(H_2O)_{12}]^{7+} \rightarrow$$
$$\equiv Si - O - Al - AlO_4Al_{11}(OH)_{23}(H_2O)_{12}^{6+} + H_2O$$

This reaction causes at least a mono layer of alumina to form on the surface of SiC and change the surface characteristic to be similar to alumina [15]. Zeta potential experiments (results are not reported here) indicated that, at a pH of about 4, SiC particles have positive charges in the alumina sol while they have negative charges in water for that same pH, which supports the proposed mechanism and is in a good agreement with previous observations by other researchers [16,40]. In addition, it was shown that a continuous layer of alumina sol entails covering the alumina surface powders by the reaction between the sol clusters with hydrolyzed Al_2O_3 nano particles, which increases the electrostatic repulsion force [41].

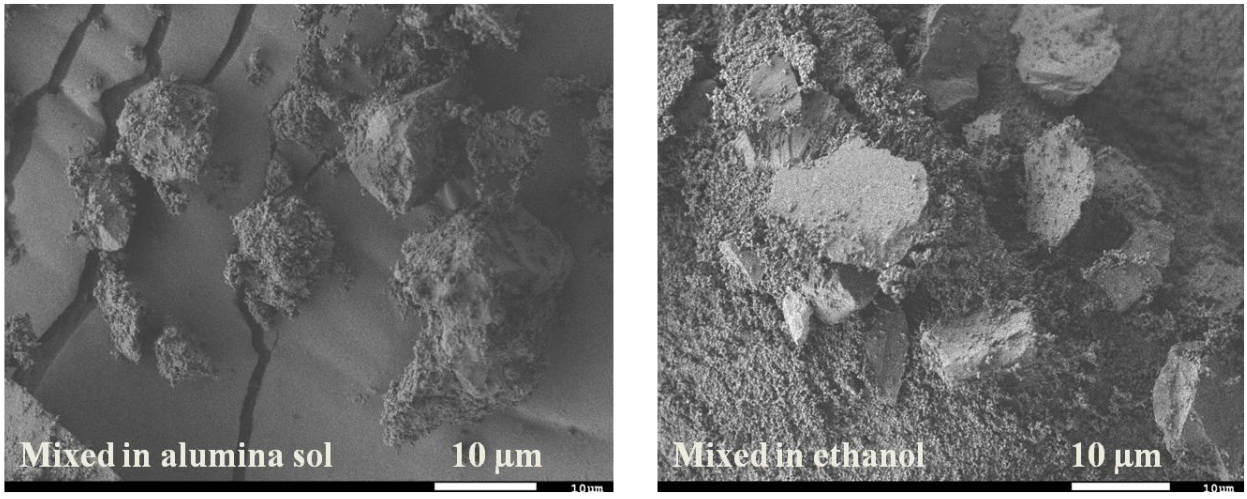

Figure 5-11 SEM micrographs SiC and alumina (35 wt. %) which was mixed in ethanol and alumina sol

Consequently, improving the mechanical properties results from the enhanced dispersion of SiC and alumina powders in alumina sol. The homogenous dispersion of SiC and alumina particles in alumina sol is attributed to the surface changes in the properties of SiC (as it acts like alumina), as well as the electrostatic and steric repulsion effects. In addition, coating SiC and alumina

particles with a thin layer of alumina sol avoids direct contact along the boundaries, which acts as a fast diffusion path and enhances the sintering process. These phenomena are not attainable when particles are mixed in ethanol.

Based on the experimental evidence presented in this study, it was confirmed that introducing a low amount of sintering additives by sol-gel routes to the starting materials enable the fabrication of porous ceramics with higher strength and porosity as compared to the traditional method. It is also worth mentioning that the thickness of the sol on the particles depends on the synthesis conditions (pH and concentration of the sol). Moreover, the total amount of sol strongly depends on the surface area of the starting particles. Application of this technique may be extended to homogenously coat starting materials with other sintering additives, such as Y_2O_3 and MgO, in sol form, when a lower amount of them is needed in the final product.

5.4 Conclusion

In this work, porous SiC ceramics were successfully produced at 1500 °C for 3 hours in air by a reaction bonding method using different sources and contents of alumina as the sintering aid. It was found that the addition of nano-sized alumina as a calcined powder increased the mechanical strength and reduced the porosity. Pore size distribution analysis also showed that the volume average pore size of the porous body shifted to smaller values as alumina nano particles were added to the starting materials. On the other hand, when alumina sol is used as the source of alumina, the mechanical strength decreased and porosity increased significantly. XRD results revealed that since there is a thin layer of alumina on SiC particles, for low amounts of alumina, the rate of mullite formation is higher due to the low mass diffusion rate between alumina and silica compared to using calcined alumina powder. Moreover, XRD and SEM analysis confirmed that, regardless of the alumina source, porous SiC substrates consist of the expected phases of mullite, cristobalite, alumina and SiC at the studied sintering temperature and mullite and cristobalite bonded SiC particles together.

Furthermore, it was found that if alumina is introduced to the system as a combination of sol and nano powder forms, the mechanical strength increased significantly compared to the specimens that were made using alumina powders alone. In this study, a flexural strength of 40.6 MPa with

a porosity of 35% was obtained when 20 wt. % of the alumina powders was replaced by an alumina sol. The improved mixing of alumina and silicon carbide in alumina sol as well as the decrease in the mass transfer resistance between alumina and silica led to improved mechanical properties of the final porous body.

Finally, it is proposed that the optimum amount of alumina as the sinter additive depends on the particle size ratio between the SiC and alumina particles. Likewise, the optimum amount of derived alumina from the alumina sol depends on the total surface area of the particles and the properties of alumina sol.

5.5 Acknowledgments

The authors would like to express their sincere thanks to NSERC for the Idea to Innovation grant, which provided the financial support for this work. They also would like to thank Sylvie St-Amour, FPInnovations, Canada, for her help with the mercury porosimetry measurements and Professor Nathalie Tufenkji, McGill University, Canada, for the use of the Zeta potential meter.

5.6 References

1. Studart, A.R., et al., *Processing routes to macroporous ceramics: A review.* Journal of the American Ceramic Society, 2006. **89**(6): p. 1771-1789.
2. Sigl, L.S. and H.J. Kleebe, *Core Rim Structure of Liquid-Phase-Sintered Silicon-Carbide.* Journal of the American Ceramic Society, 1993. **76**(3): p. 773-776.
3. She, J.H., et al., *Oxidation bonding of porous silicon carbide ceramics.* Journal of Materials Science, 2002. **37**(17): p. 3615-3622.
4. She, J.H., T. Ohji, and S. Kanzaki, *Oxidation bonding of porous silicon carbide ceramics with synergistic performance.* Journal of the European Ceramic Society, 2004. **24**(2): p. 331-334.

5. Ding, S.Q., et al., *Fabrication of mullite-bonded porous silicon carbide ceramics by in situ reaction bonding.* Journal of the European Ceramic Society, 2007. **27**(4): p. 2095-2102.

6. Kumar, B.V.M., et al., *Effect of aluminum source on flexural strength of mullite-bonded porous silicon carbide ceramics.* Journal of the Ceramic Society of Japan, 2010. **118**(1373): p. 13-18.

7. S., T.Y., *Thermophysical properties of matter. (IFI/Plenum Data Company Press, New York.* 1979. **13**.

8. Ding, S.Q., et al., *Effect of Y2O3 addition on the properties of reaction-bonded porous SiC ceramics.* Ceramics International, 2006. **32**(4): p. 461-466.

9. Choi, Y.H., et al., *Effect of alkaline earth metal oxide addition on flexural strength of porous mullite-bonded silicon carbide ceramics.* Journal of Materials Science, 2010. **45**(24): p. 6841-6844.

10. Liu, S.F., Y.P. Zeng, and D.L. Jiang, *Effects of CeO2 addition on the properties of cordierite-bonded porous SiC ceramics.* Journal of the European Ceramic Society, 2009. **29**(9): p. 1795-1802.

11. Eom, J.H. and Y.W. Kim, *Effect of additive composition on microstructure and strength of porous silicon carbide ceramics.* Journal of Materials Science, 2009. **44**(16): p. 4482-4486.

12. Li, J.F., H. Lin, and J.B. Li, *Factors that influence the flexural strength of SiC-based porous ceramics used for hot gas filter support.* Journal of the European Ceramic Society, 2011. **31**(5): p. 825-831.

13. Chi, W.G., et al., *Sintering behavior of porous SiC ceramics.* Ceramics International, 2004. **30**(6): p. 869-874.

14. Chun, Y.S. and Y.W. Kim, *Processing and mechanical properties of porous silica-bonded silicon carbide ceramics.* Metals and Materials International, 2005. **11**(5): p. 351-355.

15. Yang, Q.Z. and T. Troczynski, *Dispersion of alumina and silicon carbide powders in alumina sol.* Journal of the American Ceramic Society, 1999. **82**(7): p. 1928-1930.

16. Prabhakaran, K., J. James, and C. Pavithran, *Surface modification of SiC powders by hydrolysed aluminium coating.* Journal of the European Ceramic Society, 2003. **23**(2): p. 379-385.

17. Xu, Y.P., A. Nakahira, and K. Niihara, *Characteristics of Al2o3-Sic Nanocomposite Prepared by Sol-Gel Processing.* Nippon Seramikkusu Kyokai Gakujutsu Ronbunshi-Journal of the Ceramic Society of Japan, 1994. **102**(3): p. 312-315.

18. Yang, Q.Z. and T. Troczynski, *Alumina sol-assisted sintering of SiC-Al2O3 composites.* Journal of the American Ceramic Society, 2000. **83**(4): p. 958-960.

19. Ortiz, A.L., et al., *A route for the pressureless liquid-phase sintering of SiC with low additive content for improved sliding-wear resistance.* Journal of the European Ceramic Society, 2012. **32**(4): p. 965-973.

20. Kayal, N., A. Dey, and O. Chakrabarti, *Incorporation of mullite as a bond phase into porous SiC by an infiltration technique.* Materials Science and Engineering a-Structural Materials Properties Microstructure and Processing, 2012. **535**: p. 222-227.

21. Yoldas, B.E., *Alumina sol preparation from alkoxides.* Ceram. Bull., 1975. **54**: p. 289.

22. Sugiyama, S., et al., *Removal and regeneration of aqueous divalent cations by boehmite.* Journal of Colloid and Interface Science, 2008. **320**(2): p. 535-539.

23. Wang, J.X., et al., *Microwave-enhanced densification of sol-gel alumina films.* Thin Solid Films, 2008. **516**(18): p. 5996-6001.

24. Tiwari, S.K., et al., *Development and characterization of sol-gel silica-alumina composite coatings on AISI 316L for implant applications.* Surface & Coatings Technology, 2007. **201**(16-17): p. 7582-7588.

25. Chandradass, J. and M. Balasubramanian, *Effect of magnesium oxide on sol-gel spun alumina and alumina-zirconia fibres.* Journal of the European Ceramic Society, 2006. **26**(13): p. 2611-2617.

26. Rinaldi, R. and U. Schuchardt, *On the paradox of transition metal-free alumina-catalyzed epoxidation with aqueous hydrogen peroxide.* Journal of Catalysis, 2005. **236**(2): p. 335-345.

27. Manivasakan, P., et al., *Effect of mineral acids on the production of alumina nanopowder from raw bauxite.* Powder Technology, 2011. **211**(1): p. 77-84.

28. Frost, R.L., et al., *Dehydroxylation and structure of alumina gels prepared from trisecbutoxyaluminium.* Thermochimica Acta, 1999. **329**(1): p. 47-56.

29. Fu, Q., C.B. Cao, and H.S. Zhu, *Preparation of alumina films from a new sol-gel route.* Thin Solid Films, 1999. **348**(1-2): p. 99-102.

30. Zu, G.Q., et al., *Preparation and characterization of monolithic alumina aerogels.* Journal of Non-Crystalline Solids, 2011. **357**(15): p. 2903-2906.

31. Boumaza, A., A. Djelloul, and F. Guerrab, *Specific signatures of alpha-alumina powders prepared by calcination of boehmite or gibbsite.* Powder Technology, 2010. **201**(2): p. 177-180.

32. Dabbagh, H.A., et al., *Formation of gamma-alumina nanorods in presence of alanine.* Materials Research Bulletin, 2011. **46**(2): p. 271-277.

33. Levin, I. and D. Brandon, *Metastable alumina polymorphs: Crystal structures and transition sequences.* Journal of the American Ceramic Society, 1998. **81**(8): p. 1995-2012.

34. Rice, R.W., *Comparison of Stress-Concentration Versus Minimum Solid Area Based Mechanical Property Porosity Relations.* Journal of Materials Science, 1993. **28**(8): p. 2187-2190.

35. Ebrahimpour, O., J. Chaouki, and C. Dubois, *Diffusional effects for the oxidation of SiC powders in thermogravimetric analysis experiments.* Journal of Materials Science, 2013. **48**(12): p. 4396-4407.

36. Kyrylyuk, A.V., A. Wouterse, and A.P. Philipse, *Percolation and Jamming in Random Heterogeneous Materials with Competing Length Scales.* Trends in Colloid and Interface Science Xxiii, 2010. **137**: p. 29-33.

37. Meng, L.Y., et al., *Shape and size effects on the packing density of binary spherocylinders.* Powder Technology, 2012. **228**: p. 284-294.

38. Kritikaki, A. and A. Tsetsekou, *Fabrication of porous alumina ceramics from powder mixtures with sol-gel derived nanometer alumina: Effect of mixing method.* Journal of the European Ceramic Society, 2009. **29**(9): p. 1603-1611.

39. Touzin, M. and F. Beclin, *Fabrication and characterization of composite sol-gel coatings on porous ceramic substrate.* Journal of the European Ceramic Society, 2011. **31**(9): p. 1661-1667.

40. Huang, Q., et al., *Effect of pretreatment on rheological properties of silicon carbide aqueous suspension.* Ceramics International, 2002. **28**(7): p. 747-754.

41. Cheng, L.T., et al., *Boehmite coating on theta-Al2O3 particles via a sol-gel route.* Ceramics International, 2008. **34**(2): p. 337-343

CHAPTER 6 ARTICLE 3: A NOVEL FABRICATION ROUTE FOR POROUS SIC CERAMICS BY COMBINING IN-SITU POLYMERIZATION AND REACTION BONDING TECHNIQUES

Omid Ebrahimpour, Babak Esmaeili, Lucie Griffon, Jamal Chaouki and Charles Dubois

Department of Chemical Engineering, École Polytechnique de Montréal, P.O. Box 6079, Station Centre-Ville, Montréal, Canada

Abstract

For the first time, in-situ polymerization technique was applied to produce mullite-bonded porous SiC ceramics via reaction bonding technique. In this work, SiC microsized particles and alumina nanopowders were successfully coated by polyethylene which was synthesised from the particles surface in a slurry phase reactor using Ziegler-Natta catalyst system. The thermal studies of the resulting samples were performed with differential scanning calorimetry (DSC) and thermal gravimetric analysis (TGA). The morphology analysis obtained by transmission electron microscopy (TEM) and scanning electron microscopy (SEM) confirmed that polyethylene was successfully grafted on the particles surface. Furthermore, the obtained porous ceramics were characterized in terms of their morphologies, phase composition, open porosity, pore size distribution and mechanical strength. SEM observations and mercury porosimtery analysis revealed that the quality of dispersion of nanosized alumina powder into microsized SiC particles was strongly enhanced when particles were coated by polymers using in-situ polymerization which resulted in higher strength as well as porosity of formed ceramic porous materials with respect to the traditional process. In addition, XRD results revealed that the amount of mullite as the binder is increased significantly for the samples fabricated by this novel method. The effects of sintering temperature, forming pressure and polymer content on the physical and mechanical properties of the final porous ceramic were also evaluated in this work.

Keywords:

Porous SiC ceramics, mullite, In-situ polymerization, Polyethylene, Ziegler-Natta catalyst.

6.1 INTRODUCTION

Porous silicon carbide ceramics have attracted great interest in a broad range of high temperature structural applications because of their superior physical properties such as low thermal expansion coefficient and good thermal shock resistance, as well as excellent chemical and mechanical stability. They have been considered as potential candidate materials in high temperature application such as hot-gas filter, membrane support, refractory plates and gas burner media [1,2]. However, because of the strong covalent nature of the Si–C bond owing to its inherent structure, it is difficult to sinter SiC ceramics at moderate temperature, and high sintering temperature (over 2000 °C) is needed to self-bond SiC together [3].

It has been reported that changing the sintering environment or adding the secondary phase bonded materials such as alumina enables the fabrication of porous SiC ceramics at lower sintering temperature [4]. This process consists of mixing SiC particles with sintering aid and pore former in a suitable medium followed by drying, pressing and, finally sintering in air instead of under an inert atmosphere. Accordingly, fugitive agents burn out and form pore structures during the heating step. At higher temperature, SiC particles partially oxidize to silica, then, they react with alumina (at more than 1400 °C) to form mullite. Consequently, SiC particles are bonded by silica (SiO_2) and mullite ($3Al_2O_3.2SiO_2$) by means of an in-situ reaction bonding [5]. The fabricated mullite-bonded porous SiC ceramics are expected to have better physical and mechanical properties due to good oxidation resistance of mullite and similar thermal expansion coefficient between mullite and SiC [6].

Being an attractive approach, this process has been investigated by various researchers to improve the final properties of the product. For example, using other additives such as Y_2O_3, CeO_2 and MgO to enhance the mechanical properties of porous SiC ceramics has been proposed [6-9]. Very recently, we have studied the effect of alumina content and sources (calcined alumina, alumina sol) on the mechanical and physical properties of porous ceramics. Results demonstrated that addition of alumina nano powder increased significantly the mechanical strength and decreased dramatically the porosity [10]. To control the porosity of the final product, some pore-formers such as graphite, yeast or polymer beads, have been employed into the starting materials [5, 11, 12].

Although considerable efforts have been devoted to improve the process, one of the main drawbacks of this method is the agglomeration of fine particles (sintering aids) due to the strong interactions between nanoparticles which results in an insufficient dispersion of the starting particles during the preparationn of the green body. For instance, it was reported that when alumina submicron-particles were added to SiC microsized particles, most of them were agglomerated. As a result of the agglomeration, the alumina particles had only a limited contact with SiC micro powders and therefore could not fully participate in the mullite reaction.[5] Furthermore, this problem can severely impairs the mechanical properties of final ceramics [5]. The dispersion of particle will be more problematic when different types of powders are used in the starting materials. For example, Ding et al. [5] used different particle sizes of graphite as the pore former in the starting materials. They observed a bimodal pore size distribution which was attributed to the weak dispersion between pore former and starting materials. This agglomeration significantly decreases the constitutive properties of the product. Therefore, it is essential to develop an effective way to mitigate this problem and improve the materials dispersion which is the key aspect in preparation of porous ceramics with excellent mechanical and physical properties.

To tackle this challenge, it is proposed in our work to modify the surface of initial materials by growing a polymer phase which can subsequently act as a pore former. This approach relies on an in-situ polymerization process known as “grafting from” rather than physical mixing of starting materials with the pore former. It is a well-known method to prepare inorganic or organic polymeric composites with enhanced properties [13,14]. Typically, in this technique, the monomer is polymerized from the active compounds (initiators) which covalently anchored on the surface of inorganic particles [15, 16]. Monomers can penetrate easily through the aggregated nanoscale particles due to their inherent small sizes. As a result, synthesized polymer chains partially filled the free volume inside the nanoparticle aggregates, and therefore the aggregated nanoparticles break out [16]. Hence, in-situ polymerization is an attractive approach to be employed for the fabrication of the porous ceramics process with desired improved mechanical and physical properties.

This method have been applied successfully to synthesize composites materials for a board range of inorganic particles such as carbon nanotubes [17], alumina [18,19], SiO_2 [20-24], clay [25-27], aluminum [28], ZnO [29], silver [30] and silicon nitride [31] with different polymerization

routes. Similarly, our research group encapsulated zirconia nano particles with polyethylene via various techniques using Ziegler-Natta catalyst [32, 33].

The main objective of this work is to investigate the implementation of in-situ polymerization as a means of enhancing the dispersion of sintering additives into the starting materials to fabricate porous SiC ceramics with improved properties. The research also aims at adjusting the porosity of the porous SiC ceramics by controlling the polymerization condition as well as materials and to manufacture porous SiC ceramics with improved mechanical and physical properties via a combination of *in situ* polymerization and reaction bonding method. To the best of our knowledge, this original work is being accomplished by our group for the first time. A comparison between the traditional process and our developed method has been made by investigating the flexural strength, open porosity and pore size distribution of final products. In addition, the effects of polymer content, sintering temperature and forming pressure on the phase composition, mechanical and physical properties of the final products were studied.

In the present study, SiC microsize particles and alumina nanoparticles are primarily coated by polyethylene via in-situ polymerization in a benchtop batch reactor using a Ziegler-Natta catalyst system. After pressing of materials to form green body, they are placed in the furnace under air. During the heating cycle, polymer is first removed by calcination, thus creating the desired porous morphology and then at higher temperature, mullite is formed by reaction between the oxidation-derived SiO_2 and alumina.

6.2 EXPERIMENTAL

6.2.1 Materials

Micro-sized α-SiC powder (99.7% purity, ρ= 3.2 g/cm^3, S_{BET}= 0.87 m^2/g) as the starting material and nanopartile α-Al_2O_3 powder (99.95% purity, ρ= 3.95 g/cm^3, S_{BET}= 8.5 m^2/g) as the sintering additive were purchased from LABMAT, Canada. As shown in Figure 6-1, SiC particles are irregular in shape and sharp at their edges as compared to alumina powders, which are more uniform. According to the particle size analysis, the volume averaged mean particle size of SiC was determined to be 11.5 µm (d_{10}=6.6 µm and d_{90}=16.2 µm) and that of alumina was 270 nm (d_{10}=188 nm and d_{90}=354 nm). Ethylene gas (99.5% purity, Canadian liquid air) was used as

monomer for the polymerization reaction. The Ziegler–Natta catalyst system was constituted of titanium tetrachloride ($TiCl_4$, Fluka) as the catalyst with triethylaluminum 1M in hexane ($AlEt_3$, Sigma-Aldrich) as co-catalyst. They were stored and handled in a glove box under argon as they are highly sensitive to moisture and oxygen. Hexanes supplied by Sigma were dried and stored for at least 24 hours on molecular sieve and used as the reaction solvent.

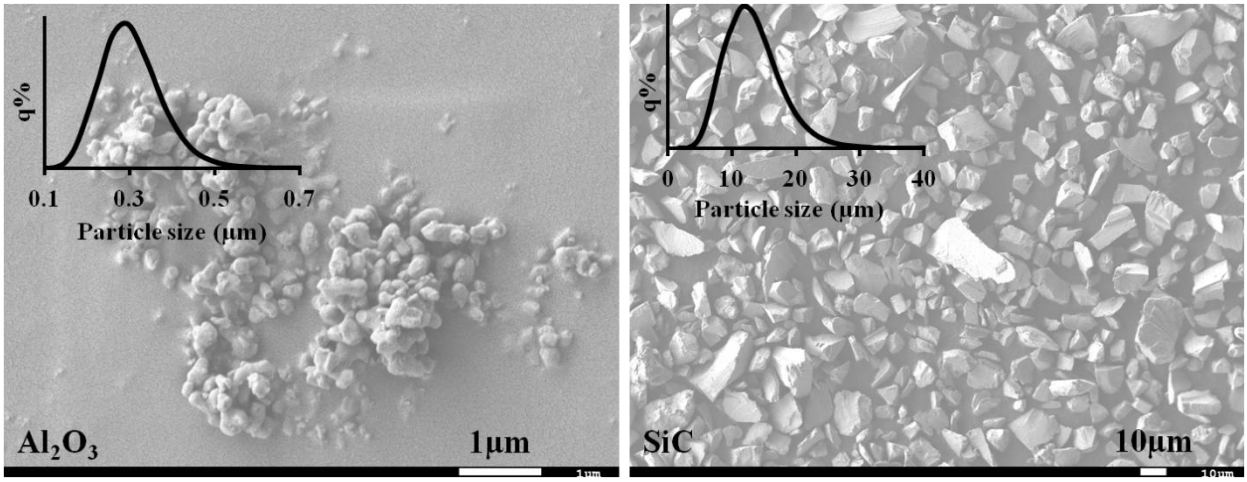

Figure 6-1 SEM micrographs and particle size distribution of starting materials.

6.2.2 In-situ Polymerization

The slurry polymerization experiments were performed in a two liter pressurized BUCHI reactor heated with an external fluid bath circulator and equipped with a magnetic drive impeller. In a typical reaction, a mixture of SiC and alumina particles (18 gr. SiC and 9.72 alumina, 35 wt % of alumina) which was previously dried in an oven at the temperature of 150 °C was added to 1.5 liter of dried hexane. The mixture was heated at desired reaction temperature for about 1 hour and continuously stirred in hexane by mechanical agitation (400 rpm). The system, then, was purged with N_2 which was dried further by passage through a molecular column sieve in order to eliminate oxygen in the medium. Subsequently, the pre-determined amount of catalyst, $TiCl_4$, was added using a syringe through a septum feeding port in the reactor. With a delay of 15 minutes after the first injection, the desired amount of co-catalyst $AlEt_3$ was also injected and the mixture was agitated for another five minutes to ensure the formation of a catalyst-co-catalyst

complex. The reaction started by initiating a flow of ethylene monomer. For all of the experiments, the reaction temperature and the pressure were maintained constant at 65 °C and a relative pressure of 48 kPa, respectively. The amount of injected catalyst was determined based on the total particle surface area of powders in the system which can be ideally coated by $TiCl_4$ (7mg cat/g powder). The molar ratio of co-catalyst to catalyst was fixed at two. After the desired reaction time, the polymerization was terminated by an injection of ethanol in the medium to hydrolyze the catalyst complex.

6.2.3 Fabrication of porous SiC ceramics

In order to manufacture the porous SiC ceramics, the polymer grafted particles were dried and passed through a 80-mesh screen. Afterward, they were pressed (25, 50 or 100 MPa) uniaxially into a rectangular bars of 4.5 mm ×10.0 mm ×50.0 mm using a stainless steel die. Subsequently, the compact compounds were placed in a box furnace and heated up to 400 °C at a heating rate of 2 °C/min for two hours to achieve polymer degradation. Subsequently, the temperature was increased up to 900 °C with a heating rate of 2 °C/min followed by a steeper ramp of 5 °C/min to reach the desired sintering temperature (1500 °C or 1550 °C). The samples were hold at the sintering temperature for three hours in air and finally the specimens were cooled down to room temperature with the cooling rate of 5 °C/min.

Alternatively, in order to compare this developed process with the more traditional method, silicon carbide and sub-micron alumina powders with a weight ratio of 35 wt % were mixed with 2.5 wt % polyvinyl butyral (PVB) as a binder in ethanol using a high energy ball mill. After drying and passing through a screen, powders were pressed and heated under air to produce porous samples. Further details about this part of the process have been reported by our group elsewhere.[125]

6.3 CHARACTERIZATION

The mean particle size and the surface area of the starting powders were measured by a Horiba LA-950 laser diffraction particle size analyzer and a Quantachrome Autosorb-1 apparatus, respectively. Before BET analysis, samples were degassed at 150 °C for 3 hours.

The quantity of polymer grafted from the particles was assessed by means of thermogravimetric analysis (TGA) using a TGA Q 5000 apparatus (TA Instruments, USA) in a temperature range from 25 °C to 600 °C at a heating rate of 10 °C/min under nitrogen atmosphere with a flow rate of 20 ml/min. The melting temperature and crystallization behaviour of the synthesized polymer on the particles were studied by differential scanning calorimetry (DSC Q 2000, TA Instruments, USA) at cooling and heating rates of 10 °C/min. The morphology observation of samples was conducted with scanning electron microscopy (SEM, Model JSM-7600 TFE, JEOL, Japan) and by transmission electron micrographs (TEM, JEOL JEM-2100F) at a 200 kV acceleration voltage. The SEM was operated at 2 kV with LEI imaging mode and a working distance of 8,5 mm. X-ray diffractions (XRD) were recorded using a Philips X'Pert diffractometer (The Netherlands) with Cu-Kα radiation (0.154 nm) at a generator voltage of 50kV and a current of 40 mA. The scanning rate was 1.2 °/min at an interval of 0.02 °. Furthermore, for the surface analysis, the coated samples and non-coated samples were analyzed by X-ray photoelectron spectroscopy (XPS) in a VG Scientific ESCALAB Mk II with Mg Kα radiation (1253.6 eV) operated at 300 W without monochromator.

The true densities of porous samples were measured by the gas volume displacement method using gas pycnometer (Accupyc II 1330 helium pycnometer). Mercury porosimetry (Micromeritics Autopore IV) was utilized to show the pore size distribution of porous samples. Open porosity was ascertained from the total mercury intrusion volume and the skeletal density of sample. Flexural strength of porous samples was measured by a three-point bending test with a support distance of 30 mm and at a constant crosshead velocity of 0.5 mm/min using an Instron Universal Testing machine (Model 1123, Instron, Canton, MA, USA) with 500 N load cell. The deflection measurement was taken using LVDT with a resolution of 0.05% and Young's modulus was calculated via standard software (Instron Bluehill-2, UK). Beams were machined and polished to 3.0 (±0.1 mm) × 4.0 (±0.1 mm) × 36.0 mm and at least three specimens were tested to obtain the average strength.

6.4 RESULTS AND DISCUSSION

6.4.1 Characterization of PE grafted SiC and Al_2O_3 particles

The amount of polymer (pore formers) in the starting materials was determined by TGA tests. The TGA curves of coated particles under inert atmosphere at different polymerization reaction time (4 min, 7 min and 15 min) are presented in Figure 6-2. As observed in the TGA curves, the weight loss occurs in two degradations steps. The first one between 150 °C and 350 °C is associated with the pyrolysis of small oligomers chain. The major weight loss took place in the temperature range of 425-485 °C. It corresponds to the decomposition of high molecular weight polyethylene to the olefinic and paraffinic components under nitrogen [34-36].

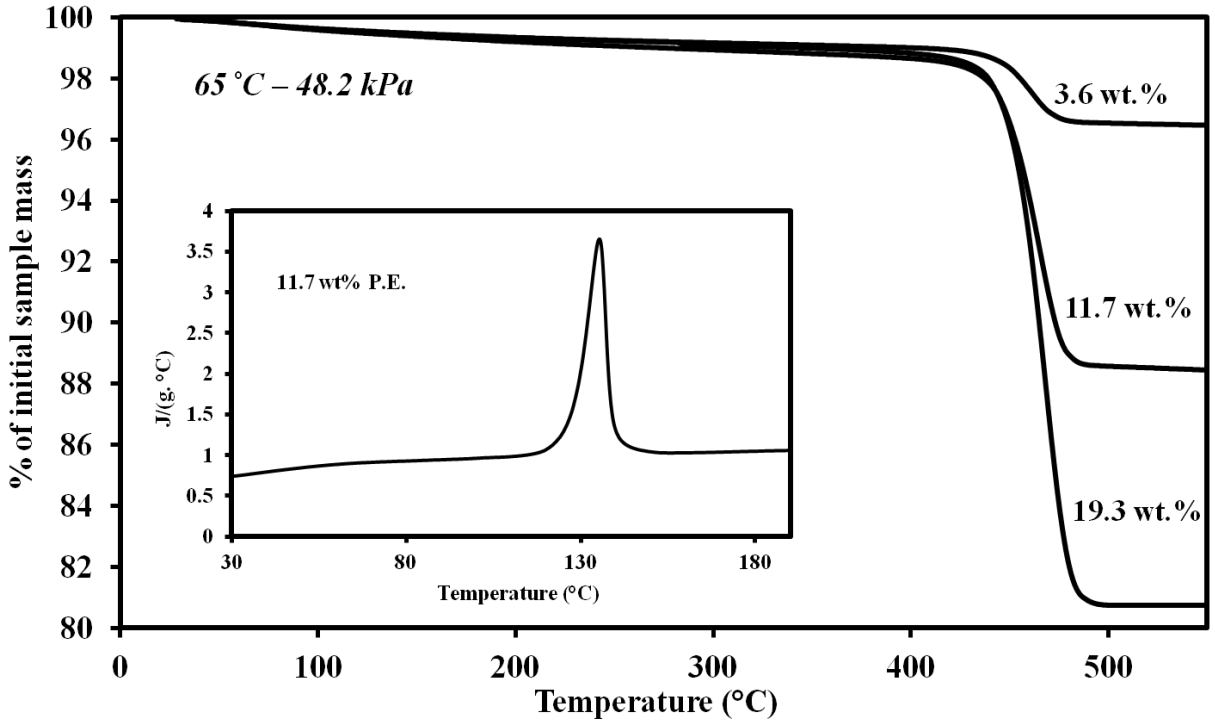

Figure 6-2 TGA of three PE coated samples

It should be noted that by increasing the polymerization time, degradation appears at higher temperature which indicates that longer polymer chains were produced. Thermal behavior of coated samples was further investigated by measuring the melting temperature and crystallinity

of the synthesized polymers via DSC. For estimating the crystallinity of HDPE component on the coated samples a value of 293 J/g was used as the reference for the heat of fusion of 100% crystalline polyethylene at the perfect crystal melting point [37]. DSC scans (Figure 6-2) showed a single melting endotherm peak corresponding to the melting temperature of the polyethylene. Typical melting temperature and degree of the crystallinity for the coating polymer (11.7 wt%) were 135.69 °C and 61%, respectively, which are in agreement with the literature reports for the characteristic properties of high density polyethylene [38].

The SEM observations for morphology study of the coated particles with different amount of polymers are presented in Figure 6-3. One can clearly see that SiC and alumina particles are coated by polymer. In addition, the presence of very thin filaments of polymer between the alumina nano powders and SiC micro powders are revealed. As SiC particles were too thick for the TEM beam to go through them, TEM analysis was only conducted on the alumina nanoparticles. Figure 6-4 shows the typical TEM–EDX micrographs obtained for coated particles with 11.7 wt % of polymer. According to the EDX analysis, the dark particles are assigned to the alumina nanoparticles and the grayish white areas represent the coating polymer. The carbon peak for the alumina particles (EDX analysis) shows the presence of the polymer on the surface of particles. It is clearly visible from TEM analysis that alumina particles are surrounded and coated by polymer and a good interfacial adhesion between polyethylene and particles are existed. High resolution TEM image presented in Figure 6-4 indicates that HDPE forms a close interface with alumina, which implies a proper wetting between matrix and particles. These observations by SEM and TEM provide strong evidence that polyethylene is successfully grafted from the surface of particles.

According to the literature, it is well established that there is a nano layer of silica on the surface of silicon carbide. Siokou and his coworkers [39] investigated the interaction between SiO_2 and $TiCl_4$ using X-ray photoelectron spectroscopy (XPS) analysis and they showed that catalyst anchors on the substrates surface through a covalent bonding between Ti and hydroxyl group on the particles.

As the surface of alumina and silica contain hydroxyl groups [40, 41] it is proposed that $TiCl_4$ reacts with the surface hydroxyl groups on the substrate as the following reaction [42, 43]:

$$x(-OH) + TiCl_4 \rightarrow (-O)_x TiCl_{4-x} + x(HCl) \qquad 6\text{-}1$$

Where x=1 for mono-functional and x=2 for bi-functional compounds. As a result, monomers are polymerized from samples surface and polymer chains builds up during the polymerization reaction [44].

Table 6.1 compares the surface elemental analysis of non coated particles with 19.3 wt% coated particles as measured by XPS. The results show that the peak intensity and therefore, the contribution of Si, Al and O elements decreased in the coated particles. On the other hand, the relative amount of carbon element increased about 4 times for coated particles. It should be noted that even at high amount of polymer, a few trace of Si and Al elements were detected by XPS analysis. One explanation is that the polymer thickness is less than 10 nm (which is in order of elemental surface composition for the used XPS) in some parts of particles as found by TEM characterization (Figure 6-5). Also, this might be due to the fact that the concentration of reactive sites on particles surface was not enough or uniform. It is worthwhile to point out that several parameters such as polymerization time, reaction temperature, pressure, and the molar ratio Al/Ti can influence the polymerization rate [45]. In addition, the reactivity of monomer strongly depends on its size. For example ethylene is five times more reactive than propylene because of the lower size of ethylene in the polymerization with the Ziegler-Natta heterogeneous catalyst.

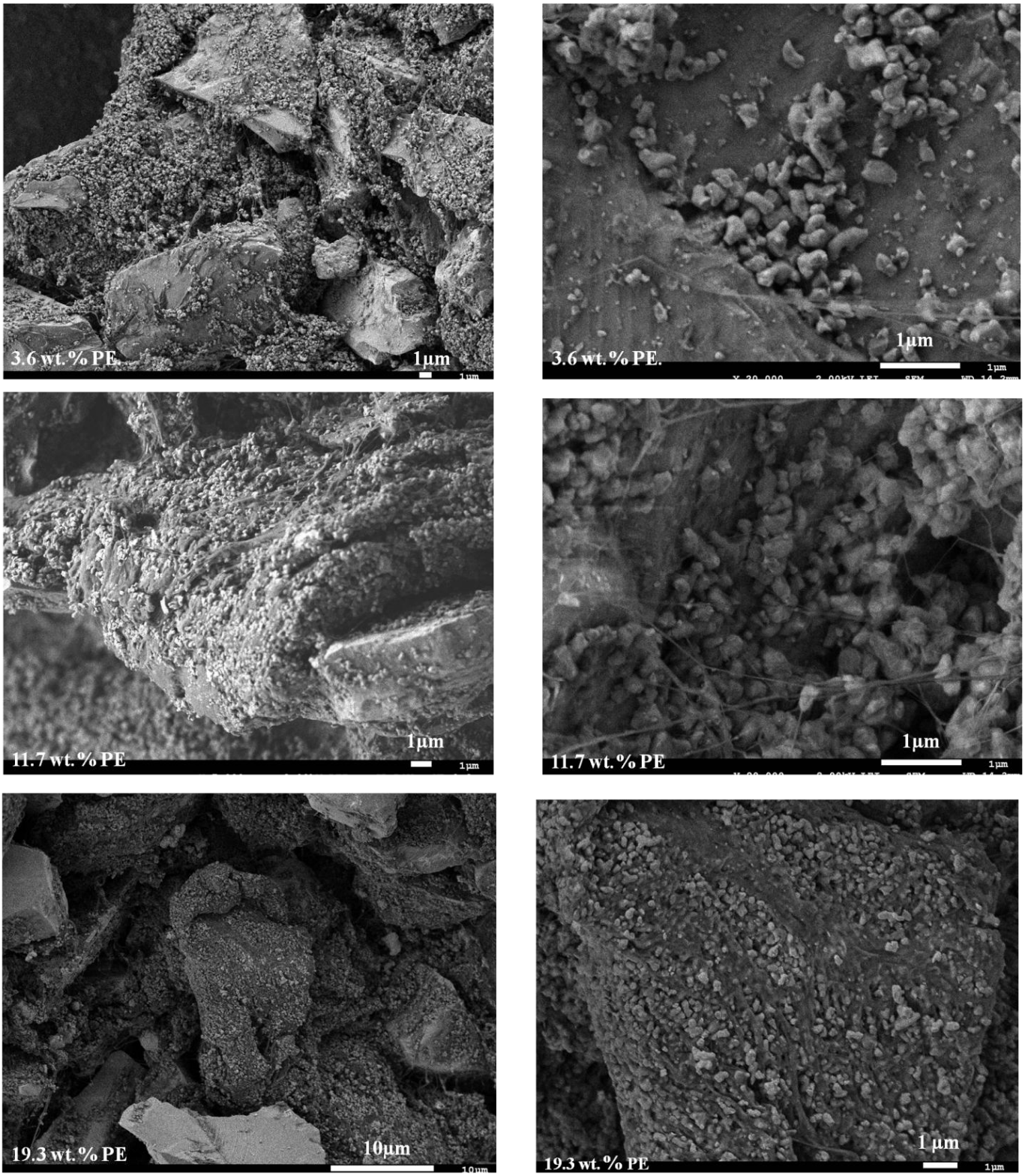

Figure 6-3 SEM images of coated SiC and Al_2O_3 particles at different amount of polymer

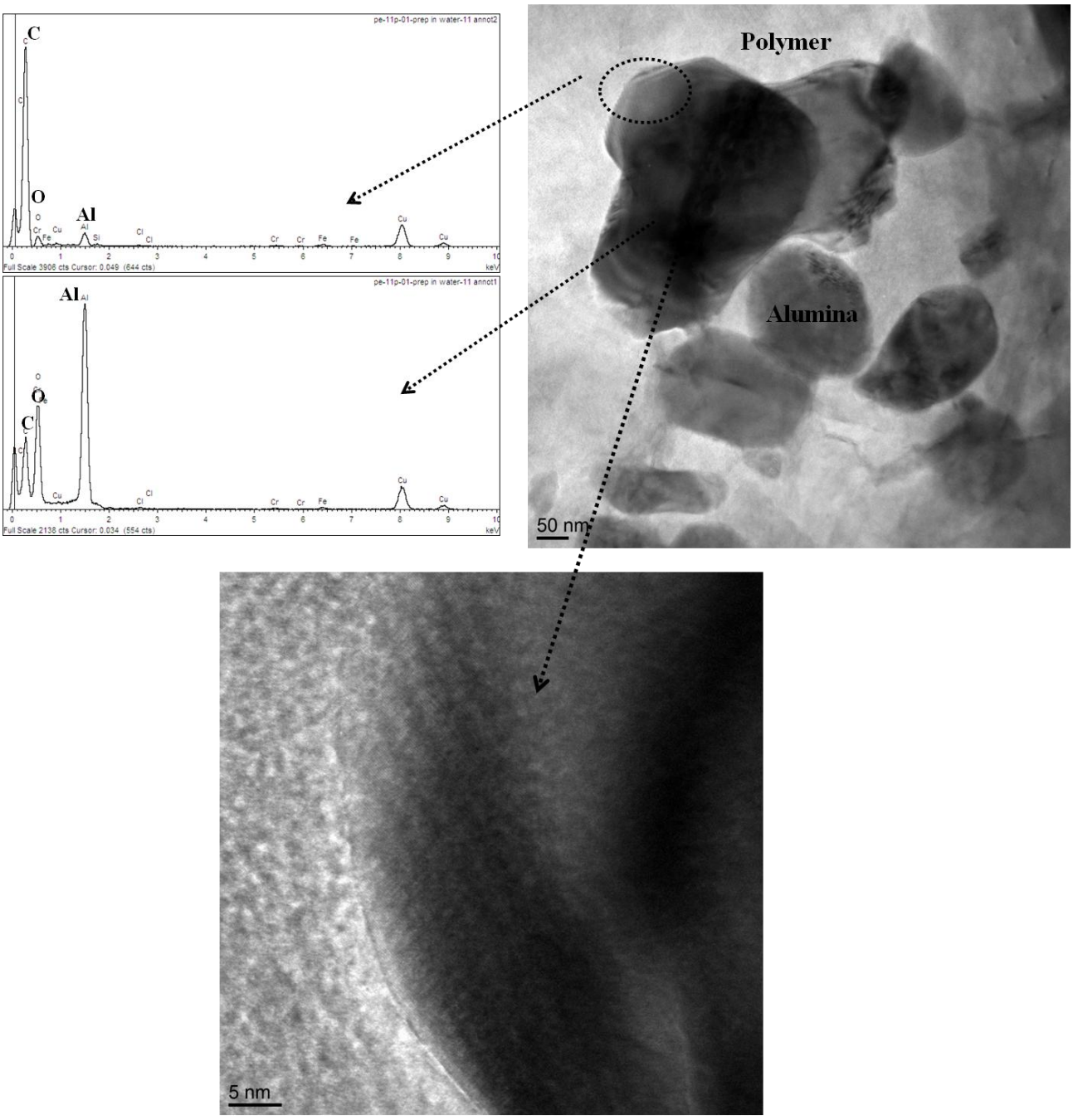

Figure 6-4 TEM images of coated particles (11.7 wt.% polymer)

Table 6.1 XPS data for original and coated particles with 19.3 wt.% polymer

Name	B.E.	At. % original	At.% coated
Al2p	75.7	21.4	2.7
Si2p	101.3	7.7	1.5
O1s	532.9	48.4	8.2
F1s	691.8	1.6	0.4
C1s	285.3	20.3	86.3
Ti2p	459.1	-	0.3
Cl2p	199.3	0.5	0.4

6.4.2 Characterization of porous SiC ceramic prepared by in-situ polymerization

The skeletal density, flexural strength, open porosity, and average pore size of porous SiC ceramic with different polymer content are summarized in Table 6.2. Samples were sintered at 1500 °C for 3 h in air with molding press of 50 MPa, where 35%wt calcined alumina was added to SiC particles. According to the results, it can be speculated that introducing polymer via in situ polymerization on particles surface could be responsible for an increase in flexural strength compared to the conventional method where particles are simply mixed without any polymerization.

Table 6.2 Influence of polymer content on the flexural strength, open porosity and pore size

polymer w/w %	Flexural strength (MPa)	Porosity (%)	Average median pore diameter (µm)	Skeletal density (g/cm^3)
0	30.9 ± 1.3	32.3	1.57	3.11
3.6	50.1 ± 3.1	31.2	1.41	3.11
11.7	41.2 ± 1.7	36.8	1.90	3.12
19.3	28.1 ± 2.3	41.0	2.53	3.09

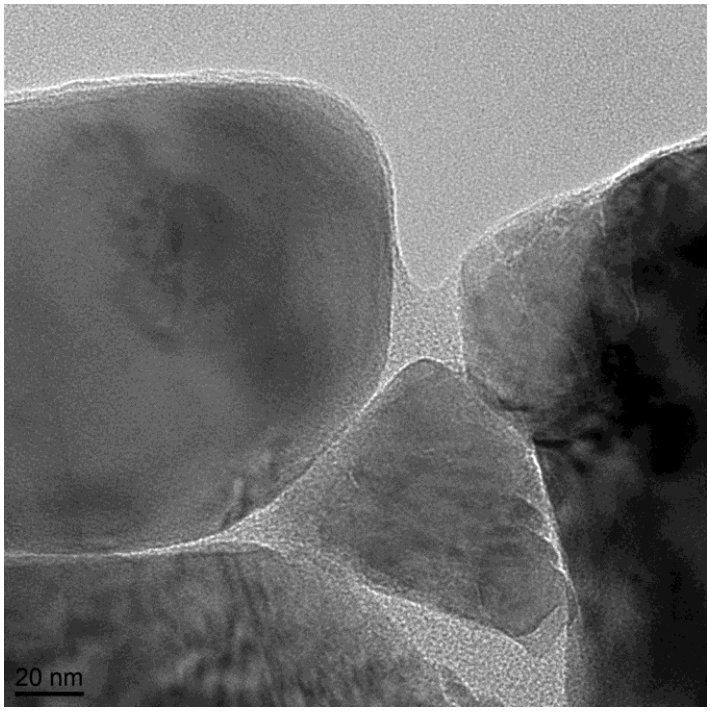

Figure 6-5 A TEM micrograph of the coated particles with 11.7 wt% of HDPE

A typical pore size distribution and SEM morphology of the samples coated with 11.7 wt% polymer are compared with the one prepared without polymerization treatment in Figure 6-6. In samples prepared with the conventional method, the pores are formed due to stacking SiC particles. As it is clear in the SEM picture, some alumina particles are agglomerated and have no contact with SiC. The agglomeration produces some small pores which causes another bump as

found in the pore size distribution results while this agglomeration has been decreased remarkably in the case of samples which are treated by in situ polymerization.

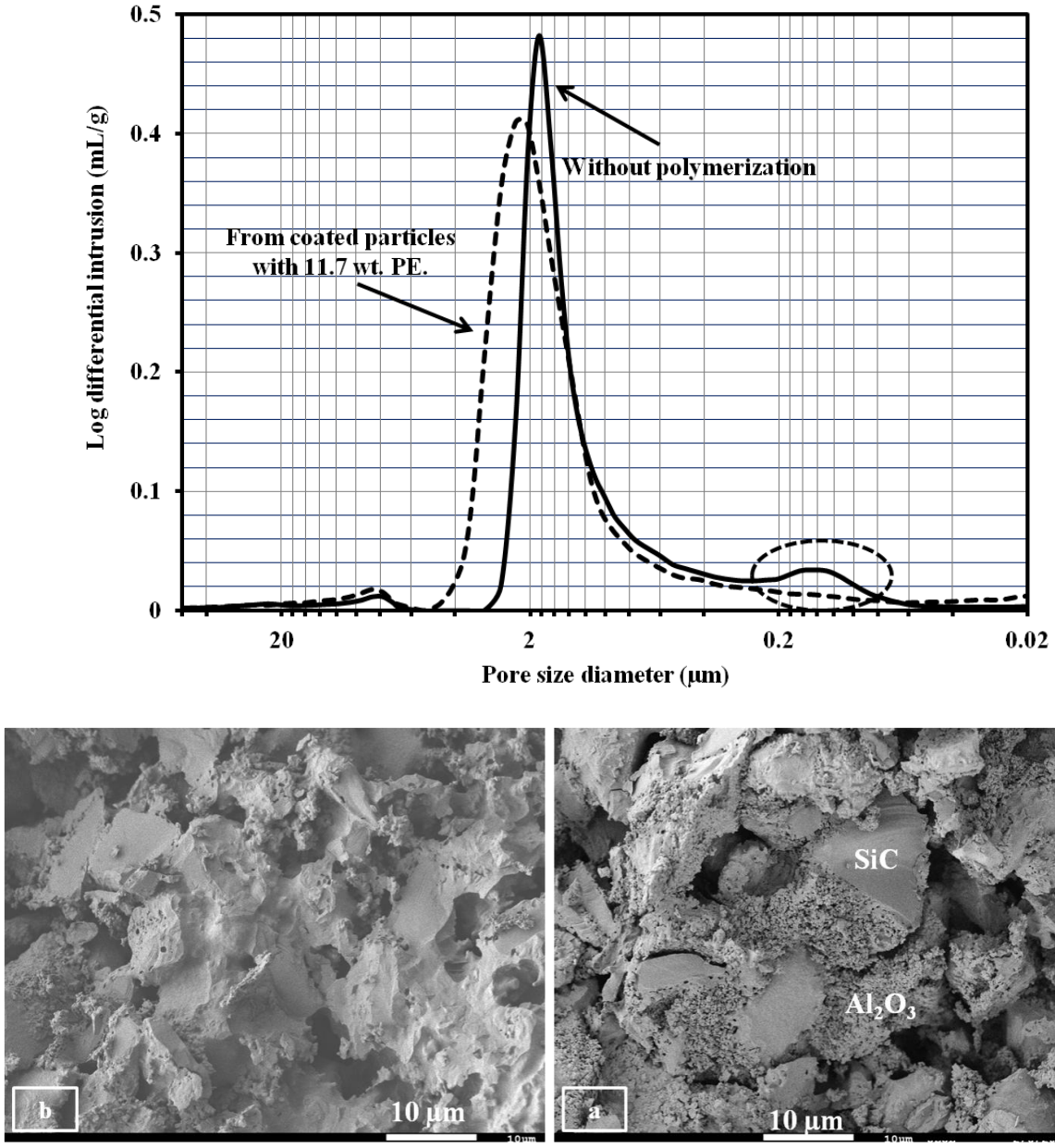

Figure 6-6 Pore size distribution and SEM of porous SiC ceramics sintered at 1500 °C for 3 h in air, where 35%wt calcined alumina was added into SiC particles and where starting particles were not coated (a) and where were coated with 11.7 wt% of polyethylene (b)

Figure 6-7 presents the XRD spectrum of samples prepared with traditional method and with the novel process at sintering temperature of 1500 °C for 3h. For both methods, the phases consist of mainly alumina, cristobalite, mullite and silicon carbide.

Typically, at temperature above 800 °C, SiC particles oxidize to silica via a passive oxidation reaction:

$$SiC + 2\,O_2 \rightarrow SiO_2(amorphous) + CO_2(g) \qquad 6\text{-}2$$

Previously, we have reported that the oxidation rate of SiC strongly depends on the reaction temperature and SiC particle size [46]. Crystalline structure of silica converts to the cristobalite phase when the temperature reaches 1200 °C:

$$SiO_2(amorphous) \rightarrow Cristobalite \qquad 6\text{-}3$$

At temperature above 1400 °C, alumina reacts with cristobalite to form mullite according to the following reaction:

$$3Al_2O_3 + 2\,SiO_2 \rightarrow 3Al_2O_3.2\,SiO_2(mullite) \qquad 6\text{-}4$$

According to the XRD pattern (Figure 6-6-a), it can be concluded that when in-situ polymerization is applied for the fabrication of porous ceramic, the relative intensity of mullite to alumina increased as compared to the samples prepared by the conventional method.

The enhancement of physical and mechanical properties of the porous samples via the developed method can be explained as follows: when SiC and alumina nanosize powders were physically mixed in ethanol, a lot of alumina powders were agglomerated in the bulk system (Figure 6-8-a), while for the samples which were introduced in polymerization most of nano alumina powders were attached on the surface of SiC powders (Figure 6-8-b) leading to homogenous dispersion of alumina particles. In fact, as a result of deposition of the Ziegler-Natta catalyst on the SiC and alumina particles, polymer chains grow from particles surface and they so generate strong repulsion between nanoparticles, eventually breaking agglomerates by their propagation between the aggregated alumina nano powders.

On the other hand, during the polymerization, polymer filaments causes to attach and bond alumina nano particles to the surface of SiC particles which provides a linkage between alumina

and SiC particles as it can be seen in Figure 6-9. In addition, since both particles (SiC and Al_2O_3) are coated by polymer, their surface properties are similar which facilitates the dispersion of powders in the solvent. Thus during the formation of the green body, more alumina particles connect to SiC particles and they have more chance to react with the derived SiO_2 to form mullite as compared to the traditional method. SEM image (Figure 6-6-b) clearly demonstrates better neck growth during the sintering of the samples as a result of more mullitization. Therefore, the increase in strength was ascribed to the better dispersion of alumina particles in SiC particles and more mullite formation via in situ polymerization.

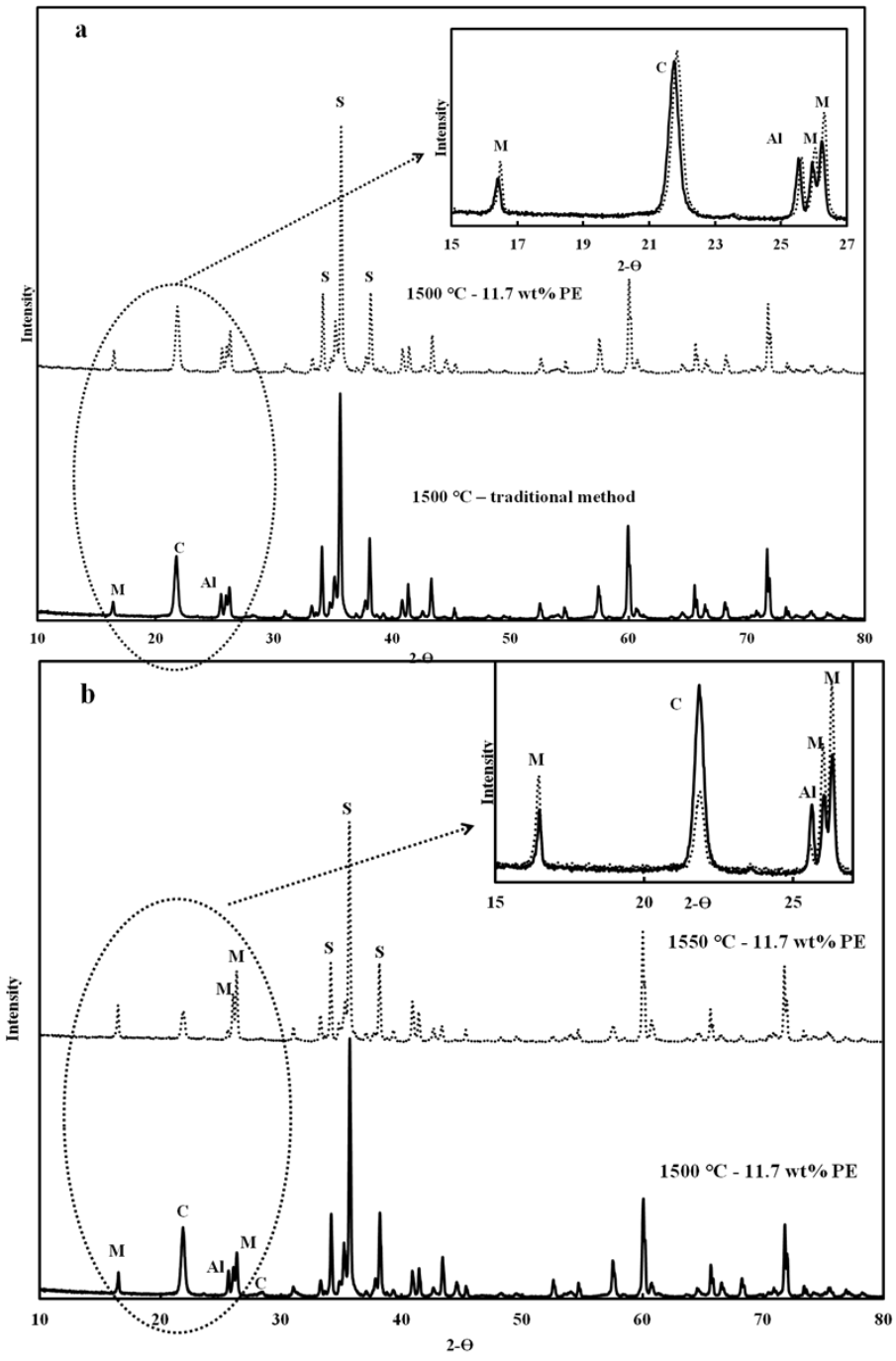

Figure 6-7 XRD patterns of porous SiC ceramics; a) effect of polymerization and b) effect of sintering temperature; (Al: alumina, C: cristobalite, M: mullite and S: silicon carbide).

Figure 6-7-b shows the effect of sintering temperature on the evolution of crystalline structure of samples which were prepared with 11.7 wt% polymer and sintered at 1500°C and 1550°C for 3 h.

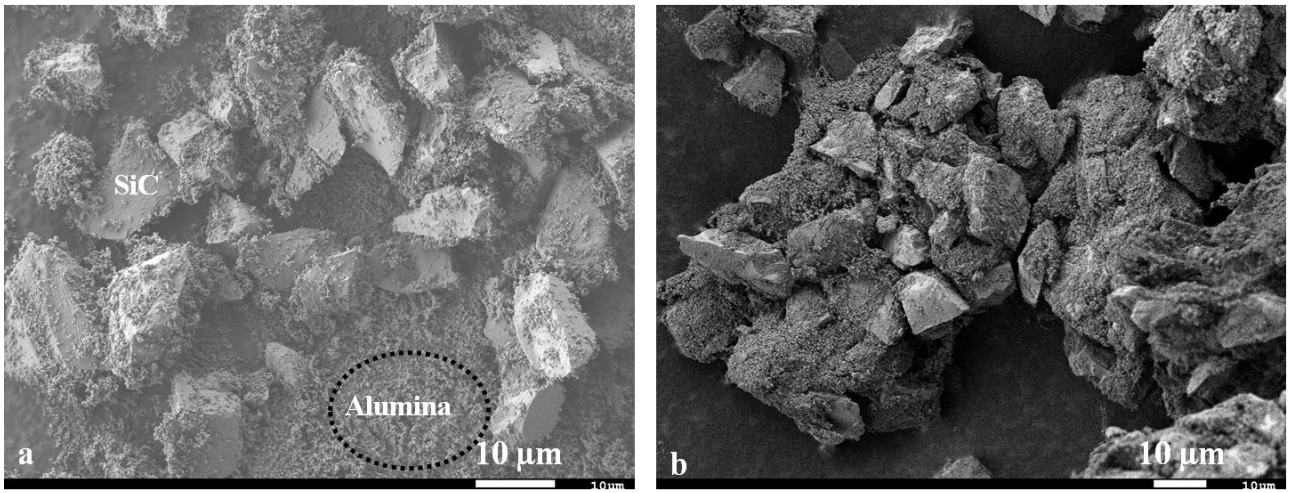

Figure 6-8 SEM micrographs SiC and alumina (35wt.%) which were mixed in ethanol (a) and coated by polymer via in situ polymerization (b)

The intensity of cristobalite and alumina decreased abruptly as a result of extensive formation of mullite with an increase in temperature. Another explanation for decreasing the intensity of cristobalite is the formation of SiO gaseous. At lower sintering temperature, oxidation occurs from diffusion of oxygen into the surface of SiC which forms a layer of silica film [46]. As temperature increases, surface of SiC particles is covered by more mullite and silica which act as an oxidation barrier. Consequently, the partial pressure of oxygen decreases which results in changing the mechanism of the oxidation from passive to active state which produces gaseous SiO.

According to the literature, mullitization is controlled by the solution-precipitation mechanism [47]. At a temperature of 1400 °C, the nucleation of mullite is occurred as a result of penetration of fine α-Al_2O_3 particles into SiO_2, which acts like viscous softening. By increasing the sintering temperature to 1450 °C, the viscosity of SiO_2 glass decreases which enhances the rate of diffusion of Al^{3+} ions into the viscous SiO_2 glass. When the sintering temperature is raised above 1500 °C, viscous-flow promotes the rate of mullitization significantly by shortening the diffusion distances between SiO_2 and alumina.

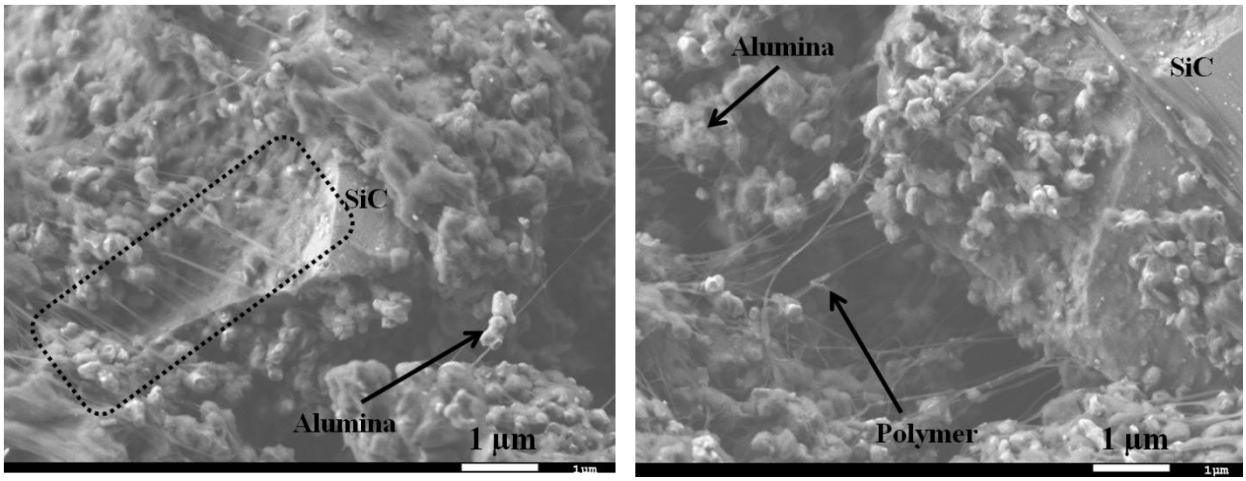

Figure 6-9 SEM micrographs of coated samples which polymer filaments attach alumina nanopowders on the SiC particles

SEM morphology (Figure 6-10) demonstrates the strong neck growth between the SiC particles as well as the formation of the needle-like mullite at sintering temperature of 1550 °C which supports strongly the XRD results. After enough formation of mullite, SiO_2 and α-Al_2O_3 must diffuse through the interfaces of SiO_2-mullite and Al_2O_3-mullite in order to conduct further reaction [48]. Therefore, the mechanism of mullitization is diffusion-controlled. Increasing the sintering temperature also leads to filling some small pores by liquid phase, and consequently, decreasing the sample porosity from 37.3 to 34.5%. For the present case, the strength of 51 MPa was obtained when the sintering temperature was increased from 1500 °C to 1550 °C.

The results in Table 6.2 indicate that the sample porosity increases substantially when the polymer content changes from 31% to 43%, whereas flexural strength decreases. The highest value of mechanical strength is found to be about 50 MPa when the particles were coated with low amount of polymer. Effect of polymer content on the morphologies and pore size distribution of porous SiC ceramics are presented in Figure 6-11. Accordingly, it can be found that by increasing the polymer content, larger pores are created in the final product. The SEM images in Figure 6-11 show the microstructure of fracture surfaces in the specimens with different amount of polymer (3.6 wt% and 19.3 wt %). One can see that in the sample with lower amount of polymer, more SiC particles were connected and larger growth necks between SiC particles are observed which enhances the mechanical strength of the produced samples.

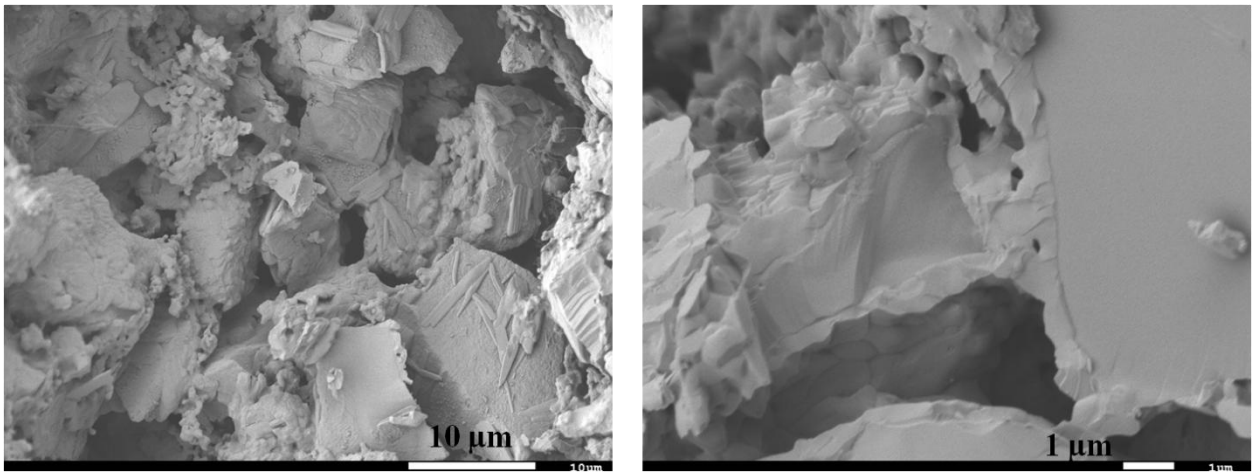

Figure 6-10 SEM of porous SiC ceramics sintered at 1550 °C for 3 h in air where 35%wt. calcined alumina was added into SiC particles and they were coated with 11.7 wt% of polyethylene

The relationship between strength of porous material and the porosity can be expressed by the following equation proposed by Rice [49]:

$$\sigma = \sigma_0 \exp(-bP) \qquad 6\text{-}5$$

Where σ_0 and σ are the strength of a non-porous structure and the strength of a porous material at a porosity P, respectively, and b is an empirical constant which depends on the pore structure and material composition. The parameters of σ_0 and b were obtained to be 235.1 MPa and 4.9, respectively by fitting of the resulted samples with different polymer content using linear-regression (R^2 = 0.977). It should be noticed that the σ_0 and b parameters depends strongly on the processing conditions. For example, She et al[4] reported the values of σ_0 =190 MPa and b=4.36 for mullite-boned porous SiC ceramics while Chun et al. [50] reported b =7.95 for the silica-bonded porous SiC ceramics.

Table 6.3 contains the physical and mechanical properties of porous samples as a function of forming pressure where 3.6 wt % of polymer was initially used and the specimens were later sintered at 1500 °C for 3h. The results show that in contrast to the polymer content, the compaction pressure has a direct effect on the strength. With increasing the forming pressure from 25 MPa to 100 MPa, the mechanical strength increases by about 100%, while the porosity and the median pore diameter were shifted to smaller values. XRD patterns analysis (results are

not shown) reveals that at higher forming pressure, the relative intensity of mullite to alumina increased slightly. Increasing the forming pressure reduces the space between particles as well as the porosity as it can be observed in Figure 6-12. Therefore, the diffusion of α-Al_2O_3 through silica particle speeds up and mullitization rate increased. Consequently, the flexural strength of porous SiC ceramics is improved as a result of well-developed necks between SiC particles.

Table 6.3 Effect of forming pressure on the flexural strength, open porosity and pore size

Forming pressure (MPa)	Flexural strength (MPa)	Porosity (%)	Median pore diameter (μm)	Skeletal density (g/cm^3)
25	32.8 ± 3.4	38.3	2.19	3.12
50	50.1 ± 3.1	31.2	1.41	3.11
100	64.4 ± 8.4	27.1	1.18	3.10

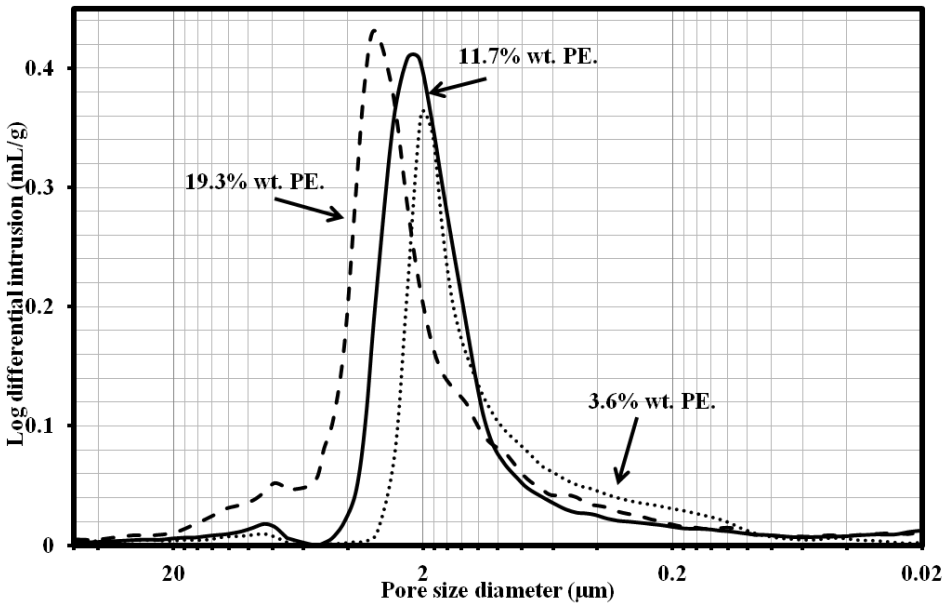

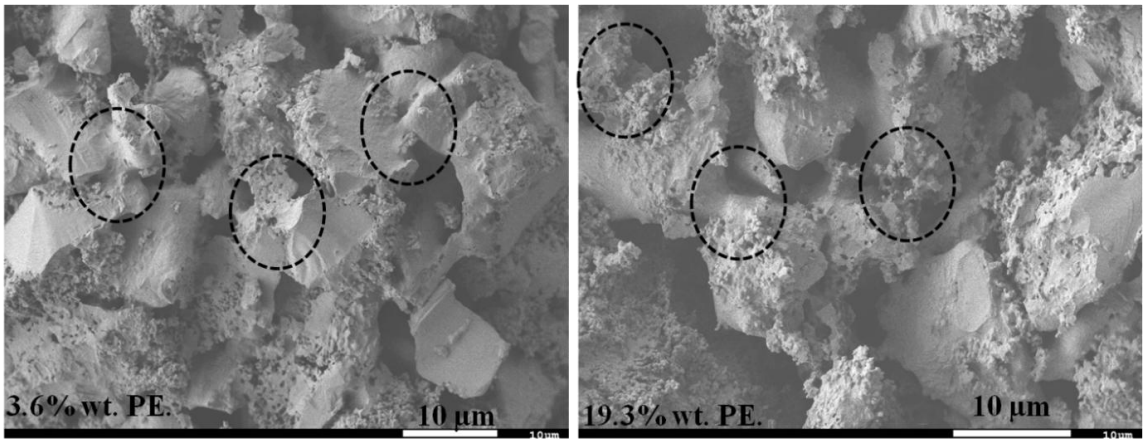

Figure 6-11 Pore size distribution and SEM of porous SiC ceramics sintered at 1500 °C for 3 h in air, where 35%wt. calcined alumina was added into SiC particles and where starting particle were coated with different amount of polyethylene

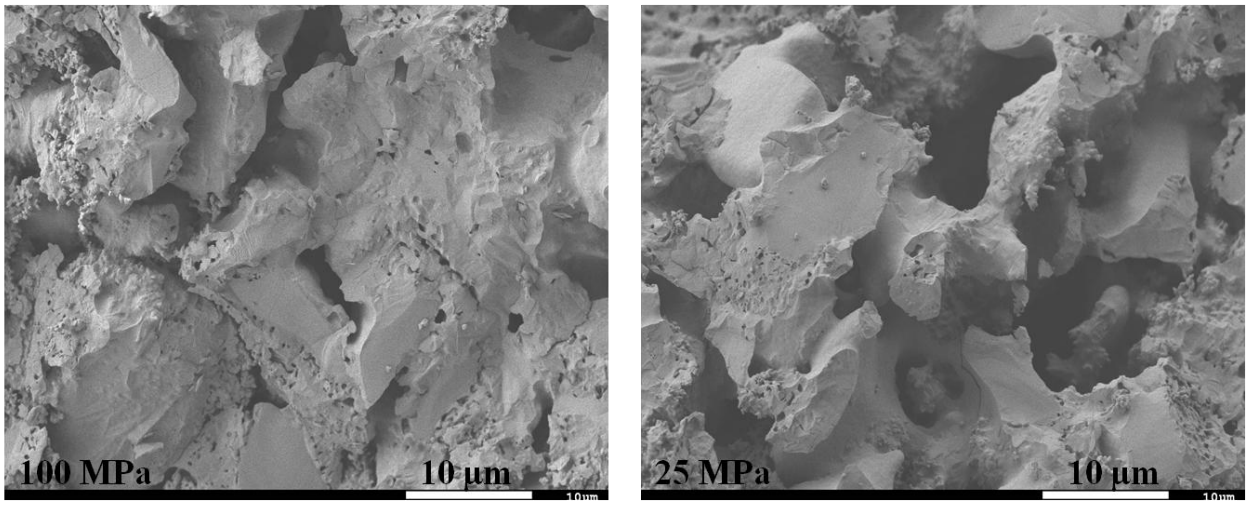

Figure 6-12 SEM morphologies of porous SiC ceramics sintered at 1500 °C for 3 hrs in air with the forming pressure of green bodies of 25 MPa and 100 MPa, where 35wt.% alumina was added into SiC particles and the starting particles were coated with 3.6 wt.% of polymer

According to the experimental results presented in this study, it is confirmed that introducing a polymer layer on the starting materials by in situ polymerization is a versatile method to produce porous ceramics with higher strength and porosity compared to the traditional method. It was

noticed that the green product formed by this technique exhibits higher strength stability which make them much safer for the handling and machining in comparison with those resulted by traditional method. This enhancement can be attributed to the strong filler/matrix interfacial adhesion during the green body formation because the polymer provides better bonding between SiC and alumina. The polymerization efficiency can be improved if the particles surface is pre-treated in order to increase the hydroxyl groups on the materials surface on which catalyst can react. For example, the modification of SiC particles and alumina nanosize powders with alumina sol before performing the polymerization may be an efficient way to increase the adhesion between matrix and the particles. This hypothesis will soon be evaluated in a future and more thorough investigation.

6.5 CONCULUSIONS

In this work, a new process was developed to produce porous SiC ceramics using a combination of *in-situ* polymerization and *in-situ* reaction bonding techniques. SiC particles as the starting materials and alumina nanoparticles as the sintering additives were successfully coated by polyethylene through an in-situ polymerization process, in which the $TiCl_4$ catalyst was initially anchored covalently on the particles surface to subsequently initiate the polymerization of ethylene from the surface of particles. TGA analysis showed that high density polyethylene was synthesized at different reaction times and SEM and TEM observations provided direct evidence for the formation of macromolecular chains on the particles.

Comparing the produced porous ceramics via novel route with the ones obtained from the more traditional method revealed that both mechanical and physical properties of the resulting products were significantly improved. In addition, it was noticed that the green product formed by this technique exhibits higher strength stability which make them much safer for the handling and machining in comparison with those resulted by traditional method. XRD and SEM analysis confirmed that SiC particles were bonded by both mullite and cristobilite. Pore size distribution analysis of the samples showed that coating of the particles with polymer via in situ polymerization induced appropriate dispersion of nano powders into micro SiC particles leading to better homogeneity of final product. As a result of better dispersion and connecting of alumina

to SiC particles by polymer chains, more mullite was produced due to the reaction between alumina and SiO_2, as observed by XRD examination.

Moreover, it was found that increasing the sintering temperature and the forming pressure has significant effects on the strength and the porosity of the porous materials. In contrast, increasing the polymer content causes less contact between SiC particles, which leads to a week neck growth and increase in porosity and decrease in mechanical strength of ceramics porous materials. In the current study, a flexural strength between 28 to 64 MPa was measured in conjunction with samples ranging from 43% to 27 % in porosity by controlling the process conditions such as forming pressure and polymer content.

6.6 ACKNOWLEDGMENTS

This research was financially supported by NSERC for the Idea to Innovation grant. The authors acknowledge Ms. Sylvie St-Amour at FPInnovations, Canada, for her assistance with the mercury porosimetry measurements and Mr. Robert Delisle from Chemical engineering department of Polytechnique Montreal for his technical support regarding to the experimental setup.

6.7 REFERENCES

1. Kennedy, G. P.; Lim, K. Y.; Kim, Y. W.; Song, I. H.; Kim, H. D., Met. Mater. Int. 17, 599 2011.

2. Liu, S. F.; Zeng, Y. P.; Jiang, D. L., International Journal of Applied Ceramic Technology 6, 617 2009.

3. Sigl, L. S.; Kleebe, H. J., Journal of the American Ceramic Society 76, 773 1993.

4. She, J. H.; Deng, Z. Y.; Daniel-Doni, J.; Ohji, T., J Mater Sci 37, 3615 2002.

5. Ding, S. Q.; Zhu, S. M.; Zeng, Y. P.; Jiang, D. L., J Eur Ceram Soc 27, 2095 2007.

6. Liu, S. F.; Zeng, Y. P.; Jiang, D. L., J Eur Ceram Soc 29, 1795 2009.

7. Ding, S. Q.; Zhu, S. M.; Zeng, Y. P.; Jiang, D. L., Ceram Int 32, 461 2006.

8. Choi, Y. H.; Kim, Y. W.; Han, I. S.; Woo, S. K., J Mater Sci 45, 6841 2010.

9. Eom, J. H.; Kim, Y. W., J Mater Sci 44, 4482 2009.

10. Ebrahimpour, O.; Dubois, C.; Chaouki, J., J Eur Ceram Soc.

11. Chi, W. G.; Jiang, D. L.; Huang, Z. R.; Tan, S. H., Ceram Int 30, 869 2004.

12. Chun, Y. S.; Kim, Y. W., Metals and Materials International 11, 351 2005.

13. Rajabian, M.; Dubois, C., Polym Composite 27, 129 2006.

14. Caruso, F., Adv Mater 13, 11 2001.

15. Esmaeili, B.; Dubois, C.; Carreau, P. J.; Heuzey, M. C., Int Polym Proc 28, 331 2013.

16. Kango, S.; Kalia, S.; Celli, A.; Njuguna, J.; Habibi, Y.; Kumar, R., Progress in Polymer Science 38, 1232 2013.

17. Trujillo, M.; Arnal, M. L.; Muller, A. J.; Laredo, E.; Bredeau, S.; Bonduel, D.; Dubois, P., Macromolecules 40, 6268 2007.

18. Zhang, X.; Simon, L. C., Macromol Mater Eng 290, 573 2005.

19. Cinausero, N.; Azema, N.; Cuesta, J. M. L.; Cochez, M.; Ferriol, M., Polym Advan Technol 22, 1931 2011.

20. Zou, H.; Wu, S. S.; Shen, J., Chem Rev 108, 3893 2008.

21. Liu, G. Y.; Li, L. Y.; Yang, X. L.; Dai, Z., Polym Advan Technol 19, 1922 2008.

22. Dubois, C.; Rajabian, M.; Rodrigue, D., Polym Eng Sci 46, 360 2006.

23. Zapata, P.; Quijada, R.; Benavente, R., J Appl Polym Sci 119, 1771 2011.

24. Azinfar, B.; Ahmad Ramazani, S. A.; Jafariesfad, N., Polym Composite, n/a 2013.

25. Nikkhah, S. J.; Ramazani, A.; Baniasadi, H.; Tavakolzadeh, F., Mater Design 30, 2309 2009.

26. Ma, J. S.; Qi, Z. N.; Hu, Y. L., J Appl Polym Sci 82, 3611 2001.

27. Zapata, P.; Quijada, R.; Covarrubias, C.; Moncada, E.; Retuert, J., J Appl Polym Sci 113, 2368 2009.

28. Esmaeili, B.; Chaouki, J.; Dubois, C., Polym Eng Sci 52, 637 2012.

29. Hong, R. Y.; Qian, J. Z.; Cao, J. X., Powder Technol 163, 160 2006.

30. Zapata, P. A.; Tamayo, L.; Páez, M.; Cerda, E.; Azócar, I.; Rabagliati, F. M., European Polymer Journal 47, 1541 2011.

31. Sohail, O. B.; Jabarullah Khan, M.; Sreekumar, P. A.; Al-Harthi, M. A., Polymer Engineering & Science, n/a 2013.

32. Esmaeili, B.; Chaouki, J.; Dubois, C., Aiche J 55, 2271 2009.

33. Esmaeili, B.; Chaouki, J.; Dubois, C., Macromol Symp 243, 268 2006.

34. Peterson, J. D.; Vyazovkin, S.; Wight, C. A., Macromol Chem Physic 202, 775 2001.

35. Marongiu, A.; Faravelli, T.; Ranzi, E., J Anal Appl Pyrol 78, 343 2007.

36. Chrissafis, K.; Paraskevopoulos, K. M.; Pavlidou, E.; Bikiaris, D., Thermochim Acta 485, 65 2009.

37. Rachtanapun, P.; Selke, S. E. M.; Matuana, L. M., J Appl Polym Sci 88, 2842 2003.

38. Osman, M. A.; Atallah, A., Macromol Rapid Comm 25, 1540 2004.

39. Siokou, A.; Ntais, S., Surf Sci 540, 379 2003.

40. McCafferty, E.; Wightman, J. P., Surf Interface Anal 26, 549 1998.

41. Ma, G.; Liu, D. F.; Allen, H. C., Langmuir 20, 11620 2004.

42. Wang, Q.; Kaliaguine, S.; Aitkadi, A., J Appl Polym Sci 44, 1107 1992.

43. Jin, Y. H.; Park, H. J.; Im, S. S.; Kwak, S. Y.; Kwak, S., Macromol Rapid Comm 23, 135 2002.

44. Siokou, A.; Ntais, S., Surf Sci 540, 379 2003.

45. Ramazani S. A, A.; Tavakolzadeh, F.; Baniasadi, H., J Appl Polym Sci 115, 308 2010.

46. Ebrahimpour, O.; Chaouki, J.; Dubois, C., J Mater Sci 48, 4396 2013.

47. Davis, R. F.; Pask, J. A., J Am Ceram Soc 55, 525 1972.

48. Saruhan, B.; Albers, W.; Schneider, H.; Kaysser, W. A., J Eur Ceram Soc 16, 1075 1996.

49. Rice, R. W., J Mater Sci 28, 2187 1993.

50. Chun, Y.-S.; Kim, Y.-W., Met. Mater. Int. 11, 351 2005

CHAPTER 7 ARTICLE 4: MANUFACTURING PROCESS FOR IN-SITU REACTION-BONDED POROUS SIC CERAMICS USING A COMBINATION OF GRAFT POLYMERIZATION AND SOL-GEL APPROACHES

Omid Ebrahimpour, Charles Dubois and Jamal Chaouki[2]

Department of Chemical Engineering, École Polytechnique de Montréal, P.O. Box 6079, Station Centre-Ville, Montréal, Canada

Abstract

A new process was successfully developed to manufacture mullite-bonded porous SiC ceramics. In this technique, SiC particles as the starting materials were coated with a sintering additive (alumina) and pore-former (high density polyethylene) in a two-step processing route composed of sol-gel and in-situ polymerization techniques, respectively. After the formation of a green body, the porous samples were produced by pressureless sintering under air. The microstructures, phase components, and physical and mechanical properties of the developed porous ceramics were examined and compared with the traditional process, which involved heating the green body (made from compacting a SiC and alumina powder mixture) under air. Comparing the results revealed that the flexural strength (35%) and porosity (8 %) as well as the pore size of the samples fabricated by the novel process significantly increased compared to the traditional method. The XRD, SEM, and mercury porosimetry analysis indicated that the enhanced

[2] Jamal.chaouki@polymtl.ca Tel.: +1-(514) 340-4711 x. 4034; fax: +1-(514)340-4159

properties of the porous ceramics were attributed to the good dispersion of the sintering additive and pore former into the SiC particles and the higher mullite formation as a result of the direct contact between the oxidation-derived SiO_2 and alumina and the presence of TiO_2 derived from the Ziegler-Natta catalyst during polymerization.

Keywords: porous SiC ceramics, mullite, TiO_2, sol-gel, in-situ polymerization, reaction bonding

7.1 INTRODUCTION

Porous silicon carbide ceramics have been recognized as promising candidates for hot gas particulate systems in different industrial processes, such as the integrated gasification combined cycle (IGCC) and coal combustion due to their unique properties, such as outstanding chemical stability, low thermal expansion number, superior thermal shock resistance and excellent mechanical strength [1-5]. However, a very high sintering temperature must be applied in the manufacturing of self-bonded porous SiC ceramics because of the strong covalent bonding in SiC and its low self-diffusion coefficient [6,7]. In addition, during the operation of this type of filter at high temperatures, especially in the presence of water vapor, SiC is oxidized to silica, which causes the failure of products, particularly during the pulse cleaning process [8].To overcome these problems, She et al. [9] first developed a promising alternative process (known as in-situ reaction bonding), which entails changing the sintering environment to air, instead of an inert atmosphere and introducing alumina powders as the sintering aids to the starting materials. During the sintering stage, SiC particles are bonded by both oxidation-derived silica and mullite formed by the reaction between alumina and silica. This process results in the formation of porous SiC ceramics at a relatively moderate sintering temperature (1500 °C) with superior oxidation resistance in the final products. In addition, due to the slight difference in the thermal expansion coefficient between mullite (5.3×10^{-6}/K at 0–1000 °C) and SiC (4.7×10^{-6}/K at 0–1000 °C) the products are durable against thermal shock [9].

As an interesting technique to fabricate porous SiC ceramics at a low sintering temperature, the reaction bonding method has been the focus of much research from various viewpoints, such as the effects of sintering additives [10-14] and starting particle sizes [3] on the characteristic

properties of porous samples as well as the evaluation of gas permeation on the manufactured samples [15]. Dey and his coworkers investigated the implementation of the infiltration technique to fabricate porous mullite-bonded SiC [16]. Kumar et al. [17] processed porous mullite-bonded SiC via different aluminum sources (Al, AlN, Al_2O_3 and $Al(OH)_3$). They reported that using alumina powders results in the highest strength and the lowest porosity.

Typically, to increase the porosity of the final product, some sacrificial fugitives, such as graphite, yeast or polymer beads, are incorporated with the raw materials [18]. During the heating process of the green body, these pore-formers burn out and pores are produced.

Although the reaction bonding technique has numerous advantages as mentioned earlier, the main disadvantage of this process is the insufficient dispersion and, particularly, the formation of nanoparticle agglomerates of sintering additives in the starting particles (SiC), which substantially initiates premature mechanical failure of the final ceramics. For instance, Ding et al. [14] reported that during the mixing of alumina nano powders with micro sized SiC, alumina were agglomerated and did not have contact with SiC particles. Therefore, the full advantages of alumina addition were not exploited as they did not react with silica to form mullite. Apart from the agglomeration of sintering additives, it was reported that because of differences between the particle size of pore formers and the starting materials and the in-homogenous dispersion of the pore former between the starting materials, the pore size distribution of the specimens exhibited the bio model [10,14]. One of the peaks derived from the burning out of pore former and another formed as a result of SiC particles being stacked due to the in-homogenous mixing between the particles. She et al. reported that even when homogenous graphite particles were used as the pore former, the pore size distribution of the porous samples was very broad [9].

Recently, our research group demonstrated that if some parts of calcined alumina were replaced by alumina sol by mixing the starting powders (SiC and alumina powders) in alumina sol, the mechanical properties were enhanced compared to the samples prepared by pure calcined alumina [19]. It was shown that sol-gel processing is an attractive approach to fabricate ceramic composites owing to its advantages, such as fine-scale mixing between alumina and SiC and lowering the processing temperature [20].

More recently, our group thought of a new idea where the starting powders (SiC and calcined alumina powders) are coated with the polymer, which acts as the pore former to improve the

dispersion of the pore former in the starting materials by means of in situ polymerization techniques. The in situ polymerization technique, known as the graft polymerization, is commonly used to fabricate in-organic-organic nanocomposites [21]. The mixture of SiC powders and calcined alumina nano powders was coated by polyethylene via the synthesis of the polymer from the surface of the particles instead of physically mixing the powders with the polymer. The obtained porous ceramics have higher mechanical properties and porosity compared to the traditional method. It was proposed that during the synthesis of the polymer from the surface of particles, the agglomeration of alumina powders was broken, which results in enhancing the mechanical properties.

The present study addresses an alternative way to fabricate porous SiC ceramics based upon our previous works, which make it possible to improve the uniform dispersion of sintering additives and pore-former onto the starting materials and have a narrow pore size distribution of the specimens as well as increasing the mechanical strength and the porosity simultaneously compared to the conventional method. The approach is schematically presented in Figure 7-1. Instead of physically mixing the starting powder, sintering additive and pore former (Figure 7-1-right), the starting powders are chemically coated by the sintering additive (using the sol-gel process) and pore former (via in-situ polymerization) as shown in Figure 7-1, left. The properties of coated particles were investigated with different techniques, such as XPS, SEM and TGA. In addition, the developed porous SiC ceramics were characterized by analyzing their phase composition, microstructure, mechanical strength, open porosity and pore size distribution and the results were compared with the specimens prepared by the conventional method. Finally, the effect of the sintering temperature in the range of 1500 °C to 1600 °C on the crystalline changes as well as the physical and mechanical properties of porous SiC ceramics has been investigated in detail.

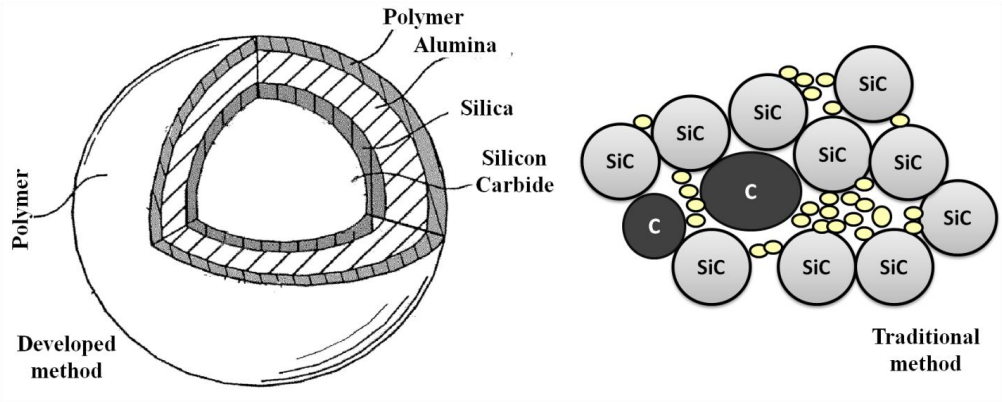

Figure 7-1 Scheme of the starting materials used for the fabrication of porous SiC ceramics: traditional process (right) developed method (left).

7.2 EXPERIMENTAL SECTION

7.2.1 MULTILAYER COATING ON SIC PARTICLES

Figure 7-2 illustrates the schematic of the fabrication procedure. In a typical experiment, 18 g α-SiC (99.7% purity, ρ= 3.2 g/cm^3, S_{BET}= 0.87 m^2/g, LabMAT, Canada) and 7.77 g α-alumina (99.95% purity, ρ= 3.95 g/cm^3, S_{BET}= 8.5 m^2/g, LabMAT, Canada) were dispersed in the alumina sol using a magnetic stirrer. The amount of alumina sol yielded 1.94 grams of alumina during the calcination process. Hence, the weight proportion of alumina in the system was kept constant to 35 wt.% $\left(\frac{Al_2O_3}{Al_2O_3+SiC}\right)$%, in which 20 wt. % of it was produced from alumina sol.

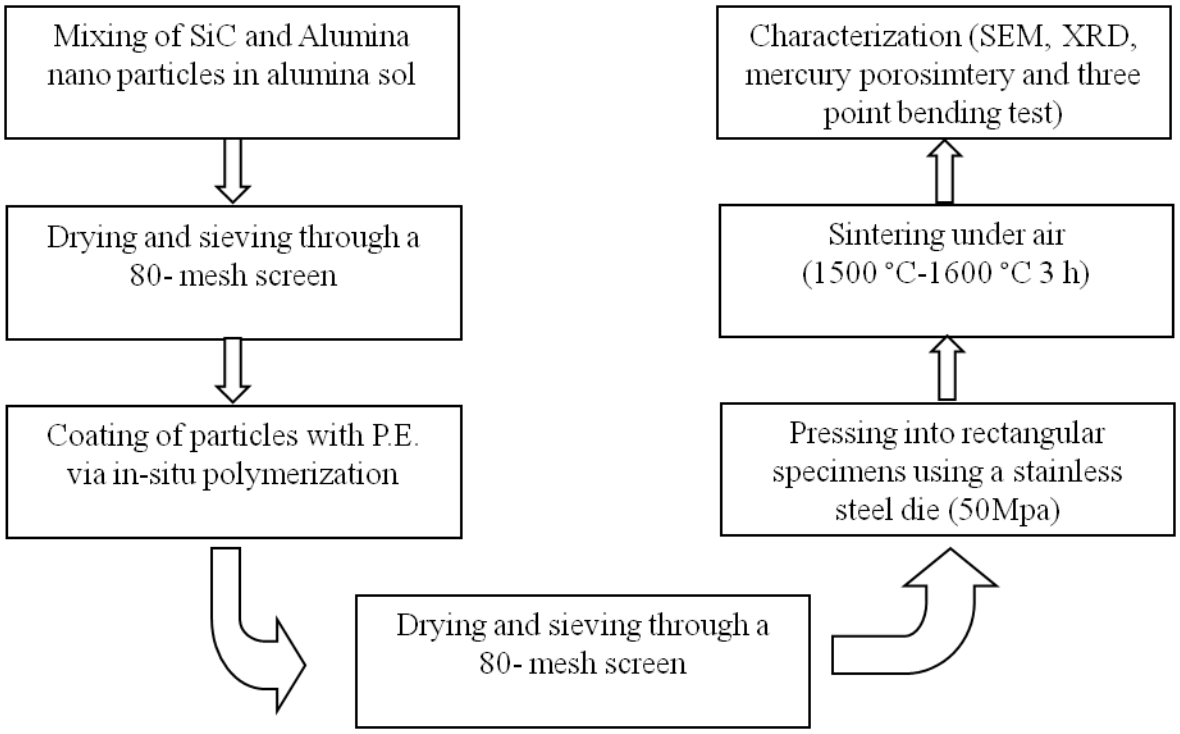

Figure 7-2 Schematic diagram of the novel fabrication route used for the preparation of porous SiC ceramics

Alumina sol was synthesized via hydrolysis and condensation of aluminum isopropoxide (AIP, Aldrich, 98%) as a precursor to the Yoldas method. The details of the synthesis and characterization of alumina sol have been described elsewhere [22]. The molar weight ratio of water to aluminum isoproxide was 100:1 and the pH of the resultant alumina sol was adjusted to about 4 leading to a stable sol. According to the TEM observation, the formed alumina sol has a needle-like shape with a thickness of 2-3 nm and a length of 15 to 25 nm [22].

After drying the powders at 150 °C for 24 hrs and passing them through an 80 mesh sieve, they were loaded into the BUCHI reactor, which was previously filled with the dried hexane (Sigma) for the polymerization of polyethylene from the surface of powders using the Ziegler Natta catalyst. Since the catalyst system was very reactive in water and oxygen, it was handled and stored in the glove-box under Argon atmosphere. The polymerization procedure can be found in detail in the previous work. In summary, in this step, the desired amount of catalyst $TiCl_4$ (Acros) was added to the system followed by an injection of the co-catalyst, triethylaluminum 1M, in hexane ($AlEt_3$, Sigma-Aldrich). The amount of injected catalyst was calculated based on the

theoretical assumption which the catalyst can cover the entire particles surface (45 mg cat/g powder) The amount of catalyst was determined on the ass7mg cat/g powder The mole ratio of co-catalyst to catalyst was kept at 2. Before the polymerization reaction, the powders were mixed by a magnetic drive impeller under nitrogen (99.5% purity, Canadian liquid air). The reaction began by introducing the ethylene monomer in the medium instead of nitrogen gas at a temperature of 65 °C and pressure of 50 kPa. The polymerization reaction was terminated by adding ethanol in the system to hydrolyze the catalyst complex. In this step, the amount of synthesized polymer on the powders was a function of reaction time.

7.2.2 Preparation of porous SiC samples

The resulted composites were dried, sieved again through an 80 mesh screen and, subsequently, compacted under a pressure of 50 MPa to form a rectangular bar 4.5 mm × 10.0 mm × 50.0 mm using a stainless steel die. Then, the green compacts were heated under air at a heating rate of 2 °C/min up to 900 °C and 5 °C / min up to the desired sintering temperatures (1500 °C, 1550 °C and 1600 °C) and held for 3 hrs at that firing temperature. To compare the physical and mechanical properties of the ceramic porous manufactured via the developed method with the conventional process, the powder mixture of SiC and alumina (35 wt. %) was ball milled in ethanol with 2.5 wt.% of polyvenyly butrilal (PVB) as the organic binder using high energy milling. The suspension was dried under circulation and subsequently sieved through an 80-mesh screen to avoid hard agglomerates. Similar steps as described above were conducted to produce porous samples.

7.2.3 Characterization of the powders

The surface area of the starting powders and after being coated with polymer was determined by a Horiba Quantachrome Autosorb-1 apparatus. Before BET analysis, samples were degassed at 150 °C for 3 hours. Particle size distribution of the powders was characterized using an LA-950 laser diffraction particle size analyzer. The morphology of untreated and coated mixed powders was observed by field emission scanning electron microscopy (SEM, Model JSM-7600 TFE, JEOL, Japan) working at 2 kV. Thermal analyses were performed using thermogravimetric

analysis (TGA Q 5000 apparatus) to determine the degradation behaviour of dried alumina sol and the quantity of polymer and alumina sol coated on the SiC particles. Typically, about 10 mg of powders were heated under nitrogen atmosphere with a heating rate of 10 °C/min and a gas flow of 20 ml/min using a palatine pan.

The surface composition of starting powders and after coating was investigated by X-ray photoelectron spectroscopy (XPS), using a VG Scientific ESCALAB Mk II with Mg Kα radiation (1253.6 eV) operated at 300 W (survey scan). The analyzer mode was held at constant pass energy (100 eV, 1 eV energy step size) with the depth up to 10 nm. The C1s line (285.0 eV) was used as a reference to correct any electrostatic charging. During the operation, the residual pressure in the chamber was below 8×10^{-9} mbar and the detection angle was perpendicular to the sample's surface.

7.2.4 Characterization of porous SiC ceramics

The crystalline phases of the porous specimens were detected by X-ray diffraction analysis using Philips *X'Pert* diffractometer (The Netherlands) with Cu-Kα radiation (0.154 nm) at a generator voltage of 50 kV and a current of 40 mA in the range of diffraction angles 2Θ of 10-80°. The microstructural examination of the porous samples fabricated by different routes was performed by SEM after first being coated by a thin layer of gold.

The bending strength of products was evaluated by the three point bending fixture using an Instron Universal Testing machine (Model 1123, Instron, Canton, MA, USA) with a 500 N load cell with a support distance of 30 mm at a constant crosshead velocity of 0.5 mm/min. The results were reported as the mean values of three measurements. The deflection measurement was taken using LVDT with a resolution of 0.05% and Young's modulus was calculated via standard software (Instron Bluehill-2, UK). After machining and polishing, the thickness and width of the samples obtained at a sintering temperature of 1500 °C was 3.0 (±0.1 mm) × 4.0 (±0.1 mm) and for the beams prepared at 1600 °C was 3.0 (±0.1 mm) × 7.0 (±0.1 mm), respectively, as it was difficult to be polished.

The pore size distribution of the porous samples was determined by mercury porosimetry (AutoPore IV 9500 V1.06, Micromeritics, USA), operated at up to maximum pressures of

125 MPa. The porosity of the porous samples after firing was determined from the intrusion mercury volume obtained from mercury porosimetry and the true density of the porous ceramic was obtained by the *gas* volume displacement method using a gas pycnometer (Accupyc II 1330 helium pycnometer) through the following equation:

$$\text{Porosity (\%)} = \frac{Total\ intrusion\ volume\ (\frac{ml}{g})}{Total\ intrusion\ volume\ (\frac{ml}{g}) + \frac{1}{Skeletal\ density(\frac{g}{ml})}} \times 100 \qquad 7\text{-}1$$

7.3 Results and discussion

7.3.1 Characterization of SiC and Al_2O_3 powders after treating with alumina sol and polyethylene

Figure 7-3 (a)-(d) represents the typical TGA results of the as-dried synthesized alumina sol and the resulted samples after treating SiC and alumina powders under different processes. During heating the dried alumina sol, the main weight loss (33 wt %) is observed at temperatures below 500 °C while the total loss was determined to be about 35 wt%. The weight loss is associated with the elimination of water and decomposition of organic components in the alumina sol. It was reported that with an increase in temperature, the phase of alumina sol is transferred from meta-stable phases to the stable α phase as follows [22,23]:

$$\text{Boehmite} \rightarrow \gamma \rightarrow \delta \rightarrow \theta \rightarrow \alpha \qquad 7\text{-}2$$

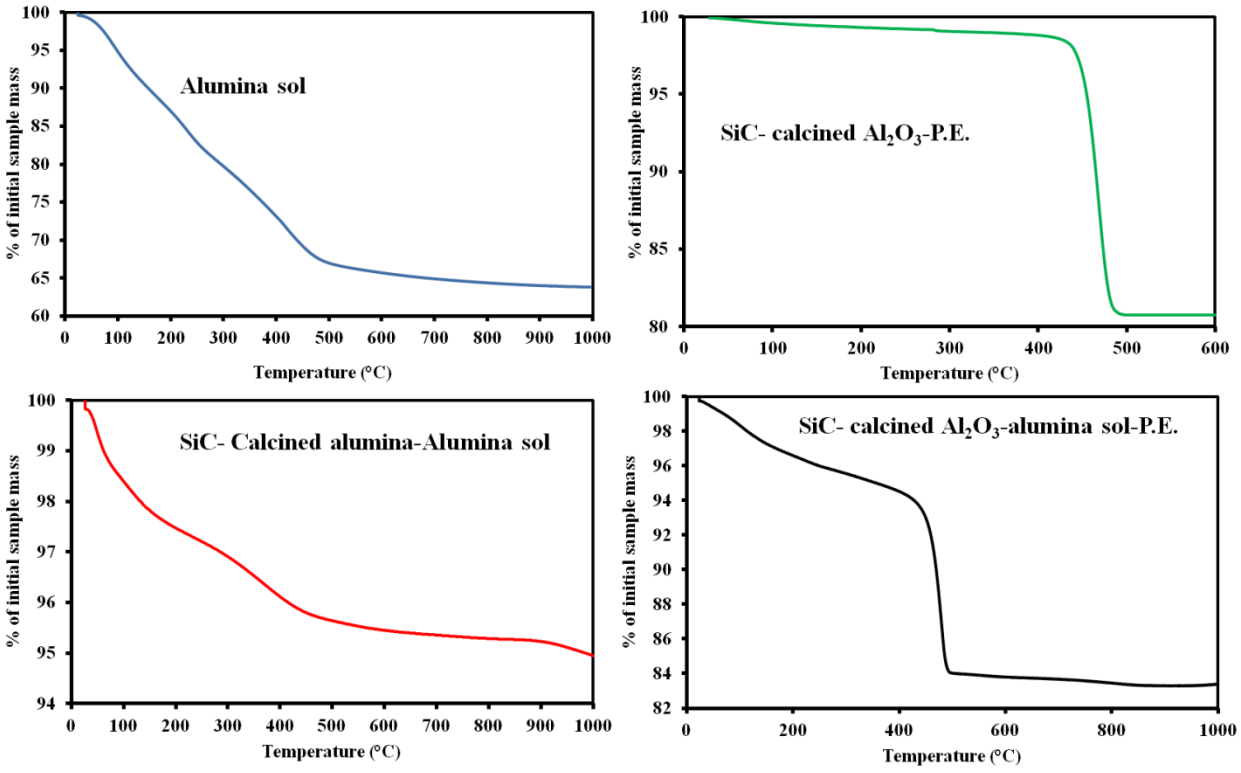

Figure 7-3 Thermal Characterization of alumina sol and coated SiC and Al2O3 powders by different routs

For the case where the mixture powders (SiC and calcined alumina (35 wt%)) were treated with polyethylene via in-situ polymerization, a sharp weight loss occurred at temperatures in the range of 425 °C-485 °C due to the degradation of high density polyethylene and olefinic and paraffinic components under nitrogen (Figure 7-3-b). It should be noted that the amount of polymer depends on the polymerization reaction time and conditions, such as pressure, temperature and mole ratio of co-catalyst to catalyst. Thermal behavior of the dried powders (SiC and calcined alumina (25 wt %)) mixed in alumina sol (Figure 7-3-c) exhibits a similar weight loss trend as observed for pure alumina sol (Figure 7-3-a) except that the total loss was much lower (5% wt). Figure 7-3-d presents the thermal analysis of the SiC and Al_2O_3 powders, which were primarily mixed in alumina sol followed by further coating with polyethylene using in-situ polymerization. The curve shows two main stages of weight loss. Compared to the results of Figure 7-3-b and Figure 7-3-c, the thermal behavior of samples obtained after sol-gel and polymerization processes behaves like the combination of individual processes (sol-gel and in-situ polymerization).

Figure 7-4 indicates the morphologies of the SiC and Al_2O_3 powder mixture before and after modification processes.

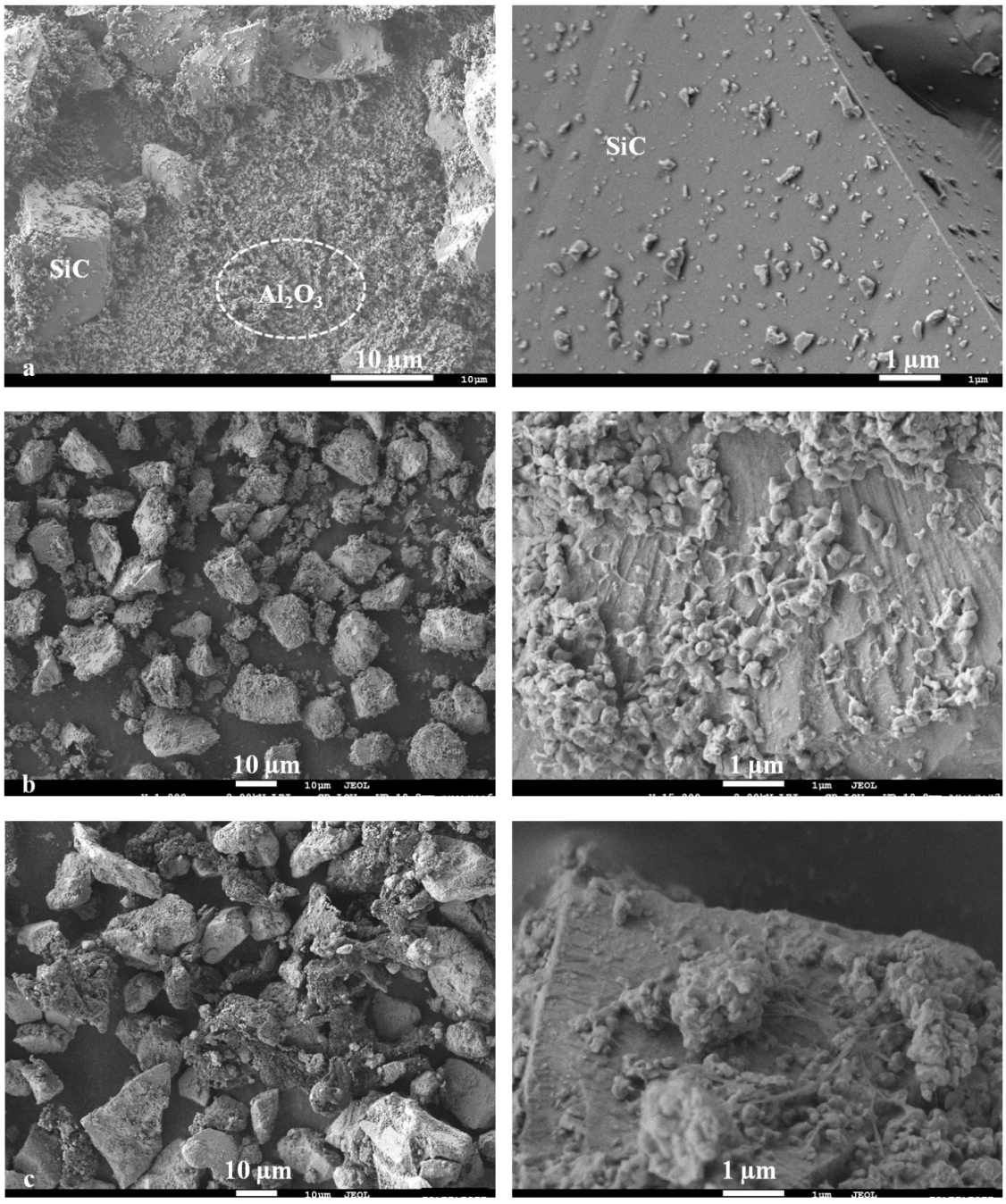

Figure 7-4 SEM images of original SiC and Al_2O_3 powders (a); after coating with alumina sol (b); after polymerization

When the powders were physically mixed in ethanol, most of the alumina nano powders were agglomerated and not homogenously dispersed between SiC particles. Before any treatment

process, the surface of SiC particles was sharp (Figure 7-4 (a) and some fine SiC powders were presented on the particles. When some parts of alumina nano particles (20 wt %) were replaced by alumina sol, the mixing of the particles was enhanced as observed by SEM characterization. Figure 7-4 -b reveals that more alumina particles attached to the surface of SiC powders. BET analysis revealed that the specific surface area of the coated powders was also notably increased to 21.38 m^2/g. This increase is attributed to the small particle size of alumina sol. Comparing the surface morphologies of powders before and after in-situ polymerization confirms the presence of the polymer chain on the surface of the particles. Implementing the surface coating leads to the blunting of the surface of SiC particles as well.

To further investigate the surface analysis of SiC and alumina powders after each treatment process, XPS measurements were conducted as shown in Figure 7-5 and element quantification from survey scans is reported in Table 7.1.

Table 7.1 XPS data for original and after coating with alumina sol and polyethylene

Name	Bonding Energy B.E. (eV)	At. % $SiC-Al_2O_3$	At.% $SiC-Al_2O_3$-AlOOH	At.% $SiC-Al_2O_3$-AlOOH-H.D.P.E.
Al2p	75.7	21.4	21.8	6.8
Si2p	101.3	7.7	2.9	-
O1s	532.9	48.4	57.1	21.1
F1s	691.8	1.6	1.4	1
C1s	285.3	20.3	15.2	67.7
Ti2p	459.1	-	-	1.3
Cl2p	199.3	0.5	1.6	2

Before any treatment on the samples, Al, Si, O, C, Cl and F elements were detected. Compared with samples after coating them with alumina sol, the weight percentage of the Si element decreased from 7.7 wt% to 2.9 wt%. In the samples that were also coated by polymer, the Si element was not detected on the surface of the substrate by the instrument. Consequently, XPS analysis revealed that the surface of SiC is completely covered by polymer and alumina sol. It should be noted that the weight percentage of the carbon element decreased slightly from 20.3 wt% to 15.2 wt% after coating the powders with alumina sol whereas after the polymerization process it increased significantly to 67.7 wt%. In the reverse trend, the weight percentage of the Al element was at first slightly increased from 48.4 wt% to 57.1 wt% after coating the powders with alumina sol due to the coating of the SiC surface by alumina sol followed by a drastic decrease to 21.1 wt% after the graft polymerization process. The first decrease corresponded to the coating of SiC particles with alumina sol and the latter increase was the result of the carbon element in polyethylene, which covers the surface of particles. Similar to the Si element, the intensity of Al is abruptly decreased from 21.4 wt% to 6.4 wt% after coating the particles with polymer. The appearance of Ti in the samples coated with polymer corresponded to the Ziegler-Natta catalyst ($TiCl_4$). It is worth mentioning that increasing the intensity of Cl is associated with the addition of HCl during the preparation of alumina sol and $TiCl_4$ during polymerization.

Yang et al. [24] proposed that when mixing SiC in alumina sol, the negatively charged silanol group (formed by the hydrolysis of the existing silica layer on the surface of SiC powders in alumina sol) reacts with $AlO_4Al_{12}(OH)_{24}(H2O)_{12}$, well-known as Al_{13}, which is positively charged in the pH range of 3.5-4. While Prabhakaran et al. [25] suggested a multi-step reaction may have occurred through the adsorption of $[Al(OH)(H_2O)]^{2+}$ and $[Al_2(OH)(H_2O)_8]^{4+}$ species on SiC particles at the studied pH range.

It is well established that the presence of the hydroxyl groups on the surface of the substrate is a key factor in the graft polymerization of polyethylene from the surface of particles [26]. It is proposed that $TiCl_4$ adheres to the substrate as follows [27]:

$$x(-OH) + TiCl_4 \rightarrow (-O)_x TiCl_{4-x} + x(HCl) \qquad 7\text{-}3$$

Where x=1 is for mono-functional and x=2 is for bi-functional compounds. Therefore, monomers are forced to be polymerized from the surface of the substrate.

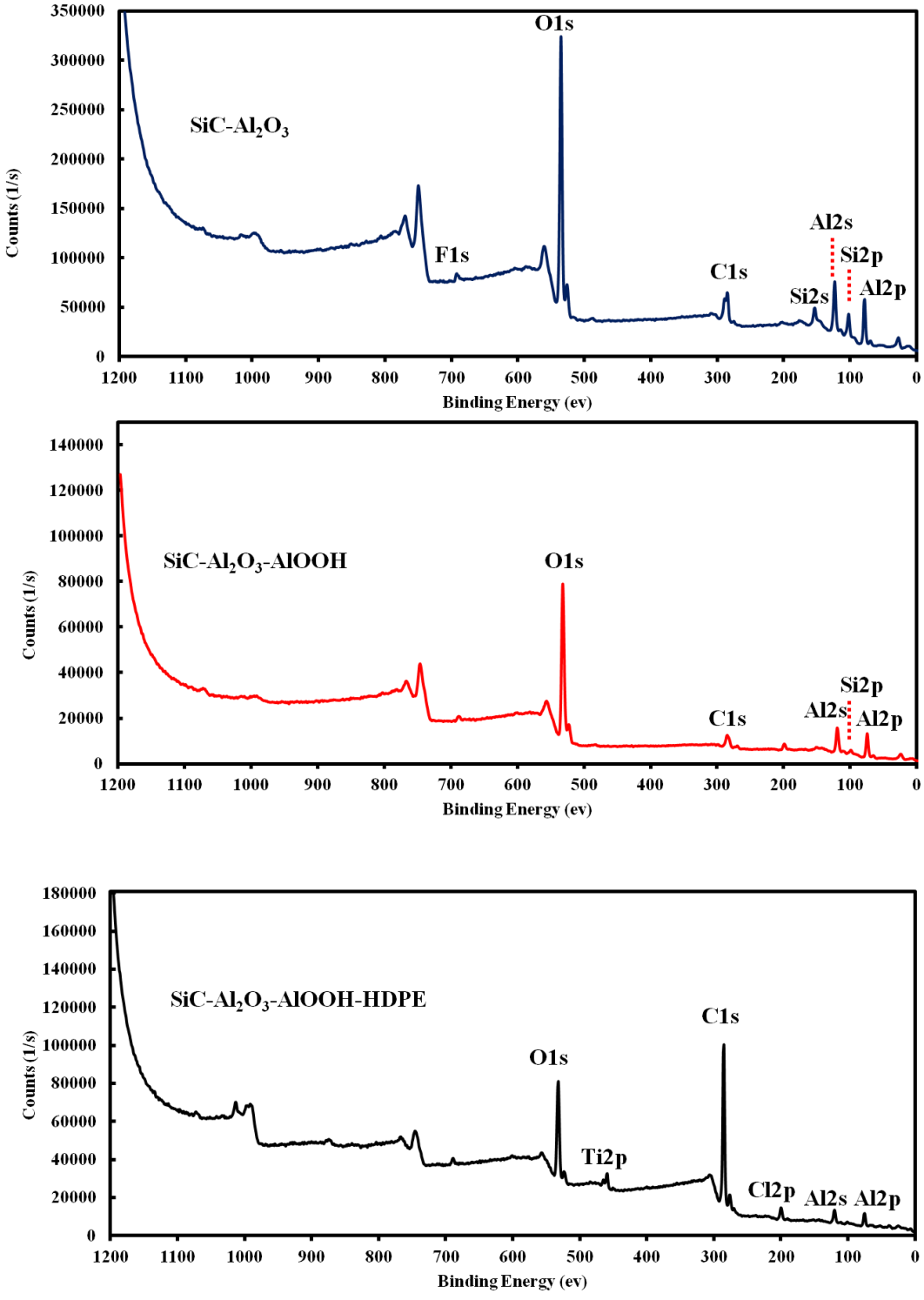

Figure 7-5 XPS spectra of original powders and after coating by alumina sol and polyethylene

According to the structure of boehmite (AlOOH), it has more hydroxyl groups compared to the SiC and calcined alumina powders. Consequently, coating the particles with alumina sol improves the interfacial adhesion between the polymer and substrate, particularly SiC powders. It is worth mentioning that XPS analysis for the particles (SiC and Al_2O_3) coated by polyethylene without any treatment detected the substrate elements (both Si and Al) even at high polymer content (18 wt%). It should be pointed out to better improve the dispersion of particles before polymerization that the surface of boehmite can be rendered by other modifications, such as stearic acid [28]. Therefore, a combination of the sol-gel process and in-situ polymerization results in the formation of the double layer of sintering additive and pore-former on the surface of SiC particles, Figure 7-6, and consequently during the pressing of these particles, the green body is formed by the uniform particles.

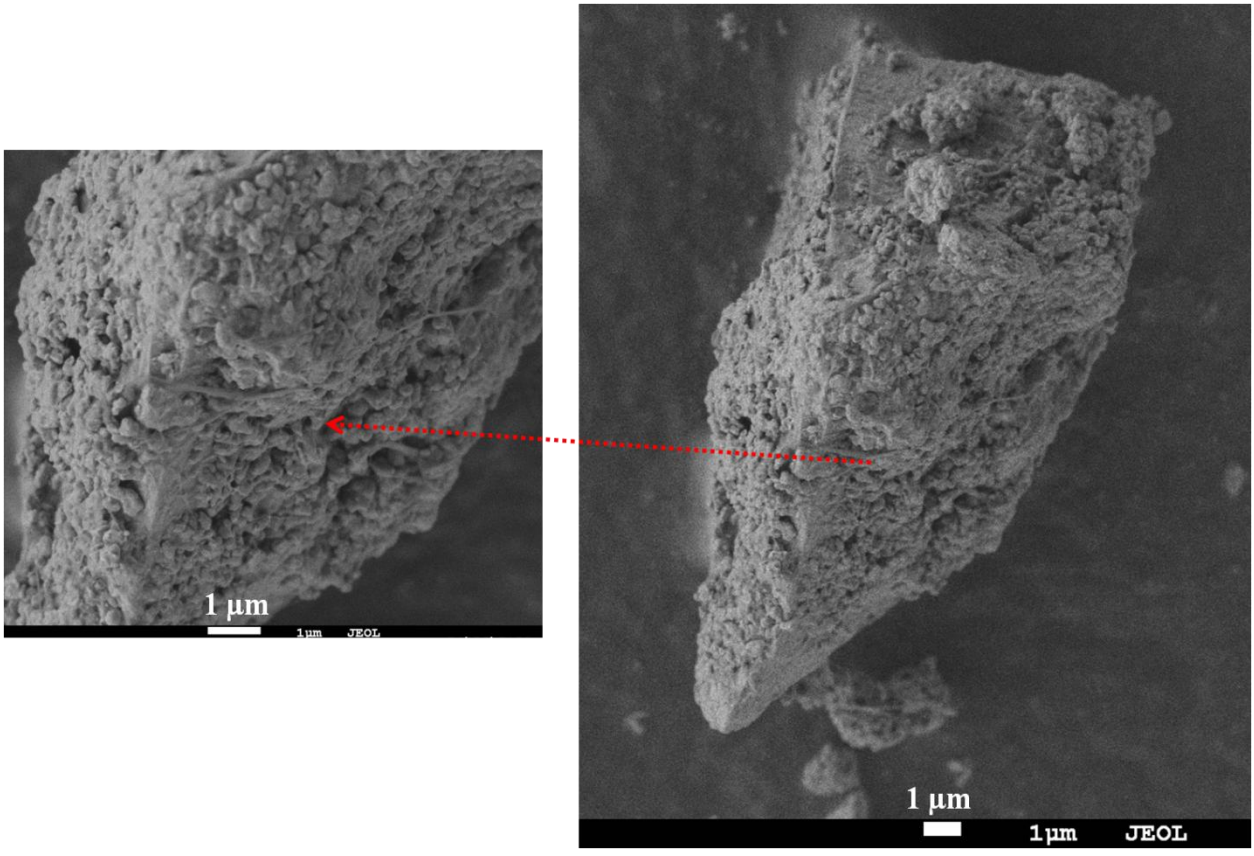

Figure 7-6 Morphology of the coated particles by sol-gel and In-situ polymerization routs

7.3.2 Characterization of porous SiC ceramics

Table 7.2 lists flexural strength, open porosity, average pore size and skeletal density of porous SiC ceramics sintered at 1500 °C for 3 hours under air (forming pressure of 50 MPa) via the developed process and the traditional method. It is clear that the incorporation of the sol-gel technique and in-situ polymerization increases significantly porosity and flexural strength compared to the conventional method.

Table 7.2 Mechanical and physical properties of the ceramics prepared by the developed method and traditional method, sintering at 1500 °C for 3hrs and forming pressure of 50 MPa

Polymer wt.%	Alumina from sol wt %	$Al_2O_3/(SiC+Al_2O_3)$ wt %	Flexural strength (MPa)	Porosity (%)	Median pore diameter (μm)	Skeletal density (g/cm^3)
0	0	35	30.9 ± 1.3	32.3	1.57	3.11
11	20	35	40.5 ± 4.2	38.7	3.85	2.90

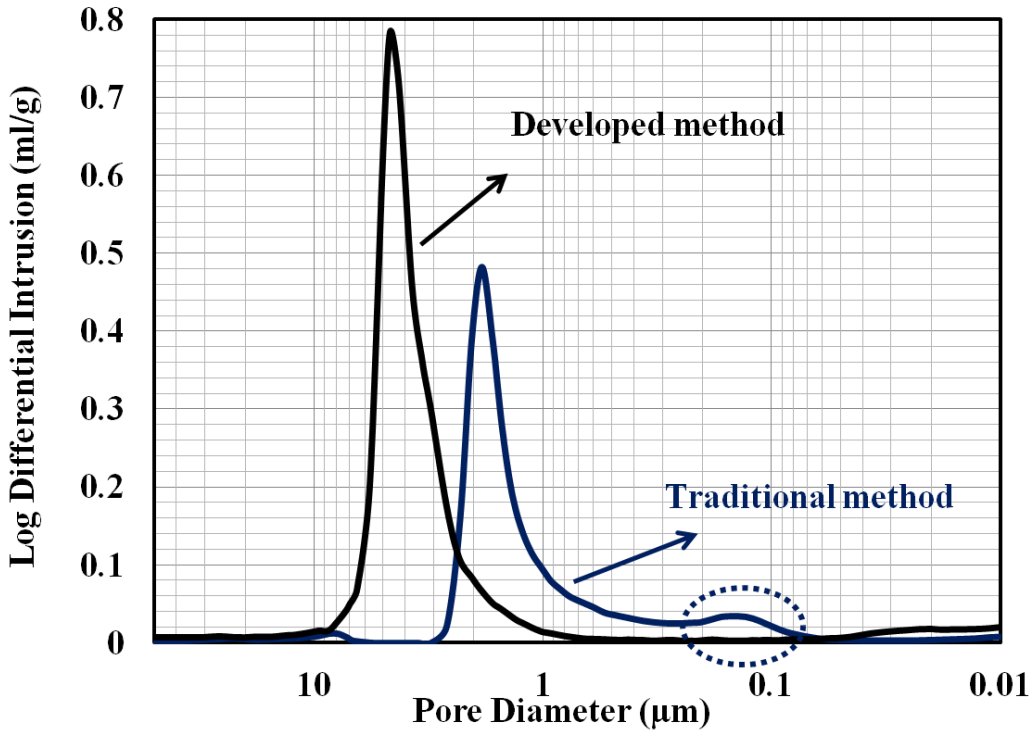

Figure 7-7 Pore size distribution of the porous SiC samples prepared by two different process, sintering temperature 1500 °C and forming pressure was 50 MPa

A typical pore size distribution of the samples via the novel process is compared with the one prepared where particles are simply mixed without any treatment in a ball mill in Figure 7-7. When no pore former was added to the system, the stacking of particles (SiC and Al_2O_3) derives pores.

As is clear in the SEM pictures (Figure 7-8), some alumina nano-particles did not make contact with SiC as a result of in-homogenous dispersion and a tendency toward agglomeration.

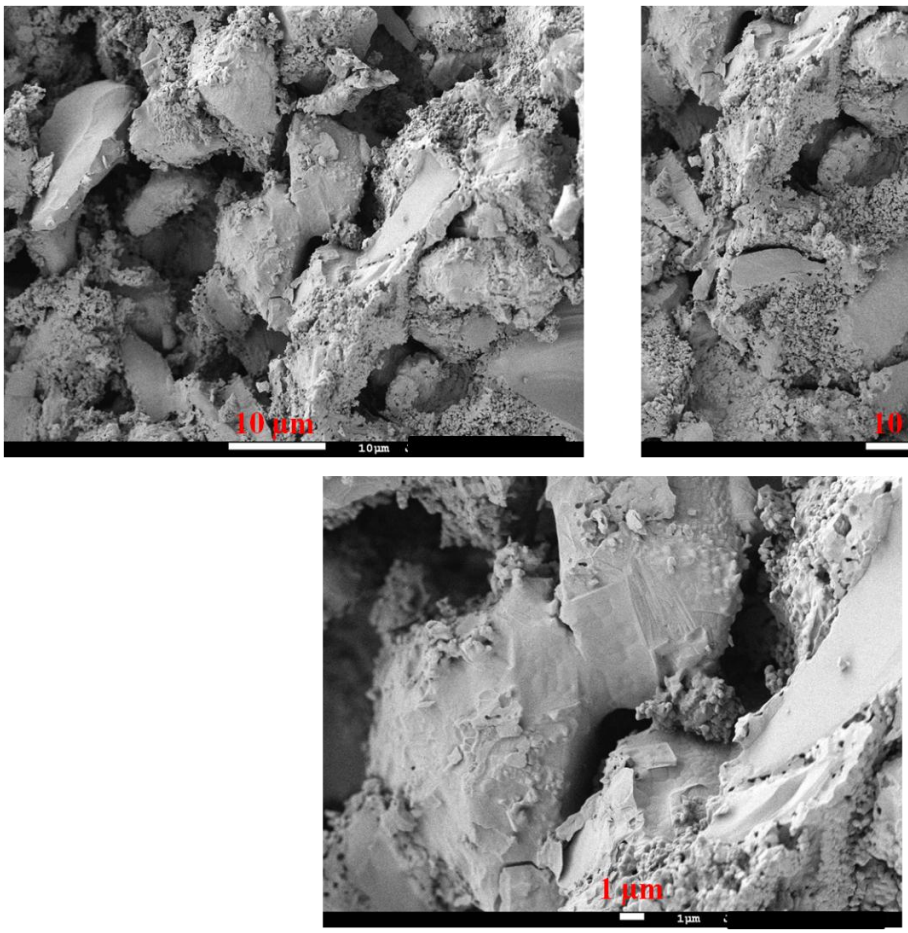

Figure 7-8 The morphology of porous SiC ceramics fabricated by the traditional method at 1500 °C under air with the 35% wt Al_2O_3

Consequently, the stacking of un-reacted alumina forms some small pores, which produce another bump as found in the pore size distribution. When particles are initially coated by both alumina sol and the polymer, the pores originate by burning out the polymer and the organic components in alumina sol as well as the stacking of SiC particles, which mostly occurs at the same position. Therefore, these phenomena results in a larger pore size than those prepared by mixing SiC and alumina powders without any pore former. In addition, the pore size distribution is much narrower compared to the samples derived by traditional methods and the agglomeration of alumina nano powders has been eliminated in the case of samples treated by sol-gel and in-situ polymerization.

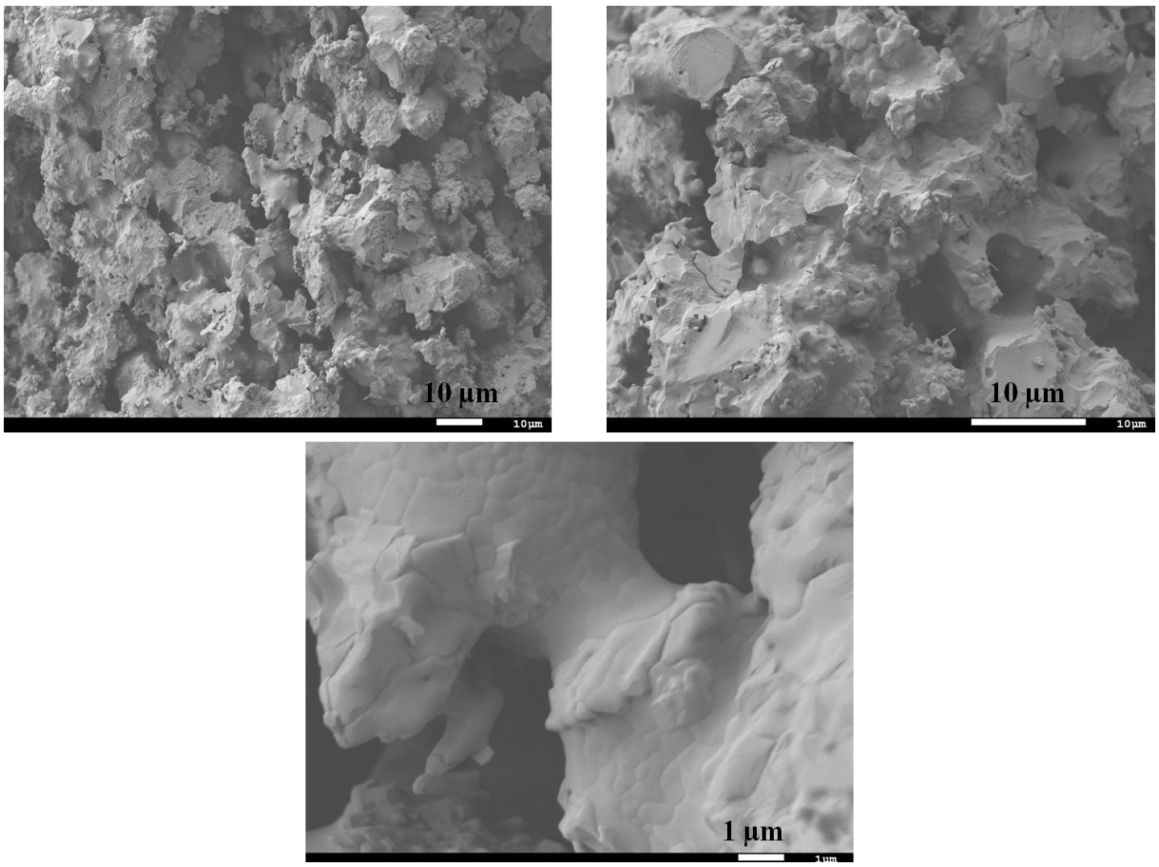

Figure 7-9 Morphology of porous SiC ceramics fabricated by the novel method at 1500 °C under air with the 35% wt Al_2O_3

Figure 7-9 shows the typical microstructure of a representative specimen fabricated by the novel method. It can be seen that the morphology of the structure completely changed compared to Figure 7-8 and most of the alumina nano powders reacted to mullite. Compared to Figure 7-8, it is evident that a greater number of SiC particles were connected together and larger growth necks

between SiC particles were developed by the novel process. This can explain the increasing mechanical strength of the produced samples obtained by a combination of sol-gel and in-situ polymerization.

To further analyze the structural changes of porous SiC ceramics with changing the process procedure, the crystalline structure was compared at the sintering temperature of 1500 °C (Figure 7-10). For both methods, the phases consist of mainly alumina, cristobalite, mullite and silicon carbide. However, in the samples fabricated with the novel route, rutile-type TiO_2 is also detected by XRD patterns as the minor phase (Figure 7-10). According to the XRD pattern, at the sintering temperature of 1500 °C, in the samples derived by the novel method, the relative intensity of mullite to alumina and cristobalite to SiC is much higher with respect to the traditional method.

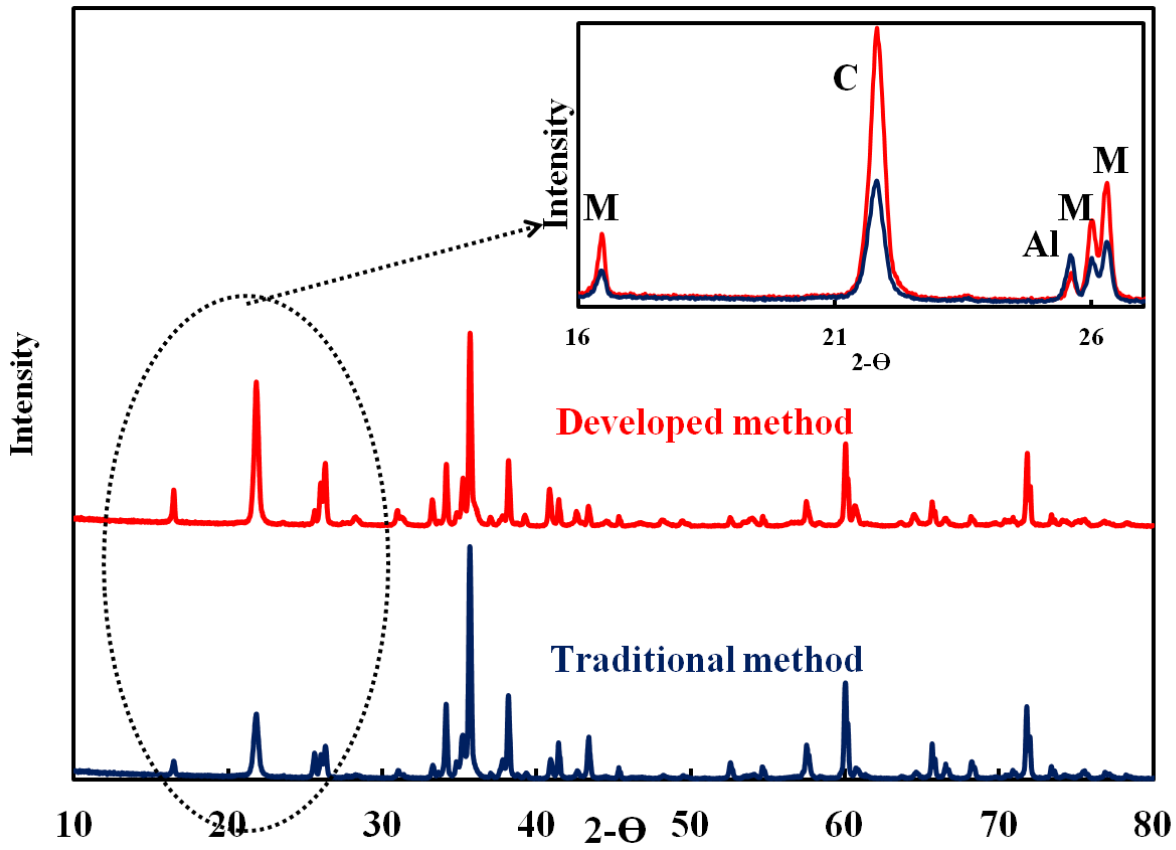

Figure 7-10 A comparison between crystalline phases of the porous SiC ceramics manufactured by the conventional method and the new process

During the passive oxidation of SiC, a coherent silica layer forms on the particle surface, resulting in the weight gain and volume expansion of particles as follows:

$$SiC + 2\,O_2 \rightarrow SiO_2(amorphous) + CO_2(g) \quad 7\text{-}4$$

As the sintering temperature is increasing, the amorphous phase of silica is transferred to the cristobalite.

$$SiO_2(amorphous) \rightarrow Cristobalite \quad 7\text{-}5$$

Previously, our research group studied the oxidation rate of SiC powders in the packed bed state. It was stated that the oxidation rate strongly depends on the reaction temperature, SiC particle size and the physical structure of the system, such as pore size and porosity in the packed bed [29]. Depending on the oxidation temperature, oxygen molecules or oxygen ions must first diffuse from the pores between SiC powders followed by diffusion through the oxide layer to reach the fresh SiC. Consequently, the oxidation rate is controlled by both inter-particle and intra-particle diffusion [29, 30].

On the other hand, it has been reported in the literature that the impurities have a favorable effect on the oxidation rate [31]. In fact, as a result of the deposition of the Ziegler-Natta catalyst on the surface of SiC and alumina particles during polymerization, $TiCl_4$ is oxidized under air as follows:

$$TiCl_4 + O_2 \rightarrow TiO_2\,(s) + 2Cl_2\,(g) \quad 7\text{-}6$$

Consequently, besides the effect of the larger pore size and porosity in the porous samples, the formation of TiO_2 could be also responsible for enhancing the oxidation rate of SiC powders in the specimen prepared by the developed method.

Typically, at a sintering temperature above 1400 °C cristobalite and silica react together to form mullite as follows:

$$3Al_2O_3 + 2\,SiO_2 \rightarrow 3Al_2O_3.2\,SiO_2(mullite) \quad 7\text{-}7$$

According to Davis and Pask [32] for the system of SiO_2-Al_2O_3, mullitization is controlled by the solution-precipitation mechanism. It was reported that the reaction rate at the interface of alumina and SiO_2 are faster than the diffusion rates and after enough formation of mullite, SiO_2 and α-

Al_2O_3 must diffuse through the interfaces of SiO_2-mullite and Al_2O_3-mullite in order to conduct further reactions [33]. Hence, the mechanism of mullitization is diffusion-controlled. Increasing the sintering temperature enhances the viscosity of SiO_2, which promotes the rate of diffusion of Al^{3+} ions into the viscous SiO_2 glass.

Another critical point to note is the effect of TiO_2 in the system of SiO_2-Al_2O_3. According to the stochiometric equation (6), the weight ratio of TiO_2 in the system is about 2.5 wt%. In the literature, it was reported that the incorporation of a small amount TiO_2 induces the mullitization rate by decreasing the viscosity of the liquid siliceous phase, which favors mass transport between alumina dissolution and silica, accordingly. The reaction temperature of the mullite formation can be reduced with the presence of titanium dioxide under its solubility limit whereas an amount in excess of that prevents the combination of silica and alumina, producing mullite [34]. It should be noted that effect of TiO_2 on mullitization is a complex phenomena and different observations have been reported [35, 36].

According to the SEM, pore size, and XRD results, the enhancement of porosity and mechanical properties of the porous samples via the developed method can be explained as follows: mixing alumina and SiC powders in alumina sol forms at least a nano layer of alumina on both the surface of SiC and calcined Al_2O_3 powders. It was shown that the dispersion of SiC and alumina powders is enhanced due to the steric and electrostatic effects. On the other hand, during polymerization the ethylene monomer, which has a small size, can easily penetrate into the agglomeration of alumina nano powders and start the reaction through the catalyst, which was anchored on the surface of the particles. During the propagation of the polymer, the agglomeration of alumina nano powders breaks out. Furthermore, it was demonstrated by our group that polymer filaments bond alumina nano particles to the SiC powders.

Thus, during the formation of the green body, more alumina particles contacted SiC particles creating more chances to react with the derived SiO_2 to form mullite compared to the traditional method. In addition, the presence of TiO_2, which homogenously attached on the surface of SiC and alumina powders, acts as the sintering additive to promote the mullitization rate. During the heating process, this polymer was burnt out producing larger pores with narrow pore size distribution as well as higher porosity. These phenomena did not occur when SiC and alumina nanosize powders were physically mixed in ethanol. In summary, the increase in strength and

porosity were ascribed to the better dispersion of alumina and pore former in SiC particles and more mullite formation.

Figure 7-11 depicts the effect of sintering temperature on the evolution of the crystalline structure of samples prepared with traditional and developed methods sintered at 1500 °C, 1550°C and 1600 °C for 3 hrs. For both samples, increasing the temperature leads to enhancing the mullite rate formation and decreasing the intensity of alumina as expected. As the temperature increases, cristobalite participates in several reactions which occur simultaneously. On the one hand, increasing the temperature results in the formation of more silica which transform to cristobalite (Equations 4 and 5).

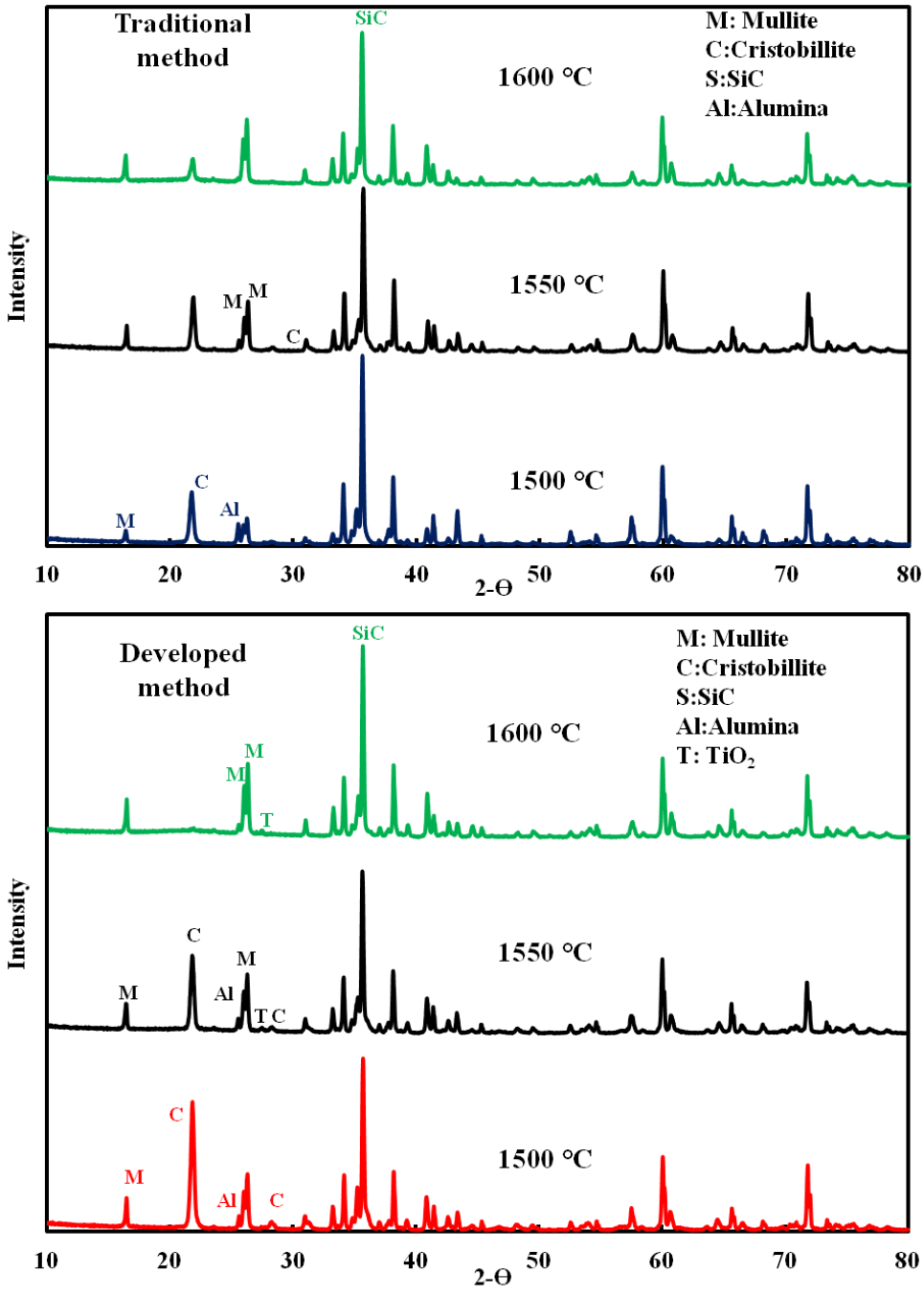

Figure 7-11 Crystalline evoulotion of porous samples as the sintering temperature increases

On the other hand, it causes more cristobalite to be consumed to form mullite (Equation 6). The formation of mullite on the surface of SiC particles can act as an oxidation barrier for further oxidation of SiC and may decrease the partial pressure of oxygen in the system resulting in changing the passive oxidation mechanism to active oxidation [37] at higher sintering temperatures (above 1550 °C) as follows:

$SiC + O_2 \rightarrow SiO\ (g) + CO\ (g)$ 7-8

Consequently, instead of forming SiO_2, SiO is produced. When this gas leaves the specimen, it reacts with the oxygen in the bulk system and produces SiO_2 on the surface of the product (Figure 7-12). The XRD analysis confirmed that the white powders are silica.

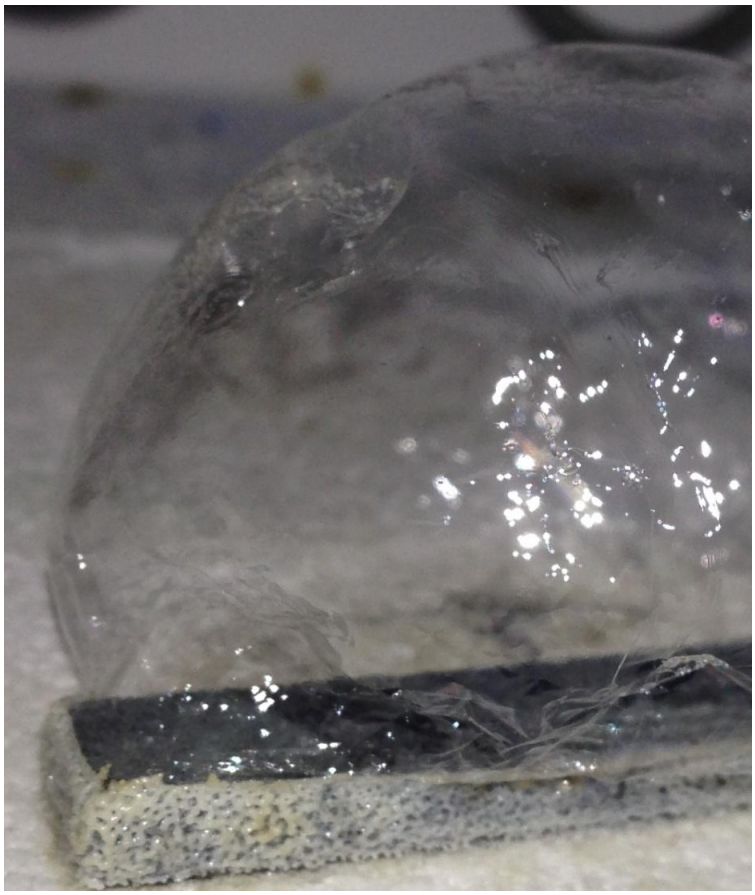

Figure 7-12 Bubble formation during sintering of the porous SiC ceramics at 1600 °C under air for 3h

Therefore, according to the XRD results, the main crystalline structures of samples prepared by the novel method at 1600 °C are only mullite and SiC. As the thermal expansion number of mullite is much more similar to the thermal expansion of silica compared to cristobalite, it would be expected that these products have a higher thermal shock resistance compared to the lower temperature. For the present case, the strength of 68.8 ± 9.0 MPa was obtained when the sintering temperature was increased from 1500 °C to 1600 °C. This significant improvement in mechanical

property of the porous samples at higher 1600 °C is attributed to the very well neck growth between SiC particles due to the formation of mullite (Figure 7-13).

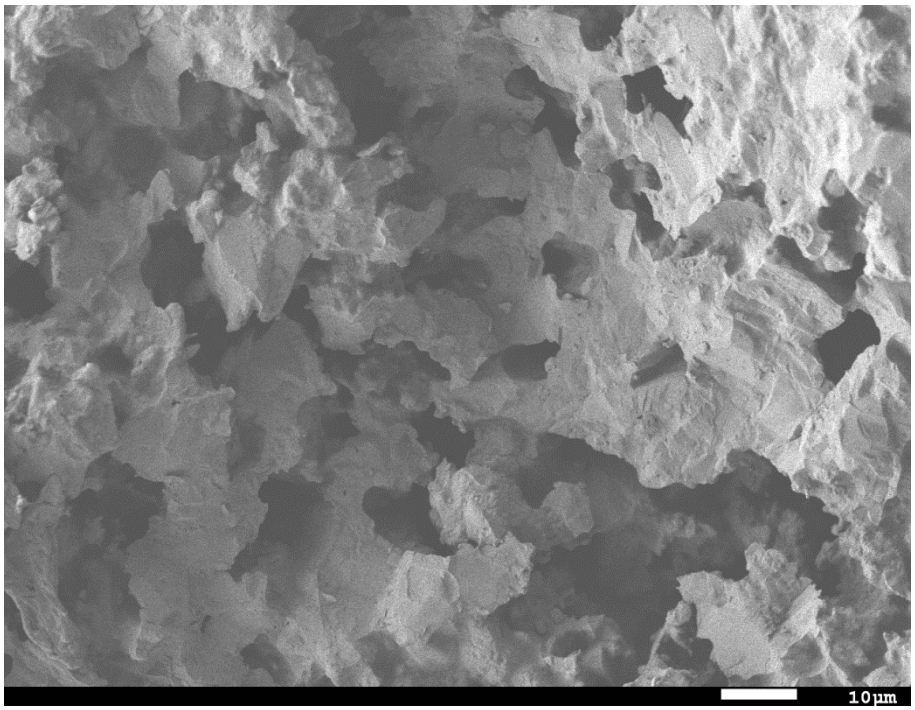

Figure 7-13 Morphology of porous SiC ceramics fabricated by the novel method at 1600 °C under air with the 35 wt% Al_2O_3

According to the experimental results presented in this study, it is confirmed that introducing the sintering additive and pore former to the starting particles via the combination of the sol-gel technique and in-situ polymerization method is a promising process to produce porous ceramics with higher strength (more than 35%) and porosity (8%) compared to the traditional method. The process was found to be flexible enough to control the amount of pore former (polymer) by adjusting the polymerization conditions which allows the production of a wide range of porosity in the final porous samples. In addition, as most parts of the starting materials are grafted by polymer, strong filler/matrix interfacial adhesion is observed during the green body formation. Therefore, the green body has more mechanical strength for the holding, transferring and even machining of the ceramic porous before firing. In the future, other physical and mechanical

properties, such as thermal shock behavior, air permeation, and the filtration efficiency of the developed porous ceramics will be evaluated.

7.4 Conclusion

Mullite bonded porous SiC ceramics with high mechanical strength and porosity have been successfully fabricated using the combination of sol-gel processing and in-situ polymerization with a reaction bonding technique. In this work, SiC particles used as the starting materials were coated by alumina nanoparticles as the sintering additives with the assistant of alumina sol followed by a coating of polyethylene through an in-situ polymerization process, in which the $TiCl_4$ catalyst was initially anchored covalently on the particle surface to subsequently initiate the polymerization of ethylene from the surface of particles. The TGA, SEM, and XPS analysis confirmed that the high density polyethylene formed on the surface of the powders. Comparing the pore size analysis obtained from the produced porous ceramics via the novel route with the ones obtained from the more traditional method revealed that coating SiC with alumina sol and polyethylene by in-situ polymerization successfully surpassed the in-homogenous dispersion problem between starting materials, sintering additives, and pore-forming.

In addition, it was noticed by XRD examination that the presence of TiO_2 as a result of the oxidation of $TiCl_4$ acted like the sintering additives, which increased the formation of mullite at a lower sintering temperature. Better dispersion of materials and a higher formation of mullite as well as the presence of polyethylene as the pore former on the SiC particles significantly induced flexural strength and porosity as well as pore size compared to the traditional method.

Moreover, it was found that increasing the sintering temperature had considerable effects on the strength and porosity of the porous materials and crystalline structure. Increasing the sintering temperature to 1600 °C resulted in the formation of porous ceramics, which consisted of mullite and SiC as the major phases with a flexural strength of 70 MPa. In summary, by controlling the process conditions, such as selecting the particle size of the starting materials, forming pressure, polymer content and sintering temperature, this novel technique can manufacture porous SiC ceramics with enhanced mechanical and physical properties at a low sintering temperature.

7.5 References

1. Studart, A.R., et al., *Processing routes to macroporous ceramics: A review.* Journal of the American Ceramic Society, 2006. **89**(6): p. 1771-1789.

2. Eom, J.-H., Y.-W. Kim, and S. Raju, *Processing and properties of macroporous silicon carbide ceramics: A review.* Journal of Asian Ceramic Societies, (0).

3. Li, J., H. Lin, and J. Li, *Factors that influence the flexural strength of SiC-based porous ceramics used for hot gas filter support.* Journal of the European Ceramic Society, 2011. **31**(5): p. 825-831.

4. Alvin, M.A., *Advanced Ceramic Materials for Use in High-Temperature Particulate Removal Systems.* Industrial & Engineering Chemistry Research, 1996. **35**(10): p. 3384-3398.

5. Wang, W., et al., *Kinetics of Ammonia Decomposition in Hot Gas Cleaning.* Industrial & Engineering Chemistry Research, 1999. **38**(11): p. 4175-4182.

6. Sigl, L.S. and H.-J. Kleebe, *Core/Rim Structure of Liquid-Phase-Sintered Silicon Carbide.* Journal of the American Ceramic Society, 1993. **76**(3): p. 773-776.

7. Kovalčíková, A., J. Dusza, and P. Šajgalík, *Thermal shock resistance and fracture toughness of liquid-phase-sintered SiC-based ceramics.* Journal of the European Ceramic Society, 2009. **29**(11): p. 2387-2394.

8. Pastila, P., et al., *Environmental effects on microstructure and strength of SiC-based hot gas filters.* Journal of the European Ceramic Society, 2001. **21**(9): p. 1261-1268.

9. She, J.H., et al., *Oxidation bonding of porous silicon carbide ceramics.* Journal of Materials Science, 2002. **37**(17): p. 3615-3622.

10. Liu, S., Y.-P. Zeng, and D. Jiang, *Fabrication and characterization of cordierite-bonded porous SiC ceramics.* Ceramics International, 2009. **35**(2): p. 597-602.

11. Kayal, N., A. Dey, and O. Chakrabarti, *Synthesis of mullite bonded porous SiC ceramics by a liquid precursor infiltration method: Effect of sintering temperature on material and mechanical properties.* Materials Science and Engineering: A, 2012. **556**(0): p. 789-795.

12. Liu, S., Y.-p. Zeng, and D. Jiang, *Effects of CeO2 addition on the properties of cordierite-bonded porous SiC ceramics.* Journal of the European Ceramic Society, 2009. **29**(9): p. 1795-1802.

13. Choi, Y.-H., et al., *Effect of alkaline earth metal oxide addition on flexural strength of porous mullite-bonded silicon carbide ceramics.* Journal of Materials Science, 2010. **45**(24): p. 6841-6844.

14. Ding, S., et al., *Effect of Y2O3 addition on the properties of reaction-bonded porous SiC ceramics.* Ceramics International, 2006. **32**(4): p. 461-466.

15. Dey, A., et al., *Investigations on Material and Mechanical Properties, Air-Permeation Behavior and Filtration Performance of Mullite-Bonded Porous SiC Ceramics.* International Journal of Applied Ceramic Technology, 2013: p. n/a-n/a.

16. Dey, A., N. Kayal, and O. Chakrabarti, *Preparation of mullite bonded porous SiC ceramics by an infiltration method.* Journal of Materials Science, 2011. **46**(16): p. 5432-5438.

17. Kumar, B.V.M., et al., *Effect of aluminum source on flexural strength of mullite-bonded porous silicon carbide ceramics.* Journal of the Ceramic Society of Japan, 2010. **118**(1373): p. 13-18.

18. Ohji, T. and M. Fukushima, *Macro-porous ceramics: processing and properties.* International Materials Reviews, 2012. **57**(2): p. 115-131.

19. Ebrahimpour, O., C. Dubois, and J. Chaouki, *Fabrication of mullite-bonded porous SiC ceramics via a sol–gel assisted in situ reaction bonding.* Journal of the European Ceramic Society, (0).

20. Hlavacek, V. and J.A. Puszynski, *Chemical Engineering Aspects of Advanced Ceramic Materials.* Industrial & Engineering Chemistry Research, 1996. **35**(2): p. 349-377.

21. Rajabian, M. and C. Dubois, *Polymerization compounding of HDPE/Kevlar composites. I. Morphology and mechanical properties.* Polymer Composites, 2006. **27**(2): p. 129-137.

22. Ebrahimpour, O., C. Dubois, and J. Chaouki, *Fabrication of mullite-bonded porous SiC ceramics via a sol–gel assisted in situ reaction bonding.* Journal of the European Ceramic Society, 2014. **34**(2): p. 237-247.

23. Derakhshan, A.A. and L. Rajabi, *Review on applications of carboxylate–alumoxane nanostructures.* Powder Technology, 2012. **226**(0): p. 117-129.

24. Yang, Q. and T. Troczynski, *Dispersion of Alumina and Silicon Carbide Powders in Alumina Sol.* Journal of the American Ceramic Society, 1999. **82**(7): p. 1928-1930.

25. Prabhakaran, K., J. James, and C. Pavithran, *Surface modification of SiC powders by hydrolysed aluminium coating.* Journal of the European Ceramic Society, 2003. **23**(2): p. 379-385.

26. Amoli, B.M., S.A.A. Ramazani, and H. Izadi, *Preparation of ultrahigh-molecular-weight polyethylene/carbon nanotube nanocomposites with a Ziegler–Natta catalytic system and investigation of their thermal and mechanical properties.* Journal of Applied Polymer Science, 2012. **125**(S1): p. E453-E461.

27. Siokou, A. and S. Ntais, *Towards the preparation of realistic model Ziegler-Natta catalysts: XPS study of the MgCl2/TiCl4 interaction with flat SiO2/Si(1 0 0).* Surface Science, 2003. **540**(2–3): p. 379-388.

28. Halbach, T.S. and R. Mülhaupt, *Boehmite-based polyethylene nanocomposites prepared by in-situ polymerization.* Polymer, 2008. **49**(4): p. 867-876.

29. Ebrahimpour, O., J. Chaouki, and C. Dubois, *Diffusional effects for the oxidation of SiC powders in thermogravimetric analysis experiments.* Journal of Materials Science, 2013. **48**(12): p. 4396-4407.

30. Zheng, Z., R.E. Tressler, and K.E. Spear, *The Effects of Cl-2 on the Oxidation of Single-Crystal Silicon-Carbide.* Corrosion Science, 1992. **33**(4): p. 557-567.

31. Opila, E., *Influence of Alumina Reaction Tube Impurities on the Oxidation of Chemically-Vapor-Deposited Silicon Carbide.* Journal of the American Ceramic Society, 1995. **78**(4): p. 1107-1110.

32. Davis, R.F. and J.A. Pask, *Diffusion and Reaction Studies in the System Al2O3-SiO2.* Journal of the American Ceramic Society, 1972. **55**(10): p. 525-531.

33. Saruhan, B., et al., *Reaction and sintering mechanisms of mullite in the systems cristobalite/α-Al2O3 and amorphous SiO2/α-Al2O3.* Journal of the European Ceramic Society, 1996. **16**(10): p. 1075-1081.

34. Baudin, C. and J.S. Moya, *Influence of Titanium Dioxide on the Sintering and Microstructural Evolution of Mullite.* Journal of the American Ceramic Society, 1984. **67**(7): p. C-134-C-136.

35. Zhang, T.S., et al., *Tailoring the microstructure of mechanoactivated Al2O3 and SiO2 mixtures with TiO2 addition.* Journal of Alloys and Compounds, 2010. **506**(2): p. 777-783.

36. Ruiz de Sola, E., et al., *Solubility and microstructural development of TiO2-containing 3Al2O3·2SiO2 and 2Al2O3·SiO2 mullites obtained from single-phase gels.* Journal of the European Ceramic Society, 2007. **27**(7): p. 2647-2654.

37. Narushima, T., et al., *High-temperature oxidation of silicon carbide and silicon nitride.* Materials Transactions Jim, 1997. **38**(10): p. 821-835

CHAPTER 8 GENERAL DISSCUSSION

In this study different strategies (implementation of sol-gel processing, graft polymerization or a combination of them) have been used to fabricate porous SiC in order to improve the physical and mechanical properties of the product compared to the traditional method, which involved mixing the starting materials in powder form. In all of the processing methods the compact SiC powders were heated under air to partially oxidize SiC to SiO_2. Therefore, since the oxidation process is an essential step in the fabrication process, the first part of this study was devoted to investigating the oxidation behavior of SiC particles using thermogravity analysis. The oxidation rate of different particle sizes of SiC powder was also investigated. Results demonstrated that at the studied temperature, besides the surface reaction and intra-particle diffusion, inter-particle diffusion should also be considered, especially when SiC particles are in compact form. To describe these limitation steps a new model was developed, which can be applied in other non-catalytic gas solid reactions where one or some of these limitation steps control the overall reaction rate of the gas-solid reaction.

In addition, the crystalline and morphology changes of the compact SiC powders during oxidation at higher temperatures have been investigated. It was found that at temperatures above 1200 °C the amorphous structure of silica transferred to cristobalite and at higher temperatures (above 1400 °C) the sintering phenomena cause the morphology of the powders to change (Figure 8-1). Although the developed model was constructed to consider all of the diffusional effects and the surface reaction as well as the physical parameters, such as porosity between the powders at the height of the samples, it assumed these physical parameters (porosity and the pore structure) were constants and would not change during oxidation. Therefore, to apply this model at higher temperatures, it should be modified to take into account the structural changes of powders compacted at higher temperatures and should be investigated in more detail.

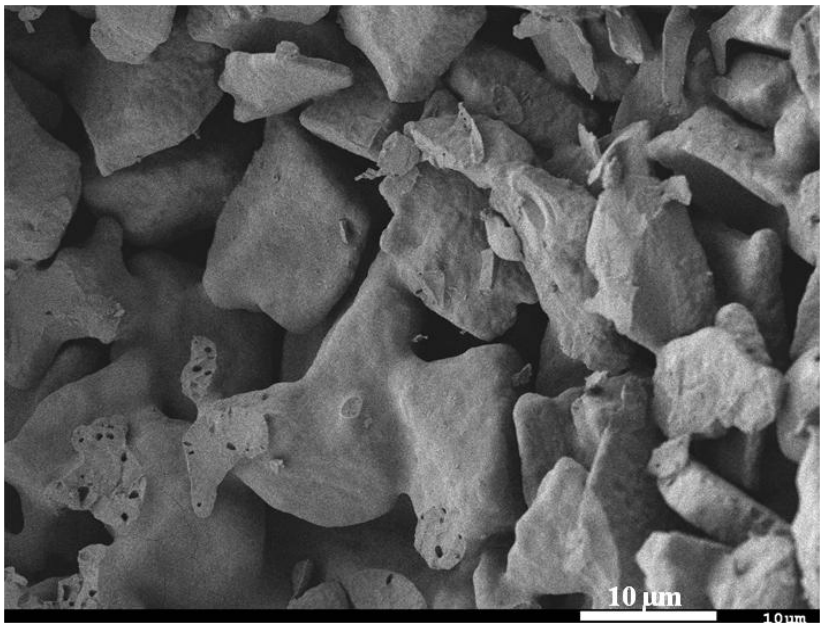

Figure 8-1 Morphology of compact α-SiC powders after the oxidation at 1500 °C/3 h

In the second phase of this research due to the controversial reports in the literature about the effect of sintering additive content during the fabrication of mullite-bonded porous SiC ceramics, it was essential to study the effect of alumina contents in powder form on the flexural strength and porosity of the produced porous ceramics. The XRD characterization identified the presence of alumina, SiC, cristobalite, and mullite in the specimen. The SEM analysis showed that porous SiC ceramics were successfully bonded by both mullite and cristobalite using the reaction bonding technique. Although the analysis showed that the addition of alumina nano powders increased the flexural strength and decreased the porosity of the samples, SEM observation confirmed that during the physical mixing of alumina nano powders with SiC powders, some of the alumina nano powders were agglomerated and did not contact the SiC particles. These agglomerations produced small pores, which were detected in the pore size analysis from the mercury results. In fact, the weight ratio of alumina nano powders to the SiC particles should be optimized to maximize the mechanical properties and porosity. Particle size ratio between SiC and alumina nano particles and their initial sizes are strongly affected by the packing density of the green body of porous ceramics. For the current study, it was proposed that the optimal condition for alumina is about 35 wt. %.

It was also found that when a small portion of alumina in the sol form was added to the SiC particles, the mullitization rate was enhanced compared with the one prepared by the addition of alumina in the calcined state. However, at a higher amount of alumina sol, the flexural strength is drastically degraded due to the large amount of shrinkage and stress during the calcination process. It was found that the addition of alumina sol beyond a certain value causes the alumina sol in the medium to saturate resulting in the formation of agglomerations of alumina nano sol in the system. Therefore, it did not coat the SiC particles. Interestingly, it was revealed that if a portion of alumina nano powders were replaced by the alumina sol, the properties of the final product would be enhanced significantly. The reason was attributed to the fine mixing and good dispersion of alumina and SiC particles in alumina sol and steric forces. Another explanation is that as the amount of alumina nano powders decreased by 20% wt%, the chance of agglomeration formation decreased. When coating alumina nano powders with alumina sol, the thickness of the alumina nano powder from the alumina sol is on the order of the size of alumina sol. Therefore, in order to coat the SiC particles with the desired amount of alumina, both alumina sol and calcined alumina should be applied. The thickness of coated alumina on the powders from the alumina sol depends on the concentration of alumina sol and the number of times the coating process is repeated. It would be interesting to study these factors to find the optimal conditions for coating alumina sol on SiC powders. As well, in this thesis, the SiC particles were coated by mixing the alumina sol using magnetic stirrers. It would be necessary to further investigate the coating performance with other methods, such as dip coating, to verify the thickness of coated alumina sol on the particles.

In the third part of the project, the feasibility of the application of in situ polymerization to fabricate porous SiC ceramics was investigated. The TGA/ DSC analysis confirmed the presence of high density polyethylene in the system and SEM and TEM analysis demonstrated that SiC and alumina particles were successfully grafted by polymer. It was found that coating the particles with polyethylene via in situ reaction was an effective way to improve the dispersion of the alumina powders in the SiC particles. Although the results confirmed that the particles were coated by polymer and most of the alumina nano powders were bonded to the surface of alumina via polymer chain, XPS analysis and SEM observation showed that the whole surface of some particles was not completely coated by polymer probably due to the low hydroxyl concentration on the surface of particles or in-homogenous mixing of the particles in the slurry phase. To obtain

a uniform polymer coating on the surface of particles, pretreatment of the particle surface would have been required. In this section, the amount of polymer was controlled by adjusting the reaction time. It was assumed that the whole surface of the particles could be covered by the catalyst and that the catalyst reacts with the hydroxyl groups on the particles. The amount of hydroxyl density of the particles has not been measured and further investigation is required to examine the chemical bonding between the $TiCl_4$ catalyst and the functional groups on the surface of particles. The high resolution of analysis with XPS is an interesting way to verify the suggested mechanisms in the literature. In this study we first grafted a catalyst to the substrate, however, some researchers originally grafted a co-catalyst on the particle before adding a catalyst. It is, therefore, interesting to compare polymerization efficiency by investigating both methods during polymerization. Furthermore, the other reaction parameters, such as the ratio of co-catalyst to catalyst or the use of other types of catalyst, would be interesting subjects to be studied to optimize the performance of polymerization.

It was found that processing parameters, such as forming pressure and polymer contents strongly affect the final properties of the porous ceramics. Morphology analysis showed that increasing the forming pressure or decreasing the polymer contents caused more SiC particles to be in contact and the neck growth to be increased. In addition, the pore size and porosity was decreased and flexural strength increased. Therefore, to produce porous SiC ceramics with the desired properties these parameters should be optimized.

The last part of this research aimed at implementing both approaches (sol-gel and in situ polymerization) to fabricate porous SiC ceramics via the reaction bonding technique. It was found that implanting these methods to fabricate porous SiC ceramics results in significantly increasing both mechanical and physical properties compared to the traditional methods. Mercury porosimtery analysis showed that the pore size distribution was narrower and the average pore size was much larger than the one produced by the conventional methods. It was expected that when the surface of alumina powders and SiC micro particles was coated by alumina sol, the amount of hydroxyl groups would increase significantly, which would help more catalysts to anchor on the surface of particles and, consequently, the thickness of the polymer would be more uniform on the particle surface compared to the samples that were polymerized without any modification.

As a result of the pre-treatment of the SiC and alumina with alumina sol the surface area of the powders increased remarkably, which was as an important factor for injecting the polymerization of the catalyst. Although the physical and mechanical properties of the porous ceramics were enhanced, in this case, it was found that the SiC particles were more oxidized compared to the traditional methods. This was attributed to the larger pore size and porosity, which helped more oxygen diffuse to the surface of SiC and react to form silica. It was also found that TiO_2 derived from the catalyst could be responsible for increasing oxidation.

Since the ideal goal was to react all of silica to mullite, the results showed that at the sintering temperature of 1500 °C both cristobalite and alumina were presented in the structure of porous ceramics. In order to speed up the mullitization rate, it was found that when the sintering temperature was increased to 1600 °C most alumina nano particles reacted with silica and formed mullite. Moreover, XRD demonstrated that the intensity of silica decreased significantly. It is believed that as the surface of SiC particles was coated by mullite, the partial pressure of oxygen decreased causing the oxidation mechanism to change and form active oxidation. Therefore, SiO gas was produced and left the porous body. When this gas reached the surface of the porous samples, some of them reacted with oxygen to produce SiO_2 and SiO amorphous powders. As a result, increasing the sintering temperature is an effective way to bond SiC particles with mullite and decrease the intensity of silica. More investigation is required to find the oxidation mechanism of the porous samples, especially the effect of alumina, TiO_2, and mullite.

CHAPTER 9 CONCLUSION AND RECOMMENDATIONS

9.1 Conclusion

In this dissertation, mullite-bonded porous SiC ceramics were fabricated via reaction bonding techniques at sintering temperature between 1500 °C to 1600 °C were fabricated. Different approaches were conducted to improve the physical and mechanical properties of the resulted specimens. Following conclusions is summarized from the work:

1- Oxidation of SiC particles depends on their initial sizes and temperature. At the studied temperature (910 °C -1010 °C), the passive oxidation rate of the powder compacts, are controlled by the surface reaction and intra and inter particle diffusion of the oxygen through the oxide layer and between particles.

2- By increasing the temperature the crystalline structure of the silica changed to the cristobalite and sintering process causes to surface structure.

3- During the heating of green samples which prepared by mixing of alumina and SiC, mullite is formed by reaction between oxidized silica and alumina and it caused to bond SiC particle together.

4- Addition of calcined alumina increased the mechanical strength and decreased the porosity while if alumina were added in the sol form, the reverse trends was observed by increasing the amount of alumina

5- It was found that when some portion of alumina nano powders were replaced by alumina sol, the dispersion of alumina nano powders between the SiC powders were improved significantly and it resulted in increase on the flexural strength and porosity.

6- For the first time, in situ polymerization was applied to fabricate porous SiC ceramics with enhanced physical and mechanical properties.

7- SEM, TGA, and TEM analysis confirmed that SiC and alumina nano powders successfully grafted by the polyethylene in the slurry phase following the anchoring of Ziegler Natta catalyst on the surface substrate.

8- The green body formed by the coated particles by polymer has adequate strength to handle and shaped in the desired form.

9- SEM analysis showed that during the polymerization, alumina particle was connected to the SiC micro particles via polymer chains.

10- The porosity and the pore size of produced porous ceramics can be controlled by the polymer contents during the polymerization via adjusting the operation conditions of the polymerization such as temperature.

11- It was confirmed that combination of sol-gel process and in-situ polymerization is an effective method to fabricate porous SiC ceramics with narrow pore size distribution, high porosity and flexural strength.

12- Forming pressure, sintering temperature and polymer contents affects notably on the resulted properties of porous samples.

13- Increasing the sintering temperature to 1600 °C caused the converting most of alumina and silica to mullite and consequently the main crystalline structure are mullite and SiC.

9.2 Recommendations

To further modify the fabrication process and investigate the potential application of the product the following recommendations are suggested:

1- It was observed that coating of the particles with polyethylene were not completely uniform during the polymerization process. It is proposed to investigate in more detail about the polymerization part to better understand the surface characterization of the particles during the polymerization and operation conditions during the polymerization to enhance the properties of coated particles.

2- Low amount of other sintering additive such as Y_2O_3 can be added to increase the mullitization rate and decrease the sintering temperature. It is proposed to investigate the addition of these sintering additives in the sol form to the starting materials.

3- It is recommended to investigate other important properties such as oxidation resistance and thermal shock properties of the resulted porous ceramics via the developed method.

4- It is proposed to design a lab scale set up to measure the pressure drop and filtration efficiency of the produced porous ceramics at high temperature.

5- It is interesting to coat the porous ceramic by some additives which can acts as the catalyst and investigate the performance of this product to adsorb some effluent gaseous.

REFERENCES

1. Eom, J.-H., Y.-W. Kim, and S. Raju, *Processing and properties of macroporous silicon carbide ceramics: A review.* Journal of Asian Ceramic Societies, 2013. **1**(3): p. 220-242.
2. Sigl, L.S. and H.-J. Kleebe, *Core/Rim Structure of Liquid-Phase-Sintered Silicon Carbide.* Journal of the American Ceramic Society, 1993. **76**(3): p. 773-776.
3. She, J.H., et al., *Oxidation bonding of porous silicon carbide ceramics.* Journal of Materials Science, 2002. **37**(17): p. 3615-3622.
4. Alvin, M.A., T.E. Lippert, and J.E. Lane, *Assessment of Porous Ceramic Materials for Hot Gas Filtration Applications.* American Ceramic Society Bulletin, 1991. **70**(9): p. 1491-1498.
5. Simeone, E., et al., *High temperature gas filtration with ceramic candles and ashes characterisation during steam-oxygen blown gasification of biomass.* Fuel, 2013. **108**: p. 99-111.
6. Heidenreich, S., W. Haag, and M. Salinger, *Next generation of ceramic hot gas filter with safety fuses integrated in venturi ejectors.* Fuel, 2013. **108**: p. 19-23.
7. Guan, X., et al., *Demonstration of hot gas filtration in advanced coal gasification system.* Powder Technology, 2008. **180**(1-2): p. 122-128.
8. Ohtsuka, Y., et al., *Recent progress in Japan on hot gas cleanup of hydrogen chloride, hydrogen sulfide and ammonia in coal-derived fuel gas.* Powder Technology, 2009. **190**(3): p. 340-347.
9. Heidenreich, S. and B. Scheibner, *Hot gas filtration with ceramic filters: Experiences and new developments.* Filtration & Separation, 2002. **39**(4): p. 22-25.
10. Heidenreich, S., *Hot gas filtration – A review.* Fuel, 2013. **104**(0): p. 83-94.
11. Schaafhausen, S., et al., *Corrosion of alumina and mullite hot gas filter candles in gasification environment.* Journal of the European Ceramic Society, 2013. **33**(15–16): p. 3301-3312.
12. Harris, G.L., *Properties of Silicon Carbide,* Institution of Engineering and Technology.

13. Hind, A.R., S.K. Bhargava, and S.C. Grocott, *The surface chemistry of Bayer process solids: a review*. Colloids and Surfaces A: Physicochemical and Engineering Aspects, 1999. **146**(1–3): p. 359-374.

14. Xie, Z.P., et al., *Influence of alpha-alumina seed on the morphology of grain growth in alumina ceramics from Bayer aluminum hydroxide.* Materials Letters, 2003. **57**(16-17): p. 2501-2508.

15. Sinton, C.W., *Raw Materials for Glass and Ceramics Sources, Processes, and Quality Control*. John Wiley & Sons, Inc., 2006.

16. Gerardin, C., et al., *Structural Investigation and Energetics of Mullite Formation from Sol-Gel Precursors.* Chemistry of Materials, 1994. **6**(2): p. 160-170.

17. Li, D.X. and W.J. Thomson, *Tetragonal to orthorhombic transformation during mullite formation.* Journal of Materials Research, 1991. **6**(04): p. 819-824.

18. Montanaro, L., et al., *Sintering of industrial mullites.* Journal of the European Ceramic Society, 1997. **17**(14): p. 1715-1723.

19. Pask, J.A., *Importance of starting materials on reactions and phase equilibria in the Al-2,O-3-SiO2 system.* Journal of the European Ceramic Society, 1996. **16**(2): p. 101-108.

20. Kaya, C., et al., *Nanostructured ceramic powders by hydrothermal synthesis and their applications.* Microporous and Mesoporous Materials, 2002. **54**(1-2): p. 37-49.

21. Pask, J.A., et al., *Effect of Sol-Gel Mixing on Mullite Microstructure and Phase Equilibria in the α-Al2O3-SiO2 System.* Journal of the American Ceramic Society, 1987. **70**(10): p. 704-707.

22. Xu, J., et al., *Protective CVD Mullite Coatings on Single-Crystal Silicon Substrates.* JOM, 2013. **65**(4): p. 567-573.

23. Rodrigo, P.D.D. and P. Boch, *High purity mullite ceramics by reaction sintering.* International Journal of High Technology Ceramics, 1985. **1**(1): p. 3-30.

24. Saruhan, B., et al., *Reaction and sintering mechanisms of mullite in the systems cristobalite/alpha-Al2O3 and amorphous SiO2/alpha-Al2O3.* Journal of the European Ceramic Society, 1996. **16**(10): p. 1075-1081.

25. Nurishi, Y. and J.A. Pask, *Sintering of α-Al2O3—Amorphous silica compacts.* Ceramics International, 1982. **8**(2): p. 57-59.

26. Kleebe, H.J., et al., *Conversion of Al2O3–SiO2 powder mixtures to 3:2 mullite following the stable or metastable phase diagram.* Journal of the European Ceramic Society, 2001. **21**(14): p. 2521-2533.

27. Schmücker, M., W. Albers, and H. Schneider, *Mullite formation by reaction sintering of quartz and α-Al2O3—A TEM study.* Journal of the European Ceramic Society, 1994. **14**(6): p. 511-515.

28. Davis, R.F. and J.A. Pask, *Diffusion and Reaction Studies in the System Al2O3-SiO2.* Journal of the American Ceramic Society, 1972. **55**(10): p. 525-531.

29. Rana, A.P.S., O. Aiko, and J.A. Pask, *Sintering of α-Al2O3/quartz, and α-Al2O3/cristobalite related to mullite formation.* Ceramics International, 1982. **8**(4): p. 151-153.

30. Bowen, N.L. and J.W. Greig, *THE SYSTEM: Al2O3.SiO2.* Journal of the American Ceramic Society, 1924. **7**(4): p. 238-254.

31. Aramaki, S. and R. Roy, *Revised Phase Diagram for the System Al2O3—SiO2.* Journal of the American Ceramic Society, 1962. **45**(5): p. 229-242.

32. Hartmut Schneider, K.O., Joseph Adam Pask, *Mullite and mullite ceramics.* J. Wiley, 1994.

33. Jiansirisomboon, S. and K.J.D. MacKenzie, *Sol-gel processing and phase characterization of Al2O3 and Al2O3/SiC nanocomposite powders.* Materials Research Bulletin, 2006. **41**(4): p. 791-803.

34. Sacks, M.D., N. Bozkurt, and G.W. Scheiffele, *Fabrication of Mullite and Mullite-Matrix Composites by Transient Viscous Sintering of Composite Powders.* Journal of the American Ceramic Society, 1991. **74**(10): p. 2428-2437.

35. Schneider, H., J. Schreuer, and B. Hildmann, *Structure and properties of mullite - A review.* Journal of the European Ceramic Society, 2008. **28**(2): p. 329-344.

36. Bartsch, M., et al., *Novel Low-Temperature Processing Route of Dense Mullite Ceramics by Reaction Sintering of Amorphous SiO2-Coated γ-Al2O3 Particle Nanocomposites.* Journal of the American Ceramic Society, 1999. **82**(6): p. 1388-1392.

37. Hench, L.L. and J.K. West, *The sol-gel process.* Chemical Reviews, 1990. **90**(1): p. 33-72.

38. C. Jeffrey Brinker, G.W.S., *Sol-gel Science: The Physics and Chemistry of Sol-gel Processing.* Gulf Professional Publishing, 1990.

39. Yoldas, B.E., *Alumina Sol Preparation from Alkoxide.* Am. Ceram. Soc. Bull., 1975. **54**(3): p. 289–290.

40. Wang, J.Q., et al., *Hydrothermal Transformation of Bayerite to Boehmite.* Science of Advanced Materials, 2009. **1**(1): p. 77-85.

41. Derakhshan, A.A. and L. Rajabi, *Review on applications of carboxylate–alumoxane nanostructures.* Powder Technology, 2012. **226**(0): p. 117-129.

42. Yimsiri, P. and M.R. Mackley, *Spin and dip coating of light-emitting polymer solutions: Matching experiment with modelling.* Chemical Engineering Science, 2006. **61**(11): p. 3496-3505.

43. L. Landau, B.L., *Dragging of a liquid by a moving plate.* Aiche Journal, 1942. **17**(1): p. 42-54.

44. Guglielmi, M., et al., *Dependence of thickness on the withdrawal speed for SiO2 and TiO2 coatings obtained by the dipping method.* Journal of Materials Science, 1992. **27**(18): p. 5052-5056.

45. Shih, W.-H., L.-L. Pwu, and A.A. Tseng, *Boehmite Coating as a Consolidation and Forming Aid in Aqueous Silicon Nitride Processing.* Journal of the American Ceramic Society, 1995. **78**(5): p. 1252-1260.

46. Yang, C.-Y. and W.-H. Shih, *Effect of Acid on the Coating of Boehmite onto Silicon Carbide Particles in Aqueous Suspensions.* Journal of the American Ceramic Society, 1999. **82**(2): p. 436-440.

47. JE Blendell, H.B., RL Coble, *High purity alumina by controlled precipitation from aluminum sulfate solutions.* American Ceramic Society Bulletin, 1984. **63**(6): p. 797-802.

48. Yang, C.-Y., W.Y. Shih, and W.-H. Shih, *Effects of Boehmite-Coating Thickness on the Consolidation and Rheological Properties of Boehmite-Coated SiC Suspensions.* Journal of the American Ceramic Society, 2001. **84**(12): p. 2834-2840.

49. Hong, C.-W., *New Concept for Simulating Particle Packing in Colloidal Forming Processes.* Journal of the American Ceramic Society, 1997. **80**(10): p. 2517-2524.

50. Zhang, Z., X. Lu, and P. Su, *Dispersion of kaolin powders in silica sols.* Applied Clay Science, 2010. **49**(1–2): p. 51-54.

51. Prabhakaran, K., J. James, and C. Pavithran, *Surface modification of SiC powders by hydrolysed aluminium coating.* Journal of the European Ceramic Society, 2003. **23**(2): p. 379-385.

52. Novak, S., et al., *Surface characterisation and modification of submicron and nanosized silicon carbide powders.* Journal of the European Ceramic Society, 2007. **27**(12): p. 3545-3550.

53. Yang, Q. and T. Troczynski, *Alumina Sol-Assisted Sintering of SiC—Al2O3 Composites.* Journal of the American Ceramic Society, 2000. **83**(4): p. 958-960.

54. Rahaman, M.N., *Ceramic Processing.* Taylor & Francis Inc, 2006.

55. Reed, J.S., *Principles of Ceramics Processing, 2nd Edition.* Wiely inter science, 1995.

56. Richerson, D., *Modern Ceramic Engineering: Properties, Processing, and Use in Design, Third Edition.* CRC Taylor & Francis, 2005.

57. Suzuki★, H. and T. Hase, *Boron Transport and Change of Lattice Parameter During Sintering of β-SiC.* Journal of the American Ceramic Society, 1980. **63**(5-6): p. 349-350.

58. Prochazka, S. and R.M. Scanlan, *Effect of Boron and Carbon on Sintering of SIC.* Journal of the American Ceramic Society, 1975. **58**(1-2): p. 72-72.

59. Xu, G., et al., *Pressureless Sintering of Carbon Nanofibre/SiC Composites and Their Properties.* International Journal of Applied Ceramic Technology, 2013: p. n/a-n/a.

60. Mulla, M.A. and V.D. Krstic, *Pressureless sintering of β-SiC with Al2O3 additions.* Journal of Materials Science, 1994. **29**(4): p. 934-938.

61. Sánchez-González, E., et al., *Effect of microstructure on the mechanical properties of liquid-phase-sintered silicon carbide at pre-creep temperatures.* Journal of the European Ceramic Society, 2011. **31**(6): p. 1131-1139.

62. Rodríguez-Rojas, F., et al., *Effect of the sintering additive content on the non-protective oxidation behaviour of pressureless liquid-phase-sintered α-SiC in air.* Journal of the European Ceramic Society, 2010. **30**(6): p. 1513-1518.

63. Rodríguez-Rojas, F., et al., *Oxidation behavior of pressureless liquid-phase-sintered α-SiC in ambient air at elevated temperatures.* Journal of Materials Research, 2008. **23**(6): p. 1689-1700.

64. Biswas, K., *Liquid phase sintering of SiC-ceramics*, 2009. p. 91-108.

65. Kim, D.-H. and C.H. Kim, *Toughening Behavior of Silicon Carbide with Additions of Yttria and Alumina.* Journal of the American Ceramic Society, 1990. **73**(5): p. 1431-1434.

66. Dai, P.Y., et al., *Fabrication of highly dense pure SiC ceramics via the HTPVT method.* Acta Materialia, 2011. **59**(16): p. 6257-6263.

67. IBuschow, K.H.J.C., Robert W.; Flemings, Merton C.; Ilschner, Bernhard; Kramer, Edward J.; Mahajan, Subhash, *Encyclopedia of Materials - Science and Technology.* Elsevier 2001. **1-11**.

68. Vaughn, W.L. and H.G. Maahs, *Active-to-Passive Transition in the Oxidation of Silicon Carbide and Silicon Nitride in Air.* Journal of the American Ceramic Society, 1990. **73**(6): p. 1540-1543.

69. Jacobson, N.S. and D.L. Myers, *Active Oxidation of SiC.* Oxidation of Metals, 2011. **75**(1-2): p. 1-25.

70. Deal, B.E. and A.S. Grove, *General Relationship for Thermal Oxidation of Silicon.* Journal of Applied Physics, 1965. **36**(12): p. 3770-&.

71. Costello, J.A. and R.E. Tressler, *Oxidation Kinetics of Silicon Carbide Crystals and Ceramics: I, In Dry Oxygen.* Journal of the American Ceramic Society, 1986. **69**(9): p. 674-681.

72. Chou, K.C., *A kinetic model for oxidation of Si-Al-O-N materials.* Journal of the American Ceramic Society, 2006. **89**(5): p. 1568-1576.

73. Levenspiel, O., *Chemical reaction engineering*. 3rd ed1999, New York: Wiley. 570, p.584.

74. Szekely, J., J. W. Evans, and H. Y. Sohn, *Gas-Solid Reactions.* Academic Press, 1976.

75. Hou, X. and K. Chou, *Model of oxidation of SiC microparticles at high temperature.* Corrosion Science, 2008. **50**(8): p. 2367-2371.

76. Presser, V. and K.G. Nickel, *Silica on Silicon Carbide.* Critical Reviews in Solid State and Materials Sciences, 2008. **33**(1): p. 1-99.

77. Shi, Z., et al., *The passive-oxidized behavior of SiC particles and their jointing characteristics.* Journal of Materials Processing Technology, 2001. **110**(2): p. 127-131.

78. Opila, E., *Influence of Alumina Reaction Tube Impurities on the Oxidation of Chemically-Vapor-Deposited Silicon Carbide.* Journal of the American Ceramic Society, 1995. **78**(4): p. 1107-1110.

79. Opila, E.J. and R.E. Hann, *Paralinear Oxidation of CVD SiC in Water Vapor.* Journal of the American Ceramic Society, 1997. **80**(1): p. 197-205.

80. Ramberg, C.E., et al., *Passive-Oxidation Kinetics of High-Purity Silicon Carbide from 800° to 1100°C.* Journal of the American Ceramic Society, 1996. **79**(11): p. 2897-2911.

81. Rong, M.Z., et al., *Improvement of tensile properties of nano-SiO2/PP composites in relation to percolation mechanism.* Polymer, 2001. **42**(7): p. 3301-3304.

82. Kango, S., et al., *Surface modification of inorganic nanoparticles for development of organic-inorganic nanocomposites-A review.* Progress in Polymer Science, 2013. **38**(8): p. 1232-1261.

83. Alexandre, M. and P. Dubois, *Polymer-layered silicate nanocomposites: preparation, properties and uses of a new class of materials.* Materials Science and Engineering: R: Reports, 2000. **28**(1–2): p. 1-63.

84. Wang, Q., S. Kaliaguine, and A. Ait-Kadi, *Catalytic grafting: A new technique for polymer–fiber composites I. Polyethylene–asbestos composites.* Journal of Applied Polymer Science, 1992. **44**(6): p. 1107-1119.

85. Dubois, C., M. Rajabian, and D. Rodrigue, *Polymerization compounding of polyurethane-fumed silica composites.* Polymer Engineering & Science, 2006. **46**(3): p. 360-371.

86. Roy, C., et al., *The dispersion and polymer coating of ultrafine aluminum powders by the Ziegler Natta reaction.* MRS Online Proceedings Library, 2003. **800**: p. null-null.

87. Esmaeili, B., J. Chaouki, and C. Dubois, *Polymerization Compounding on the Surface of Zirconia Nanoparticles.* Macromolecular Symposia, 2006. **243**(1): p. 268-276.

88. Rong, J.F., et al., *A polyethylene nanocomposite prepared via in-situ polymerization.* Macromolecular Rapid Communications, 2001. **22**(5): p. 329-334.

89. Du, Z.J., et al., *A novel polyethylene/palygorskite nanocomposite prepared via in-situ coordinated polymerization.* Polymer Bulletin, 2002. **49**(2-3): p. 151-158.

90. Ramazani, A., F. Tavakolzadeh, and H. Baniasadi, *In situ polymerization of polyethylene/clay nanocomposites using a novel clay-supported Ziegler-Natta catalyst.* Polymer Composites, 2009. **30**(10): p. 1388-1393.

91. Wei, L., T. Tang, and B. Huang, *Synthesis and characterization of polyethylene/clay–silica nanocomposites: A montmorillonite/silica-hybrid-supported catalyst and in situ polymerization.* Journal of Polymer Science Part A: Polymer Chemistry, 2004. **42**(4): p. 941-949.

92. Yang, F., et al., *Preparation and properties of polyethylene/montmorillonite nanocomposites by in situ polymerization.* Journal of Applied Polymer Science, 2003. **89**(13): p. 3680-3684.

93. Alexandre, M., et al., *Polyethylene-layered silicate nanocomposites prepared by the polymerization-filling technique: synthesis and mechanical properties.* Polymer, 2002. **43**(8): p. 2123-2132.

94. Takamura, M., T. Yamauchi, and N. Tsubokawa, *Preparation and dispersibility of poly(L-lactide)-grafted silica nanoparticle.* Journal of Applied Polymer Science, 2012. **124**(5): p. 3854-3860.

95. Eom, J.-H., Y.-W. Kim, and S. Raju, *Processing and properties of macroporous silicon carbide ceramics: A review.* Journal of Asian Ceramic Societies, (0).

96. Fukushima, M., Y. Zhou, and Y.-I. Yoshizawa, *Fabrication and microstructural characterization of porous silicon carbide with nano-sized powders.* Materials Science and Engineering: B, 2008. **148**(1–3): p. 211-214.

97. Liu, G., et al., *Fabrication of wood-like porous silicon carbide ceramics without templates.* Journal of the European Ceramic Society, 2011. **31**(5): p. 847-854.

98. Kim, Y., et al., *Formation of porous SiC ceramics via recrystallization.* Journal of the European Ceramic Society, 2012. **32**(13): p. 3611-3615.

99. Fukushima, M., et al., *Microstructural Characterization of Porous Silicon Carbide Membrane Support With and Without Alumina Additive.* Journal of the American Ceramic Society, 2006. **89**(5): p. 1523-1529.

100. Zhou, Y., et al., *Preparation and characterization of tubular porous silicon carbide membrane supports.* Journal of Membrane Science, 2011. **369**(1–2): p. 112-118.

101. Fukushima, M., Y. Zhou, and Y.-i. Yoshizawa, *Fabrication and microstructural characterization of porous SiC membrane supports with Al2O3–Y2O3 additives.* Journal of Membrane Science, 2009. **339**(1–2): p. 78-84.

102. Jang, B.K. and Y. Sakka, *Influence of microstructure on the thermophysical properties of sintered SiC ceramics.* Journal of Alloys and Compounds, 2008. **463**(1–2): p. 493-497.

103. Yao, X., et al., *Effect of recoating slurry viscosity on the properties of reticulated porous silicon carbide ceramics.* Ceramics International, 2006. **32**(2): p. 137-142.

104. Sieber, H., et al., *Biomorphic Cellular Ceramics.* Advanced Engineering Materials, 2000. **2**(3): p. 105-109.

105. Vogli, E., H. Sieber, and P. Greil, *Biomorphic SiC-ceramic prepared by Si-vapor phaseinfiltration of wood.* Journal of the European Ceramic Society, 2002. **22**(14–15): p. 2663-2668.

106. Studart, A.R., et al., *Processing Routes to Macroporous Ceramics: A Review.* Journal of the American Ceramic Society, 2006. **89**(6): p. 1771-1789.

107. Jin, Y.-J. and Y.-W. Kim, *Low temperature processing of highly porous silicon carbide ceramics with improved flexural strength.* Journal of Materials Science, 2010. **45**(1): p. 282-285.

108. Kim, Y.-W., et al., *Fabrication of Open-Cell, Microcellular Silicon Carbide Ceramics by Carbothermal Reduction.* Journal of the American Ceramic Society, 2005. **88**(10): p. 2949-2951.

109. Eom, J.-H., et al., *Microstructure and properties of porous silicon carbide ceramics fabricated by carbothermal reduction and subsequent sintering process.* Materials Science and Engineering: A, 2007. **464**(1–2): p. 129-134.

110. Dey, A., N. Kayal, and O. Chakrabarti, *Preparation of porous SiC ceramics by an infiltration technique.* Ceramics International, 2011. **37**(1): p. 223-230.

111. Ding, S., et al., *Effect of Y2O3 addition on the properties of reaction-bonded porous SiC ceramics.* Ceramics International, 2006. **32**(4): p. 461-466.

112. Liu, S., Y.-p. Zeng, and D. Jiang, *Effects of CeO2 addition on the properties of cordierite-bonded porous SiC ceramics.* Journal of the European Ceramic Society, 2009. **29**(9): p. 1795-1802.

113. Kumar, B.V.M., et al., *Effect of aluminum hydroxide content on porosity and strength of porous mullite-bonded silicon carbide ceramics.* Journal of the Ceramic Society of Japan, 2011. **119**(1389): p. 367-370.

114. Jing, Y., et al., *Fabrication and properties of SiC/mullite composite porous ceramics.* Ceramics International, 2014. **40**(1, Part B): p. 1329-1334.

115. Choi, Y.-H., et al., *Effect of alkaline earth metal oxide addition on flexural strength of porous mullite-bonded silicon carbide ceramics.* Journal of Materials Science, 2010. **45**(24): p. 6841-6844.

116. Dey, A., et al., *Evaluation of Air Permeation Behavior of Porous SiC Ceramics Synthesized by Oxidation-Bonding Technique.* International Journal of Applied Ceramic Technology, 2013. **10**(6): p. 1023-1033.

117. Alvin, M.A., *Impact of char and ash fines on porous ceramic filter life.* Fuel Processing Technology, 1998. **56**(1–2): p. 143-168.

118. Alvin, M.A., *Advanced Ceramic Materials for Use in High-Temperature Particulate Removal Systems.* Industrial & Engineering Chemistry Research, 1996. **35**(10): p. 3384-3398.

119. Dou, B., et al., *Research progress of hot gas filtration, desulphurization and HCl removal in coal-derived fuel gas: A review.* Chemical Engineering Research and Design, 2012. **90**(11): p. 1901-1917.

120. Sharma, S.D., et al., *A critical review of syngas cleaning technologies - fundamental limitations and practical problems.* Powder Technology, 2008. **180**(1-2): p. 115-121.

121. Ding, S., et al., *Fabrication of mullite-bonded porous silicon carbide ceramics by in situ reaction bonding.* Journal of the European Ceramic Society, 2007. **27**(4): p. 2095-2102.

122. Yoldas, B.E., *Alumina sol preparation from alkoxides.* Ceram. Bull., 1975. **54**: p. 289.

123. Brunauer, S., P.H. Emmett, and E. Teller, *Adsorption of Gases in Multimolecular Layers.* Journal of the American Chemical Society, 1938. **60**(2): p. 309-319.

124. Washburn, E.W., *The Dynamics of Capillary Flow.* Physical Review, 1921. **17**(3): p. 273-283.

125. Ebrahimpour, O., C. Dubois, and J. Chaouki, *Fabrication of mullite-bonded porous SiC ceramics via a sol–gel assisted in situ reaction bonding.* Journal of the European Ceramic Society, (0).

ANNEXE 1 – **POROUS SIC CERAMIC AND METHOD FOR THE FABRICATION THEREOF**

(12) INTERNATIONAL APPLICATION PUBLISHED UNDER THE PATENT COOPERATION TREATY (PCT)

(19) World Intellectual Property Organization
International Bureau

(43) International Publication Date
28 February 2013 (28.02.2013)

WIPO | PCT

(10) International Publication Number
WO 2013/026168 A1

(51) International Patent Classification:
C04B 38/06 (2006.01) ***C04B 35/565*** (2006.01)

(21) International Application Number:
PCT/CA2012/050586

(22) International Filing Date:
24 August 2012 (24.08.2012)

(25) Filing Language: English

(26) Publication Language: English

(30) Priority Data:
61/526,849 24 August 2011 (24.08.2011) US

(71) Applicant *(for all designated States except US)*: **POLYVALOR, SOCIÉTÉ EN COMMANDITE** [CA/CA]; 3535, chemin Queen-Mary, Bureau 220, Montréal, Québec H3V 1H8 (CA).

(72) Inventors; and
(75) Inventors/Applicants *(for US only)*: **CHAOUKI, Jamal** [CA/CA]; 180, ave de la présentation, Dorval, Québec H9S 3L4 (CA). **EBRAHIMPOUR, Omid** [IR/CA]; #720, 3328 av Troie, Montréal, Québec H3V 1B1 (CA). **DUBOIS, Charles** [CA/CA]; 8115 Saguenay, Brossard, Québec J4X 1N2 (CA).

(74) Agent: **GOUDREAU GAGE DUBUC**; 2000, McGill College, #2200, Montréal, Québec H3A 3H3 (CA).

(81) Designated States *(unless otherwise indicated, for every kind of national protection available)*: AE, AG, AL, AM, AO, AT, AU, AZ, BA, BB, BG, BH, BN, BR, BW, BY, BZ, CA, CH, CL, CN, CO, CR, CU, CZ, DE, DK, DM, DO, DZ, EC, EE, EG, ES, FI, GB, GD, GE, GH, GM, GT, HN, HR, HU, ID, IL, IN, IS, JP, KE, KG, KM, KN, KP, KR, KZ, LA, LC, LK, LR, LS, LT, LU, LY, MA, MD, ME, MG, MK, MN, MW, MX, MY, MZ, NA, NG, NI, NO, NZ, OM, PE, PG, PH, PL, PT, QA, RO, RS, RU, RW, SC, SD, SE, SG, SK, SL, SM, ST, SV, SY, TH, TJ, TM, TN, TR, TT, TZ, UA, UG, US, UZ, VC, VN, ZA, ZM, ZW.

(84) Designated States *(unless otherwise indicated, for every kind of regional protection available)*: ARIPO (BW, GH, GM, KE, LR, LS, MW, MZ, NA, RW, SD, SL, SZ, TZ, UG, ZM, ZW), Eurasian (AM, AZ, BY, KG, KZ, RU, TJ, TM), European (AL, AT, BE, BG, CH, CY, CZ, DE, DK, EE, ES, FI, FR, GB, GR, HR, HU, IE, IS, IT, LT, LU, LV, MC, MK, MT, NL, NO, PL, PT, RO, RS, SE, SI, SK, SM, TR), OAPI (BF, BJ, CF, CG, CI, CM, GA, GN, GQ, GW, ML, MR, NE, SN, TD, TG).

Published:
— *with international search report (Art. 21(3))*

WO 2013/026168 A1

(54) **Title**: POROUS SIC CERAMIC AND METHOD FOR THE FABRICATION THEREOF

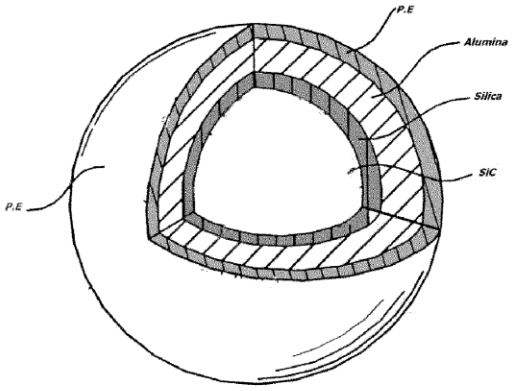

Figure 18. Schematic of final coated SiC particles.

(57) **Abstract**: There is provided a method for the fabrication of porous SiC ceramic. The method comprises oxidizing particles of SiC ceramic thereby forming amorphous silica on the surface of the particles. The oxidized SiC particles are then mixed with an additive. Alternatively, layer(s) of the additive is (are) deposited on their surface by sol-gel technique. The oxidized SiC particles mixed or coated with the additive are then mixed with at least one pore-former. Alternatively, the oxidized SiC particles mixed or coated with the additive are coated with layer(s) of a polymer or pore-former by in-situ polymerization. In embodiments where the oxidized SiC particles are mixed with an additive and a pore-former or polymer, a further additive may be used. In each of these embodiments, the resulting product is then compacted into a green body which is heated and sintered to yield the porous SiC ceramic material. There is also provided a porous SiC ceramic fabricated by the method according to the invention.